Fall 2014

# Dopamine Transporter (DAT), Nicotinic Acetylcholine Receptor (nAChR), and Metabotropic Glutamate Receptor 2 (mGlu2) Irreversible Probes For Identifying Anti-Psychostimulant Therapeutics

Shaili Aggarwal

# DOPAMINE TRANSPORTER (DAT), NICOTINIC ACETYLCHOLINE RECEPTOR (nAChR), AND METABOTROPIC GLUTAMATE RECEPTOR 2 (MGLU2) IRREVERSIBLE PROBES FOR IDENTIFYING ANTI-PSYCHOSTIMULANT THERAPEUTICS

A Dissertation

Submitted to the Mylan School of Pharmacy

Duquesne University

In partial fulfillment of the requirements for

the degree of Doctor of Philosophy

By

Shaili Aggarwal

December 2014

DOPAMINE TRANSPORTER (DAT), NICOTINIC ACETYLCHOLINE RECEPTOR (nAChR), AND METABOTROPIC GLUTAMATE RECEPTOR 2 (MGLU2) IRREVERSIBLE PROBES FOR IDENTIFYING ANTI-PSYCHOSTIMULANT THERAPEUTICS

By

Shaili Aggarwal

Approved October 20th, 2014

| | |
|---|---|
| David J. Lapinsky, Ph.D.<br>Committee Chair, Associate Professor of Medicinal Chemistry, Graduate School of Pharmaceutical Sciences, Duquesne University, Pittsburgh, PA | Aleem Gangjee, Ph.D.<br>Committee Member, Professor of Medicinal Chemistry, Graduate School of Pharmaceutical Sciences, Duquesne University, Pittsburgh, PA |
| Patrick T. Flaherty, Ph.D.<br>Committee Member, Associate Professor of Medicinal Chemistry, Graduate School of Pharmaceutical Sciences, Duquesne University, Pittsburgh, PA | Marc W. Harrold, Ph.D.<br>Committee Member, Professor of Medicinal Chemistry, Graduate School of Pharmaceutical Sciences, Duquesne University, Pittsburgh, PA |
| Christopher K. Surratt, Ph.D.<br>Committee Member, Professor of Pharmacology, Graduate School of Pharmaceutical Sciences, Duquesne University, Pittsburgh, PA | James K. Drennen, Ph.D.<br>Committee Member, Associate Dean, Research and Graduate Programs, Duquesne University, Pittsburgh, PA |

ABSTRACT

DOPAMINE TRANSPORTER (DAT), NICOTINIC ACETYLCHOLINE RECEPTOR (nAChR), AND METABOTROPIC GLUTAMATE RECEPTOR 2 (MGLU2) IRREVERSIBLE PROBES FOR IDENTIFYING ANTI-PSYCHOSTIMULANT THERAPEUTICS

By

Shaili Aggarwal

December 2014

Dissertation supervised by Dr. David J. Lapinsky

Numerous *in vitro* and *in vivo* studies implicate that certain ligands that interact with DAT, nAChRs, and mGlu2 have tremendous potential as anti-addiction therapeutics. However, understanding how these promising anti-addiction compounds interact with their major drug targets at the molecular level is limited because of the absence of human DAT, nAChRs, and mGlu2 x-ray crystal structures. This knowledge gap is important towards rationally designing new therapeutics for psychostimulant abuse and addiction. The objective of this research was to develop irreversible chemical probes based on promising anti-addiction lead compounds (i.e., pyrovalerone, bupropion, BINA, etc) to map their binding sites and poses within the DAT, select nAChR subtypes, or mGlu2. The central hypothesis was that these compounds could be rationally derivatized, without significant alteration in their pharmacological activity, with a photoreactive group capable of forming a covalent bond to their target protein and a tag for

application of a "Binding Ensemble Profiling with (f)Photoaffinity Labeling (BEProFL)" experimental approach. BEProFL rationally couples photoaffinity labeling, chemical proteomics, and computational molecular modeling to allow structure-function studies of the target proteins. This central hypothesis was tested by pursuing three specific aims: 1.) Identification of non-tropane photoprobes based on pyrovalerone (PV) suitable for DAT structure-function studies, 2.) Identification of bupropion (BP)-based photoprobes suitable for DAT, and nAChR structure-function studies, and 3.) Identification of irreversible mGlu2 PAM ligands as chemical probes suitable for mGlu2 structure-function studies. In the first aim, PV, a non-tropane DAT inhibitor, was structurally modified to contain a photoreactive group (i.e., an aryl azide) and a tag (i.e., $^{125}$I). These photoprobes were then pharmacologically evaluated to identify suitable candidates for DAT structure-function studies. In the second aim, BP was structurally modified to contain an aryl azide and $^{125}$I. This probe successfully identified the exact location of the bupropion-binding site within the *Torpedo* nAChR. Under the third aim, biphenyl-carboxylic acid indanone- and pyridone-based mGlu2 PAMs were structurally modified to contain a photoreactive group (e.g., aryl azide, acetophenone) and a tag (e.g., terminal alkyne, aliphatic azide). These compounds, at present, are being subjected to mGlu2 pharmacological evaluation to identify suitable chemical probe candidates for mGlu2 structure-function studies.

DEDICATION

*Dedicated to my parents,*

*and my husband Sameer,*

*for their unconditional love and support*

ACKNOWLEDGEMENTS

I would like to express my deepest gratitude to my research advisor, Dr. David J. Lapinsky for his help and guidance throughout these years. He has constantly inspired and encouraged me to become a better scientist. I thank him for his insightful advice, consistent accessibility and, most of all, patience that was instrumental in the completion of this research work.

I would like to acknowledge my dissertation committee members, Dr. Aleem Gangjee, Dr. Patrick T. Flaherty, Dr. Marc W. Harrold, Dr. Christopher K. Surratt, and Dr. James K. Drennen for their valuable time and advice throughout my graduate school career. I would also like to thank Dr. Christopher K. Surratt, Dr. Roxanne Vaughan, Dr. Hugo Arias, Dr. Michael Blanton, and Dr. Karen Gregory for the biological evaluation of my compounds. I will forever be grateful to Ms. Jackie Farrer, Ms. Nancy Hosni, Ms. Deborah Willson, and Ms. Mary Caruso for their unconditional help and support in administrative affairs. I would also like to thank the Graduate School of Pharmaceutical Sciences at Duquesne University and funding from the research grant NIDA R03DA027081 for providing me with financial aid as a teaching and research assistant.

My survival in graduate school would have been impossible without my friends and fellow graduate students at Duquesne University, with whom I have spent the most memorable and wonderful times of my life. I thank them for their love and care, and for never letting me feel alone while being so far away from home.

Finally, I would like to thank my best friend and dear husband, Sameer. His enthusiasm, optimism, and amazing sense of humor have kept me sane throughout these years. He has never

failed to put a smile on my face when I was most depressed. He has helped me survive through the toughest phases of my life and has always been by my side when I needed him the most. He continues to motivate me every single day and I am grateful to have him in my life. Without his encouragement, emotional support, and love, it would have been impossible to finish this work. I love him with all my heart and soul.

Last, but not least, a special thanks to my loving parents, Vandana and Arun Aggarwal. They have made the greatest sacrifice of letting their only child go far away from them to study abroad. I thank them dearly for giving me this opportunity and for always believing in me. Their humble nature has always kept me grounded and have made me a better person. There are no words to adequately express how much I love and miss them.

TABLE OF CONTENTS

LIST OF FIGURES

LIST OF SCHEMES

LIST OF TABLES

ABBREVIATIONS

| | |
|---|---|
| ASA | American Psychiatric Association |
| AMPA | α-Amino-3-hydroxy-5-methyl-4-isoxazole propionic acid |
| BEPro(f)L | Binding ensemble profiling with (f)photoaffinity labeling |
| α-BgTx | α-Bungarotoxin |
| cAMP | Cyclic adenosine monophosphate |
| Carb | Carbamylcholine |
| BP | Bupropion |
| DAT | Dopamine transporter |
| DCM | Dichloromethane |
| DMF | Dimethylformamide |
| dDAT | *Drosophila* dopamine transporter |
| EtOAc | Ethyl acetate |
| FDA | Food and Drug Administration |
| GPCR | G protein-coupled receptor |
| hDAT | Human dopamine transporter |
| HPLC | High performance liquid chromatography |
| iGlu | Ionotropic glutamate receptor |
| ISC | Intersystem crossing |
| LeuT | Leucine transporter |
| MAO | Monoamine oxidase |
| MeOH | Methanol |
| mGlu2 | Metabotropic glutamate receptor 2 |

| | |
|---|---|
| mGlu5 | Metabotropic glutamate receptor 5 |
| mAChR | Muscarinic acetylcholine receptor |
| MP | Melting point |
| MS | Mass spectrometry |
| nAChR | Nicotinic acetylcholine receptor |
| NAM | Negative allosteric modulator |
| NBS | N-Bromosuccinimide |
| NET | Norepinephrine transporter |
| NIDA | National Institute on Drug Abuse |
| NMDA | *N*-Methyl-D-aspartate |
| NSS | Neurotransmitter/sodium symporter |
| PAM | Positive allosteric modulator |
| PKC | Protein kinase C |
| PLC | Phospholipase C |
| PV | Pyrovalerone |
| SAR | Structure-activity relationship |
| SDS-PAGE | Sodium dodecyl sulfate polyacrylamide gel electrophoresis |
| SLC6 | Solute carrier 6 |
| THF | Tetrahydrofuran |
| TLC | Thin layer chromatography |
| TM | Transmembrane |
| U.S. | United States |

## CHAPTER ONE

## 1. Biological Literature Review

### 1.1. The Problem of Drug Addiction

Substance abuse is characterized by a compulsive, incontrollable need to seek and intake a psychostimulant despite its deleterious effects on the personal and social well being of the individual. It is a chronic condition leading to severe medical, psychiatric, and psychosocial problems (LeMoal and Koob, 2007; Koob and Volkow, 2010). According to the 5th edition of *Diagnostic and Statistical Manual of Mental Disorders* (DSM) from the American Psychiatric Association (ASA), substance dependence is characterized by a loss of control in limiting abuse, and the emergence of a negative emotional state, (e.g. anxiety and irritability due to withdrawal) when access to a substance is prevented. It demonstrates the presence of an acquired abnormal state wherein regular administration of an adequate amount of a substance is essential to maintain normal physiological equilibrium. According to the 2012 National Survey on Drug Use and Health (NSDUH), about 27 million people in the US alone suffer from drug addiction; approximately 200,000 people died due to drug abuse in 2012 (Kobeissy *et al.*, 2014). Therefore, development of effective strategies for treatment of substance abuse and dependence is essential considering its negative impact on the individual and society, as well as the unprecedented economic burden attributed to health care costs, loss of productivity and legal system expenditures.

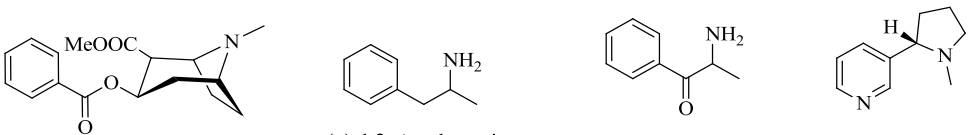


**1.1**, Cocaine (±)-**1.2**, Amphetamine (±)-**1.3**, Cathinone (-)-**1.4**, Nicotine

**Figure 1.1.** Chemical structures of some major drugs of abuse

Some of the most commonly abused drugs include cocaine (**(-)-1.1**), amphetamine (**(±)-1.2**), cathinone (**(±)-1.3**) and nicotine (**(-)-1.4**) (Klein and Rowland, 2013; Figure 1.1). These drugs of abuse cause long-term neuroadaptive changes in the mesocorticolimbic region of the brain, ultimately leading to the problems of substance abuse, dependence, tolerance, and relapse (Hyman and Malenka, 2001; Hyman *et al.*, 2006). Apart from severe socioeconomic losses faced by drug addicts, such individuals also suffer from acute CNS effects including euphoria, insomnia, increased libido, tremors, and convulsions.

Cocaine (**1.1**, Figure 1.1) is a tropane alkaloid originally obtained from the leaves of the coca plant *Erythroxylum coca* in 1855. It is a Schedule II drug and one of the most potent psychostimulants known, possessing very high addictive properties (Freye, 2010). More than 1.6 million Americans were addicted to cocaine in 2012 according to a report by the US Department of Health and Human Services (see http://www.samhsa.gov/data/NSDUH/2012SummNatFindDetTables/NationalFindings/NSDUHresults2012.htm). The hydrochloride salt of cocaine is administered intravenously, whereas its free base is used *via* inhalation. Cocaine, upon administration, elicits physiological effects such as euphoria, increased cardiovascular activity, hypothermia, and hypertension, with chronic abuse leading to a higher risk for stroke, heart, and pulmonary diseases. Furthermore, individuals who abuse cocaine are also more susceptible to infectious diseases such as HIV/AIDS, Hepatitis B, and Hepatitis C (Parikh *et al.*, 2012; Zimmerman, 2012). In addition, cocaine withdrawal results in severe stages of depression, paranoia, and hallucinations, and addicts require a strong desire and tremendous willpower to quit. In most cases, severity of cocaine withdrawal symptoms forces addict to ultimately relapse. Currently, effective FDA-approved pharmacotherapies to treat cocain addiction are non-existent, and the addicts have to

rely mainly on behavioral therapies for treating cocaine abuse and addiction (Herdener *et al*., 2012).

Phenethylamine-containing psychostimulants (i.e., amphetamine (**(±)-1.2**), methamphetamine (**(±)-1.5**) and MDMA (3,4-methylenedioxy-N-methylamphetamine, (**(±)-1.6** or "ecstasy"), as well as their β-keto derivative, cathinone (**(±)-1.3**) and its synthetic analogs (also called "designer cathinones" or "bath salts") are another category of psychostimulants with severe abuse potential (see Figure 1.2) (Banks *et al.*, 2014; Iversen *et al.*, 2014).

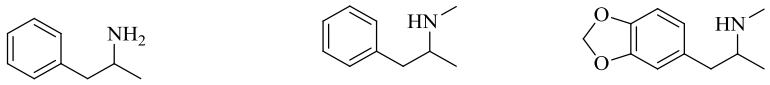


**(±)-1.2**, Amphetamine **(±)-1.5**, Methamphetamine **(±)-1.6**, MDMA

**Figure 1.2.** Chemical structures of the amphetamine-class of psychostimulants.

Amphetamine (**(±)-1.2**) addiction causes severe loss of appetite, agitation, paranoia, hallucinations, and delusions (Goncalves *et al.*, 2014). The *N*-methyl analog, methamphetamine (**(±)-1.5**, METH) is even more potent and toxic than amphetamine. METH is highly lipophilic, less prone to enzymatic degradation, with a half life of 10-12 hours, and reaches the brain faster than any other psychostimulant (Cruickshank and Dyer, 2009; Schep *et al.*, 2010). METH abuse is a major public health problem in the U.S. The 2012 NSDUH reported 1.2 million people using METH, with 440,000 users in a single month (see http://www.drugabuse.gov/sites/default/files/methrrs_web.pdf). METH exists in several physical forms and can be smoked, inhaled, injected, or orally ingested. The short-term effects of METH abuse include increased attention, decreased fatigue, increased activity and wakefulness, decreased appetite, euphoria, and hyperthermia. Consequently, chronic long-term METH use leads to memory loss, fatal seizures, psychosis, impaired motor skills, aggressive and violent behavior, weight loss, hemorrhage, depression, and death. The abusive intake of MDMA (**(±)-**

**1.6** or "ecstasy"), another amphetamine analog, can cause damage to the brain, kidney, liver, and heart tissue. Its long term effects include myocardial infarction, multiple organ failure, and ultimately death (Reid *et al.*, 2007). In addition, MDMA (**(±)-1.6**) metabolizes systemically into a variety of reactive quinone or thioether precursors, that produce free radicals that can cause further damage to the physiological system (Green *et al.*, 2003).

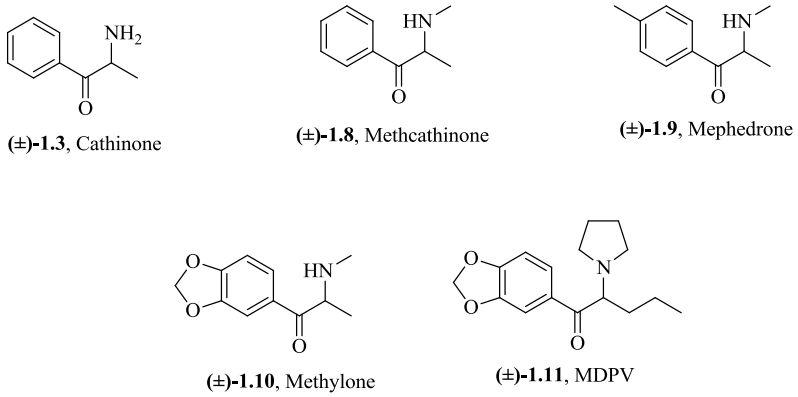


**Figure 1.3.** Chemical structures of cathinone and its synthetic derivatives.

Cathinone (**(±)-1.3**, Figure 1.3), found in the plant *Catha edulis*, or "khat", is a naturally occurring β-keto analog of amphetamine that producing psychostimulant effects similar to the amphetamines but with greater potency (Al'Absi and Grabowski, 2012; Al Suwaidi *et al.*, 2013). Its first synthetic analog, methcathinone (**(±)-1.8**) discovered through structure-activity studies of **(±)-1.3**, was found to be as potent as METH, and is presently widely abused (Glennon *et al.*, 1987; Calkins *et al.*, 1995; Bonano *et al.*, 2014). Between 2005 and 2011, several synthetic analogs of cathinone with a common α-aminophenylketone moiety emerged called as "designer cathinones" (or "bath salts" or "legal highs"). Most of these drugs are now being sold legally on the internet under different street names (German *et al.*, 2014). Due to their convenient accessibility *via* chemical synthesis and inadequate regulatory policies to limit their illegal use, these designer drugs have posed growing health risks. Many cases of severe neurological

disorder and deaths due to their overdose have been increasing at an alarming rate (Johnson *et al.*, 2013). Moreover, the synthetic cathinone derivatives are relatively easier to synthesize and several analogs with subtle structural changes versus cathinone can be generated to evade legal constraints (Coppola and Mondola, 2012; Gunderson *et al.*, 2013; Simmler, Buser *et al.*, 2013; Zawilska and Wojcieszak, 2013). Among the designer cathinones, the most popularly abused are mephedrone (**(±)-1.9**), methylone (**(±)-1.10**) and methylenedioxypyrovalerone (**(±)-1.11**, MDPV) which were labeled as Schedule I controlled substances in 2011 (Bonano *et al.*, 2014). These synthetic cathinone derivatives, despite slight structural divergence from cathinone, can either have pharmacological effects similar to methamphetamine, cocaine, MDMA, and cathinone, or can produce completely unknown complex neurological and cardiovascular effects that can last up to days (Marinetti and Antonides, 2013).

Physiologically, the psychostimulant effects of the aforementioned drugs of abuse, (i.e., cocaine, amphetamine-like compounds and synthetic cathinones) are mediated through direct or indirect stimulation of the dopaminergic or glutamatergic nervous systems (Nestler, 2005).

Another form of drug addiction is tobacco dependence from cigarette smoking. *L*-nicotine (**(-)-1.4**, Figure 1.1), a tertiary amine alkaloid, is the main psychoactive constituent of tobacco. Nicotine mediates its psychoactive actions such as mood elevation, increased arousal, improved attentiveness, and muscle relaxation, by activating nicotinic acetylcholine receptors (nAChRs), thereby causing stimulation of the cholinergic nervous system, which in turn affects dopaminergic neurotransmission (Benowitz, 2009). Despite the harmful consequences of tobacco smoking, which is known to increase the risks of cardiovascular diseases, stroke, and cancer, the compulsive use of tobacco is the major cause of deaths associated with addiction in developing countries (George and O'Malley, 2004).

Treatment of psychostimulant abuse currently remains a major challenge. No medications have yet been approved by the Food and Drug Administration (FDA) for treatment of cocaine or methamphetamine abuse. In addition, smoking cessation therapies available for nicotine addiction, such as nicotine replacement products, varencline (Chantix®), and bupropion (Zyban®) are inadequate, as 80% of addicts relapse within a month of treatment (Benowitz, 2009). Furthermore, the growing number of more potent, newer synthetic cathinones with continuously changing names, many routes of administration, several preparations with diverse drug constituents, and the difficulties in legally controlling them, are leading to overdose deaths. This observation warrants the urgent need for discovery and development of psychostimulant abuse therapeutics. As a result, over the past many years, numerous studies have focused on elucidating the detailed structural and functional properties of protein targets that control the neurotransmission within the dopaminergic, glutamatergic, and cholinergic systems, which are directly implicated in drug addiction.

### 1.2. The Dopaminergic System

The dopaminergic system refers to the mesocorticolimbic pathway (Figure 1.4) which includes dopaminergic neurons projecting from the midbrain region, comprised of the ventral tegmental area and substantia nigra (Arias-Carrion *et al.*, 2010).

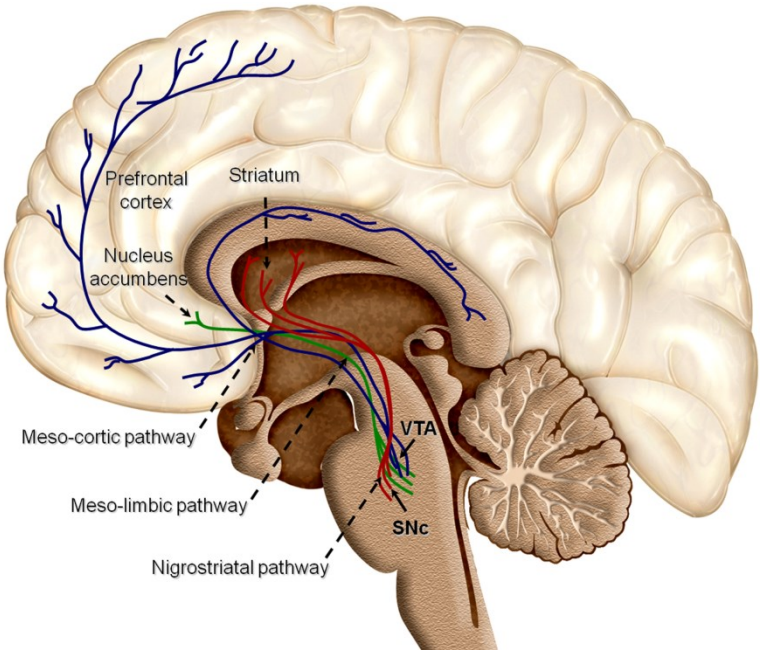


**Figure 1.4.** Overview of the mesocorticolimbic system of the human brain containing the dopaminergic projections passing through different regions of the human brain (Arias-Carrion *et al.*, 2010. Reprinted with permission from *Int. Arch. Med.* **2010**, *3*, 24. Copyright 2010, BioMed Central).

These neurons, originating from the ventral tegmental area and the substantia nigra, synthesize and release dopamine as a chemical messenger into the nucleus accumbens, frontal cortex and the striatum. Dopamine (**1.13**, Figure 1.5) is a catecholamine neurotransmitter biosynthesized from tyrosine by tyrosine hydroxylase and is stored in vesicles of presynaptic neurons (Tritsch and Sabatini, 2012).

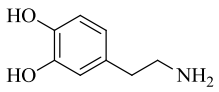


**1.13**, Dopamine

**Figure 1.5.** Chemical structure of dopamine (**1.13**) as a neurotransmitter.

Dopamine, released from presynaptic neurons into the synaptic cleft due to $Ca^{2+}$ influx, activates G protein-coupled dopamine receptors located on postsynaptic neurons. In turn, dopamine regulates important brain functions such as reward, addiction, attention, memory,

cognition, and motor control by activating dopamine receptors (Di Chiara and Bassareo, 2007). Dopamine is then slowly cleared from the synaptic cleft by reuptake into presynaptic neurons, where it is metabolized by monoamine oxidase (MAO).

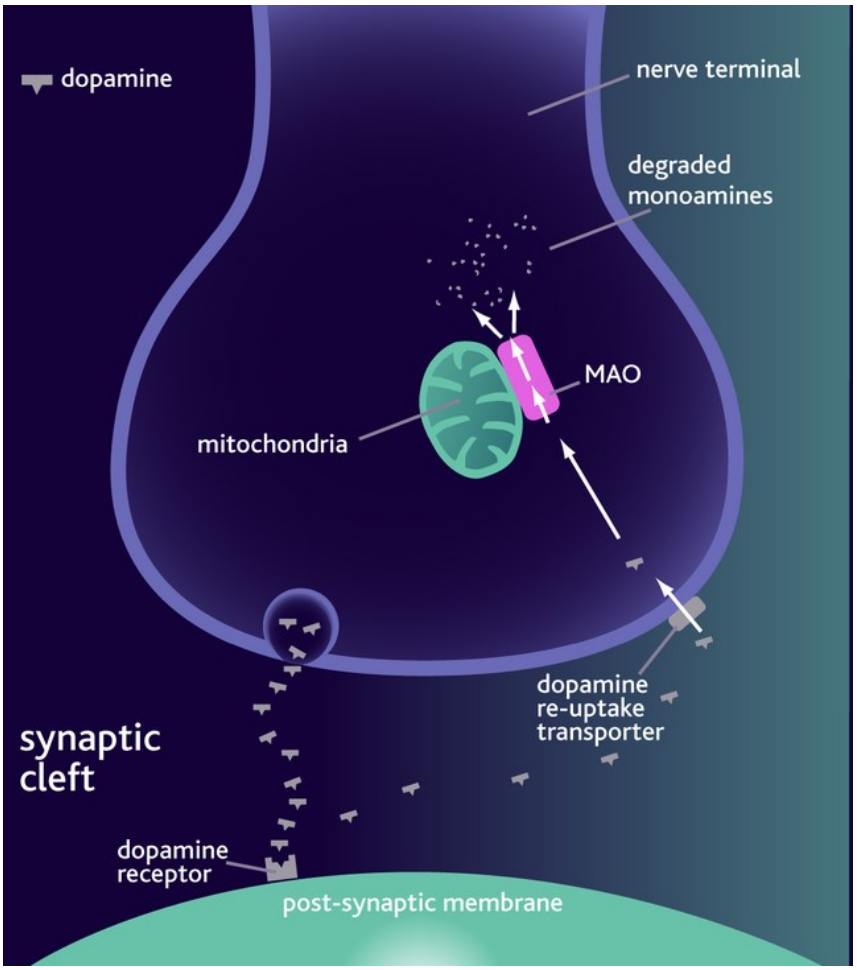


**Figure 1.6.** Dopaminergic neurotransmission (Reprinted with permission from https://www.cnsforum.com/educationalresources/imagebank/substance_abuse/mao_cocaine. Copyright 2014, accessed on 11/02/2014).

The duration and intensity of dopaminergic neurotransmission mediated by dopamine is controlled by the dopamine transporter (DAT) (Jaber *et al.*, 1997). The DAT belongs to the family of $Na^+/Cl^-$ dependent transporters. It is a plasma membrane protein located presynaptically that rapidly terminates dopamine neurotransmission by facilitating dopamine reuptake into the presynaptic terminals of dopaminergic neurons (Figure 1.6). Therefore, the

DAT plays a pivotal role in controlling the signal amplitude and duration of dopaminergic neurotransmission by altering dopamine concentration.

### 1.2.1. Role of the DAT in Drug Addiction

The mesocorticolimbic dopamine pathway in the brain is implicated in the acute rewarding actions of all psychostimulants by direct or indirect influence (Pierce and Kumaresan, 2006; Zhu and Reith, 2008; Schmitt and Reith, 2010). In particular, cocaine and amphetamine-like compounds stimulate the dopaminergic system by directly controlling DAT function and expression through different mechanisms (Caron, 1996; Figures 1.7 and 1.8).

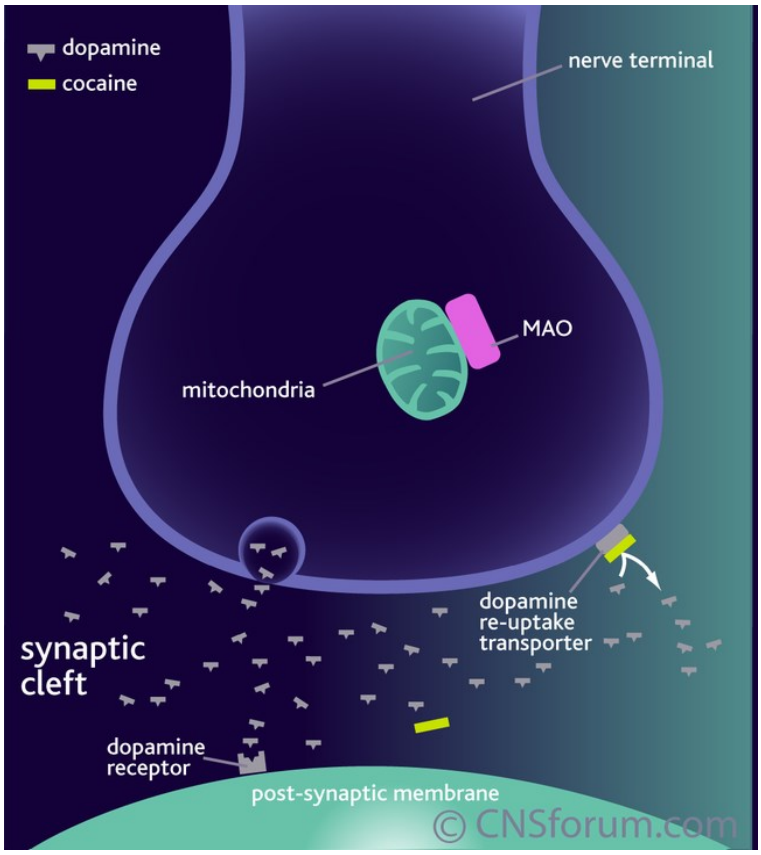


**Figure 1.7.** Inhibition of dopamine reuptake upon binding of cocaine to the DAT (Reprinted with permission from https://www.cnsforum.com/educationalresources/imagebank/substance_abuse/drug_amphet_low. Copyright 2014, accessed on 11/02/2014).

In particular, various *in vitro* and *in vivo* studies have established the DAT as the key protein for cocaine binding (Woolverton and Johnson, 1992). According to the widely accepted mechanism for cocaine-mediated increase in dopamine neurotransmission, cocaine binds to the DAT within presynaptic neuronal membranes of dopaminergic neurons, competitively blocking the reuptake of dopamine from the synaptic space. This results in an increase in extracellular dopamine concentration, that mediates the rewarding and reinforcing effects of cocaine by the activation of dopamine receptors located on postsynaptic neurons. Another potential mechanism of action of cocaine recently being explored is that cocaine might be acting as a DAT "inverse agonist" that "allosterically" reverses the direction of DAT transport, thereby releasing dopamine into the synaptic cleft (Heal *et al*., 2014).

Consequently, chronic use of cocaine results in a long-term functional upregulation of DAT in the presynaptic neurons by increasing its cell surface expression, which in turn reduces the basal levels of extracellular dopamine, thus leading to decreased rewarding or stimulatory effects (Letchworth *et al.*, 2001; Daws *et al.*, 2002). This leads to self-administration of cocaine to experience the rewarding effects, which ultimately results in chronic cocaine dependence and addiction. The cocaine-induced elevated DAT membrane expression further creates abnormal neurobiological conditions that are responsible for causing severe withdrawal symptoms, and ultimately relapse after discontinuation of cocaine use (Kuhar, *et al.*, 1991; Kuhar and Pilotte, 1996; Kalivas *et al.*, 1998; Kahlig and Galli, 2003).

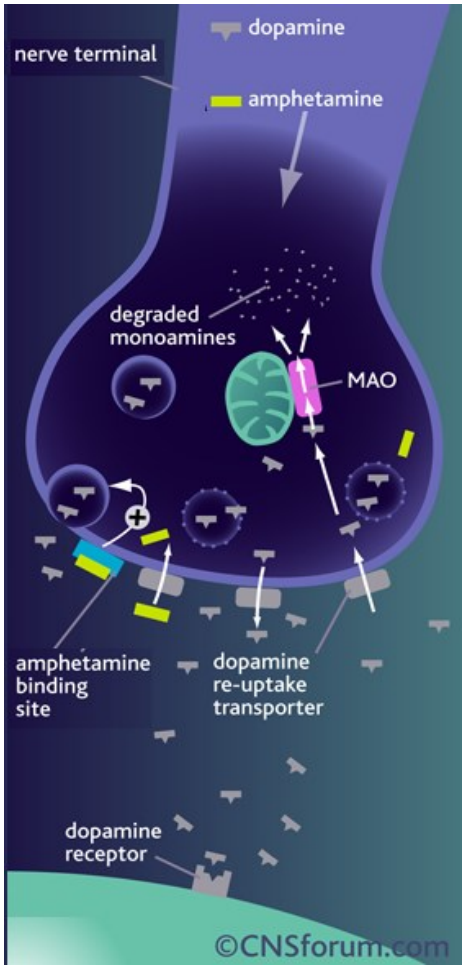


**Figure 1.8.** Mechanism of action of amphetamine (Adapted with permission from https://www.cnsforum.com/educationalresources/imagebank/substance_abuse/drug_amphet_low. Copyright 2014, accessed on 11/02/2014).

On the other hand, amphetamine-like psychostimulants, due to their structural similarity to dopamine, act as DAT substrates and are translocated into dopaminergic neurons. This triggers efflux of dopamine, thus resulting in an elevated dopamine concentration in the synapse (Kahlig *et al.*, 2005) (Figure 1.8). Furthermore, amphetamines also act as substrates for vesicular monoamine transporters (VMAT), triggering a release of dopamine stores from the vesicles into the intracellular environment that further promotes dopamine efflux (Sulzer *et al.*, 1995; Partilla *et al.*, 2006). Likewise, synthetic cathinones like mephedrone and methylone have amphetamine-like action on the DAT and stimulate the synaptic efflux of dopamine (Baumann *et*

*al.*, 2012; Simmler, Rickli *et al.*, 2013). MDPV (**(±)-1.11**), on the other hand, is a potent blocker of the DAT and increases dopamine neurotransmission by a mechanism similar to cocaine (Baumann *et al.*, 2013).

In conclusion, the DAT is a major target for psychostimulants and plays a key role in mediating their reward and stimulant behavioral effects, principally by controlling dopamine levels in the brain (Zhu and Reith, 2008). It is therefore important to understand the structural and functional features of the DAT, in particular, the binding sites of drugs of abuse within the DAT. A better understanding of DAT binding sites is expected to enable efforts to discover and develop new and improved therapeutics for the treatment of addiction associated with cocaine, amphetamines, and cathinones.

## 1.3. The DAT

### 1.3.1. Structural and Functional Features of the DAT

The DAT belongs to the neurotransmitter:sodium symporter (NSS) or solute carrier 6 (SLC6) family of $Na^+/Cl^-$ dependent membrane transporters (Pramod *et al.*, 2013). Other members of this family include the serotonin (SERT) and norepinephrine transporters (NET) (Torres *et al.*, 2003). The DAT is an approximately 80,000 dalton protein composed of 620 amino acids. It contains 12 transmembrane (TM) domains with both N- and C-termini located on the intracellular side of the membrane (Figure 1.9). The large extracellular loop (Loop e2, Figure 1.9) connecting TM3 and TM4 contains several *N*-glycosylation sites for the stability and plasma membrane trafficking of the DAT, whereas TM1 and TM6 are considered to be critical for ions, substrate, and cocaine binding as shown in Figure 1.9 (Chen and Reith, 2000).

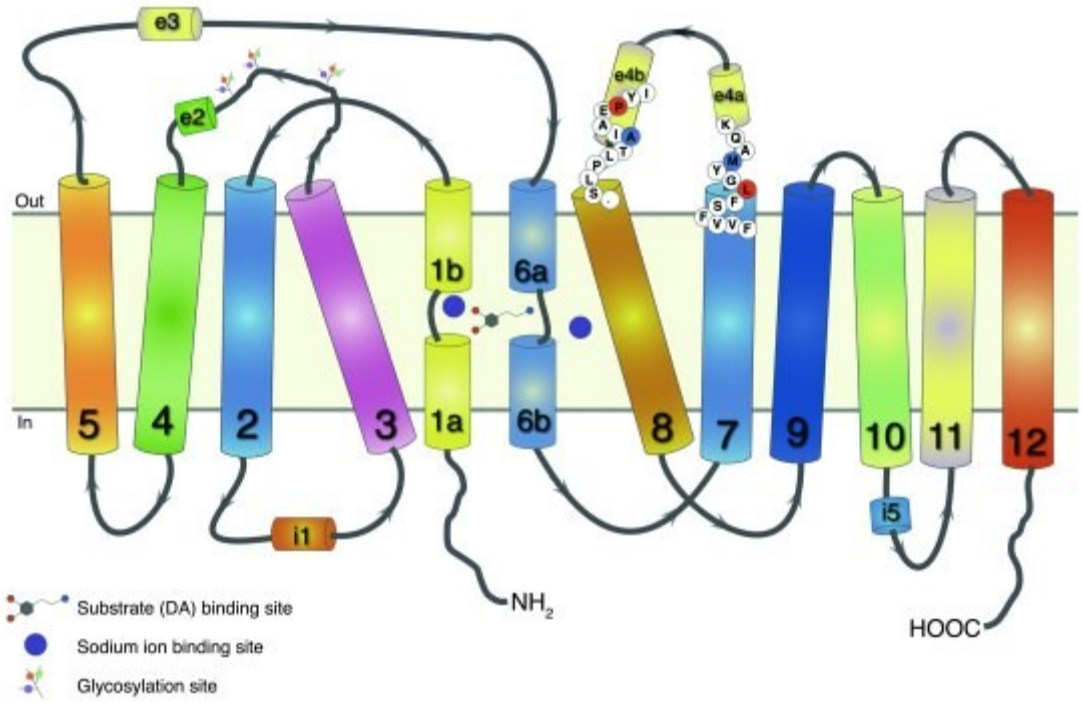


**Figure 1.9.** Diagram of membrane topology of the hDAT based on bacterial leucine transporter (LeuT) crystal structures. Full TM helices are numbered 1–12 and intra- and extracellular loops are numbered 1–5 with prefixes either 'i' or 'e' respectively (Schmitt *et al.*, 2008. Reprinted with permission from *J. Neurochem.* **2008**, *107*, 928-940. Copyright 2008, International Society for Neurochemistry).

Many aspects of the 3-D structure of human DAT (hDAT) currently remain unknown. As a result, approaches such as site-directed mutagenesis, photoaffinity labeling, and computer-aided homology models of hDAT have provided extensive information on DAT structure, transport mechanism, and binding sites. In particular, x-ray crystal structures of the bacterial (*Aquifex aeolicus*) leucine transporter (LeuT) (Yamashita *et al.*, 2005; Zhou *et al.*, 2007 and 2009; Singh *et al.*, 2007 and 2008; Quick *et al.*, 2009; Nyola *et al.*, 2010; Krishnamurthy and Gouaux, 2012; Loland, 2014; Penmatsa and Gouaux, 2014), possessing with 22% sequence homology to hDAT, and the recent *Drosophila melanogaster* DAT crystal structure (Penmatsa *et al.*, 2013), with greater than 50% homology with hDAT, have provided a more detailed understanding of DAT 3-D structure. Furthermore, several groups have generated homology models of the hDAT using the high resolution LeuT-crystal structure to predict the hDAT's

tertiary structure (e.g., Huang and Zhan, 2007; Indarte *et al.*, 2008; Manepalli *et al.*, 2012). Such studies have suggested that LeuT and hDAT share several common structural features, including the presence of a substrate binding pocket between TM1 and TM6. In addition, site-directed mutants of hDAT with single and multiple amino acid substitutions have been employed to study hDAT/cocaine interactions (Kitayama *et al*., 1992; Uhl and Lin, 2003; Wu and Gu, 2003; Chen *et al.*, 2004; Loland *et al*., 2004; Volz and Schenk, 2005). Photoaffinity labeling studies of the DAT with photoreactive compounds based on cocaine, its analogs, and several other known DAT inhibitors have also been utilized in elucidating the location of binding sites within the DAT (Grigoriadis *et al.*, 1989; Kline *et al.*, 1994; Vaughan, 1998, 1999, 2001, 2005 and 2007; Dutta *et al.*, 2001; Zou *et al.*, 2001; Newman *et al.*, 2006; Parnas *et al.*, 2008; Dahal *et al.*, 2014). Despite these efforts, the molecular mechanism and exact binding site of cocaine and other DAT inhibitors, as well as the molecular determinants of inhibitor selectivity, remain largely unknown. In particular, direct and indirect effects of mutations on substrate and inhibitor binding are difficult to predict with the absence of an accurate hDAT 3-D structure (Beuming *et al*., 2008). Furthermore, the LeuT structure, despite its many similarities to hDAT, also shows several distinct functional features. For instance, DAT homology models built using co-crystal structures of LeuT with desipramine and other tricyclic antidepressants (Singh *et al.*, 2007; Zhou *et al.*, 2007) do not provide reliable information on substrate interaction with the DAT, since tricyclic antidepressants show low affinity for hDAT (Schmitt *et al.*, 2008). In addition, cocaine, which is a potent DAT inhibitor, does not display inhibitory potency against LeuT. The comparison of LeuT crystal structure with the recently discovered dDAT crystal structure (Penmatsa *et al*., 2013) in complex with tricyclic antidepressant nortriptyline further provides many direct evidences of disparaties between the two transporters. In particular, the primary or

S1 binding site in dDAT is occupied by nortriptyline in contrast to LeuT-antidepressant co-crystal structures in which the TCAs inhibit LeuT *via* non-competitive mechanism by binding to the S2 binding site. The interactions made by Asp46 residue present in the TM1 region of dDAT compensates for the absence of carboxylate group present in the biogenic amine substrates as compared to the binding interactions of leucine substrate within LeuT. In dDAT, a hydrogen bond formed between the Asp46 side chain and the hydroxyl group of Tyr124 is similar to the interactions between the carboxylate group of leucine substrate and Tyr108 within the LeuT substrate binding pocket. The intracellular cytoplasmic gate in dDAT is capped by a carboxy-terminal helix like a latch which is absent in LeuT. Moreover, unlike in LeuT crystal structures, a cholesterol molecule is present in dDAT crystal structure between TMs 1a, 5 and 7 which is critical for its stabilization in an outward-open conformation. Such observations indicate the disparate features in the structure of dDAT and LeuT, and possibly between hDAT and LeuT, and warrant the need for more direct and valid experimental approaches for hDAT structure and function elucidation.

### 1.3.2. Proposed Conformational Cycles and Reuptake Mechanism of the DAT

The transport of dopamine by the DAT is favored by the energy gradient produced by the movement of $Na^+$ ions inside the cell, and driven by the concentration gradient created by $Na^+/K^+$ ATPase. DAT co-transports two $Na^+$ ions and a $Cl^-$ ion with each dopamine molecule through a series of sequential binding and conformational changes to facilitate influx (Sonders *et al.*, 1997; Gether *et al.*, 2006; Forrest *et al.*, 2011). This sequence begins with initial binding of $Na^+$ ions on the extracellular side of the membrane, followed by binding of dopamine, which triggers conformational changes in the protein.

The very first model of DAT substrate uptake was proposed by Jardetzky almost half a century ago, wherein DAT was proposed to exist in outward- (open to extracellular side) and inward-facing (open to intracellular side) conformation (Jardetzky, 1966) (see Figure 1.10, A and E). Initially, ions and dopamine bind to the open-outward conformation (as shown in Figure 1.10, A and B), which triggers a rearrangement sequence, subsequently closing the outward opening while simultaneously exposing the bound substrate to the intracellular side of the membrane, thus leading to dissociation of substrate in the intracellular milieu *via* diffusion. The subsequent discovery of crystal structures of the LeuT, followed by molecular dynamic studies and molecular simulations *via* DAT homology models, validated and further refined the alternating access model of Jardetzky (Yamashita *et al.*, 2005; Schmitt *et al.*, 2013). These studies revealed that the putative dopamine-binding site within DAT (called the S1 site or the primary binding site) lies in the center of the membrane channel, and is large enough to hold two $Na^+$ ions and the dopamine (Singh *et al.*, 2008). Furthermore, LeuT crystal structures have also revealed a third low-energy conformational state: a dually occluded, substrate bound state in addition to the outward- and inward-conformational states of the Jardetzky model for NSS proteins (Figure 1.10, C). According to this newer, three conformational state model, the initial outward-facing DAT conformation exposed to the extracellular milieu promotes the binding of $Na^+$ ions to stabilize the outward-open conformation (Claxton *et al.*, 2010; Krishnamurthy and Gouaux, 2012). This ion-bound, open conformation then facilitates the binding of dopamine to the S1 site. Once the dopamine is bound to the S1 site, the extracellular gate closes leading to the dopamine-bound occluded state, where both the ions and dopamine are in the middle of the channel protected from both the periplasmic and the cytoplasmic space by gating networks (Nyola *et al.*, 2010; Forrest *et al.*, 2011) (Figure 1.10, C). In hDAT, the extracellular gate

consists of a salt bridge between Arg85 and Asp476, and a cation-π interaction between Phe320 and Arg85. In addition, the aromatic rings of Tyr156 and Phe320 obstruct the S1 site during the occluded state by forming a lid with the help of a hydrogen bond interaction between Tyr156 and Asp79. The intracellular side of the S1 site also consists of a series of gating networks (i.e., salt-bridge between Arg60 and Asp436, cation-π interaction between Arg60 and Tyr335, and hydrogen bond interaction between Glu428 and Tyr335). Next, the occluded state is followed by the opening of the intracellular gate, leading to an inward-open conformation (Figure 1.10, D), which releases the ions and dopamine into the cytoplasm *via* diffusion facilitated by hydration of the site (Zhao, *et al.*, 2010 and 2011; Zhao and Noskov, 2011).

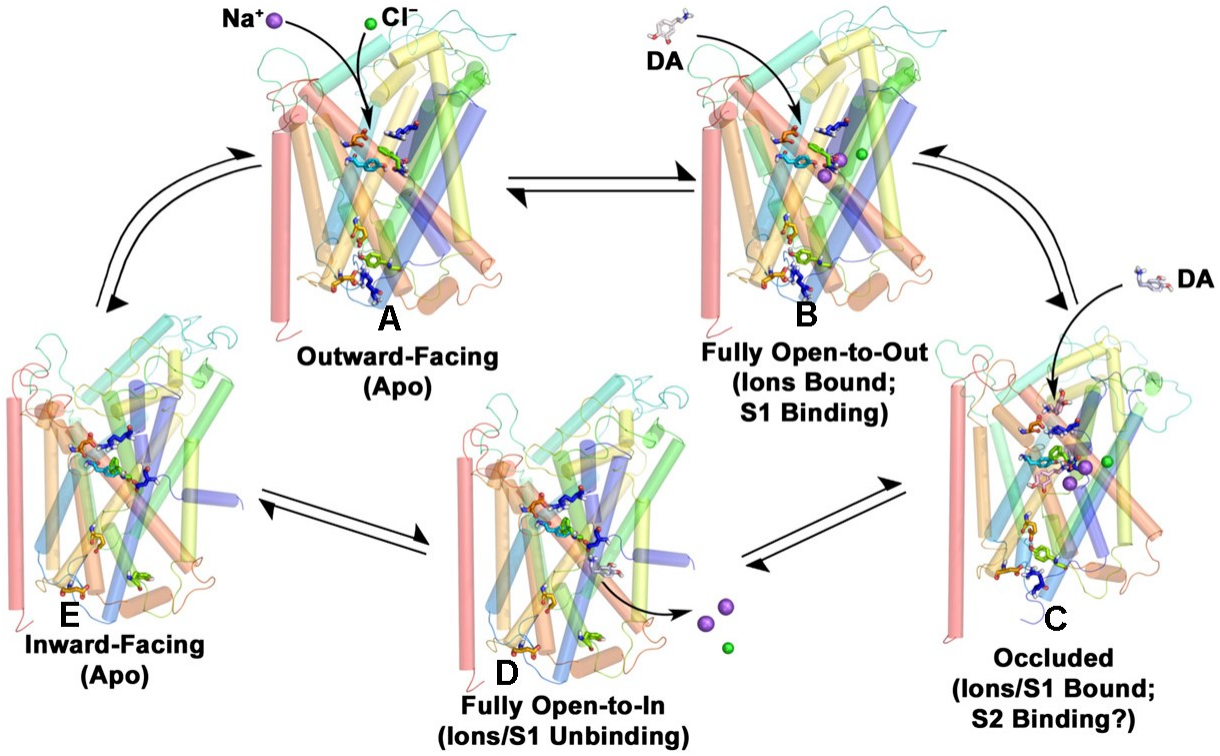


**Figure 1.10.** Putative conformational cycle of the DAT protein for translocation of dopamine (DA) (Schmitt *et al.*, 2013. Adapted with permission from *J. Pharmacol. Exp. Ther.* **2013**, *346,* 2-10. Copyright 2013, JPET Online by American Society for Pharmacology and Experimental Therapeutics).

Though the three-state, alternating access model proposes the presence of a single, putative substrate binding site, (i.e., the primary or the S1 site), Shi and coworkers, through molecular dynamic simulations, predicted the presence of a secondary, high-affinity allosteric site (S2) in LeuT occupied by a second leucine molecule (Figure 1.10, C) (Shi *et al.*, 2008; Quick *et al.*, 2012). This site was proposed to be present approximately 11Å above the S1 site towards the extracellular side of the membrane. The S2 site in LeuT has been shown to accommodate a wide variety of ligands such as tricyclic antidepressants, selective serotonin reuptake inhibitors (Zhou *et al.*, 2007 and 2009), and alkylglucoside detergents (Quick *et al.*, 2009). However, the existence of a similar S2 site in the human DAT, and its relevance, is highly controversial, and is currently a topic of debate in the scientific community. Some mutagenesis, comparative modeling, and photoaffinity studies support the hypothesis that DAT inhibitors like cocaine interact with the S1 site and competitively inhibit the substrate binding (Beuming *et al*., 2008; Bisgaard *et al*., 2011; Dahal *et al*., 2014), whereas other studies propose that cocaine binds to the S2 site and allosterically modulates binding at the substrate-binding site (Huang *et al*., 2009; Heal *et al*., 2014). Another hypothesis proposes that cocaine initially binds to the low affinity S2 site, and then transitions into a high affinity S1 site through conformational movements (Schmitt *et al*., 2013).

## 1.4. DAT Ligands

### 1.4.1. DAT Substrates

Amphetamine (**(±)-1.2**, Figure 1.2) and its analogs are drugs of abuse that cause euphoric actions by excessively increasing extracellular dopamine concentrations in the brain. Amphetamines, due to their structural similarity to dopamine (**1.13**), act as exogenous substrates

for the DAT. They are transported into presynaptic neurons causing reverse transport of dopamine into the synapse (Sitte *et al.*, 1998; Sulzer *et al.*, 2005). This is triggered by the fact that $Na^+$ influx accompanying the uptake of amphetamine increases the intracellular $Na^+$ concentration that promotes dopamine efflux (Sulzer *et al.*, 1995). In addition to causing efflux of dopamine, amphetamines also compete with dopamine for the unoccupied DAT binding site, which prevents dopamine reuptake from the synapse, thus resulting in a further increase in dopamine concentration. Furthermore, these drugs also act as substrates for vesicular monoamine transporters (VMAT), triggering a release of dopamine stores from vesicles into the intracellular environment that further promote dopamine efflux (Pifl *et al.*, 1995; Nickell *et al.*, 2014).

### 1.4.2. DAT Inhibitors

One proposed strategy to treat cocaine addiction has been to generate competitive inhibitors of cocaine binding without inhibiting dopamine reuptake. Ideally such a medication is expected to serve as a cocaine substitute with respect to its pharmacological actions and abuse liability, but should be able to gradually eliminate self-administration of cocaine without having any reinforcing effects (Rothman *et al.*, 1989; Carroll, *et al.*, 1999). In addition, compounds that have a slow onset of action and longer durations of actions are also considered as promising candidates for cocaine abuse treatment (Froimowitz *et al.*, 2000). Such an approach to find treatments for cocaine abuse has been challenging due to poor understanding of DAT's 3D structure and binding sites, which limits rational structure-based drug design of DAT ligands. Therefore, all DAT inhibitors to date have been developed by ligand-based drug design using known DAT ligands as lead compounds. In particular, such compounds can be categorized as

tropane- or non-tropane inhibitors based on their chemical structure. These compounds can be further differentiated based on their distinct behavioral effects as "cocaine-like" or "atypical" inhibitors.

### 1.4.2.1. Tropane Class of DAT Inhibitors

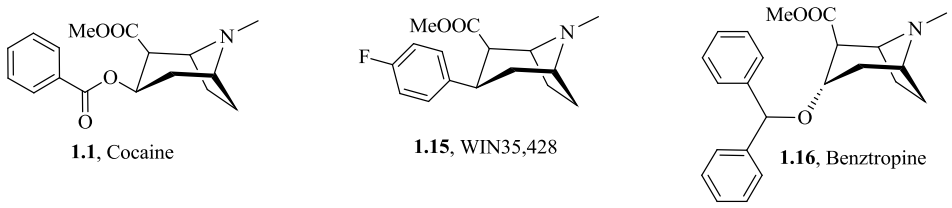


**1.1**, Cocaine

**1.15**, WIN35,428

**1.16**, Benztropine

**Figure 1.11.** Chemical structures of tropane-based DAT inhibitors

Cocaine is a tropane analog that mediates its psychostimulant effects by binding to the DAT and inhibiting dopamine uptake (hDAT $K_i$ = 285 ± 27 nM, DA uptake $IC_{50}$ = 230 ± 40 nM; Zou *et al*., 2003). SAR studies *via* a large number of cocaine analogs containing the tropane moiety have been conducted to find antagonists that can compete with cocaine for DAT binding sites, but do not inhibit dopamine uptake (Carroll *et al.*, 1992; Newman *et al.*, 1994). Such efforts have led to the identification of tropane analogs such as WIN-35,428 (**1.15**) and benztropine (**1.16**) (Figure 1.11). WIN-35,428 (hDAT $K_i$ = 37 ± 30 nM; DA uptake $IC_{50}$ = 30 ± 4 nM) is a highly potent competitive inhibitor of cocaine with 8-fold greater affinity at the DAT as compared to cocaine, and displays strong cocaine-like stimulatory effects *in vivo* (Clarke *et al.*, 1973; Madras *et al.*, 1989). WIN-35,428 is a cocaine analog without the metabolically labile benzoate ester of cocaine, thus making it a more stable analog with a longer half-life relative to cocaine. Therefore, a radioactive version of WIN-35,428 (i.e., [$^3$H]-WIN-35,428) is used in pharmacological assay studies of DAT ligands (Carroll *et al.*, 1991 and 1994). Benztropine (**1.16**, Cogentin®) is another tropane analog that inhibits the dopamine transporter (hDAT $K_i$ =

118 ± 10.6 nM; DA uptake $IC_{50}$ = 66 ± 25 nM; Zou *et al*., 2003). It is also an anticholinergic agent and is used clinically for symptomatic treatment of Parkinson's disease. In contrast to cocaine, benztropine analogs, despite having high affinity for the DAT, do not demonstrate cocaine-like behavioral effects in animal models of cocaine abuse (Katz *et al.*, 2001; Ukairo *et al.*, 2005; Schmitt *et al.*, 2008). This class of atypical inhibitors does not effectively stimulate locomotor activity in mice relative to cocaine. In addition, benztropines failed to substitute for cocaine in discriminative stimulus studies in rats (Hiranita *et al.*, 2009). Moreover, benztropine analogs have a slower onset of action and a longer duration than cocaine when administered i.p.. Furthermore, benztropine is not self-administered in rhesus monkeys as effectively as cocaine (Woolverton *et al.*, 2000). Therefore, owing to their non-addictive behavior profile, benztropine analogs have been actively explored for the treatment of cocaine dependence (Katz *et al.*, 2001 and 2004; Rothman *et al.*, 2008; Kopajtic *et al.*, 2010).

### 1.4.2.2. Non-Tropane Class of DAT Inhibitors

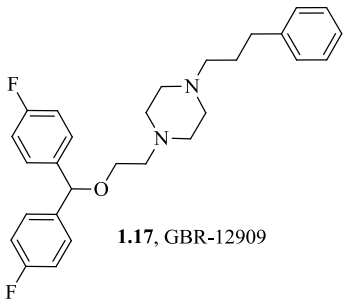


**1.17**, GBR-12909

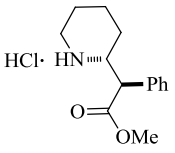


**1.18**, Methylphenidate

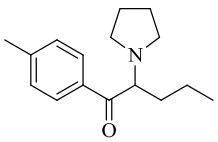


**(±)-1.19**, Pyrovalerone

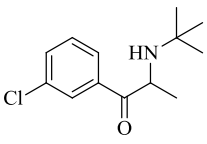


**(±)-1.20**, Bupropion

**Figure 1.12.** Structures of non-tropane DAT inhibitors.

**1.4.2.2.1. GBR-12909.** GBR-12909 (**1.17**; Figure 1.12) is a non-tropane DAT inhibitor with a significantly different behavioral profile than cocaine (Tella *et al.*, 1996). Furthermore, GBR-12909 (hDAT $K_i$ = 3.7 nM) is a highly potent and selective DAT inhibitor with a slow onset and a long duration of action (Rothman *et al.*, 2008). GBR-12909 has been shown to reverse the cocaine-induced upregulation of DAT and reduces dopamine levels in the mesolimbic system (Tella *et al.*, 1996). However, despite GBR-12909's ideal pharmacokinetic and pharmacodynamic properties as a psychostimulant abuse treatment, it was discontinued after Phase 1 clinical trial in cocaine-dependent subjects because it caused undesirable prolongation of the QTc interval, which can cause ventricular arrhythmias (Goldsmith *et al.*, 2007).

**1.4.2.2.2. Methylphenidate.** Another non-tropane DAT inhibitor, methylphenidate (**1.18**, Concerta®, Ritalin®; Figure 1.12), is a marketed drug for attention-deficit hyperactivity disorder (ADHD). Methylphenidate is a potent DAT inhibitor with affinity 2-fold higher than cocaine. Despite methylphenidate's similar structural features to cocaine (i.e., a methyl ester, basic nitrogen, and an aromatic ring), its reinforcing effects in humans are much lower than cocaine. As a result, methylphenidate has gathered significant attention as the potential agent for the treatment of cocaine addiction (Misra *et al.*, 2010).

**1.4.2.2.3. Pyrovalerone.** Pyrovalerone ((±)-**1.19**; PV; Figure 1.13) is a high affinity and potent DAT inhibitor (hDAT $K_i$ = 21.4 ± 4.6 nM; DA uptake $IC_{50}$ = 52.0 ± 20 nM) and NET inhibitor (NET $K_i$ = 195 ± 26 nM; NE uptake $IC_{50}$ = 28.3 ± 8.1 nM) with little effect on serotonin trafficking (SERT $K_i$ = 3770 ± 560 nM; SER uptake $IC_{50}$ = 2780 ± 590 nM) (pharmacology data from Meltzer *et al.*, 2006). Additionally, being structurally similar to rapidly emerging, highly

abusive designer cathinones (also called "bath salts"; Simmler *et al.*, 2013; Zawilska and Wojcieszak, 2013; Bonano *et al.*, 2014; Glennon, 2014) (see Figure 1.13), as well as the amphetamines, pyrovalerone possesses significant abuse and addiction liability. In particular, pyrovalerone is known to produce psychostimulant effects similar to amphetamine in humans (Holliday *et al.*, 1964) and is a schedule V controlled substance in the United States.

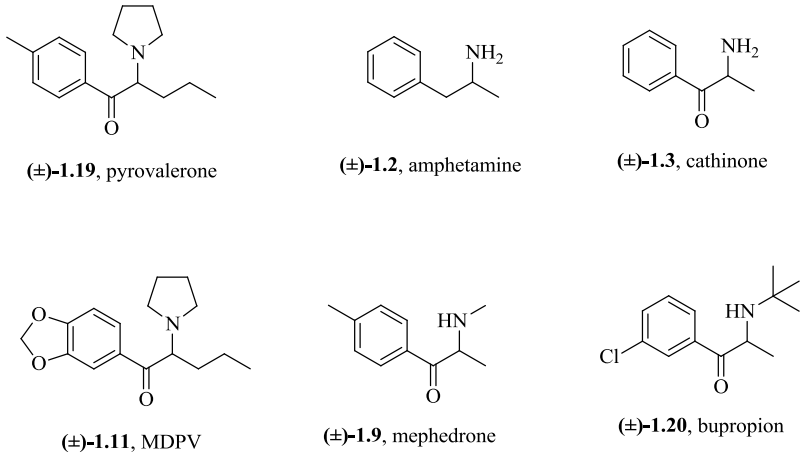


**Figure 1.13.** Structural comparison of the DAT inhibitor pyrovalerone (**(±)-1.19**) to DAT-interactive psychostimulant drugs of abuse (e.g., **(±)-1.3**, **(±)-1.11**, and **(±)-1.9**) and the marketed drug bupropion (**(±)-1.20**; Wellbutrin, Zyban, featuring the common β-aminopropiophenone moiety), and amphetamine (**(±)-1.2**) bearing the phenethylamine moiety.

Methylenedioxypyrovalerone (MDPV, **(±)-1.11**, Figure 1.13), a close pyrovalerone analog with a dioxole moiety, is a common constituent of "bath salts" and is a highly abused cathinone derivative currently posing a substantial threat for compulsive use that is potentially greater than that for METH (Meyer *et al.*, 2010; Baumann *et al.*, 2013; Cameron *et al.*, 2013; Marusich *et al.*, 2014; Watterson *et al.*, 2014). PV and MDPV are potent DAT inhibitors that block dopamine uptake resulting in an excessive increase in dopamine concentration in the mesolimbic system, thus causing reinforcing/stimulatory effects. However, due to its notable structural resemblance to the non-addictive marketed drug bupropion (**(±)-1.20**, Figure 1.13), and 20-fold greater DAT affinity than cocaine ([$^{125}$I]-RTI-55 binding inhibition; hDAT $K_i$ = 432 ± 29

nM for cocaine versus hDAT $K_i$ = 21.4 ± 4.6 nM for PV), pyrovalerone has garnered interest as a potential scaffold to search for new and potent DAT inhibitors devoid of stimulatory properties for treatment of treat cocaine dependence. In this regard, Meltzer and colleagues reported a host of pyrovalerone analogs for their evaluation as potential cocaine abuse therapeutics (Meltzer *et al.*, 2006).

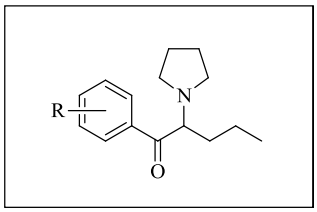


| | R | hDAT $K_i$ (nM) ([$^{125}$I]RTI-55 Inhibition) | [$^3$H]-Dopamine reuptake inhibition $IC_{50}$ (nM) |
|---|---|---|---|
| **(±)-1.19** | 4-$CH_3$ | 21.4 ± 4.6 | 52.0 ± 20 |
| **(*S*)-1.19** | 4-$CH_3$ (*S*) | 18.1 ± 3.0 | 16.3 ± 2.3 |
| **(*R*)-1.19** | 4-$CH_3$ (*R*) | 1330 ± 300 | 1790 ± 320 |
| **(±)-1.21** | 2-$CH_3$ | 59.7 ± 9.0 | 63.0 ± 19 |
| **(±)-1.22** | 3-$CH_3$ | 51.0 ± 14 | 62.9 ± 6.9 |
| **(±)-1.23** | H | 33.7 ± 5.4 | 52.3 ± 6.2 |
| **(±)-1.24** | 4-Br | 51.0 ± 6.7 | 39.5 ± 7.5 |
| **(±)-1.25** | 4-F | 82.0 ± 25 | 185 ± 62 |
| **(±)-1.26** | 4-I | 81.4 ± 9.2 | 32.0 ± 11 |
| **(±)-1.27** | 3-I | 109 ± 32 | 52.0 ± 16 |
| **(±)-1.28** | 3,4-$Cl_2$ | 11.5 ± 1.4 | 43.0 ± 20 |
| **(±)-1.29** | 4-$NO_2$ | 266 ± 32 | 1110 ± 340 |
| **(±)-1.30** | 4-$OCH_3$ | 329 ± 33 | 283 ± 66 |
| **(±)-1.31** | 4-$CO_2CH_3$ | 360 ± 140 | 154 ± 50 |
| **(±)-1.32** | 4-$NHCOCH_3$ | 30.2 ± 2.0 | 67.9 ± 8.4 |

**Table 1.1.** Structure-activity relationship studies of some pyrovalerone analogs reported by Meltzer *et al.* 2006.

Results showed that pyrovalerone enantiomer (2*S*)-**1.19** (hDAT $K_i$ = 18.1 ± 3.0 nM, DA uptake $IC_{50}$ = 16.3 ± 2.3 nM) was more active at DAT with affinity and potency 100-fold greater

than that of (2*R*)-**1.19** enantiomer (hDAT $K_i$ = 1330 ± 300 nM, DA reuptake $IC_{50}$ = 1790 ± 320 nM). Pharmacological results of various pyrovalerone analogs with different substitutions at the aromatic ring suggested high tolerability of this ring to a variety of functional groups. For example, changing the *para*-methyl group of lead **(±)-1.19** to the *ortho*- (**(±)-1.21**) or the *meta*-position (**(±)-1.22**) did not have any drastic change in the potency of the compounds, with only 2-fold loss in DAT affinity of both **(±)-1.21** (hDAT $K_i$ = 59.7 ± 9.0 nM) and **(±)-1.22** (hDAT $K_i$ = 51.0 ± 14 nM) versus **(±)-1.19** (hDAT $K_i$ = 21.4 ± 4.6 nM), while dopamine uptake inhibition potency remained unchanged. Notably, compound **(±)-1.23**, which is completely devoid of any substitutions on the phenyl ring retained the affinity and potency of the lead compound. On the other hand, different halogen substitutions at the *para*-position failed to provide any discernible correlation of DAT affinity and potency with variations in the electronics or bulk of the phenyl ring. For example, though the 4'-bromo substitution in **(±)-1.24** (hDAT $K_i$ = 51.0 ± 6.7 nM, $IC_{50}$ = 39.5 ± 7.5 nM) slightly reduced the affinity towards DAT as compared to PV, this substitution did not drastically affect the potency of dopamine uptake inhibition. Furthermore, while compound **(±)-1.26** with a 4'-iodo functional group was equipotent to **(±)-1.25** with a 4'-fluoro substituent in terms of DAT affinity, the functional potency difference between the two compounds was almost 6-fold different. In addition, though the 3'-iodo substitution (**(±)-1.27**, hDAT $K_i$ = 109 ± 32 nM, DA reuptake $IC_{50}$ = 52.0 ± 16 nM) showed a 5-fold loss in DAT affinity as compared to pyrovalerone, it still retained dopamine uptake inhibition. The most potent compound in terms of affinity in this series was 3',4'-$Cl_2$ substituted **(±)-1.28** ($K_i$ = 11.5 ± 1.4 nM, $IC_{50}$ = 43.0 ± 20 nM). Furthermore, large and more polar functional group substitutions at the *para*-position lacked impressive potency at the DAT. For example, an electron withdrawing 4'-nitro group (**(±)-1.29**), electron donating 4'-methoxy (**(±)-1.30**), and the 4'-

methylester (**(±)-1.31**) substitutions resulted in more than 10-fold loss in potency, which further makes it difficult to draw a correlation between the preferred electron density of the ring and the corresponding biological activity. However, **(±)-1.32** with a 4'-amide replacement showed quite a different profile with respect to both DAT affinity and dopamine uptake inhibition potency, almost equivalent to pyrovalerone. Nevertheless, a subset of pyrovalerone analogs with promising pharmacological activity displayed a dose-dependent stimulation of locomotor activity in mice. In addition, a few compounds were also progressed into *in vivo* studies in rat for behavioral pharmacological evaluation, the results of which currently remain undisclosed (Meltzer *et al*., 2006).

**1.4.2.2.4. Bupropion.** Bupropion (BP, **(±)-1.20**, Figure 1.13), an aminoketone, is a well-known FDA-approved drug marketed for the treatment of major depressive disorder and seasonal affective disorder (as Wellbutrin®) (Dhillon *et al*., 2008), and also as a smoking cessation aid (Zyban®) (Fava *et al.*, 2005; Tong *et al.*, 2006). Furthermore, clinical studies of bupropion on cocaine and methamphetamine dependence have indicated its effectiveness in reducing drug cravings in light abusers either alone or in combination with methadone (Poling *et al.*, 2006; Newton *et al.*, 2006; Elkashef *et al.*, 2008). Though its antidepressant actions and smoking cessation properties are mainly attributed to norepinephrine reuptake inhibition and non-competitive inhibition of select nAChRs, bupropion's weak dopamine reuptake inhibitory action *via* DAT binding was suggested to be responsible for reducing drug cravings during withdrawal (Stahl *et al.*, 2004). Interestingly, despite having structural similarities with highly abusive amphetamine (**(±)-1.2**), cathinone (**(±)-1.3**) and pyrovalerone (**(±)-1.19**) (see Figure 1.13), bupropion shows no undesirable psychostimulant activity in humans at low doses. As a result,

bupropion has been disclosed as a clinically promising lead compound for potential development into a pharmacotherapeutic for cocaine and methamphetamine dependence (Reichel *et al.*, 2009; Heinzerling *et al.*, 2014). In this regard, Carroll and coworkers reported the synthesis and pharmacological properties of a number of bupropion analogs as potential treatments for cocaine and methamphetamine dependence in addition to smoking cessation (Carroll *et al.*, 2009 and 2014) (Table 1.2).

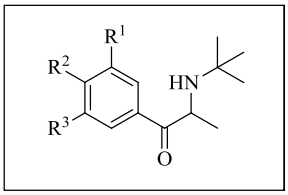


| Compound number | R | $R^1$ | $R^2$ | $R^3$ | hDAT $K_i$ (nM) [$^{125}$I]RTI55 binding inhibition | [$^3$H]-Dopamine reuptake inhibition $IC_{50}$ (nM) |
|---|---|---|---|---|---|---|
| Bupropion, **(±)-1.20** | -Me | Cl | H | H | 871 ± 126 | 945 ± 213 |
| **(±)-1.35** | -Me | H | H | H | 5730 ± 480 | 2310 ± 750 |
| **(±)-1.36** | -Me | F | H | H | 4510 ± 460 | 1460 ± 220 |
| **(±)-1.37** | -Me | Br | H | H | 4200 ± 1200 | 950 ± 210 |
| **(±)-1.38** | -Me | Me | H | H | >10,000 | ND |
| **(±)-1.39** | -Me | H | Cl | H | 2195 ± 151 | 2319 ± 429 |
| **(±)-1.40** | -Me | H | Br | H | 1918 ± 221 | 1295 ± 375 |
| **(±)-1.41** | -Me | H | Me | H | >10,000 | ND |
| **(±)-1.42** | -Me | F | F | H | >10,000 | ND |
| **(±)-1.43** | -Me | Cl | Cl | H | 472 ± 81 | 271 ± 96 |
| **(±)-1.44** | -Me | Cl | Me | H | 1150 ± 370 | 650 ± 150 |
| **(±)-1.45** | -Me | Me | Br | H | 1740 ± 440 | 950 ± 310 |
| **(±)-1.46** | -Me | F | H | F | 5660 ± 490 | 5600 ± 1800 |
| **(±)-1.47** | -Me | Cl | H | Cl | >10,000 | ND |
| **(±)-1.48** | -Ethyl | Cl | H | H | 459 ± 50 | 31 ± 9 |
| **(±)-1.49** | -Propyl | Cl | H | H | 96 ± 20 | 33 ± 7 |

**Table 1.2.** Structure-activity relationship studies of some bupropion analogs with respect to DAT inhibition and dopamine reuptake inhibition (Carroll *et al*., 2009).

The goal of this study was to find bupropion analogs with stronger dopamine reuptake inhibition (i.e., lower $IC_{50}$ values), slow onset and longer duration of action leading potentially to low abuse potential. Such compounds were expected to show promise as pharmacotherapies for cocaine and methamphetamine addiction. Bupropion analogs **(±)-1.35** to **(±)-1.47** (Table 1.2), featuring a wide range of hydrophobic substitutions on the phenyl ring, displayed varying DAT inhibitory activity patterns. For example, **(±)-1.43** with a 3',4'-dichlorophenyl substitution ([$^3$H]DA $IC_{50}$ = 271 ± 96 nM) and **(±)-1.44** with 3'-chloro-4'-methylphenyl substitution ([$^3$H]DA $IC_{50}$ = 650 ± 150 nM) inhibited dopamine reuptake 3.5- and 1.5-times more potently than bupropion ([$^3$H]DA $IC_{50}$ = 945 ± 213 nM) respectively. However, 3'-bromophenyl (**(±)-1.37**, [$^3$H]DA $IC_{50}$ = 950 ± 210 nM) and 4'-bromo-3'-methylphenyl (**(±)-1.45**, [$^3$H]DA $IC_{50}$ = 950 ± 310 nM) analogs were as potent as BP ([$^3$H]DA $IC_{50}$ = 945 ± 213 nM) in inhibiting dopamine reuptake. Further investigations of substituent tolerance on the phenyl ring showed that **(±)-1.35** with an unsubstituted phenyl ring or **(±)-1.36** with a 3'-F substituent led to reduced potency. Single substitutions at the *para*-position (i.e., in **(±)-1.39** (4'-Cl) and **(±)-1.40** (4'-Br)) were not tolerated, as these changes resulted in a significant decrease in DAT affinity ($IC_{50}$ = 2319 ± 429 nM for **(±)-1.39**; $IC_{50}$ = 1295 ± 375 nM for **(±)-1.40**). Compound **(±)-1.41** (4'-Me) showed a complete loss in DAT inhibitory activity. Difluoro substitutions in **(±)-1.42** (3',4'-diF) and **(±)-1.46** (3',5'-diF) also failed to provide potent DAT inhibitors. Overall, these results suggested that, in contrast to the pyrovalerone scaffold, which was less sensitive to lipophilic aromatic substitutions (Section 1.2.4.2.2.3), bupropion analogs containing a di-substituted phenyl ring with lipophillic functional groups (i.e. –Me, -Br and –Cl) were, in general, more potent (with the exception of di-fluoro compounds **(±)-1.42** and **(±)-1.46**) than mono-substituted compounds. Furthermore, replacement of the α-methyl group of bupropion with bulkier ethyl and propyl

groups gave analogs **(±)-1.48** and **(±)-1.49**, respectively, showing remarkably reduced $IC_{50}$ values compared to BP ([$^3$H]DA $IC_{50}$ = 31 ± 9 nM for **(±)-1.48**, [$^3$H]DA $IC_{50}$ = 33 ± 7 nM for **(±)-1.49** versus [$^3$H]DA $IC_{50}$ = 945 ± 213 nM for BP). In conclusion, bupropion analogs **(±)-1.43** (2',3'-dichloro), **(±)-1.48** (ethyl side chain) and **(±)-1.49** (propyl side chain) represented the most potent dopamine uptake inhibitors in the series relative to BP. In addition, these analogs were also tested for their NE uptake properties to develop compounds with lower noradrenergic activity to reduce the potential of cardiotoxicity. The results indicated that **(±)-1.43** (NE reuptake $IC_{50}$ = 2100 ± 380 nM) and **(±)-1.48** (NE reuptake $IC_{50}$ = 969 ± 410 nM) displayed 5-fold and 2-fold reduced NE uptake inhibition, respectively, when compared to BP (NE reuptake $IC_{50}$ = 443 ± 245 nM) whereas NE inhibition potency remain unchanged for **(±)-1.49** (NE reuptake $IC_{50}$ = 472 ± 93 nM). Subsequently, promising analogs **(±)-1.43** and **(±)-1.48** with desirably higher dopamine reuptake potency (i.e., lower $IC_{50}$ values) and lower NE inhibition were further evaluated for their effect on locomotor activity and drug discrimination tests in cocaine administered rats. The resulting animal behavior profile of the analogs failed to provide any correlation with the *in vitro* data and further studies are required to evaluate the effect of the nature of metabolites on different behavioral profiles (Carroll *et al*., 2014).

### 1.4.3. Unique Behavioral Responses of DAT Inhibitors

Though the widely accepted mechanism of cocaine's psychostimulant behavioral effects have been attributed to an increase in perisynaptic dopamine concentration by inhibition of the DAT, the discovery of several other potent DAT inhibitors which lack cocaine's abuse liability is suggestive of a different mechanism involved in eliciting reinforcing or stimulatory effects. DAT inhibitors such as GBR12909, bupropion, and benztropine do not share a stimulatory

behavioral profile and high abuse potential when compared to cocaine (Desai *et al.*, 2005; Schmitt *et al.*, 2008). Such findings have suggested that different structural classes of DAT inhibitors display contrasting psychostimulant effects due to the disparate nature of their molecular interactions with the DAT. This means that DAT inhibitors may induce unique transporter conformational states of the DAT, which in turn could dictate their addictive liability (Reith *et al.*, 2001). Many researchers have supported this concept of conformation-specific activity by presenting experimental evidence that cocaine and benztropine have different effects on the accessibility of cysteine residues present near DAT's extracellular side towards reaction with sulfhydryl reducing reagents (Ferrer and Javitch, 1998; Reith *et al.*, 2001). Consequently, site-directed mutagenesis studies provided further verification of this theory. In particular, Chen and coworkers showed that DAT mutants W84L and D313N, producing a stabilized outward-open conformation had greater affinity for cocaine and methylphenidate but not for non-addictive benztropine, GBR-12909 and bupropion, while still maintaining binding affinity of DAT substrates such as dopamine and amphetamine (Chen *et al.*, 2001 and 2004). On the other hand, the mutation Y335A, which stabilizes the inward-facing DAT conformational state, increased the affinity of benztropine analogs, but decreased the efficacy of cocaine the indicating that atypical DAT inhibitors that lack the addiction potential apparently have preferential binding for an inward-facing closed DAT conformation (Loland *et al.*, 2002 and 2008). One possible explanation proposed for how atypical DAT inhibitors access the inward-conformation might be that they enter the extracellular DAT vestibule, and then are partially translocated in DAT in a manner similar to the substrates, but eventually stabilize the inward-facing conformation and are released slowly into the intracellular side (Schmitt *et al.*, 2013). This, to some extent, might also further explain the *in vivo* slow onset of action of these agents which ultimately result in their

reduced behavioral reinforcing effects (Wee *et al.*, 2006). These results corroborate the hypothesis that "atypical" DAT inhibitors have either low abuse potential or are completely devoid of "cocaine-like" stimulatory and rewarding effects because of their preferential interactions with the inward-facing DAT conformational state (Loland *et al.*, 2008; Kopajtic *et al.*, 2010; Schmitt and Reith, 2011).

In conclusion, additional structural studies to elucidate detailed molecular requirements of "cocaine-like" and "atypical" DAT inhibitors are needed in order to determine their binding profile and addiction liability, which can further facilitate the development of therapeutics for cocaine addiction.

## 1.5. The Cholinergic Nervous System

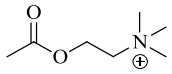

Acetylcholine, **1.50**

**Figure 1.14.** Chemical structure of the neurotransmitter acetylcholine (**1.50**).

The cholinergic system comprises two broad classes of cholinergic receptors: muscarinic acetylcholine receptors (mAChRs) and nicotinic acetylcholine receptors (nAChRs). Both receptors are activated by the endogenous neurotransmitter acetylcholine (ACh), which is present in the peripheral and central nervous system. These receptors mediate neurotransmission by converting a chemical response characterized by ACh release from the nerve ending into a electrical response *via* ion flux through the cellular transmembrane in neurons or muscles (Jensen *et al.*, 2005). Muscarinic acetylcholine receptors, activated by the toxin, muscarine, are G-protein coupled receptors which once activated, mediate slow synaptic transmission of ACh through reduced cAMP formation, phospholipase c stimulation and increased $K^+$ conductance.

On the other hand, nicotinic acetylcholine receptors (nAChRs), are ligand-gated ion channels activated by the exogenous tertiary alkaloid nicotine, and mediate a fast stimulatory response (Jensen *et al.*, 2005). nAChRs are further classified into muscle and neuronal subtypes based on their locations. The muscle type is located at all neuromuscular junctions and is mainly present postsynaptically. Their function is to control and mediate electrical transmission through neuromuscular junctions to maintain skeletal muscle tone. As a result, they are the targets of several known muscle relaxants. On the other hand, neuronal nAChRs are located both pre- and postsynaptically throughout the CNS and in autonomic ganglia. Their function is to control several processes such as cognitive function, learning, and memory, reward, and arousal principally by modulating the postsynaptic neuronal transmission and also by facilitating $Ca^{2+}$-dependent release of other neurotransmitters such as dopamine and glutamate (Albuquerque *et al*., 2009).

### 1.5.1. Structural and Functional Features of nAChRs

nAChRs are allosteric proteins composed of multiple subunits and contain multiple orthosteric and allosteric binding sites through which they modulate their function. Studies from x-ray crystallographic structures of nAChRs from different species, such as nAChRs from the fish *Torpedo* (Miyazawa *et al*., 2003; Rucktooa *et al.*, 2009), Ach-binding proteins (AChBP) from the snail *Lymnaea stagnalis* (Celie, Kasheverov*, et al.*, 2005), *Aplysia californica* (Rucktooa *et al.*, 2012; Atkinson *et al.*, 2014), and *Bulinus truncatus* (Celie, Klaassen*, et al.*, 2005), have provided a great deal of information regarding the 3-D structural features of human nAChRs. The general structure of nAChRs includes a heteropentameric arrangement created by any five subunits (α, β, δ, γ, and ε) assembled in different stoichiometries to form a central pore

permeable to $Na^+$, $K^+$, and $Ca^+$ ions (Figure 1.15, B). To date, 17 nAChR subunits are known, which are divided into muscle types ($\alpha1$, $\beta1$, $\delta$, $\gamma$, and $\varepsilon$) and neuronal types ($\alpha2 - \alpha10$ and $\beta2 - \beta4$) (Lukas *et al.*, 1999). All the subunits have the following common structural features: an ~200 amino acid-containing, highly conserved extracellular N-terminal domain connected to three transmembrane domains (TM1 to TM3), which lead to an intracellular cytoplasmic loop connecting TM4, whose size and composition varies in different types of subunits (Figure 1.15, A). The orthosteric binding site for ACh is located in the N-terminal domain located between adjacent subunits. The N-terminal domain of all $\alpha$ subunits contain a cystein-loop that is critical for agonist binding. TM2 of all five subunits line the central ion channel and TM1-3 lie in the periphery to protect TM2 from the lipid bilayer (Figure 1.15, B; Corringer *et al*., 2000). About 90% of neuronal nAChRs in the CNS are heteropentameric $\alpha4\beta2$ receptors that have high affinity for nicotine (Figure 1.15, D). In contrast, $\alpha3\beta4$ receptors (Figure 1.15, D) are mainly located in autonomic ganglia, the adrenal medulla and in few selected parts of CNS neurons. Heteromeric nAChRs contain two orthosteric binding site each located at the interface between $\alpha$ and $\beta$ subunits. Another type present in the CNS are homopentameric $\alpha7$ nAChRs containing only $\alpha$ subunits (Figure 1.15, C).

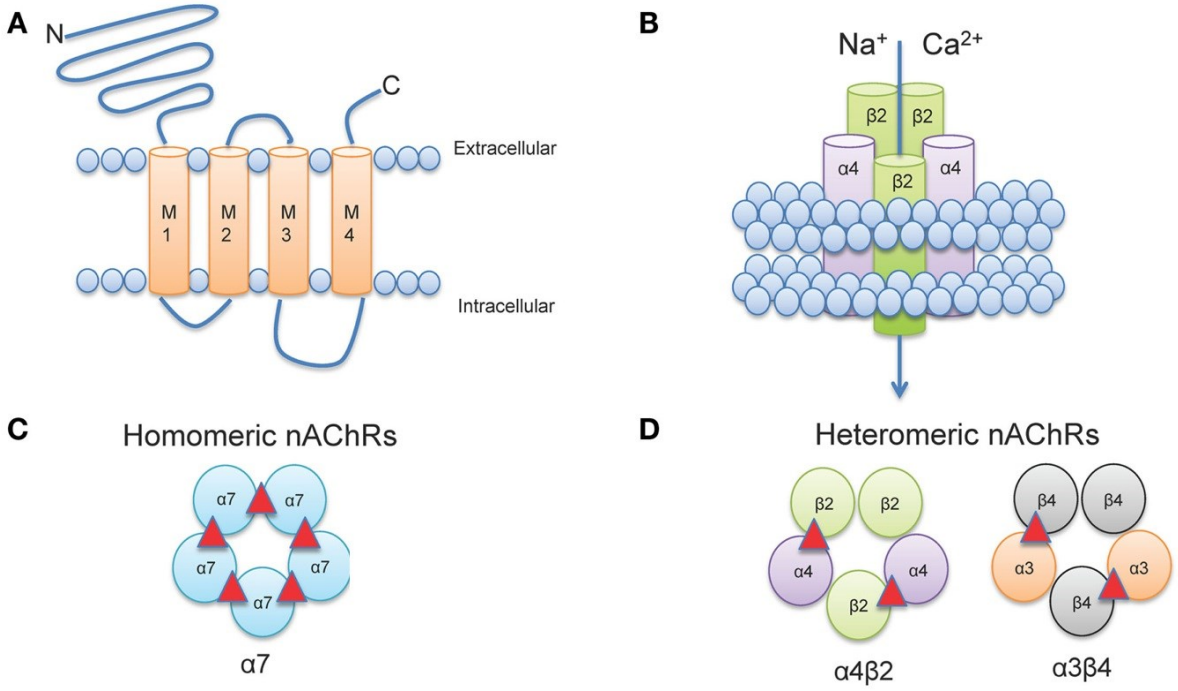


**Figure 1.15.** Pictorial representation of structural and functional organization of nAChR subtypes. A. Schematic representation of four transmembrane domains (TM1-4) with extracellular N- and C-terminal. B. Organization of five subunits to form central channel for ion permeability. C. Arrangement of subunits in α7 nAChR subtype with five Ach binding sites. D. Arrangement of subunits in α4β2 and α3β4 nAChR subtypes with two Ach binding sites at the interface of α and β subunits (Hendrickson *et al.*, 2013. Adapted with permission from *Front. Psychiatry* **2013**, *4*, 1-16. Copyright 2013 Hendrickson, Guildford and Tapper).

The intracellular and extracellular ends of the ion channel are lined with negatively charged residues and the central portion is composed of a number of non-polar amino acid residues to facilitate the influx and passage of cations. Allosteric binding sites for nAChRs are presumably located within the ion channel (Albuquerque *et al.*, 2009). nAChRs exist in three conformational transition states: a resting state (or closed) in which the ion channel remains closed and is stabilized by competitive antagonists; an active (or open) state with low affinity for agonists, which when agonist-bound results in channel-opening to allow passage of ions; and the desensitized state which is occupied by competitive agonists, but the ion channel remains closed (Monod *et al.*, 1965; Jackson, 1984 and 1990; Changeux and Edelstein, 1998; Hurst *et al.*, 2013).

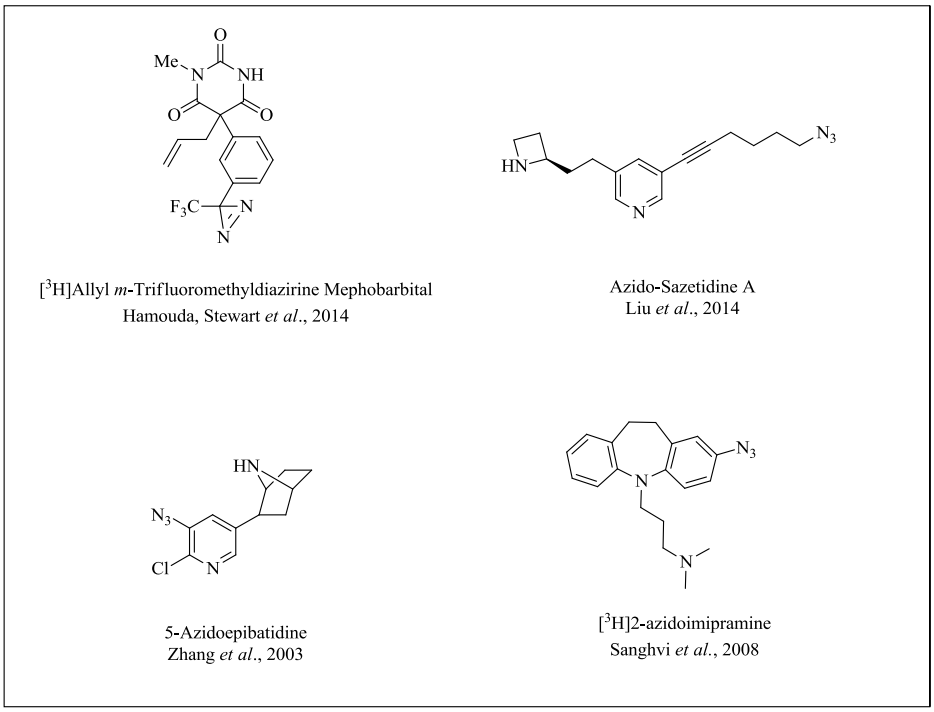


**Figure 1.16.** Chemical structures of some irreversible chemical probes utilized in nAChR structure-function studies.

Though the homology models of human nAChRs based on x-ray crystal structures of bacterial and invertebrate pentameric receptors coupled with mutagenesis studies (for representative examples, see Pavlovicz *et al*., 2011; Grishin *et al*., 2013; Marotta *et al*., 2014) has been worthwhile in predicting molecular organization, structure, and location of binding sites, the accuracy and usefulness of these models are still in question for structure based drug discovery. Photoaffinity labeling studies using irreversible chemical probes (for e.g., Hamouda, Steward *et al*., 2014; Liu *et al*., 2014; Sanghvi *et al*., 2008; Zhang *et al*., 2003; Figure 1.16), on the other hand, have provided more direct identification of location and amino acid composition of many orthosteric and allosteric sites within nAChRs (reviewed in Hamouda, Jayakar *et al.*, 2014).

### 1.5.2. The Role of nAChRs in Drug Addiction

Nicotine (**1.4**, Figure 1.1) is the main psychoactive component of tobacco used in cigarette smoking. Nicotine mainly acts on neuronal nAChRs to manifest its stimulatory or reinforcing effects on the human brain. Due to nicotine's high lipophilicity, it crosses the blood-brain barrier rapidly and accumulates in the brain near nAChRs for a much longer time than ACh. Furthermore, unlike ACh, nicotine is not metabolized by acetylcholinesterase enzymes present in the CNS, which further prolongs its duration of action.

Nicotine addiction progresses in three different stages: initiation of addiction, neuroadaptations, and withdrawal (De Biasi and Dani, 2011). The midbrain region, consisting of dopamine neurons, express as nAChRs that are mainly composed of β2 subunits in combination with α4 or occasionally α6 subunits. Activation of nAChRs, located on dopaminergic cells in the VTA by nicotine provides the excitatory drive to release dopamine in high concentrations in the mesolimbic region, which initiates the development of addiction and reward behavior, and ultimately nicotine dependence (Benowitz, 2008). Recently, the role of the β2 subunit has been irrefutably proved by studies using β2−knockout mice, which lacked nicotine induced dopamine release and did not show reinforcing effects to nicotine (Simmons and Gould, 2014). Furthermore, prolonged exposure to nicotine and the continued process of its addiction produces neuroadaptations in neuronal cells that include the upregulation of nAChRs (De Biasi and Dani, 2011). The upregulation of nAChRs occurs due to the fact that the presence of nicotine for prolonged periods favors excessive desensitization of nAChRs. To counteract this phenomenon, the cellular machinery upregulates nAChRs as part of the homeostatic response in the cortex, midbrain, and hypothalamus regions of the brain (Colombo *et al.*, 2013). Consequently, since nAChRs regulate the release of other neurotransmitters in the brain, (i.e., increase in dopamine

and glutamate as well as decrease in GABA transmission), their excessive upregulation subsequently creates a widespread irregularity in neurotransmission. In particular, the receptors that exhibit the highest level of upregulation are α4β2 nAChRs, which contain high-affinity nicotine binding sites. Consequently, due to such neuroadaptations during chronic nicotine exposure, the brain eventually adapts to this new environment and requires the presence of nicotine for continued maintenance. This creates a state of imbalance in brain neurochemistry and leads to a withdrawal state when the nicotine consumption is discontinued (Koob and Volkow, 2010). Withdrawal symptoms are often characterized by anxiety, anger, sleep disturbances, weight gain, and irritability.

In conclusion, since nAChR-mediated nicotine addiction significantly impairs cognitive activities such as decision making, behavioral inhibition, and problem solving, nAChR targeted compounds have garnered considerable attention in order to develop therapeutics to counteract tobacco addiction.

## 1.6. nAChR Ligands and Their Significance in Smoking Cessation

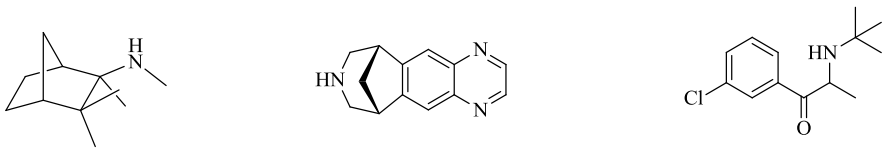


**1.51**, Mecamylamine **1.52**, Varenicline **(±)-1.53**, Bupropion

**Figure 1.17.** Chemical structure of nAChR ligands used as marketed therapies for the treatment of nicotine addiction.

Medicinal chemistry efforts towards the development of nAChR ligands as agonists, competitive antagonists and allosteric modulators have shown promise as therapeutic agents targeting a wide range of disorders such as nicotine and alcohol dependence, depression,

schizophrenia, Alzheimer's disease, ADHD, Parkinson's disease, pain, and inflammation (Holladay *et al.*, 1997).

**1.6.1. Mecamylamine.** Mecamylamine (**1.51**), a potent nAChR antagonist, blocks the effects of nicotine in the human brain (Reid *et al.*, 1999). Mecamylamine has been shown to be an effective smoking cessation agent when co-administered alongside a transdermal nicotine patch during the pre-clinical studies (Rose *et al.*, 1994).

**1.6.2. Varencline.** Varencline (**1.52**, Chantix® and Champix®), a marketed therapy for tobacco dependence, is a partial agonist of α4β2 nAChRs, which effectively reduces nicotine withdrawal effects and at the same time provides rewarding effects by moderately releasing dopamine in the mesolimbic region (Coe *et al.*, 2005).

**1.6.3. Bupropion.** Bupropion (**(±)-1.20**), initially developed as an antidepressant (as Wellbutrin®), was later serendipitously found to have smoking cessation properties (Balfour, 2001). Apart from its norepinephrine (NE) and dopamine (DA) reuptake inhibitor activity, bupropion is also a moderately potent noncompetitive antagonist of nAChRs, in particular the α4β2 and α3β4 sutypes. Studies in rodents have shown that bupropion decreases the reinforcing properties of nicotine and also relieves withdrawal symptoms associated with nicotine (Shiffman *et al.*, 2000; Cryan *et al.*, 2003; West *et al.*, 2008). Although there is no experimental evidence to precisely determine whether bupropion's smoking cessation activity resides in its monoamine uptake inhibition or nAChR inhibition, it has been suggested that since the inhibition of DAT and NET alone cannot alleviate nicotine's reinforcing effects, the noncompetitive antagonism of

nAChRs might be playing a more important role in inhibiting upregulated nAChRs during nicotine dependence and help prevent nicotine relapse (Arias, 2009).

However, despite its status as a FDA-approved drug for major depressive disorder, seasonal affective disorder, and an aid to help people stop smoking by reducing cravings and other withdrawal effects, the molecular determinants of how bupropion interacts with select nAChR subtypes remains unknown. As a result, in order to identify improved therapeutics targeting nAChRs, it is important to understand, in detail, how clinically approved ligands like bupropion interact with binding sites within select nAChR subtypes. This information is currently lacking in the nAChR field due to the unavailability of high-resolution x-ray crystal structures of human $\alpha4\beta2$ and $\alpha3\beta4$ nAChR subtypes. Despite predictions that bupropion binds near the middle of the nAChR ion channel between M2-6 and M2-13 by pharmacological, electrophysiological, and computational approaches (Arias *et al.*, 2009 and 2010), currently there is a dearth of direct experimental evidence regarding the precise location of bupropion-binding sites within the DAT and select nAChR subtypes. Pharmacological studies in nAChRs expressed in HEK-293 cells have shown that bupropion exhibits differential inhibition towards two different conformational states of nAChRs (Arias *et al.*, 2009 and 2010). Bupropion apparently binds preferentially to the resting or desensitized state of nAChRs within the lumen of the ion channel and promotes the conformational transition to the desensitized state. Furthermore, Unwin and Fujiyoshi in 2012 provided a much more direct observation regarding the possible mechanism of bupropion's inhibition of nAChRs (Unwin and Fujiyoshi, 2012). These researches showed that during the resting / closed state, the M2 helices of nAChRs are bent towards each other and are stabilized by helix-to-helix interactions, thus obstructing the passage of ions through the ion channel. When an agonist (e.g., nicotine or acetylcholine) binds

to the orthosteric-binding site, the helix-to-helix interactions are disrupted by causing a conformational change in the receptor's 3-D structure which results in opening of the ion channel. On the other hand, when bupropion binds to its allosteric site present within the nAChR ion-channel, it further reinforces or facilitates M2 helix-to-helix interactions, thereby stabilizing the 'bent' conformation of the M2 helices that result in ion channel blockade.

Despite the growing global health problem of nicotine dependence, currently available pharmacotherapies for treating tobacco use are inadequate in helping smokers maintain long term abstinence (Johnston *et al*., 2002). This warrants an urgent need for new and improved drugs for the treatment of tobacco abuse. Due to the promising effects of bupropion as smoking cessation aid, structure activity studies have been conducted to further develop more potent bupropion analogs in order to create much more superior smoking cessation aids that are more effective in maintaining long term abstinence in smokers. Since the smoking cessation activity of bupropion is mediated through a combination of DAT/NET inhibitory activity and nAChR antagonistic activity, the goal for developing improved pharmacotherapies for nicotine dependence relies on a multi-targeted approach. In this regard, bupropion analogs that were previously explored for cocaine and methamphetamine abuse treatment (see Section 1.4.2.2.4) by Carroll and coworker, were also evaluated against nAChR subtypes, as well as DA/NE reuptake inhibition, in order to find ligands with better smoking cessation properties (Carroll *et al.*, 2010).

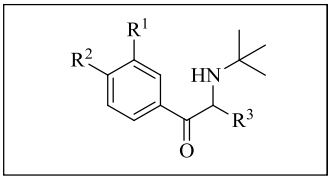


| | | | | Monoamine uptake inhibitor $IC_{50}$ (nM)[1] | | nAChR inhibition[2] $IC_{50}$ (μM) | |
|---|---|---|---|---|---|---|---|
| **Compound number** | **$R^1$** | **$R^2$** | **$R^3$** | **[$^3$H]DA** | **[$^3$H]NE** | **α3β4*** | **α4β2** |
| Bupropion, **(±)-1.20** | Cl | H | $CH_3$ | 658 ± 178 | 1850 ± 300 | 1.8 (1.15) | 12 (1.15) |
| **(±)-1.36** | F | H | $CH_3$ | 2320 ± 860 | 6500 ± 270 | 4.4 (1.07) | 21 (1.12) |
| **(±)-1.37** | Br | H | $CH_3$ | 511 ± 33 | 5600 ± 1300 | 1.3 (1.07) | 15 (1.12) |
| **(±)-1.38** | $CH_3$ | H | $CH_3$ | 1470 ± 170 | 6200 ± 3500 | 1.5 (1.07) | 19 (1.07) |
| **(±)-1.39** | H | Cl | $CH_3$ | 1090 ± 150 | 2070 ± 660 | 2.4 (1.10) | 33 (1.12) |
| **(±)-1.40** | H | Br | $CH_3$ | 689 ± 229 | 2540 ± 740 | 1.4 (1.07) | 23 (1.10) |
| **(±)-1.41** | H | $CH_3$ | $CH_3$ | 1950 ± 390 | 2350 ± 560 | 2.4 (1.10) | 17 (1.07) |
| **(±)-1.42** | F | F | $CH_3$ | 7978 ± 4437 | 6480 ± 2100 | 2.6 (1.10) | 45 (1.12) |
| **(±)-1.43** | Cl | Cl | $CH_3$ | 463 ± 104 | 1670 ± 250 | 6.8 (1.07) | 29 (1.10) |
| **(±)-1.44** | Cl | $CH_3$ | $CH_3$ | 410 ± 75 | 2040 ± 280 | 0.65 (1.10) | 9.2 (1.07) |
| **(±)-1.45** | $CH_3$ | Br | $CH_3$ | 2810 ± 590 | 7250 ± 2370 | 2.9 (1.07) | 32 (1.10) |
| **(±)-1.53** | Cl | Cl | $C_3H_7$ | 31 ± 9.4 | 180 ± 69 | 0.62 (1.29) | 9.8 (1.07) |

[1]Values for mean ± standard error of three independent experiments, each conducted with triplicate determination.
[2]Mean micromolar $IC_{50}$ values from three independent experiments for inhibition of functional responses to an $EC_{80}$-$EC_{90}$ concentration of carbamylcholine mediated by nAChR subtypes composed of the indicated subunits (where the asterisk (*) indicates that additional subunits are or may be additional assembly partners with the subunits specified.

**Table 1.3.** Structure-activity relationship studies of bupropion and some of its analogs: monoamine reuptake inhibition and select nAChR inhibition (Carroll *et al*., 2010).

All of these bupropion analogs were synthesized and pharmacologically evaluated as their racemic mixtures since bupropion is also marketed as a racemic mixture. Exploration of aromatic substitutions on the phenyl ring led to analog **(±)-1.43** with a 3',4'-dicloro substitution that showed higher inhibitory potency for dopamine and norepinephrine uptake than the 3'-Cl substitution in BP ([$^3$H]DA $IC_{50}$ = 463 ± 104 nM, [$^3$H]NE $IC_{50}$ = 1670 ± 250 nM for **(±)-1.43** versus [$^3$H]DA $IC_{50}$ = 658 ± 178 nM, [$^3$H]NE $IC_{50}$ = 1850 ± 300 nM for BP). In addition, **(±)-**

**1.37** (3'-Br) was the most selective dopamine reuptake inhibitor in this series versus norepinephrine uptake inhibition ([$^3$H]DA $IC_{50}$ = 511 ± 33 nM, [$^3$H]NE $IC_{50}$ = 5600 ± 1300 nM). The overall results in nAChR inhibition indicated that all of these BP analogs were more selective towards the inhibition of α3β4 nAChRs as compared to the α4β2 subtype. The 6-fold selectivity of BP for α3β4 nAChR ($IC_{50}$ = 1.8 μM) over α4β2 ($IC_{50}$ = 12 μM) increased to 11-fold for 3'-bromo analog **(±)-1.37** (α3β4 $IC_{50}$ = 1.3 μM; α4β2 $IC_{50}$ = 15 μM), 13-fold for 3'-Me analog **(±)-1.38** (α3β4 $IC_{50}$ = 1.5 μM; α4β2 $IC_{50}$ = 19 μM), and 16-fold for 4'-Br substituted **(±)-1.40** (α3β4 $IC_{50}$ = 1.4 μM; α4β2 $IC_{50}$ = 23 μM).

In conclusion, the best balance of potency for DA and NE uptake inhibition, along with nAChR subtype antagonism, was displayed by the 3'-chloro-4'-methyl derivative **(±)-1.44**, the 3'-bromo derivative **(±)-1.37**, and 4'-bromo compound **(±)-1.40**. These compounds were also more potent than bupropion in blocking nicotine induced locomotor activity as well as antinociception in a tail-flick test. Several of these compounds showed potential as leads for further drug development for better smoking cessation therapy. In particular, extended side chain analog **(±)-1.53** with 41- and 7.5-fold greater DA and NE uptake potency, and 3-fold higher potency in α3β4 inhibition than bupropion, was the most interesting compound in the series as it demonstrated that replacing the α-methyl group in 3,4-dichloro substituted **(±)-1.43** with a larger alkyl chain produced a compound with better overall efficacy. Consequently, this compound also displayed 9-fold greater potency when compared to bupropion in antagonizing nicotine-induced antinociception effects in a mouse tail-flick experiment. These results support the hypothesis that targeting compounds with higher inhibitory potency at multiple targets (i.e., DAT, NET, and nAChRs) can lead to new pharmacotherapies potentially with higher efficacy as aids to smoking cessation (Carroll *et al*., 2010).

**1.6.4. Hydroxybupropion.** Several i*n vivo* pharmacokinetic studies on bupropion in humans have consequently revealed that only 10% of orally administered bupropion is excreted in the urine as the parent compound and a majority of it is systemically metabolized by cytochrome P450 2B6 oxidation to its metabolites, (i.e., (2*S*,3*S*)-hydroxybupropion, (2*R*,3*R*)-hydroxybupropion, *threo*-hydrobupropion and *erythro*-hydrobupropion) (Figure 1.18; Laizure *et al*., 1985; Benowitz *et al*., 2013; Zhu *et al*., 2014).

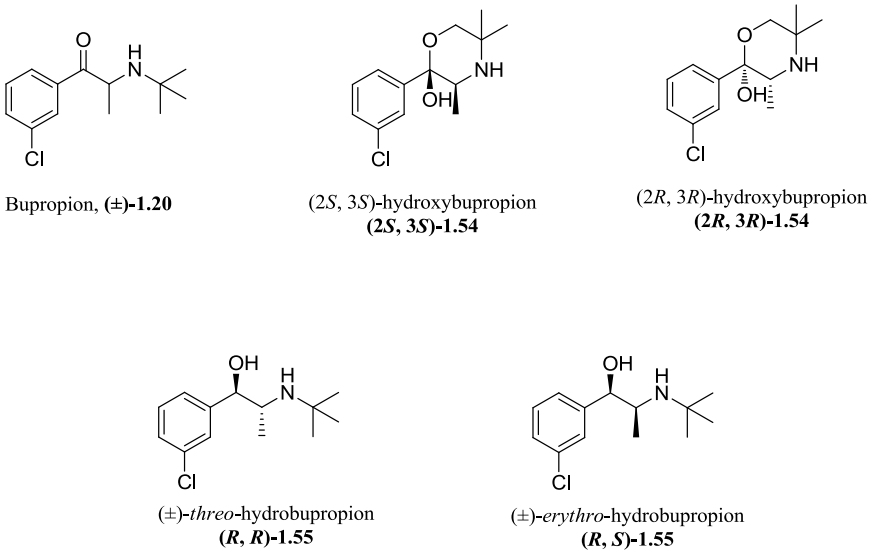


**Figure 1.18.** Chemical structures of bupropion metabolites.

Among these metabolites, the hydroxylated form, (2*S*,3*S*)-hydroxybupropion (**(2*S*,3*S*)-1.54**) is the main pharmacologically active metabolite. In a recent randomized clinical study of bupropion for its smoking cessation activity, Zhu and coworkers demonstrated that the smoking cessation effect in patients increased with an increase in bupropion metabolism and subsequent increase in hydroxybupropion concentration (Zhu *et al.*, 2012). This irrefutably established that bupropion's efficacy as a smoking cessation aid is mainly associated with this active metabolite. In particular, it has been observed that the (2*S*,3*S*)-hydroxybupropion isomer is significantly more pharmacologically active and displays the highest steady state plasma levels versus other

metabolites in a number of behavioral-, monoamine-, and nAChR-based pharmacological assays (Damaj *et al.*, 2004 and 2010; Benowitz *et al*., 2013). Furthermore, (2*S*,3*S*)-hydroxybupropion displays higher potency and a longer elimination half-life than bupropion (Yeniceli *et al.*, 2011; Parekh *et al.*, 2012; Laib *et al.*, 2014). In addition, (2*S*,3*S*)-hydroxybupropion is 3-10 times more potent that BP in antagonizing nicotine-induced hypomobility and hypothermia, plus analgesia in the tail-flick and hot plate tests in mice. As a result, (2*S*,3*S*)-hydroxybupropion has been suggested to represent a better drug candidate for developing smoking cessation therapeutics versus bupropion.

In this regard, Lukas and coworkers in 2010 synthesized and pharmacologically evaluated several analogs of (2*S*,3*S*)-hydroxybupropion in the search for better drugs for the treatment of nicotine addiction (Lukas *et al.*, 2010) (Table 1.4).

Analogous to the structure-activity relationship studies of bupropion analogs, hydroxybupropion analogs were also tested for potency against nAChR subtypes as well as DA/NE reuptake inhibition. In terms of monoamine reuptake inhibition potency, **(2*S*,3*S*)-1.54** ([$^3$H]NE $IC_{50}$ = 241 ± 60 nM) showed 9-fold greater NE reuptake inhibition versus BP ([$^3$H]NE $IC_{50}$ = 1850 ± 300 nM), while the DA reuptake inhibition potency remained unchanged. Moreover, (2*S*,3*S*)-hydroxybupropion is more potent than bupropion towards inhibiting α4β2-nAChR over α3β4-nAChR (α4β2-nAChR $IC_{50}$ = 3.3 μM for **(2*S*,3*S*)-1.54** versus $IC_{50}$ = 12 μM for BP; whereas α3β4-nAChR $IC_{50}$ = 11 μM for **(2*S*,3*S*)-1.54** versus $IC_{50}$ = 1.8 μM for BP).

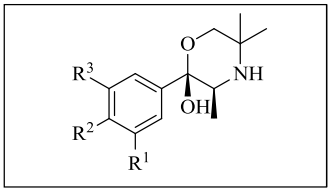


| | | | | Monoamine uptake inhibition, $IC_{50}$ (nM)[1] | | nAChR inhibition $IC_{50}$ (μM)[2] | |
|---|---|---|---|---|---|---|---|
| **Compound number** | **$R^1$** | **$R^2$** | **$R^3$** | **[$^3$H]DA** | **[$^3$H]NE** | **α3β4*** | **α4β2** |
| Bupropion, **(±)-1.20** | | | | 658 ± 178 | 1850 ± 300 | 1.8 (1.15) | 12 (1.15) |
| (2*S*, 3*S*)-Hydroxybupropion, **1.54** | Cl | H | H | 630 ± 50 | 241 ± 60 | 11 (1.48) | 3.3 (1.07) |
| **1.56** | F | H | H | 1380 ± 360 | 740 ± 150 | 15 (1.12) | 1.3 (1.17) |
| **1.57** | Br | H | H | 3340 ± 680 | 920 ± 300 | 3.2 (1.12) | 0.55 (1.23) |
| **1.58** | $CH_3$ | H | H | 2600 ± 400 | 1130 ± 20 | 8.6 (1.12) | 6.0 (1.20) |
| **1.59** | H | Cl | H | 285 ± 70 | 830 ± 90 | 5.1 (1.07) | 9.2 (1.17) |
| **1.60** | H | $CH_3$ | H | 832 ± 260 | 1680 ± 330 | 8.6 (1.12) | 12 (1.12) |
| **1.61** | F | F | H | 2140 ± 180 | 740 ± 110 | 11.9 (1.15) | 12 (1.07) |
| **1.62**[3] | Cl | Cl | H | 70 ± 20 | 114 ± 30 | 2.6 (1.10) | 20 (1.07) |
| **1.63** | F | H | F | 1020 ± 190 | 151 ± 43 | 11 (1.15) | 6.3 (1.51) |
| **1.64**[3] | Cl | H | Cl | 8250 ± 720 | 2440 ± 730 | 3.9 (1.07) | 11 (1.05) |

[1]Values for mean ± standard error of three independent experiments conducted with triplicate determination.
[2]Mean micromolar $IC_{50}$ values from three independent experiments for inhibition of functional responses to an $EC_{80}$-$EC_{90}$ concentration of carbamylcholine mediated by nAChR subtypes composed of the indicated subunits (where the asterisk (*) indicates that additional subunits are or may be additional assembly partners with the subunits specified.
[3]Racemic.

**Table 1.4.** Structure-activity relationship studies of (2*S*,3*S*)-hydroxybupropion and some of its analogs: monoamine reuptake and nAChR inhibition as reported by Lucas *et al*., 2010.

Likewise, hydroxybupropion analogs also showed more selectivity for α4β2-nAChR versus α3β4-nAChRs. Changes in the 3'-chlorophenyl group in **(2*S*, 3*S*)-1.54** to 3'-bromo **(2*S*, 3*S*)-1.56** or 3'-fluoro **(2*S*, 3*S*)-1.57** substituents afforded analogs with improved affinity and selectivity for α4β2-nAChRs while significantly losing monoamine inhibition potency. The racemic *threo*-3',4'-dichlorophenyl derivative (±)-*threo*-**1.62** (DA uptake inhibition $IC_{50}$ = 70 ± 20 nM; [$^3$H]NE $IC_{50}$ = 114 ± 43 nM) and 4'-chloro **(2*S*,3*S*)-1.59** ([$^3$H]DA $IC_{50}$ = 285 ± 70 nM;

[$^3$H]NE $IC_{50}$ = 830 ± 90 nM) had higher DA and NE inhibitory potency than (2*S*,3*S*)-hydroxybupropion ([$^3$H]DA $IC_{50}$ = 630 ± 50 nM; [$^3$H]NE $IC_{50}$ = 241 ± 60 nM) and bupropion ([$^3$H]DA $IC_{50}$ = 658 ± 178 nM; [$^3$H]NE $IC_{50}$ = 1850 ± 300 nM) with significant loss in α4β2-nAChR potency. Compound **(2*S*,3*S*)-1.61** (3',5'-difluoro) displayed the highest selectivity for NE uptake inhibition ([$^3$H]NE $IC_{50}$ = 151 ± 43 nM) over DA uptake inhibition ([$^3$H]DA $IC_{50}$ = 1020 ± 190 nM). The bromo-analog **(2*S*,3*S*)-1.57** (α4β2 inhibition $IC_{50}$ = 0.55 μM) and 3-F' analog **(2*S*,3*S*)-1.56** (α4β2 inhibition $IC_{50}$ = 1.3 μM) were the most potent α4β2 nAChR antagonists in the series.

Concomitantly, hydroxybupropion and its analogs were also tested in *in vivo* models of nicotine and smoking dependence, such as nicotine-induced effects in tail-flick, hot-plate, locomotor activity, and hypothermia assays (Carroll *et al.*, 2010). The results indicated that (2*S*,3*S*)-hydroxybupropion was more potent than its analogs, as well as bupropion, in blocking nicotine-induced effects in hot-plate, locomotor activity and hypothermia assays. However, in contrast, almost all of the hydroxybupropion analogs (except 3,4-dicloro analog (±)-*threo*-**1.62**) were more potent in blocking the nicotine-induced antinociception effects in tail-flick assay than (2*S*,3*S*)-hydroxybupropion.

Despite the development of several analogs, currently there are no hydroxybupropion-related compounds in clinical trial specifically for smoking cessation. This is principally due to the observation that the behavioral response of these compounds do not correlate with their *in vitro* nAChR and DA/NE uptake inhibition data (Carroll *et al.*, 2014). Furthermore, the mechanistic rationale behind the smoking cessation property of these compounds, and the importance of nAChR inhibition versus DA/NE reuptake inhibition, is still unclear.

## 1.7. The Glutamatergic System

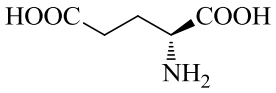


**Figure 1.19.** The chemical structure of *L*-glutamate (**1.68**) as a neurotransmitter.

Glutamate (*L*-glutamic acid; **1.68**, Figure 1.19) is the major excitatory neurotransmitter in the central nervous system (CNS) of mammals. Glutamate plays a critical role in regulating various brain functions by activating the glutamate family of receptor distributed abundantly in the CNS. The two classes of glutamate receptors are ionotropic and metabotropic glutamate receptors (Figure 1.20) (Kew and Kemp, 2005).

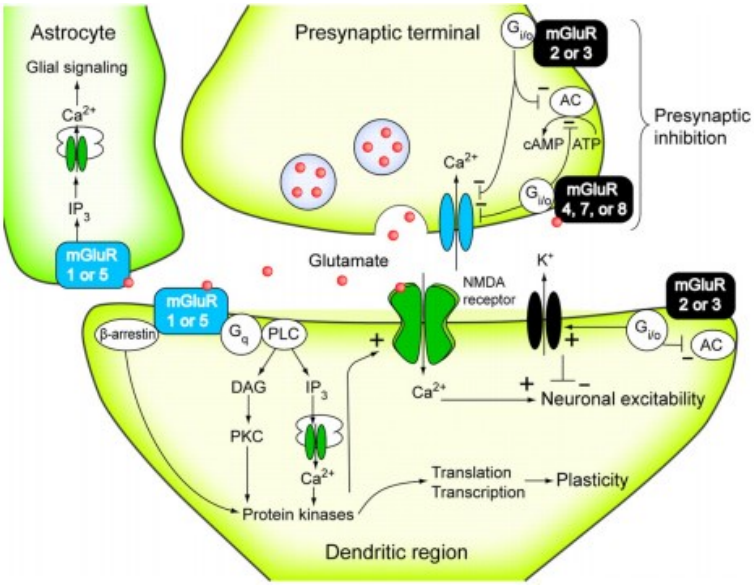


**Figure 1.20.** A general pictorial representation of location, distribution, and function of glutamate receptors in neurons (Benarroch, 2008. Reprinted with permission from *Neurology* **2008**, *70*, 964-968. Copyright 2008, AAN Enterprises, Inc.).

Ionotropic glutamate receptors (iGluRs) are ligand-gated cation channels that mediate fast excitatory neurotransmission and are divided into three major types, named according to the agonists that activate them selectively: *N*-methyl-*D*-aspartate (NMDA), α-amino-3-hydroxy-5-

methyl-4-isoazolepropionic acid (AMPA), and 2-carboxy-3-carboxymethyl-4-isopropenylpyrrolidine (kainate) receptors.

In contrast, metabotropic glutamate receptors (mGluRs) are G-protein coupled glutamate receptors that regulate neuronal excitability, synaptic transmission, and plasticity by activating slow excitatory synaptic potentials (Pin and Duvoisin, 1995). mGluRs are broadly classified into three groups (I to III) based on their sequence homology, second messenger coupling, and pharmacology (Figure 1.20) (Niswender and Conn, 2010). Group I receptors comprises mGlu1 and mGlu5, which are located on post-synaptic neurons and are positively linked to phospholipase C *via* $G_q/G_{11}$. Therefore, direct activation of mGlu1/5 results in increased phosphoinositide turnover resulting in an increase of intracellular $Ca^{2+}$. In contrast, Group II (mGlu2 and mGlu3) and III (mGlu4, mGlu6, mGlu7, and mGlu8) receptors inhibit adenylyl cyclase activity *via* $G_i/G_o$. Their activation leads to inhibition of forskolin-stimulated cyclic AMP formation. Group II mGlu receptors are located presynptically and are primarily distributed in forebrain regions. These receptors represent classic autoreceptors that upon agonist binding inhibit the release of glutamate into the synapse. In contrast, group III mGlu2 receptors are expressed both presynaptically and postsynaptically, and are localized in the cerebellum, striatum and hippocampus regions (Vinson and Jeffrey, 2012).

### 1.7.1. The Role of mGlu2 in Drug Addiction

The abundunce of mGlu receptors located throughout the limbic and cortical brain regions, which are implicated in drug addiction, has led to the emerging role of mGlus in regulating the behavioral and physiological effects of psychostimulants (Kenny and Markou, 2004; Knackstedt *et al*., 2009; Cleva and Olive *et al*., 2012; Pomierny-Chamiolo *et al*., 2014).

Glutamatergic neuronal projections originate from the prefrontal cortex (PFC) and reach up to the nucleus accumbens (NAc) and ventral tegmental area (VTA). Increased glutamate transmission innervates the dopaminergic system in the VTA leading to reward and response-initiating effects of drugs of abuse. Moreover, repeated use of addictive drugs causes long term cellular adaptations in the glutamatergic system, leading to the characteristic behaviors of addiction (Cornish and Kalivas, 2000; Gass and Olive, 2008; Kalivas, *et al.*, 2009; Schmidt and Pierce, 2010; Uys and Reissner, 2011). Extensive preclinical studies employing animal models of addiction for drug self-administration, reinstatement, and conditioned place preference have strongly suggested the potential of various mGlu ligands as anti-addiction therapeutics (reviewed in Pomierny-Chamioło *et al.*, 2014). Furthermore, changes in the function of mGlu2 under the influence of drugs of abuse have been observed that contribute towards the progression of drug dependence and the occurrence of withdrawal symptoms (Moussawi and Kalivas, 2010). In particular, studies have shown that functional downregulation of mGlu2 occurs during withdrawal from chronic abuse of morphine and cocaine (Vandergriff and Rasmussen, 1999; Rasmussen *et al.*, 2004; Xie and Steketee, 2008 and 2009). In addition, receptor mediated neuroplasticity and coupling to G-protein is significantly impaired after chronic drug abuse (Neugebauer *et al.*, 2000; Martin *et al.*, 2006; Huang *et al.*, 2007; Moussawi *et al.*, 2009; Beveridge *et al.*, 2011; Lu *et al.*, 2012). This dysfunctional neurotransmission could also explain the failure of drug addicts to control compulsive urges of drug seeking behavior. To support this, it has been shown that self-administration of drugs of abuse such as cocaine and nicotine, as well as the reinstatement of drug seeking behavior in animals, was suppressed with administration of mGlu2/3 agonists LY379268 and LY404039 (Figure 1.22) (Fundytus and Coderre, 1997; Baptista *et al.*, 2004; Greenslade and Mitchell, 2004; Adewale *et al.*, 2006; Peters and Kalivas,

2006; Kufahl *et al.*, 2013). Additionally, Morishima and coworkers found that mGlu2-knockout mice show greater locomotor sensitization as well as conditioned placed preference, in response to cocaine (Morishima *et al.*, 2005).

In conclusion, increasing evidence suggests that mGlu2 is strongly implicated in regulating drug seeking and reward processes during chronic drug addiction. This corroborates the importance of developing ligands that efficiently enhance mGlu2 function for anti-addiction therapy.

### 1.7.2. Structural and Functional Features of mGlu2

All the existing Class C GPCRs, including the mGlu receptor family, are known to share common structural features consisting of seven transmembrane structures, an extracellular N-terminus, and an intracellular C-terminus (Rosenbaum *et al.*, 2009). The extracellular N-terminus of mGluRs form a bi-lobed clam shell-shaped structure called the Venus Flytrap Domain (VFD) (Figure 1.21). This domain contains a highly conserved orthosteric agonist (i.e., glutamate) binding site that has been validated by x-ray crystallography (Kunishima *et al.*, 2000), ligand-binding studies (Tsuchiya *et al.*, 2002; Pin *et al.*, 2003), and mutagenesis reports (Sato *et al.*, 2003; Muto *et al.*, 2007). The 7-transmembrane domain is connected to the VFD *via* a conserved cystein-rich domain, which transmits conformation changes between the two domains and promotes subsequent signal transduction. Allosteric binding sites for these GPCRs are proposed to be embedded within the 7-transmembrane structure (Kunishima *et al*., 2000).

Once glutamate binds to the orthosteric site of mGlu2, it stabilizes the closed conformation of the extracellular domain, which then activates the G-protein coupling mechanism, thereby initiating second messenger pathways. More specifically, upon activation of

mGlu2, $G_{i/o}$ proteins get activated, which inhibit the activity of adenylyl cyclase (AC), thereby decreasing intracellular concentrations of cAMP (Kenny and Markou, 2004).

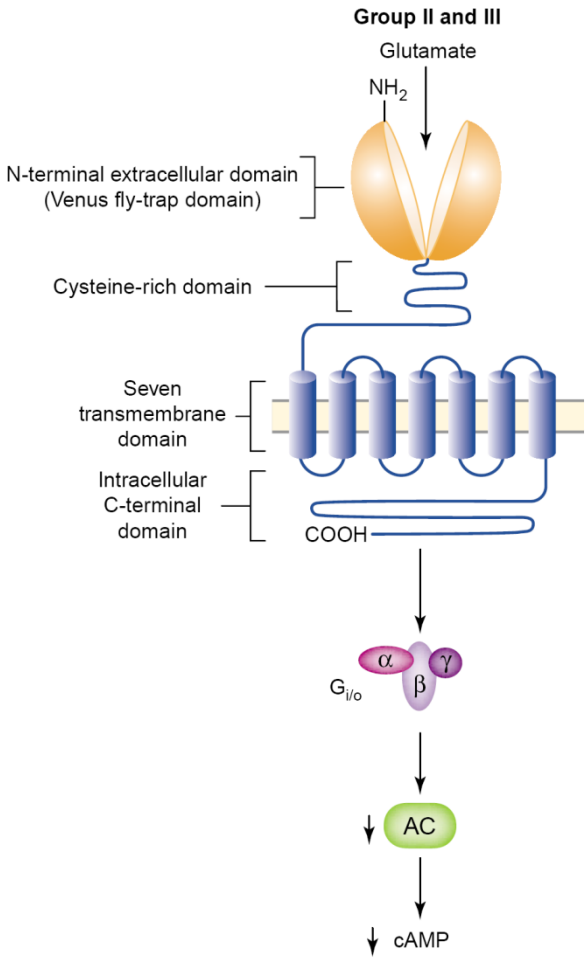


**Figure 1.21.** Structural and functional representation of mGlu2 as a family C G-protein coupled receptor (Kenny and Markou, 2004. Reprinted with permission from *Trends in Pharmacol. Sc.* **2004**, *25*, 265-272. Copyright 2004, Elsevier Ltd.)

## 1.8. mGlu2 Ligands

### 1.8.1. Orthosteric Ligands

A majority of mGlu2 orthosteric agonists and antagonists have been designed based on structural modifications to the endogenous ligand, *L*-glutamate (Figure 1.22) (e.g., see Monn *et al.*, 1997; Kingston *et al.*, 1999; Monn *et al.*, 1999; Wright *et al.*, 2001; Chaki *et al.*, 2004; Rorick-Kehn, Johnson, Burkey, *et al.*, 2007; Rorick-Kehn, Johnson, Knitowski, *et al.*, 2007).

Such orthosteric ligands have helped in understanding the functional role of these receptors and their implication in a corresponding disease state. However, given that these compounds are amino acid derivatives that have a high polar surface area, they lack appropriate hydrophobicity to cross the blood-brain barrier and reach the CNS where the majority of mGlu2 receptors are located. Additionally, since the glutamate-binding site is highly conserved structurally amongst the entire mGluR family, orthosteric ligands frequently lack appropriate receptor subtype selectivity (Conn and Pin, 1997; Schoepp *et al.*, 1999; Cartmell and Schoepp, 2000).

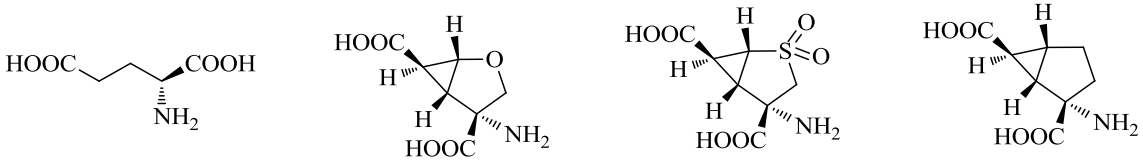


Glutamate LY379268 LY404039 LY354740

**Figure 1.22.** Structural examples of mGlu2 agonists targeting the orthosteric- / glutamate-binding site of mGlu2.

### 1.8.2. Allosteric Modulators

In order to overcome the drawbacks associated with the traditional approach of targeting the orthosteric site, studies have now focused on exploring allosteric mechanisms to control glutamate neurotransmission by modulating the activity of mGlu2 receptors. Allosteric modulators exert a range of pharmacological responses, such as positive allosteric modulation (PAM), negative allosteric modulation (NAM), and silent allosteric modulation (SAM) (Langmead and Christopoulos, 2014). PAMs bind to an allosteric site and enhance receptor function by increasing the affinity or efficacy of the orthosteric ligand. NAMs, on the other hand, decreases the affinity or efficacy of the orthosteric ligand upon binding to an allosteric site. Ligands that have no effect on the binding or function of the orthosteric ligand when bound to the allosteric site are the SAMs which, in turn, sterically block the binding of other allosteric

modulators. Allosteric ligands provide several advantages over the orthosteric ligands, namely 1.) Since the allosteric site is topographically distinct from the orthosteric site, receptor subtype selectivity can be better achieved with allosteric ligands, 2.) an allosteric modulator can exert its effect only in the presence of the endogenous ligand, (e.g., *L*-glutamate), and 3.) allosteric modulators frequently show better chemical tractability and more ligands can be designed with greater drug-like properties (Jensen and Spalding, 2004; Lewis *et al.*, 2008; Conn *et al.*, 2009; Rocheville and Garland, 2010; Smith *et al.*, 2011).

Despite these advantages, small molecule drug discovery programs of allosteric modulators are associated with several challenges. mGlu allosteric modulators routinely display "flat" SAR, wherein a minimal change to the structure can result in a significant loss in pharmacological activity (Zhao *et al*., 2007). Furthermore, the SAR studies of allosteric modulators are complicated by the phenomenon of "molecular switches", whereby a subtle or minimal structural change to an allosteric ligand can completely change the mode of pharmacology or selectivity of a ligand for a given receptor subtype (Wood *et al.*, 2011). This problem of molecular switches poses a serious challenge towards developing SAR based on a single mode of pharmacology. Additionally, allosteric ligands can also display ligand-biased pharmacology in which a single modulator can exert different pharmacological responses (Kenakin, 2012). In addition, the problem of probe-dependent allosteric interactions exists wherein the same allosteric modulator can enhance the efficacy of one orthosteric ligand, while acting as a NAM or SAM for another. Moreover, structure-based lead optimization of allosteric modulators towards developing clinically-relevant candidates is currently impossible due to the lack of accurate and reliable mGlu2 3-D structural information. In contrast to the extracellular N-terminal, an x-ray crystal structure of the transmembrane domain is yet to be determined for

mGlu2. Though computer-aided homology models of mGlu1 (Malherbe, Pari, Kratochwil, Knoflach, *et al.*, 2003) and mGlu5 (Malherbe, Pari, Kratochwil, Zenner, *et al.*, 2003) using Class A GPCRs as templates, and their subsequent crystal structures (Doré *et al.*, 2014; Wu *et al.*, 2014) have provided insights into the structure of allosteric binding sites of these subtypes, currently only a single low-resolution homology model of the TM domain of mGlu2 exists in the literature (Radchenko *et al.*, 2014). Nevertheless, site-directed mutagenesis and the construction of chimeric receptors of mGlu2 have provided, to some extent, information on the molecular determinants of allosteric modulator-binding site interactions within the mGlu2 TM domain (Malherbe, *et al.*, 2001; Schaffhauser *et al.*, 2003; Hemstapat *et al.*, 2007). In particular, Rowe and coworkers prepared a series of mutant receptors by exchanging various single or multiple amino acids between hmGlu2 and hmGlu3 residues (Rowe *et al.*, 2008). The results showed that replacing hmGlu2 amino acid residues between Leu656 and Arg750 in TM3-4 region with homologous hmGlu3 segments resulted in a complete loss of the potentiator activity of mGlu2-specific PAMs. On the other hand, substitution of hmGlu2 residues Ser688, Gly689, and Asn735 into the homologous region of hmGlu3 created an active hmGlu2 allosteric modulation site within mGlu3 which was potentiated by mGlu2-specific PAMs, suggesting the importance of these three residues in the potentiation effect.

#### 1.8.2.1. Positive Allosteric Modulators of mGlu2

Regardless of the complexities associated with optimizing the activity of allosteric modulators, discovery efforts towards selective PAMs of mGlu2 are still gaining tremendous momentum as they represent promising drug candidates for a number of disease states including

schizophrenia (Fell *et al*., 2012), drug abuse (Moussawi and Kalivas, 2010), impaired cognition, and depression (Goeldner *et al*., 2013).

#### 1.8.2.1.2. SAR of Biphenyl-Carboxylic Acid-Indanone-Based mGlu2 PAMs

The study of mGlu2 PAMs as anti-addiction therapeutics has been principally aided by the discovery of 3'-[[(2-cyclopentyl-2,3-dihydro-6,7-dimethyl-1-oxo-1*H*-inden-5-yl)oxy]methyl]-[1,1'-biphenyl]-4-carboxylic acid (BINA **(±)-1.71**; hmGluR2 GTP-γS $EC_{50}$ = 111 nM). BINA (**(±)-1.71**, Table 1.5), which originated from extensive SAR efforts by Merck in an attempt to improve the physicochemical properties of an initial hit compound discovered *via* mGlu2 high-throughput screening (Pinkerton *et al.*, 2005). BINA is a selective, brain-penetrant, and potent mGlu2 PAM that produces long-lasting antipsychotic and anxiolytic effects in various behavioral animal models (Galici *et al.*, 2006). Furthermore, BINA has been shown to consistently reduce the reinforcing properties of cocaine, amphetamine, and alcohol in squirrel monkeys and rats (Adewale *et al.*, 2006; Jin *et al.*, 2010). Moreover, animals addicted to cocaine, amphetamine, and alcohol showed reduced drug-seeking behavior and relapse upon treatment with BINA (Kim *et al.*, 2005; Zhao *et al.*, 2006). Additionally, since BINA non-competitively potentiates the function of mGlu2, it did not show off-site actions such as attenuation of response to food which is a natural reward stimulant often seen in the case of non-selective orthosteric agonists (Jin *et al.*, 2010). However, despite promising results from BINA, this compound significantly lacked *in vivo* and *in vitro* potency as well as possessed low oral bioavailability. Therefore, in an effort to improve the efficacy, potency and drug-like properties of BINA, several structural modifications of BINA were further reported (Bonnefous *et al.*, 2005; Pinkerton *et al.*, 2005; Galici *et al.*, 2006; Pinkerton *et al.*, 2006; Dhanya *et al.*, 2011).

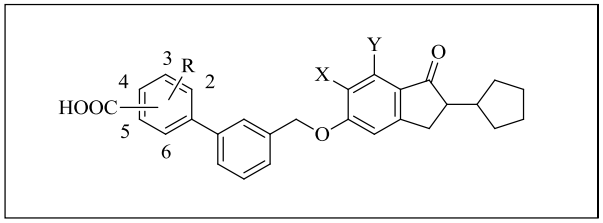


| Entry | -COOH | -R | -X | -Y | hmGlu2 [$^{35}$S]GTP-γS $EC_{50}$ (nM) | % glutamate potentiation |
|---|---|---|---|---|---|---|
| **(±)-1.70** | C3 | -H | $CH_3$ | $CH_3$ | 69 | 118 |
| **(±)-1.71** | C4 (BINA) | -H | $CH_3$ | $CH_3$ | 111 | 114 |
| **(±)-1.72** | C3 | 2-$CH_3$ | $CH_3$ | $CH_3$ | 252 | 94 |
| **(±)-1.73** | C4 | 2-$CH_3$ | $CH_3$ | $CH_3$ | 353 | 103 |
| **(±)-1.74** | C3 | 6-$OCH_3$ | $CH_3$ | $CH_3$ | 36 | 114 |
| **(±)-1.75** | C3 | 4-Cl | $CH_3$ | $CH_3$ | 24 | 109 |
| **(±)-1.76** | C3 | -H | $CH_3$ | Cl | 64 | 122 |
| **(±)-1.77** | C4 | -H | $CH_3$ | Cl | 49 | 110 |
| **(±)-1.78** | C3 | 4-Cl | $CH_3$ | Cl | 67 | 121 |
| **(±)-1.79** | C3 | 4-Cl | Cl | Cl | 5 | 117 |

**Table 1.5.** SAR of a biphenyl-indanones: mGlu2 PAM potencies reported by Bonnefous *et al*., 2005.

The pharmacological evaluation of all analogs for their mGlu2 PAM activity was reported in terms of their functional efficacy in glutamate potentiation (i.e., $IC_{50}$ values) rather than their binding affinity (i.e., $K_i$ values) at mGlu2 due to the absence of a suitable radiolabelled ligand for mGlu2 allosteric sites. The effects of substitutions on the indanone and the terminal phenyl ring are briefly summarized as follows: the acid at C3 (**(±)-1.70**; hmGluR2 GTP-γS $EC_{50}$ = 69 nM, glutamate potentiation 118%) was slightly more preferred over C4 (BINA, **(±)-1.71**; hmGluR2 GTP-γS $EC_{50}$ = 111 nM, glutamate potentiation 114%) when X = Y = $CH_3$. Further exploration of SAR at the terminal phenyl ring revealed that the 2'-position of the phenyl ring was not tolerable to methyl substitutions wherein both **(±)-1.72** and **(±)-1.73** displayed 4-fold (hmGluR2 GTP-γS $EC_{50}$ = 252 nM, glutamate potentiation 94%) and 5-fold (hmGluR2 $EC_{50}$ =

353 nM, glutamate potentiation 103%) reduced potency respectively when compared to **(±)-1.70** (hmGluR2 GTP-γS $EC_{50}$ = 69 nM). In contrast, 6'-methoxy analog **(±)-1.74** (hmGluR2 GTP-γS $EC_{50}$ = 36 nM, % glutamate potentiation = 114) and 4'-chloro analog **(±)-1.75** (hmGluR2 GTP-γS $EC_{50}$ = 24 nM, % glutamate potentiation = 109) displayed 2-fold and 3-fold higher mGlu2 potency, respectively, relative to parent compound **(±)-1.70** (hmGluR2 GTP-γS $EC_{50}$ = 69 nM, % glutamate potentiation = 118), while their glutamate potentiation ability remained unchanged. Position Y on the indanone ring, when substituted with a -Cl group, consistently increased the potency of the compounds irrespective of the position of the carboxylic acid group (**(±)-1.76** to **(±)-1.79**). Though the potency was not affected when the 4'-position of the phenyl ring was substituted with 4'-Cl (**(±)-1.78**, hmGluR2 GTP-γS $EC_{50}$ = 67 nM, glutamate potentiation 121%) when compared to **(±)-1.76** (hmGluR2 GTP-γS $EC_{50}$ = 64 nM, glutamate potentiation 122%), there was a large boost in the potency when the substituent on position X was replaced with a Cl atom (**(±)-1.79**, hmGluR2 GTP-γS $EC_{50}$ = 5 nM, glutamate potentiation 117%). Racemic compound **(±)-1.79** was the most potent mGlu2 PAM synthesized in this biphenyl-indanone series.

#### 1.8.2.1.3. SAR of Pyridone-Based mGlu2 PAMs

Another series of mGlu2 PAMs identified through high throughput screening (HTS) were 1,5-disubstituted 2-pyridones **1.82** and **1.83** (Cid *et al.*, 2010). In particular, 1,5-substituted pyridones emerged as a promising class of potent and selective mGlu2 PAMs *via* high throughput screening (HTS) efforts at Addex Pharmaceuticals using a mGluR2 PAM FLIPR (fluorometric imaging plate reader) assay (Cid *et al.*, 2010). Though the mGlu2 PAM activity of the two initial hits was low (hmGlu2 GTP-γS binding $EC_{50}$ = 6.29 μM, glutamate potentiation

$E_{max}$ = 138% for **1.82** and $EC_{50}$ = 4.47 μM, $E_{max}$ = 133 % for **1.83**), these compounds were reasonable starting points for lead optimization efforts.

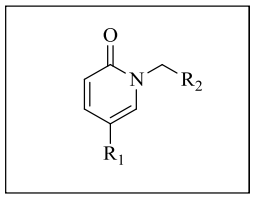


| Entry | $R_1$ | $R_2$ | hmGlu2 [$^{35}$S]-GTPγS $EC_{50}$ (μM) | Glutamate potentiation $E_{max}$ (%) |
|---|---|---|---|---|
| **1.82** | 4-MeO-Ph- | -Ph | 6.29 | 138 |
| **1.83** | $HOCH_2CH_2O$-Ph- | 2-F-4-Cl-Ph- | 4.47 | 133 |
| **1.84** | 4-MeO-Ph- | 2-F-Ph- | 1.00 | 44 |
| **1.85** | 4-MeO-Ph- | 3-F-Ph- | 1.91 | 96 |
| **1.86** | 4-MeO-Ph- | 4-Cl-Ph- | 1.41 | 189 |
| **1.87** | 4-MeO-Ph- | 2,3-diF-Ph- | 10 | 131 |
| **1.88** | 4-MeO-Ph- | 2,4-diF-Ph- | 4.79 | 128 |
| **1.89** | 4-MeO-Ph- | 2-F-4-Cl-Ph- | 0.53 | 194 |
| **1.90** | 4-MeO-Ph- | 2-F-4-CF3- | 3.16 | 124 |
| **1.91** | 3-F-4-MeO-Ph- | 2-F-4-Cl-Ph- | 0.71 | 241 |
| **1.92** | Ph- | 2-F-4-Cl-Ph- | 6.31 | 138 |
| **1.93** | 4-($PhC(O)CH_2CH_2O$)-Ph- | 2-F-4-Cl-Ph- | 1.26 | 196 |
| **1.94** | 4-($CNCH_2O$)-Ph- | 2-F-4-Cl-Ph- | 3.39 | 184 |

**Table 1.6.** SAR of some 1,5-substituted pyridones: mGlu2 PAMs reported by Cid *et al*., 2010.

Initial efforts focused on examining the effect of introducing halogen substitutions on the benzyl ring of **1.82**. Although the 2'-F substitution in **1.84** increased mGlu2 potency as compared to the lead **1.82** by 6-fold, this substitution resulted in a marked decrease in glutamate potentiation ability (hmGlu2 GTP-γS binding $EC_{50}$ = 1.00 μM, glutamate potentiation = 44% for **1.84** versus hmGlu2 GTP-γS $EC_{50}$ = 6.29 μM, glutamate potentiation = 138% for **1.82**). Subsequently, compounds **1.85** (3'-F), **1.86** (4'-Cl), **1.87** (2',3'-di-F), and **1.90** (2'-F-4'-$CF_3$) showed significant improvements in the percentage potentiation of glutamate versus **1.84** (2'-F).

Notably, a ten-fold increase in mGlu2 potency was observed with 2'-F-4'-Cl- substituted **1.89** (hmGlu2 GTP-γS $EC_{50}$ = 0.53 μM, glutamate potentiation = 194%) versus 2',4'-difluoro substituted **1.88** (hmGlu2 GTP-γS $EC_{50}$ = 4.79 μM, glutamate potentiation = 128%) suggesting the preference for larger groups at the *para*-position. Furthermore, slight improvements in the mGlu2 potency were observed with the 3'-F-4'-MeO containing **1.91** (hmGlu2 GTP-γS $EC_{50}$ = 0.71 μM, glutamate potentiation 241% ). The unsubstituted phenyl analog (**1.92**) of the second HTS hit **1.83** resulted in the same level of *in vitro* mGlu2 potency as compared to **1.83** (hmGlu2 GTP-γS $EC_{50}$ = 6.31 μM, glutamate potentiation = 139% for **1.92** versus hmGlu2 GTP-γS $EC_{50}$ = 4.47 μM, glutamate potentiation = 133% for **1.83**). Exploration of other alkyl chains with H-bond acceptor groups at the *para*-position of the phenyl ring slightly improved the mGlu2 potency (**1.93** hmGlu2 GTP-γS $EC_{50}$ = 1.26 μM, glutamate potentiation = 196%; **1.94** hmGlu2 GTP-γS $EC_{50}$ = 3.39 μM, glutamate potentiation = 184%).

Among all 2-pyridone derivatives, compound **1.89** displayed the most promising results during *in vivo* evaluation in mice. Upon intraperitoneal administration, **1.89** markedly attenuated the increase in phencyclidine-induced locomotor activity in animal models of psychosis. Such results were similar to other previously known mGlu2 PAMs. Furthermore, **1.89** also displaced appreciable bioavailability and brain penetration upon iv administration. However, despite the promising results of **1.89**, further studies with this compound were discontinued due to its poor metabolic stability (Cid *et al*., 2010). As a result, since the poor pharmacokinetic properties of this compound precluded its further development, more advanced leads with improved potency and drug-like properties were later pursued (Cid *et al*., 2012).

## CHAPTER TWO

## 2. Determination of Drug-Target Interactions *via* Small-Molecule Photoaffinity Labeling: a Concise Literature Review

### 2.1. Introduction

In order to vertically advance the DAT, mGlu2, and nAChR fields towards rational structure-based drug design, it is imperative to obtain detailed 3-D structural information regarding ligand-binding sites within these therapeutically significant proteins. In this regard, the most common experimental methods towards acquiring detailed 3-D structural information of proteins are x-ray crystallography (Garman, 2014), site-directed mutagenesis (Shortle *et al.*, 1981), computational modeling (Rodrigues and Bonvin, 2014), and photoaffinity labeling (Sumranjit and Chung, 2013).

Currently, x-ray crystal structures of human forms of the DAT, mGlu2, and nAChRs are not available. In particular, procuring 3-D structural information regarding membrane-bound proteins such as the DAT, mGlu2, and nAChRs by x-ray crystallography and NMR analysis is very challenging due to their complex heterogeneity and insolubility in water (Bill *et al.*, 2011). Most recently, multiple research groups have computationally built human DAT molecular models (e.g., Stockner *et al.*, 2013; Huang and Chang-Guo, 2007) based on 3-D structural information obtained from several available bacterial $LeuT_{Aa}$ leucine transporter crystal structures (e.g., Singh *et al.*, 2007; Yamashita *et al.*, 2005; Zhou *et al.*, 2007 and 2009). In turn, these computer homology models have aided in characterizing ligand-binding sites within the DAT (e.g., Beuming *et al.*, 2006 and 2008; Bisgaard *et al.*, 2011; Indarte *et al.*, 2008). Likewise, homology models of human nAChRs are known (e.g., Hu *et al.*, 2009; Bisson *et al.*, 2008; Saladino *et al.*, 2005; Law and Lightstone, 2009) based on crystallographic structures of *Torpedo*

nAChRs (e.g., Unwin, 2005) and several AChBPs (e.g., Brejc *et al.*, 2001). However, due to significant differences between the human DAT, nAChRs, and their corresponding protein templates for computational homology modeling, careful experimental validation and critical refinement of these molecular models is necessary in order to understand the structure, function, and pharmacological properties of these proteins. In a similar light, structure-function studies of allosteric binding sites within mGlu2 are minimal (Lundstrom *et al.*, 2011; Schaffhauser *et al.*, 2003), and only one research group has recently disclosed a molecular modeling study of the transmembrane domain of mGlu2 featuring a proposed binding site for positive allosteric modulators (Radchenko *et al.*, 2014). As a result, there is a critical need for direct mapping of ligand-binding sites within the DAT, nAChRs, and mGlu2 in order to rationally develop therapeutics for numerous disease states associated with these proteins.

To date, the status quo towards gaining insight into DAT, nAChR, and mGlu2 regions where ligands bind and confer pharmacology has been provided by mutagenesis-based studies coupled with homology modeling (e.g. for the DAT: Severinsen *et al.*, 2014, Stockner *et al.*, 2013, Guptaroy *et al.*, 2011, Bisgaard *et al.*, 2011; Schmitt *et al.*, 2008; e.g. for nAChRs: Marotta *et al.*, 2014; Grishin *et al.*, 2013; Pavlovicz *et al.*, 2011). However, in the absence of detailed 3-D structural information it is difficult to confirm if the impact of certain amino acid mutations are due to disruptions of specific ligand-protein binding sites, or to alterations of protein structure that *indirectly* impact binding sites. These shortcomings have prevented advancement of the fields involving these target proteins and bring into question the validity of the 3-D structures of ligand-protein complexes generated by coupling site-directed mutagenesis with homology modeling. In contrast, what objectively sets affinity and photoaffinity labeling apart from this status quo is that these experimental approaches allow *direct* identification of binding

sites and poses of ligands when coupled with homology modeling, thus allowing one to understand the structural basis for a particular ligand's pharmacology at the molecular level.

## 2.2. The Concept of Photoaffinity Labeling

The concept of photoaffinity labeling was first proposed in 1962 (Singh *et al.*, 1962). In turn, Chakrabarti and Khorana were the first to implement this method in order to directly investigate sites of lipid−protein interactions at the molecular level in biomembranes (Chakrabarti and Khorana, 1975).

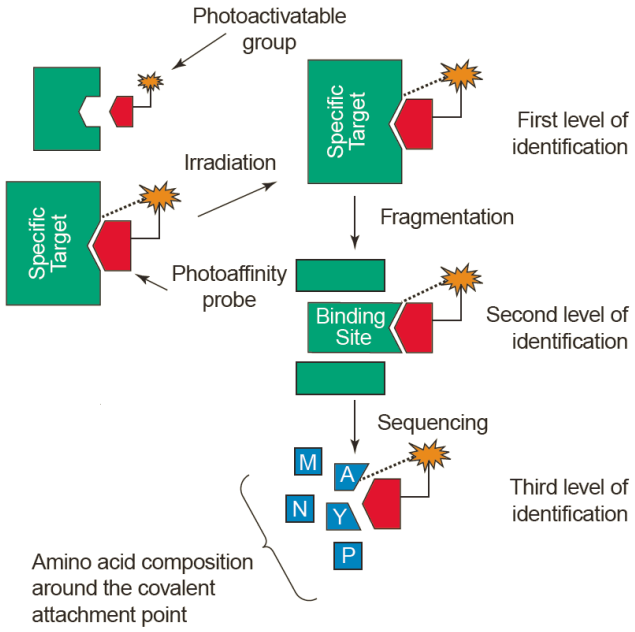


**Scheme 2.1.** An overview of identification levels possible *via* photoaffinity labeling (Dorman and Prestwich, 2000. Reprinted with permission from *Trends in biotech*. **2000**, *18*, 64-77. Copyright 2000, Elsevier).

Photoaffinity labeling represents one of the most direct approaches towards elucidating ligand-binding sites within target proteins. Although this experimental approach has been employed extensively with the DAT (e.g., Agoston *et al.*, 1997; Lever *et al.*, 2005; Newman *et al.*, 2006; Parnas *et al.*, 2008; Vaughan *et al.*, 1999, 2005, and 2007; Vaughan and Kuhar, 1996;

Zou *et al.*, 2001; Lapinsky *et al.*, 2009, 2011, and 2012) and select nAChRs (e.g., Hamouda *et al.*, 2009, 2011, and 2013; Srivastava *et al.*, 2009; Chiara *et al.*, 2009; Tantama *et al.*, 2008; Sanghvi *et al.*, 2008; Garcia *et al.*, 2007; Nirthanan *et al.*, 2008), this dissertation has contributed the first ever probes to conduct photoaffinity labeling experiments with mGlu2.

In photoaffinity labeling, known ligands are typically derivatized with a reporter tag and a photoreactive group, which is capable of forming an irreversible, covalent bond with a target protein after initial reversible target binding and subsequent exposure to UV light (Scheme 2.1). Under normal ambient light conditions, photoreactive groups tend to remain inert and chemically unreactive. However, upon irradiation with an appropriate wavelength of UV light, photoreactive groups can be converted into highly reactive, radical-based intermediates. When such reactive intermediates are formed within the binding site of a target protein, they can react irreversibly with proximal amino acid residues found within their vicinity. Photo-crosslinking products are then traditionally identified and analyzed using methods such as SDS-PAGE and HPLC coupled with MS (Robinette *et al.*, 2006). In particular, proper photoaffinity experiments can be used to identify the targets of biologically active compounds, determine the affinity and selectivity of ligand-target complexes, interrogate the structure and function of target biological macromolecules, investigate ligand-receptor interactions, identify amino acids at biological macromolecule interfaces (e.g., protein-protein interactions, lipid-protein interactions), and also isolate and identify unknown enzymes or receptors (Lapinsky, 2012).

A set of criteria has been disclosed regarding ideal photoprobes, namely: (1) they utilize a wavelength-selective activation that does not damage other components in the testing system; (2) they possess high stability in the dark under various pH conditions; (3) they form a stable adduct with their target biological macromolecule(s) and survive subsequent characterization and

detection methodology; (4) they bear a structural resemblance to the parent ligand with similar binding affinity and pharmacology; (5) they have the ability to react with any type of bond or residue without any preference; (6) they are sterically non-congested; and (7) they generate highly reactive, short-lived photo-intermediates upon irradiation with UV light (Das, 2011; Vodovozova, 2007). Despite being employed for decades in biochemical research, so far there have been no reports of photoprobes that possess all of the previously mentioned characteristics.

Arguably the most important component of a photoaffinity probe is the photoreactive functional group. The most widely used photoreactive functional groups in photoaffinity labeling are aromatic azides, benzophenones and acetophenones, and aliphatic (Das, 2011) and aromatic diazirines (e.g., Dubinsky *et al.*, 2012; Hashimoto and Hatanaka, 2011). These functional groups can also be classified according to their photochemically-generated reactive species, principally nitrenes, diradicals, and carbenes, respectively (Fleming, 1995). Given that this dissertation features chemical probes containing an aromatic azide, benzophenone, or acetophenone photoreactive group, only these functional groups in terms of photoaffinity labeling are reviewed below.

### 2.2.1. Discussion of Select Photoreactive Groups Employed in This Dissertation

#### 2.2.1.1. Aryl Azides as Photoreactive Groups in Photoaffinity Labeling

Aryl azides represent the most frequently employed photoreactive group in photoaffinity probes, mainly because of their small size and straightforward synthetic routes for incorporation into parent ligands *via* conventional aniline diazotization and azide displacement. Aryl azides remain chemically inert in the dark and are relatively stable to multiple synthetic transformation

conditions. These functional groups possess high reactivity upon photoirradiation, wherein they generate reactive nitrene species with presumably longer lifetimes than carbenes.

The photochemistry of aryl azides (e.g., **2.1**) is well established and proceeds after photoirradiation under UV light (Morris *et al.*, 2013) (Scheme 2.2). Once activated, a singlet nitrene (**2.2**) is generated upon the release of nitrogen. The *in situ* generated reactive singlet nitrene (**2.2**) undergoes bond insertion into proximal carbon-hydrogen or heteroatom-hydrogen bonds (pathway A) of amino acids within the binding pocket resulting in photolabeling to form a covalent complex (**2.3**). Apart from this desired reaction pathway, the nitrene can also undergo other side reactions, namely ring expansion to form a ketenimine (**2.7**) (pathway B) or intersystem conversion (pathway C) to form a triplet intermediate (**2.4**). These latter pathways are generally less desirable and tend to account for non-specific protein labeling and lower yields during photoaffinity labeling experiments. In particular, the resulting ketenimine from pathway B is an electrophile that can react with nucleophiles to form azepines (**2.8**) in either a desirable (i.e., specific) or undesirable (i.e., non-specific) manner. In order to increase the stability of the desired singlet nitrene (**2.2**) to favor the insertion reaction pathway (pathway A) while avoiding side reactions (pathways B and C), electron-withdrawing groups (e.g., one or more fluorine atoms) have traditionally been incorporated into the aromatic ring bearing the photoreactive aryl azide. In particular, it has been experimentally shown that fluorinated aryl azides impede ring expansion reactions and favor bond insertion reactions in a desirable manner (Schnapp *et al.*, 1993).

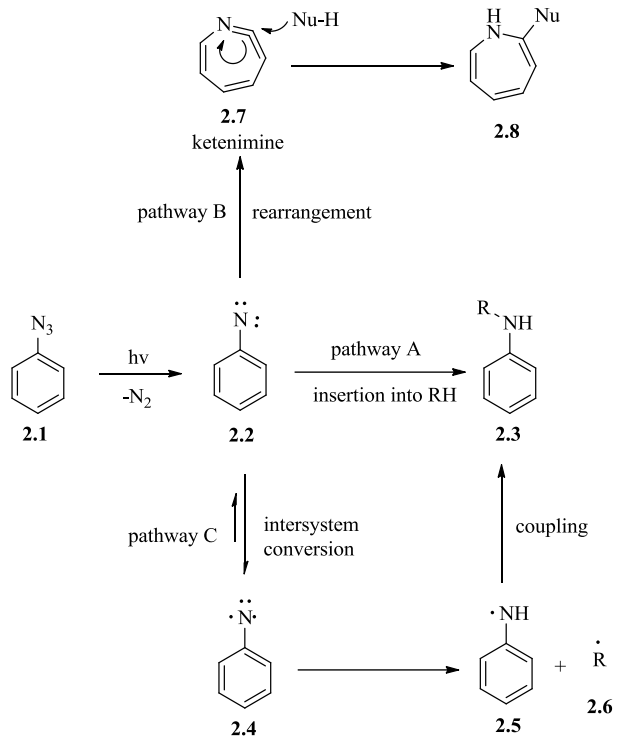


**Scheme 2.2.** The photochemistry of aryl azides as photoreactive groups in photoaffinity labeling.

Photoactivation of phenylazides is achieved at their maximal absorption wavelength of around 260 nm. This amount of energy can be highly unfavorable to biomacromolecules such as proteins and nucleic acids given they have an absorption maxima around 260-280 nm. As a result, it is possible that the photoactivation of aryl azides can cause considerable damage to the biological system being studied during photoaffinity labeling. In order to overcome this potential problem, several groups have successfully shifted the absorption wavelength of photoreactive aryl azides beyond 300 nm, principally by substituting the phenyl ring with electron-withdrawing groups such as a nitro functional group (Mohr, 2004).

### 2.2.1.2. Benzophenones and Acetophenones as Photoreactive Groups in Photoaffinity Labeling

Benzophenones (**2.9**), as well as their more conformationally flexible counterparts, acetophenones (**2.10**), are common precursors to reactive free radicals generated during photoaffinity labeling (Scheme 2.3). Benzophenone and acetophenone moieties get converted into a triplet biradical (**2.11**) upon photoactivation. This triplet biradical can subsequently abstract a hydrogen atom from a nearby amino acid to form two free radicals (**2.12** and ·CProt). These two radicals can then combine to result in the formation of a photoadduct (**2.13**).

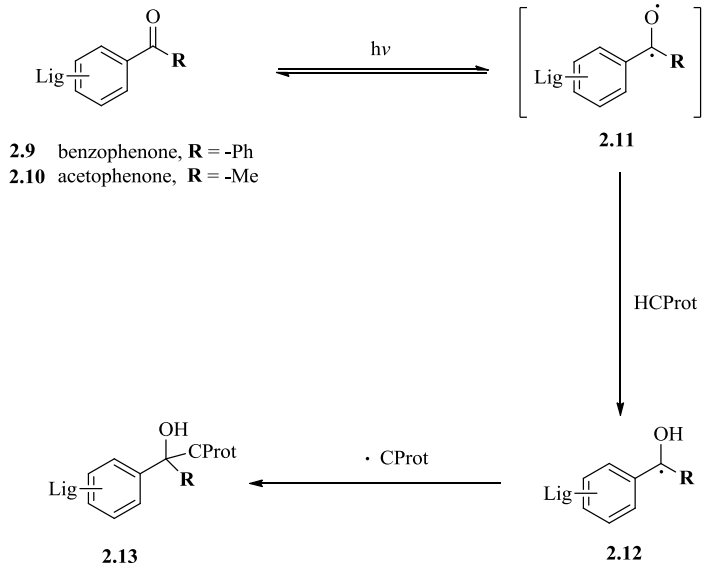


**Scheme 2.3.** The photochemistry of benzophenone and acetophenone as photoreactive functional groups in photoaffinity labeling.

Despite their large size, which could potentially adversely affect reversible formation of the photoprobe-protein complex prior to irradiation, benzophenones offer several advantages over other photoaffinity labeling groups (Dorman and Prestwich, 1994). The maximal absorption of a benzophenone functional group for photoactivation is 350-360 nm, which in sharp contrast to aryl azides, lies well outside the energy range that causes damaging effects to living cells. As a result, benzophenone-containing photoprobes routinely show success in cell

cultures or other living systems. Additionally, a number of benzophenone-containing building blocks are commercially available for photoprobe synthesis, and this functional group is stable in most organic solvents and compatible with multiple synthetic strategies. Benzophenones also tend to possess much higher chemical stability when compared to other nitrene and carbene precursors. In particular, the reversible nature of the biradical species **2.11** generated during acetophenone and benzophenone photochemistry also increases the labeling efficiency for probes that contain these particular photoreactive groups. In addition, benzophenones can preferentially react with inactive C-H bonds in the presence of water. Besides their bulkiness that could hinder reversible binding to a biological target, another principal disadvantage associated with benzophenone-containing photoprobes is that they normally require longer irradiation times versus aryl azide-containing probes, thus potentially resulting in higher amounts of non-specific labeling.

Similar to benzophenones, the acetophenone moiety (**2.10**) has long been known to undergo photochemical reactions upon photoactivation (Berger and Steel, 1975; Huix-Rotllant *et al.*, 2013). However, its use as a photoreactive group in photoaffinity labeling (e.g., van Scherpenzeel *et al.*, 2010) is significantly less when compared to aryl azides, benzophenones, and diazirines.

#### 2.2.1.3. Pyrimidones as Photo-masked Electrophiles for Affinity Labeling

In contrast to photoaffinity labeling, affinity labeling features a compound that is designed to be structurally similar to a ligand that is known to bind to a target biological macromolecule of interest, but already inherently contains an electrophilic functional group capable of covalently reacting with proximal nucleophilic amino acids (Miller and Cornish,

2005) (Scheme 2.4). The expectation is that the affinity label will initially form a reversible probe-target complex and, once bound at a specific site, will react in a proximal, irreversible manner with a nearby nucleophilic amino acid within the binding site. Application of this technique can result in tagging of a particular ligand-binding site within a specific protein or in the labeling of one protein within a complex mixture of proteins.

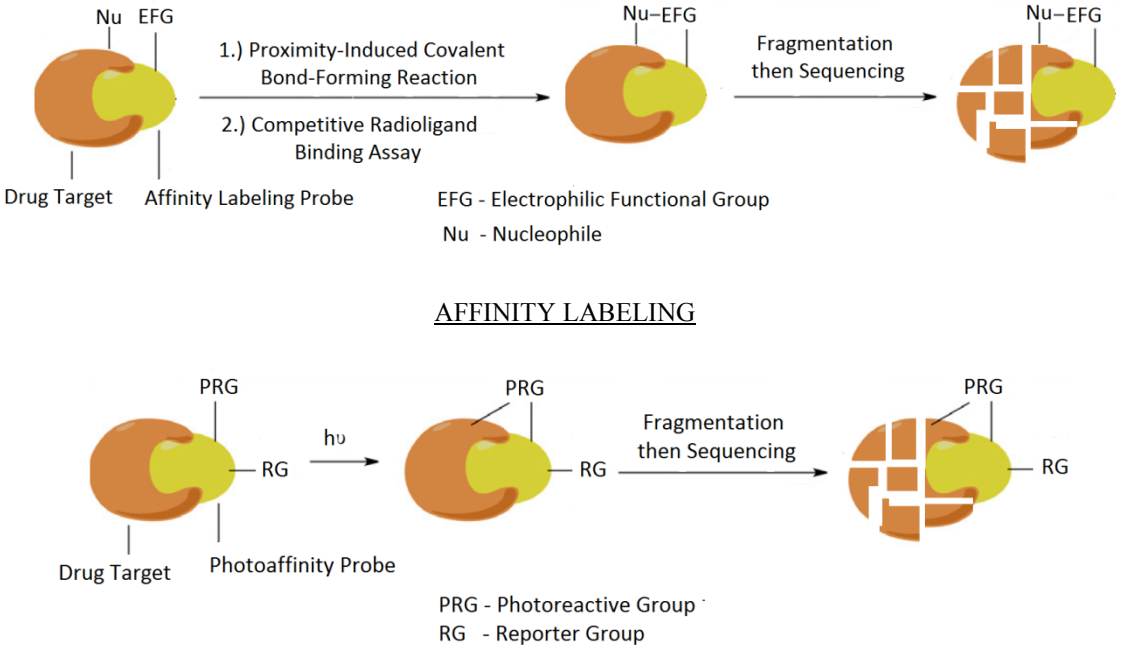


**Scheme 2.4.** Schematic representation of affinity labeling versus photoaffinity labeling towards determining the binding site of a ligand within a drug target (Lapinsky *et al*., 2012. Adapted with permission from *Bioorg. Med. Chem.* **2012**, *20*, 6237-6247. Copyright 2012, Elsevier).

In contrast to aryl azides, benzophenones, and acetophenones, pyrimidones (**2.15**, Scheme 2.5) are unique chemical structures that upon irradiation are known to photochemically generate isocyanate-based electrophiles (**2.17**), which can then covalently react with proximal nucleophiles in ligand-binding sites *via* affinity labeling (Battenberg *et al.*, 2011). Since pyrimidones are present in many natural products (e.g., bufadienolides, zebularine, and citreoviridin), this moiety can be potentially exploited as an intrinsic photoreactive group

naturally present within a lead compound. As a result, this circumvents the need to incorporate non-natural functional groups (e.g., photoreactive azide and diazirine functional groups) into a lead compound that could potentially negatively disrupt protein-ligand interactions prior to photo-unmasking affinity labeling.

The photochemistry of pyrimidones is induced by UV irradiation ranging between 290-320 nm and proceeds *via* a Norrish type 1 reaction to form a reactive isocyanate (**2.17**) or a bicyclic intermediate (**2.20**) (Scheme 2.5). In turn, the electrophilic carbon of the isocyanate moiety is susceptible to nucleophilic attack by proximal alcohol- or amine-containing derivatives (e.g., the amino acid side chains serine and lysine, respectively) to give rise to a stable covalent adduct (**2.19**).

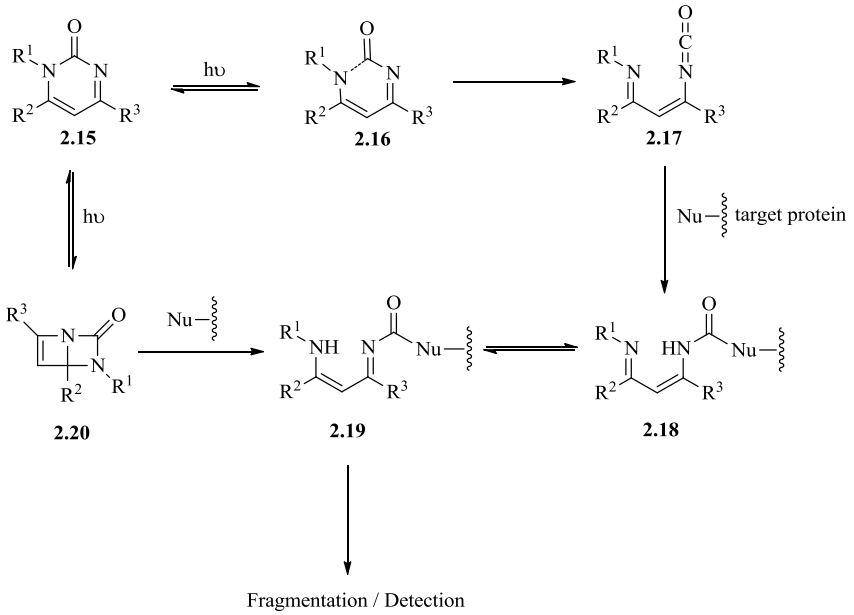


**2.15** **2.16** **2.17** **2.20** **2.19** **2.18**

**Scheme 2.5.** Photochemistry of pyrimidones as photomasked electrophiles for affinity labeling.

## 2.3. Select Reporter Groups Traditionally Employed in Affinity and Photoaffinity Probes

In addition to a functional group that can eventually form a covalent bond to a ligand-binding site within a target biological macromolecule, affinity and photoaffinity chemical probes also traditionally require incorporation of a reporter group within the probe structure (Sadaghiani *et al.*, 2007). Examples include radioactive isotopes (e.g., $^{125}$I), affinity tags (e.g., biotin), or fluorophores. These reporter groups function to facilitate visualization, identification, enrichment, or isolation of probe-labeled covalent adducts associated with irreversible labeling experiments.

### 2.3.1. Radioactive Isotopes as a Reporter Group in Chemical Probes

Radioactive isotopes are commonly used in biological applications for the detection of a wide variety of biological molecules. In particular, $I^{125}$ represents one of the most frequently used radioactive isotope tags in biochemistry owing to its ease of incorporation *via* simple synthetic steps, relatively small size, and highly sensitive signal for easy detection and quantification (Gevaert *et al.*, 2008). However, the relatively short half-life associated with $I^{125}$ prevents storage of probes and reagents containing this radioisotope for prolonged periods of time. In addition, the synthesis of probes labeled with $I^{125}$ requires a special laboratory setting wherein extra care during handling is necessary given as $I^{125}$ is a harmful radioactive health hazard.

### 2.3.2. 'Clickable' Handles as Chemical Reporters in Tandem Photoaffinity Labeling-Bioorthogonal Conjugation

In order to facilitate complete proteomic analysis following photoaffinity labeling and address the shortcomings associated with radioactive isotopes as reporter groups, alternatives such as biotin (Tomohiro *et al.*, 2012), epitope tags (e.g., FLAG peptide), or fluorophores can be directly incorporated into the structure of photoaffinity probes. These moieties frequently allow easy enrichment, detection, and/or isolation of photolabeled products after photoaffinity labeling. However, biotin, epitope tags, and fluorophores are somewhat notoriously large in size, cell impermeable, and may adversely affect pharmacological activity relative to a parent compound by sterically disrupting key interactions between the photoprobe and the target biological macromolecule.

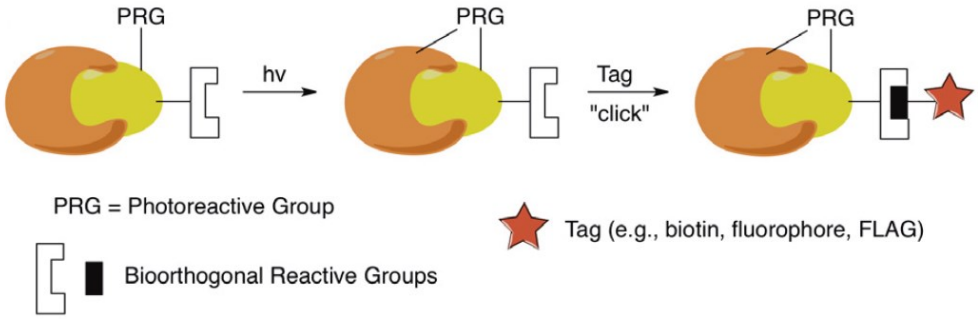


**Scheme 2.6.** Tandem photoaffinity labeling-bioorthogonal conjugation chemical proteomics strategy. (Lapinsky, 2012. Reprinted with permission from *Bioorg. Med. Chem.* **2012**, *20*, 6237-6247. Copyright 2012, Elsevier).

In order to overcome the disadvantages previously noted, tandem photoaffinity labeling-bioorthogonal conjugation has emerged as a powerful chemical proteomics strategy within the past decade (Lapinsky, 2012) (Scheme 2.6). In this strategy, a terminal alkyne or an aliphatic azide is incorporated into the structure of photoprobes to serve as a 'clickable' handle / chemical reporter. Following the formation of a covalent probe-target complex after photoirradiation (Step 1, Scheme 2.6), a variety of tags such as biotin, fluorophores, or FLAG peptide can be

subsequently attached specifically to the terminal alkyne or aliphatic azide functional group within the photoprobe *via* bioorthogonal conjugation reactions, e.g., copper-catalyzed Huisgen 1,3-dipolar cycloaddition (Rostovtsev *et al.*, 2002) ('click' reaction) or Staudinger-Bertozzi ligation (Saxon and Bertozzi, 2000) (Scheme 2.7). Due to their relatively small size, biological compatibility, and easy incorporation, terminal alkynes and aliphatic azides as bioorthogonal chemistry handles (Sletten and Bertozzi, 2009) have proven to be highly advantageous given they are less likely to potentially disrupt key ligand-target interactions during irreversible labeling experiments.

**Staudinger-Bertozzi Ligation**

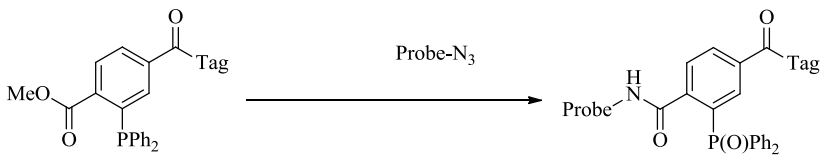


**2.21** **2.22**

**Copper-catalyzed Huisgen 1,3-dipolar cycloaddition**

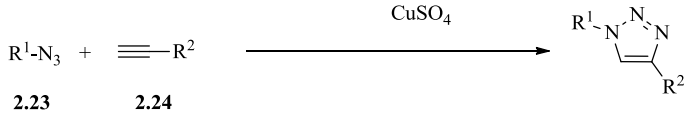


**2.23** **2.24** **2.25**

$R^1$ = Probe or Tag
$R^2$ = Tag or probe

**Scheme 2.7.** Bioorthogonal conjugation chemistries traditionally employed during tandem photoaffinity labeling-bioorthogonal conjugation.

It should be noted that the only apparent disadvantage associated with tandem photoaffinity labeling-bioorthogonal conjugation is that yields of the bioorthogonal conjugation

step (Step 2, Scheme 2.6) can vary in different systems. In particular, it has been reported that higher yields are frequently observed when copper-catalyzed Huisgen 1,3-dipolar cycloaddition is employed in the bioorthogonal conjugation step during protein labeling experiments versus Staudinger-Bertozzi ligation (Speers *et al.* 2003). Despite this variability in bioorthogonal conjugation yield, the noteworthy advantages of tag flexibility, high-throughput analysis, and *in vivo* use makes this strategy the current method of choice for analysis of probe-labeled products after photoaffinity labeling.

## 2.4. Binding Ensemble Profiling with (f)Photoaffinity Labeling (BEProFL)

It is well established that the basis of medicinal chemistry, pharmacophore research, structure-activity relationships, and drug development is fundamentally linked to understanding how a ligand interacts in a 3-D manner with its biological macromolecular target(s) at the molecular level (Keiser *et al.*, 2010; Leach *et al.*, 2010; Nicholls *et al.*, 2010). In particular, combining tandem photoaffinity labeling-bioorthogonal conjugation with LC-MS and molecular modeling studies represents a powerful experimental approach towards determining the 3-D structure of a ligand-target complex. This approach features a synergism of chemical biology, proteomics, and computational chemistry in order to determine key ligand-target binding interactions and conformational preferences for both the biological target and the ligand being analyzed. In turn, high quality 3-D information from this combined experimental approach aids in validation or refinement of biological target molecular models to be used for computer-aided drug discovery and development (e.g., virtual / *in silico* screening, structure-based drug design) (Sliwoski *et al.*, 2013). In particular, this merged experimental approach was coined "BEProFL

(binding ensemble profiling with (f)photoaffinity labeling)" in the late 2000s by the Petukhov group (He et al., 2009).

In BEProFL, a ligand-target covalent complex formed *via* photoaffinity labeling is subjected to traditional proteomic experiments in order to determine the biological target's amino acid(s) directly attached to the photoprobe (Scheme 2.8). Such results are then coupled with computational studies of the probe-target complex in order to unambiguously map the binding pose(s) and site(s) of probe compounds within the biological target.

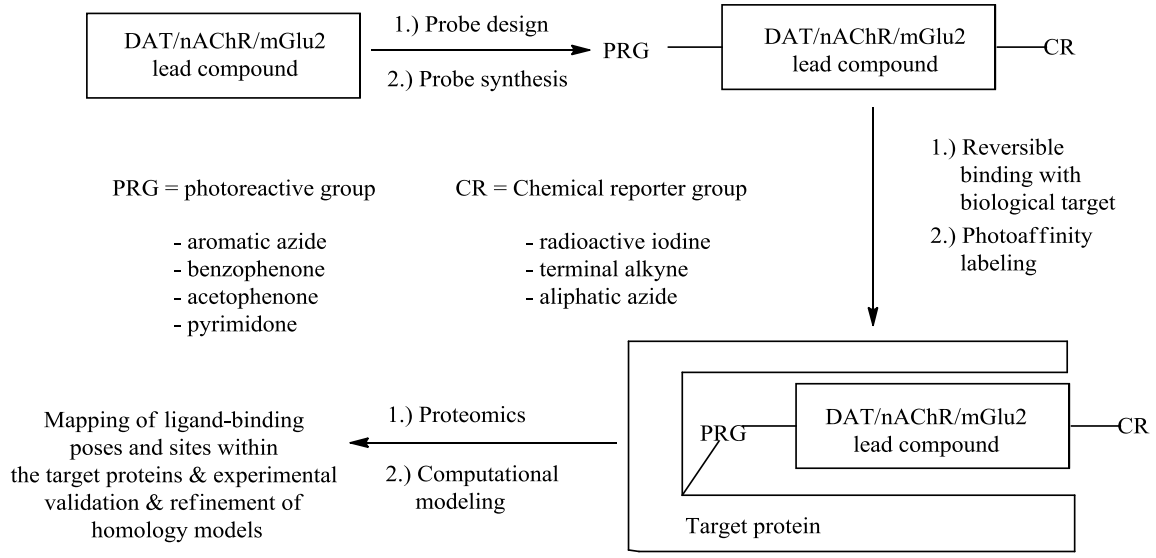


**Scheme 2.8.** Binding ensemble profiling with (f)photoaffinity labeling (BEProFL) towards mapping the binding sites and poses of drug candidates within the DAT, nAChRs, and mGlu2.

With the aim of gaining 3-D structural information on how promising drug candidates interact with either the DAT, nAChRs, or mGlu2 at the molecular level, the Lapinsky lab has a history of pursuing the BEProFL strategy towards understanding the binding modes and poses of promising CNS therapeutics, particularly anti-addiction lead compounds (Lapinsky *et al.*, 2009, 2011, and 2012). In particular, the work described in this dissertation features derivatization of known DAT inhibitors, nAChR antagonists, and mGlu2 PAMs as lead compounds for BEPRoFL studies *via* modifying the synthesis of these compounds to include a photoreactive group and a

chemical reporter. Following pharmacological evaluation in order to identify suitable probe candidates for irreversible labeling experiments *via* collaboration, photoprobes are then subjected to traditional photoaffinity labeling with a biological target of interest. Analysis of the photoprobe-target covalent adduct then proceeds *via* a multi-step sequential protocol of bioorthogonal conjugation, fragmentation, LC-MS/MS, and coupling with computational modeling in order to specifically determine the binding sites and poses of DAT/nAChR/mGlu2 lead compounds within their corresponding biological target. Continued utilization of this innovative and collaborative research approach is expected to experimentally validate and refine current DAT, nAChR, and mGlu2 homology models, thus aiding in the discovery and development of therapeutics associated with these proteins.

## CHAPTER THREE

## 3. Known Synthetic Approaches to Lead Compounds

### 3.1. Review of Synthetic Approaches for Pyrovalerone as a Lead Compound for DAT Photoprobe Design

Heffe developed the first chemical synthesis of racemic pyrovalerone (**(±)-1.19**) in 1962 *via* Stevens rearrangement of an unsymmetrical olefin (Heffe, 1964) (Scheme 3.1). This approach begins with displacement of 2-bromo-4'-methylacetophenone (**3.1**) with pyrrolidine, followed by formation of the hydrobromide salt of 2-pyrrolidino-4'-methylacetophenone (**3.2**). This salt was then converted to the free base and subsequently reacted with allylbromide to provide *N*-allyl-*N*-(*p*-methylphenacyl)-pyrrolidinium bromide (**3.3**) in 85% yield. Subsequent Stevens rearrangement using basic conditions resulted in key migration of the allyl group alpha to the ketone to provide unsaturated pyrovalerone analog **(±)-3.4** in 89% yield. Final hydrogenation of the alkene analog then provided racemic pyrovalerone **(±)-1.19** in 91% yield.

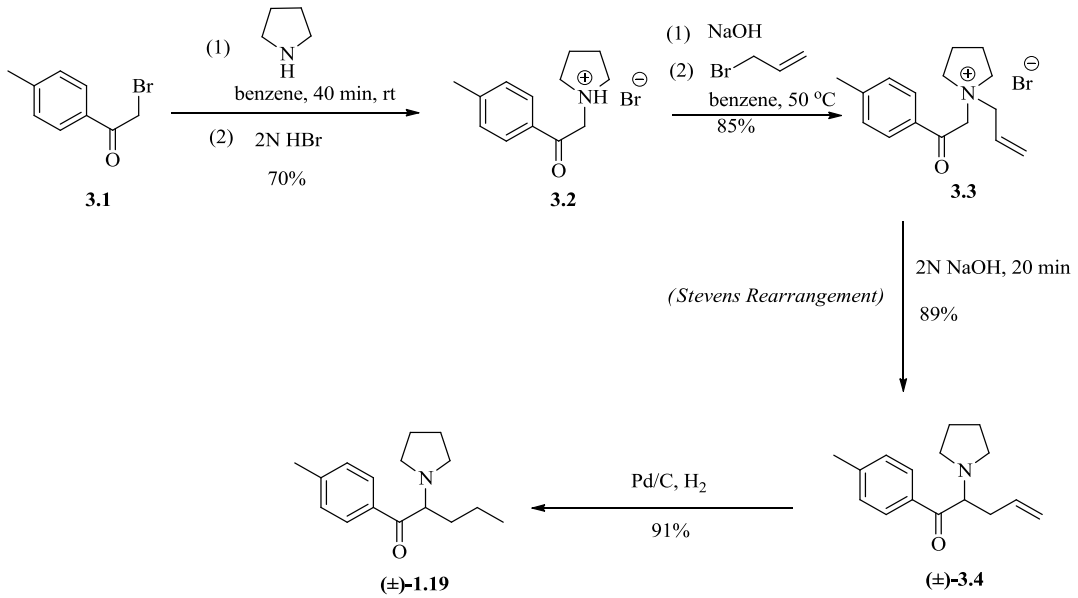


**Scheme 3.1.** Synthesis of racemic pyrovalerone (**(±)-1.19**) according to Heffe, 1962.

Lancelot and coworkers reported a short, simple three-step route for accessing thiophene analogs of pyrovalerone in 1992 (Lancelot *et al.*, 1992) (Scheme 3.2). In their approach, 2,5-disubstituted thiophene ketones (**3.6**) were first obtained by Friedel-Crafts acylation of 2-substituted thiophenes (**3.5**) with a mixed anhydride of valeric acid. Subsequent α-bromination and nucleophilic displacement with a variety of cycloaliphatic amines (e.g., pyrrolidine, piperidine, morpholine) readily provided substituted thiophene analogs of pyrovalerone (**(±)-3.7**) in yields between 60 to 80%.

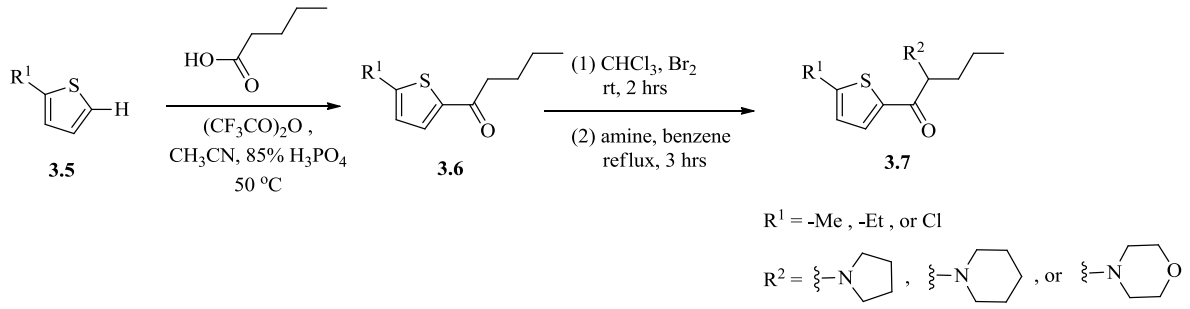


**Scheme 3.2.** Synthesis of racemic thiophene analogs of pyrovalerone (**(±)-3.7**) reported by Lancelot and coworkers (Lancelot *et al.*, 1992).

Meltzer and coworkers described a synthesis of pyrovalerone analogs for their evaluation as potential drug candidates to treat cocaine abuse (Meltzer *et al.*, 2006). In particular, their synthesis of pyrovalerone was accomplished analogous to the strategy previously reported by Lancelot for thiophene analogs (see Scheme 3.2). Beginning with 1-(4-methylphenyl)pentan-1-one (**3.8**), which was synthesized by Friedel-Craft's acylation of toluene with valeryl chloride, α-bromination followed by nucleophilic displacement with pyrrolidine provided racemic pyrovalerone (**(±)-1.19**) in 68% yield (Scheme 3.3). Enantiomerically pure forms of pyrovalerone (**(2*R*)-1.19**) and **(2*S*)-1.19**) were then accessed *via* diastereomeric salt resolution of racemic pyrovalerone using either dibenzoyl-*D*- or *L*-tartaric acid and multiple recrystallizations in ethanol. In particular, assignment of the stereochemistry associated with the resolved

enantiomers of pyrovalerone was achieved by x-ray crystallography of the tartarate-based diastereomeric salts.

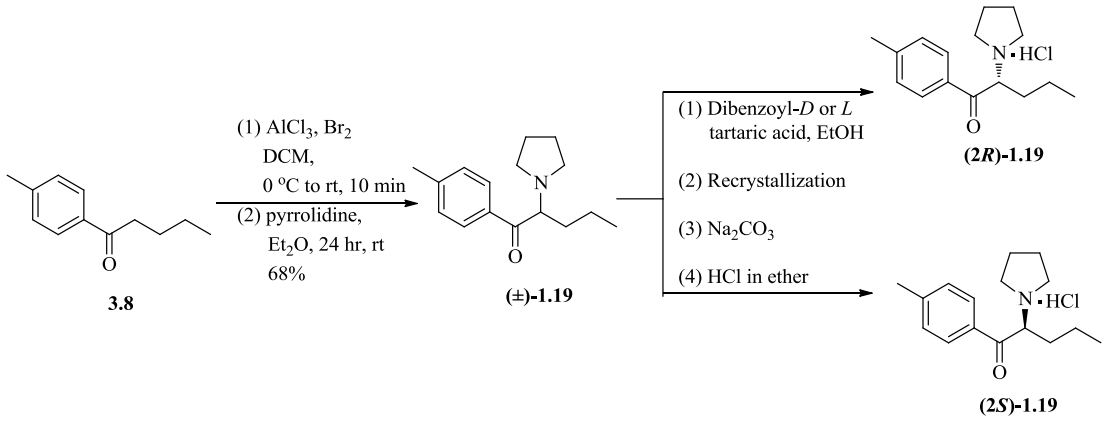


**Scheme 3.3.** Synthesis of optically pure (2*R*) and (2*S*)-pyrovalerone *via* diastereomeric salt formation (Meltzer *et al.*, 2006).

As a precursor to accessing pyrovalerone analogs for pharmacological evaluation *via* the established synthetic methodology, Meltzer and colleagues also reported the synthesis of a variety of substituted aryl ketones (**3.10**) by reacting *n*-BuMgCl with a variety of substituted aryl nitriles (**3.9**), followed by acidic hydrolysis (Scheme 3.4) (Meltzer *et al.*, 2006).

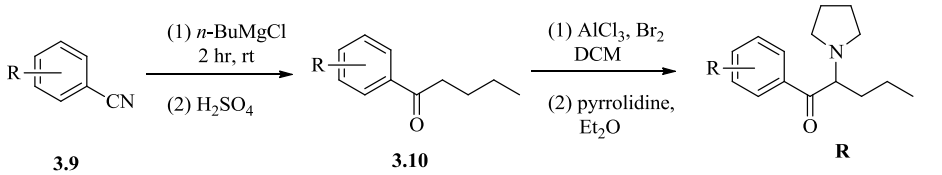


**(±)-1.21** 2-$CH_3$
**(±)-1.22** 3-$CH_3$
**(±)-1.27** 3-I
**(±)-1.28** 3,4-$Cl_2$
**(±)-3.11** 4-$CF_3$
**(±)-3.12** 3,4-$(OCH_3)_2$

**Scheme 3.4.** Synthesis of some pyrovalerone analogs stemming from substituted aryl nitriles (Meltzer *et al.*, 2006).

## 3.2. Review of Synthetic Approaches for Bupropion as a Lead Compound for DAT and nAChR Photoprobe Design

The first reported preparation of racemic bupropion (**(±)-1.20**) was described by Mehta in 1975 (Mehta, 1975) (Scheme 3.5). This work began with reaction of *m*-chlorobenzonitrile (**3.15**) with ethylmagnesium bromide, followed by imine hydrolysis, to give *m*-chloropropiophenone (**3.16**), which upon α-chlorination with sulfuryl chloride provided *m*-chloro-α-chloropropiophenone (**(±)-3.17**) in 90% yield. Subsequent nucleophilic displacement of the α-iodo group (generated *in situ* from **(±)-3.17**) with *t*-butylamine in acetonitrile, followed by treatment with HCl, in turn provided racemic bupropion hydrochloride (**(±)-1.20**). Alternatively, the synthesis of racemic bupropion hydrochloride could also be achieved through *m*-chloro-α-bromopropiophenone (**(±)-3.18**) in an analogous manner; however, *in situ*-generation of an iodo leaving group was not needed in this case.

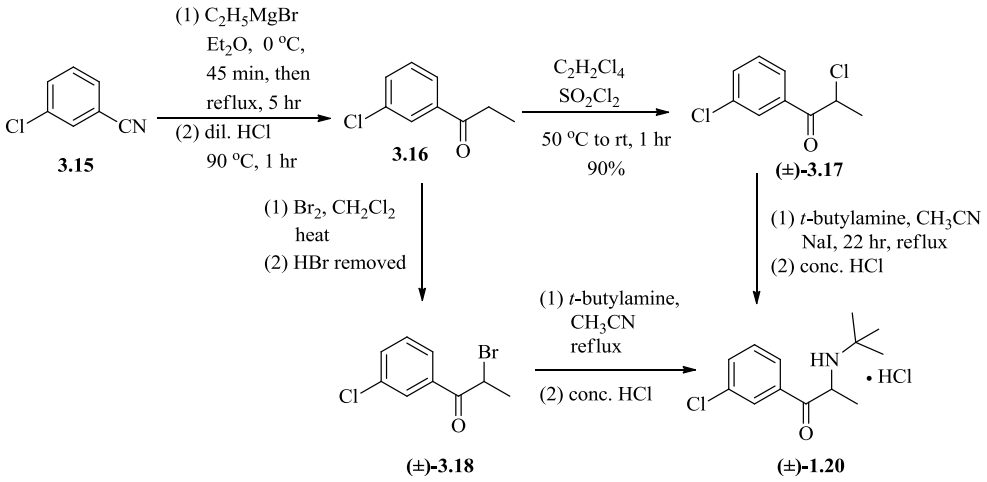


**Scheme 3.5.** Synthesis of racemic bupropion hydrochloride (**(±)-1.20**) reported by Mehta, 1975.

In order to address problems associated with long displacement reaction times of *t*-butylamine with α-bromo intermediate **(±)-3.18**, further modifications to the Mehta route were made by Perrine and co-workers, who employed *N*-methyl-2-pyrrolidine (NMP) as a solvent

during the *N*-alkylation step instead of acetonitrile (Scheme 3.6). This slight change in solvents during displacement of α-bromo leaving group significantly reduced the reaction time to 10 minutes and increased the overall yield to 80% (Perrine *et al.*, 2000). Additionally, Hamad and coworkers used a similar method with slightly different reaction conditions to synthesize bupropion for the generation of tripartate codrugs of naltrexone and 6β-naltrexol with hydroxybupropion as potential alcohol abuse and smoking cessation agents (Hamad *et al.*, 2006).

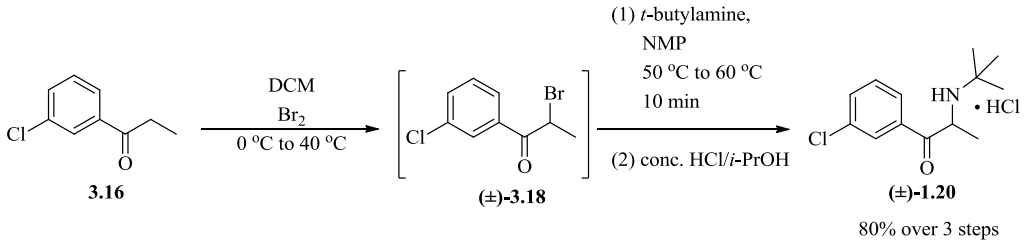


**Scheme 3.6.** Racemic bupropion hydrochloride (**(±)-1.20**) synthesis reported by Perrine *et al.*, 2000.

Slight improvements were made to Scheme 3.6 in order to avoid evaporation of $CH_2Cl_2$ after bromination and NMP after *N*-alkylation. As a result, Dabak and coworkers accomplished a much safer, one-pot synthesis of bupropion by using excess *tert*-butylamine as a solvent and a reactant in the bromination and *N*-alkylation steps, respectively, thus circumventing the need to evaporate additional solvents (Dabak *et al*., 2004) (Scheme 3.7). In this process, 3'-chloropropiophenone (**3.16**) was first dissolved in excess *tert*-butylamine as a solvent, and then bromine was added dropwise in order to directly isolate the desired free base of bupropion. The HCl salt of racemic bupropion (**(±)-1.20**) was then obtained by treating the free base with 1N HCl and isopropyl alcohol (yields were not disclosed).

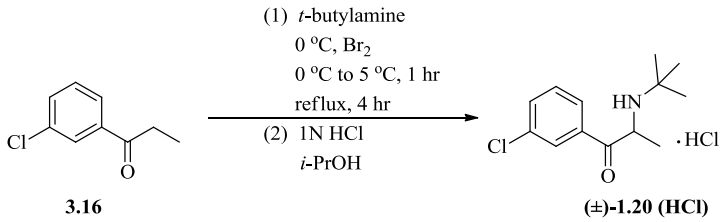


**3.16** **(±)-1.20 (HCl)**

**Scheme 3.7.** One-pot synthesis of racemic bupropion hydrochloride (**(±)-1.20**) according to Dabak *et al*., 2004.

Deshpande and colleagues reported additional changes in bupropion synthesis reaction conditions that were much simpler, economical, and applicable in an industrial setting (Deshpande *et al*., 2008). In this work, the α-bromination of *m*-chloropropiophenone (**3.16**) was carried out using liquid bromine in water, instead of DCM. In particular, the entrapment of HBr gas released during the bromination step required special equipment when the reaction was carried out in dichloromethane, thus making the process inconvenient at an industrial level. However, when the reaction was carried out in water, the HBr side-product remained in water, thus allowing the resulting product to be easily isolated *via* simply partitioning with an organic solvent.

In order to avoid using toxic liquid bromine during a scalable synthesis of racemic bupropion, Reddy and co-workers reported *N*-bromosuccinimide (NBS) as an efficient brominating agent by carrying out the halogenation reaction in the presence of *p*-toluenesulfonic acid (*p*-TSA) as a catalyst (Scheme 3.8) (Reddy *et al*., 2010). *m*-Chloro-α-bromopropiophenone (**3.18**) was then reacted with *t*-butylamine in a mixture of *N*-methyl-2-pyrrolidine (NMP) and toluene to obtain the free base of bupropion, which was subsequently converted to the HCl salt (**(±)-1.20**) in 75% overall yield and 100% purity.

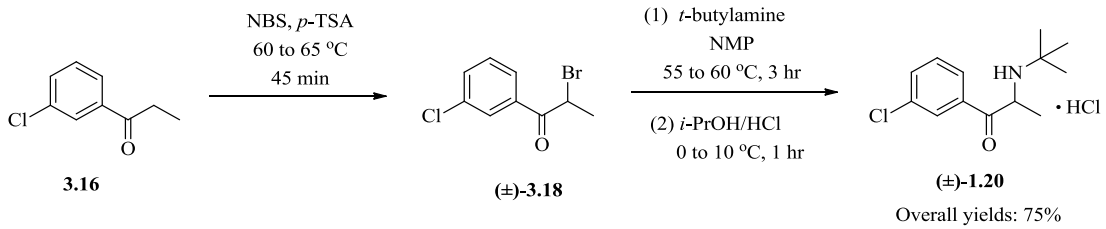


**Scheme 3.8.** Commercially scalable synthesis of racemic bupropion (**(±)-1.20**) reported by Reddy *et al*., 2010.

As a logical application to this known chemistry, Carroll and coworkers synthesized a number of racemic bupropion analogs as fumarate salts (**(±)-1.35 - (±)-1.43**) for investigation as potential pharmacotherapies for cocaine addiction and smoking cessation (Carroll *et al*., 2009 and 2010). In particular, the general reaction scheme for synthesizing these analogs is outlined in the Scheme 3.9 and utilizes strategies and reactions conditions previously discussed in this chapter.

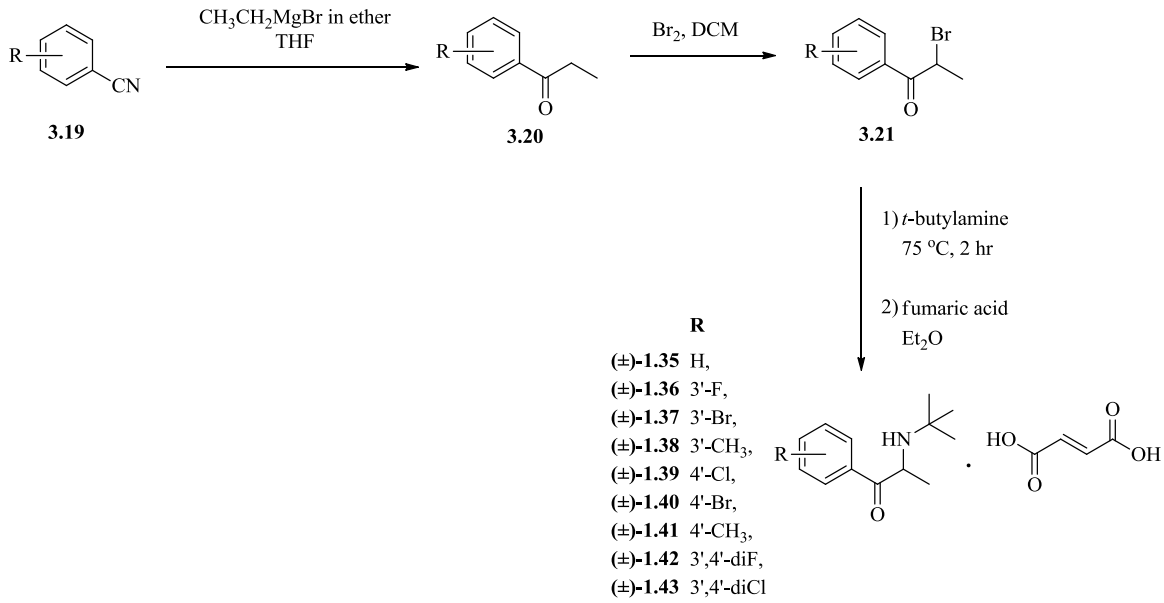


**Scheme 3.9.** General synthetic scheme reported by Carroll and coworkers (Carroll *et al*., 2009 and 2010) for the synthesis of bupropion analogs (**(±)-1.35 - (±)-1.43**).

In a lengthy, but rather unique process as 'proof-of-principle', Amarante and coworkers reported a seven-step synthesis of racemic bupropion in 27% overall yield using Morita-Baylis-

Hillman (MBH) adducts (Scheme 3.10) (Amarante *et al*., 2008 and 2011). This method began with MBH acid **(±)-3.28**, derived in almost quantitative yield using 3 steps starting from 3-chlorobenzaldehyde (**3.25**). MBH acid **(±)-3.28** was then treated with ethyl chloroformate to form a carbonate derivative, which was converted to an acyl azide intermediate by reaction with sodium azide. The acylazide intermediate was then subjected to Curtius rearrangement by refluxing in toluene for 2 hours, followed by 12 hr reflux in water to obtain acyloin **(±)-3.29** in 45% yield. In turn, acyloin **(±)-3.29** was subjected to keto-reduction, deprotection, and selective α-oxidation to provide α-hydroxyketone derivative **(±)-3.32**, which was treated with triflic anhydride and 2,6-lutidine at -78ºC to form the corresponding α-ketotriflate derivative *in situ*, which upon stirring at -40ºC followed by *t*-butylamine addition provided racemic bupropion (**(±)-1.20**) in 75% yield.

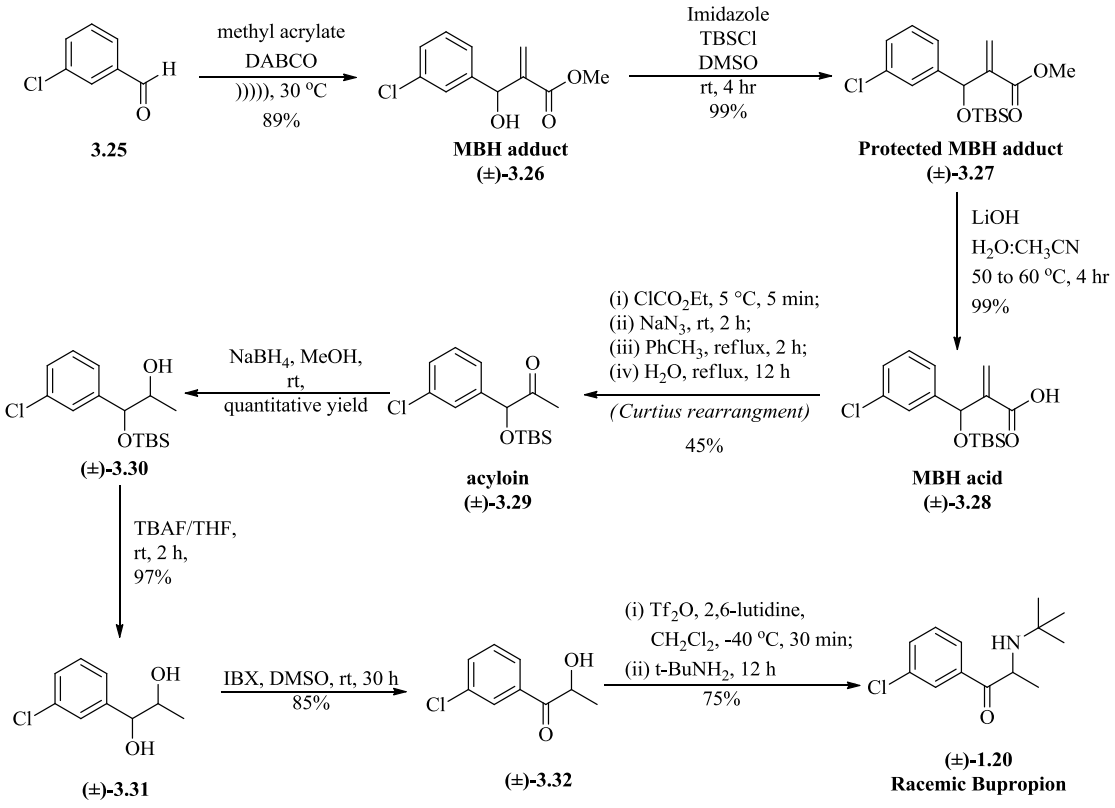


**Scheme 3.10.** Synthesis of racemic bupropion (**(±)-1.20**) from Morita-Baylis-Hillman adduct **3.26** (Amarante *et al*., 2008 and 2011).

Synthesis of the optically pure enantiomers of bupropion has been accomplished *via* several methods. Musso and colleagues attempted to resolve racemic bupropion (**(±)-1.20**) *via* recrystallization of the corresponding diastereomeric salts by employing chiral acids such as (+)- and (-)-tartaric acid (Musso *et al*., 1993). However, this conventional resolution method was unsuccessful because of the ability of chiral aminoketones to racemize in the absence of strong acids (Berrang *et al*., 1982). In order to overcome this problem, these researchers first reduced the aminoketone moiety of racemic bupropion to the corresponding chiral amino alcohols (**(±)-*threo*-1.55** and **(±)-*erythro*-1.55**) using $BH_3$-THF (Scheme 3.11) (Musso *et al*., 1993 and 1997).

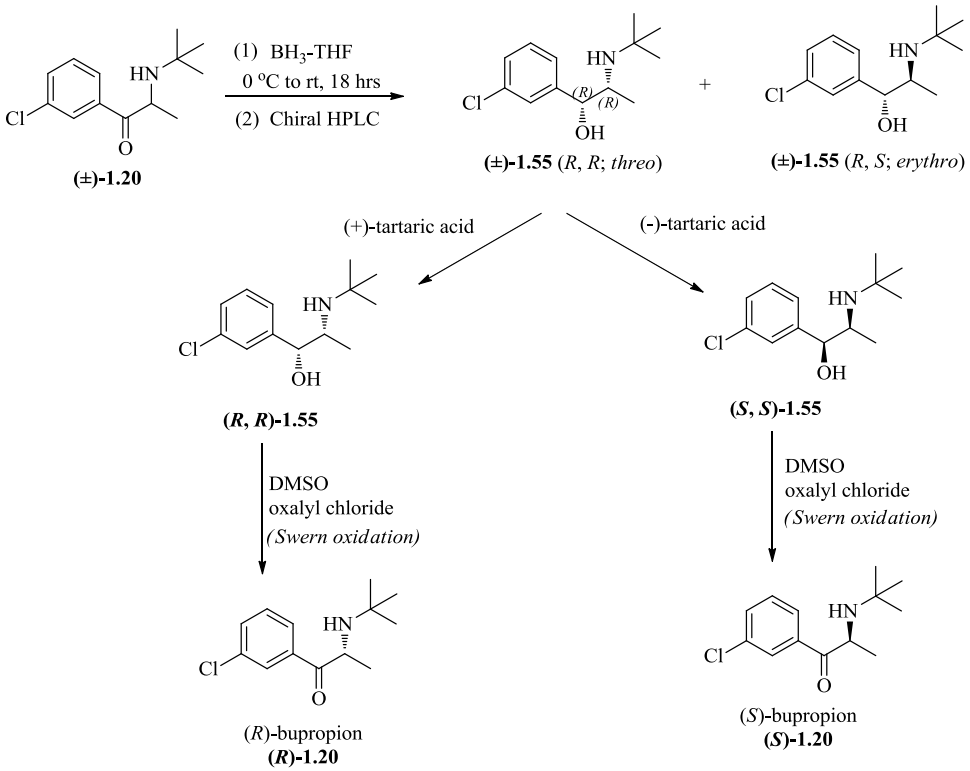


**Scheme 3.11.** Synthesis of optically-pure bupropion enantiomers *via* aminoalcohol derivative **1.55** (Musso *et al*., 1993).

Racemic amino alcohols **(±)-1.55** (*R*,*R*; *threo*) and **(±)-1.55** (*R*,*S*; *erythro*) were then separated *via* preparative liquid chromatography (Musso and Mehta, 1981). Subsequent resolution of **(±)-1.55** (*R*,*R*; *threo*) was accomplished *via* distereomeric salt formation with (+)-

and (-)-tartaric acid, followed by recrystallization. Swern oxidation of the corresponding enantiomeric amino alcohols then successfully provided both enantiomers of bupropion in approximately 50% yield each.

However, the most efficient route for obtaining the enantiomers of bupropion is *via* asymmetric synthesis employing readily accessible enantiopure α-hydroxy ketones (*S*)-**3.32** and (*R*)-**3.32** as key intermediates, which are synthesized *via* Sharpless's asymmetric dihydroxylation of silyl enol ether **3.35** (Scheme 3.12) (Fang *et al*., 2000). During this work, 3'-chlorophenyl propanone (**3.16**) was first converted to its corresponding enolate by treatment with LDA and trapped by reaction with TBSCl. The resulting enantiopure α-hydroxyphenylketones (*S*)-**3.32** and (*R*)-**3.32** were then obtained *via* Sharpless's asymmetric dihydroxylation in 82% overall yield with 98% and 99% ee, respectively. Subsequently, enantiopure (*R*)-α-hydroxyphenylketone (*R*)-**3.32** was converted to ketotriflate intermediate (*R*)-**3.36**, which was then subjected to nucleophilic attack by *t*-butylamine, proceeding with complete inversion of chemistry to provide (*S*)-bupropion in 98% ee (Scheme 3.13). In turn, (*R*)-bupropion was obtained in an analogous manner starting with **(*S*)-3.32**.

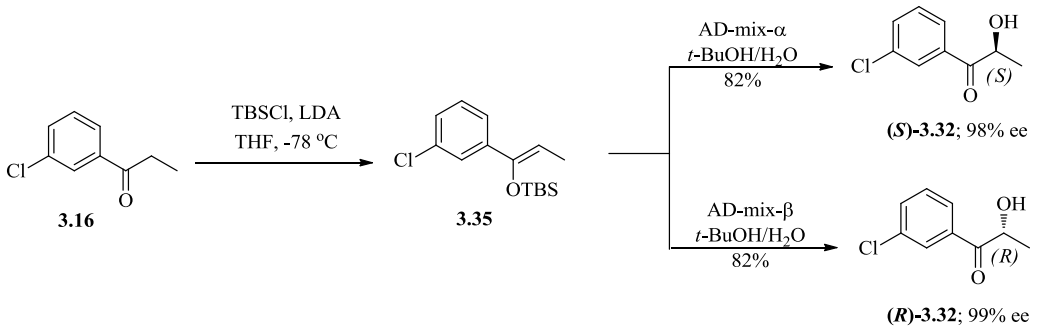


**Scheme 3.12.** Asymmetric synthesis of enantiomerically pure keto alcohols **(*S*)-3.32** and **(*R*)-3.32** *via* Sharpless dihydroxylation (Fang *et al*., 2000).

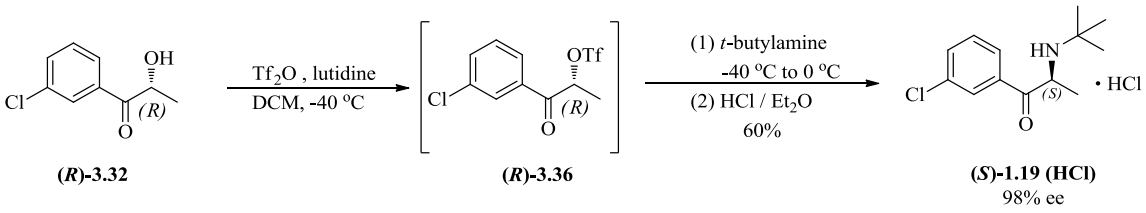


**Scheme 3.13.** Asymmetric synthesis of bupropion enantiomer **(*S*)-1.19** according to Fang *et al*., 2000.

## 3.3. Review of Synthetic Approaches for (2*S*,3*S*)-Hydroxybupropion as a Lead Compound for DAT and nAChR Photoprobe Design

Since the free base and HCl salt of bupropion are prone to undergo racemization readily, considerable attention has been focused on the synthesis of bupropion's most active and conformationally stable metabolite, (2*S*,3*S*)-hydroxybupropion (**1.54**). In particular, treatment of (*R*)-α-hydroxyketone **(*R*)-3.32** with trifluoroacetic anhydride, followed by reaction with 2-amino-2-methyl-1-propanol, gives (2*S*,3*S*)-hydroxybupropion **1.54** in 98% ee (Scheme 3.14) (Fang *et al*., 2000). Additionally, attempts to isolate optically pure (2*S*,3*S*)-hydroxybupropion (**(2*S*,3*S*)-1.54**) *via* resolution of diastereomeric salts employing chiral acids have been reported. However, asymmetric synthesis remains the most widely used route for accessing pure (2*S*,3*S*)-hydroxybupropion (Fang *et al*., 2001 and 2002; Jerussi *et al*., 2000). Furthermore, Lukas and other groups have reported a wide range of (2*S*,3*S*)-hydroxybupropion analogs following a similar synthetic strategy (Carroll, Blough, *et al*., 2011; Carroll, Muresan, *et al*., 2011; Lukas *et al*., 2010).

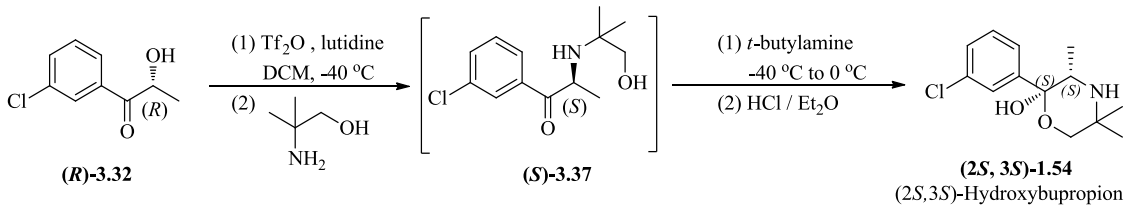


**Scheme 3.14.** Asymmetric synthesis of (2*S*,2*S*)-hydroxybupropion (**1.54**) reported by Fang *et al*., 2000.

## 3.4. Review of Synthetic Approaches for Racemic BINA as a Lead Compound for mGlu2 Photoprobe Design

Biphenyl-carboxylic acid indanone **(±)-1.71** and several of its analogs emerged from SAR efforts based on a combination of compounds identified from high throughput screening (Bonnefous *et al*., 2005; Pinkerton *et al*., 2005). These compounds were synthesized following the synthetic route outlined in Scheme 3.15 (Pinkerton *et al*., 2006; Sidique *et al*., 2012).

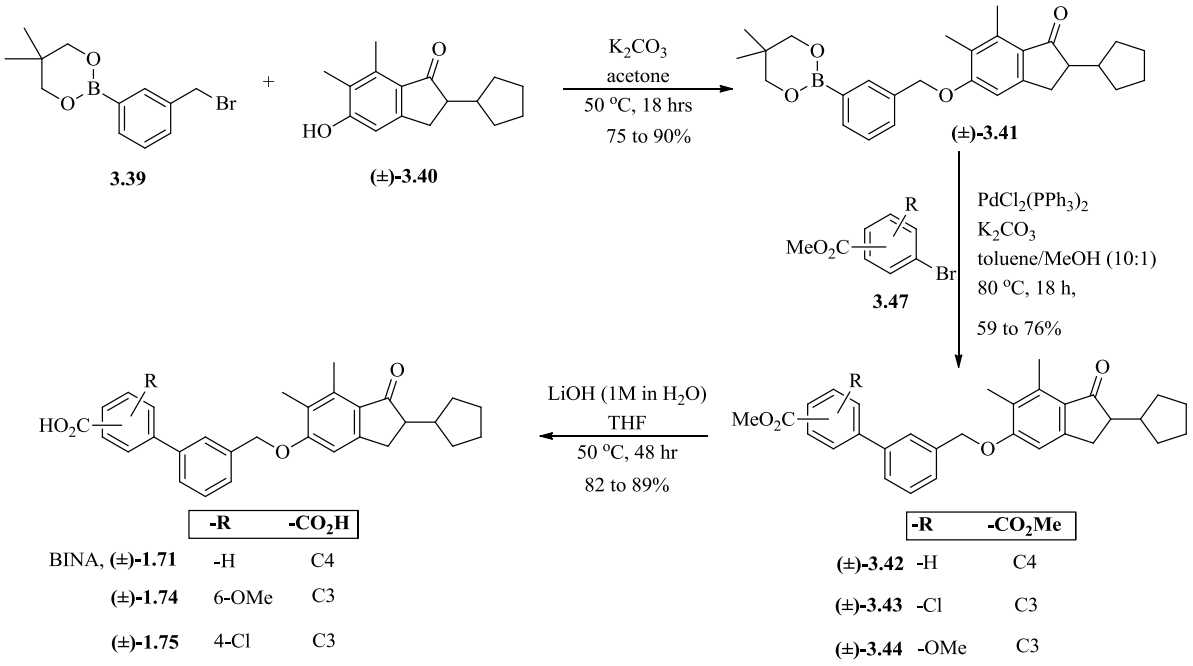


**Scheme 3.15.** Synthesis of BINA (**(±)-1.71**) and some of its analogs (Bonnefous *et al*., 2005).

As depicted, Bonnefous and coworkers (Bonnefous *et al.*, 2005) first synthesized boronic ester intermediate **(±)-3.41** *via O*-alkylation of known hydroxy indanone **(±)-3.40** (Woltersdorf *et al*., 1977; DeSolms *et al*., 1978) with 2-[3-(bromomethyl)phenyl]-5,5-dimethyl-1,3,2-dioxaborinane (**3.39**) (Scheme 3.15). Subsequent Suzuki coupling of benzyl ether **(±)-3.41** with substituted aryl bromides (**3.47**) then gave ester derivatives **(±)-3.42 – (±)-3.44**. The final products (**(±)-1.71**, **(±)-1.74**, **(±)-1.75**) were then obtained by ester hydrolysis using aqueous LiOH.

In an alternate scheme, Galici and colleagues synthesized BINA in 9 steps with 16% overall yield (Galici *et al*., 2006). This approach featured initial synthesis of 3-toluoyl zinc bromide **3.49** by treating 3-bromotoluene with *n*-butyl lithium and zinc chloride (Scheme 3.16). Simultaneously, 4-ethoxycarbonylphenyl-bis(triphenylphosphine) palladium (**3.52**) was synthesized from ethyl 4-iodobenzoate and bis(triphenylphosphine)palladium dichloride. According to conditions in a previous report (Klein *et al*., 1998), compounds **3.49** and **3.52** were then combined to form key building block **3.50** (Scheme 3.16).

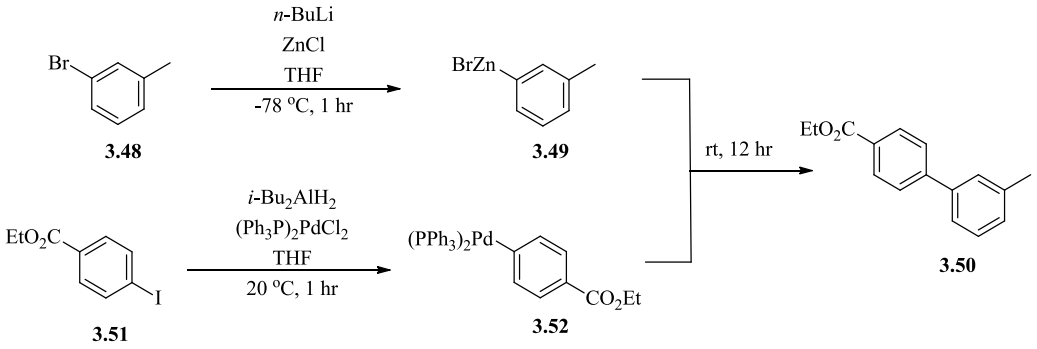


**Scheme 3.16.** Synthesis of intermediate **3.50** for the preparation of BINA (Galici *et al*., 2006).

Free radical bromination of biphenyl **3.50** using *N*-bromosuccinimide in the presence of AIBN produced benzyl bromide **3.53** in 86% yield (Scheme 3.17). Subsequent *O*-alkylation of known hydroxy-indanone **(±)-3.40** (Bonnefous *et al*., 2005; DeSolms *et al*., 1978; Woltersdorf *et al*., 1977) with benzyl bromide **3.53** then provided ether **(±)-3.42**, whose ester was hydrolyzed with 2N NaOH to provide BINA (**(±)-1.71**) in 63% yield.

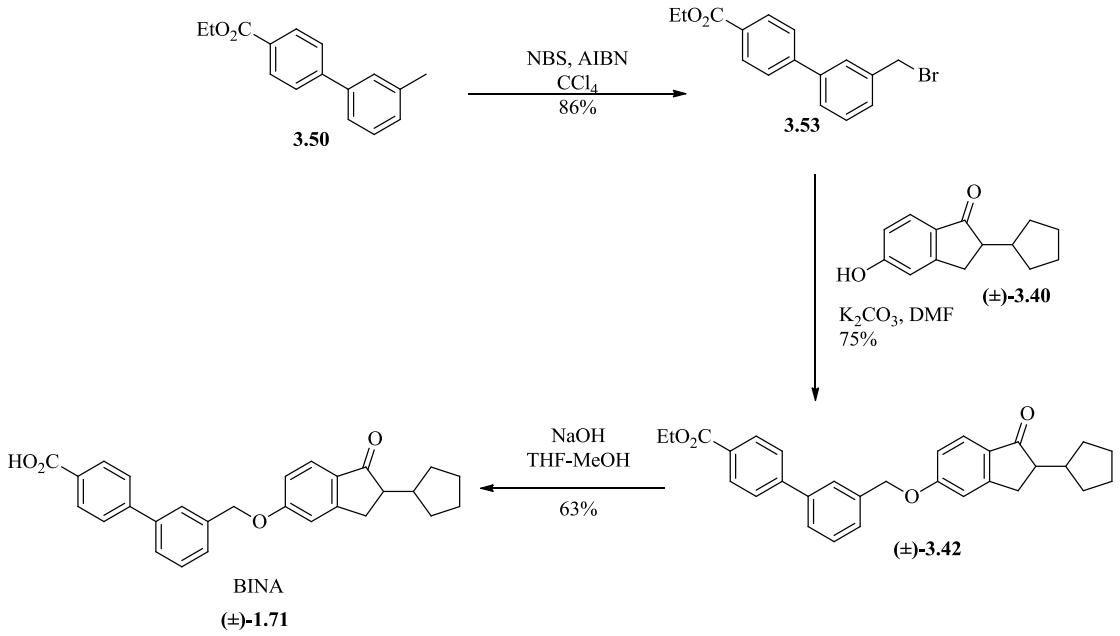


**Scheme 3.17.** Synthesis of BINA (**(±)-1.71**) according to Galici *et al*., 2006.

## 3.5. Review of Synthetic Approaches for 1,5-Substituted Pyridones as Lead Compounds for mGlu2 Photoprobe Design

Using a high throughput screening FLIPR (fluorimetric image plate reader) assay, Addex Pharmaceuticals discovered several 1,5-substituted pyridones as moderately potent and selective mGlu2 PAMs (Cid *et al*., 2010). Further SAR was developed by sequential modification of substituents at positions 1 and 5 of the pyridone ring, from which compound **1.89** emerged as the most potent mGlu2 PAM from their studies (Cid *et al*., 2010; Imogai *et al*., 2006). Compound **1.89** was synthesized *via* a simple 3-step synthetic route depicted in Scheme 3.18. First, bromohydroxy pyridine **3.55** was *N*-alkylated with benzyl bromide **3.56** to provide pyridone **3.57** in 79% yield. Subsequent Suzuki coupling with the *para* boronic acid derivative of anisole (**3.58**) then provided mGlu2 PAM **1.89** in 30% yield.

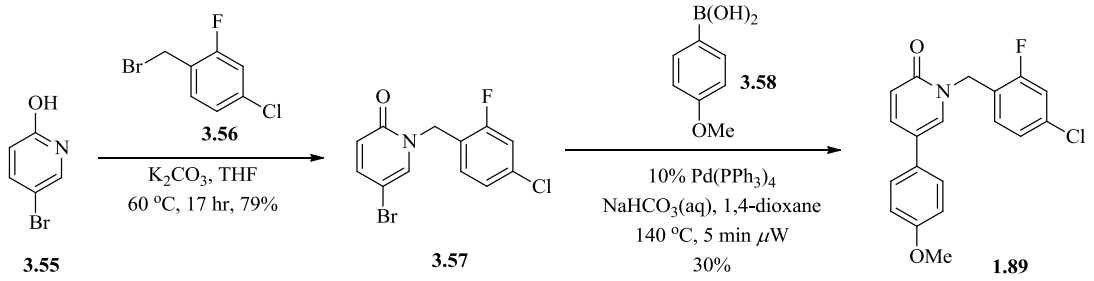


**Scheme 3.18.** Synthesis of pyridone lead compound **1.89** by Cid *et al*., 2010.

Several compounds with modifications at the 5-phenyl substituent could then be synthesized as shown in Scheme 3.19. For example, deprotection of methyl ether **1.89** using $BBr_3$ provided phenol analog **3.59** in 83%. Subsequent *O*-alkylation under microwave conditions then provided acetophenone **1.93** in 34% yield.

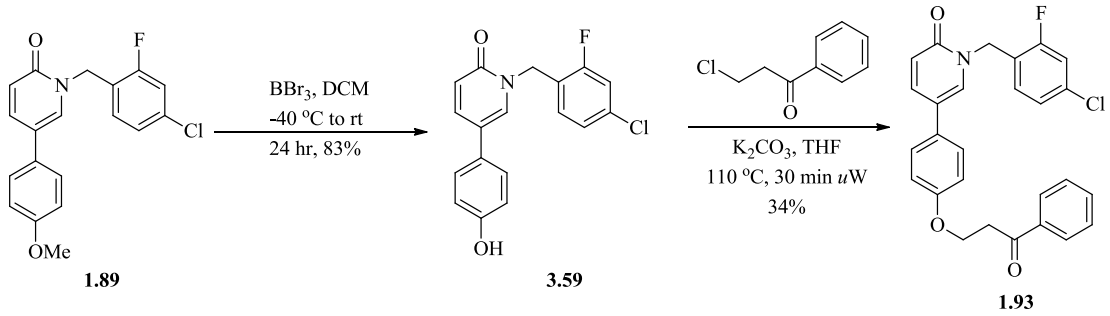


**Scheme 3.19.** Synthesis of an acetophenone-containing pyridone (**1.93**) reported by Cid *et al*., 2010.

# CHAPTER FOUR

## 4. Statement of Research Problems

### 4.1. Current Knowledge Gaps

#### 4.1.1. DAT Structure-Function Knowledge Gap

Despite the emergence of several LeuT-based DAT homology models (e.g., Koldsoe *et al.*, 2013; Stockner *et al.*, 2013; Seddik *et al.*, 2013; Gedeon *et al.*, 2010; Huang and Zhan, 2007; Huang *et al.*, 2009; Indarte *et al.*, 2008) and the identification of a plethora of DAT-interactive compounds (reviewed in Runyon and Carroll, 2006), details regarding the transport inhibition mechanism, structural elements, conformational states, and ligand-binding sites associated with the DAT remain poorly understood. In particular, it is still not clear how the DAT discriminates substrates (e.g., dopamine, amphetamines), inhibitors (e.g., cocaine, bupropion, methylphenidate, GBR-12909, pyrovalerone), highly abused compounds (e.g., cocaine, amphetamines, cathinones), and therapeutic compounds (e.g., bupropion, methylphenidate) at the molecular level. Furthermore, establishment of the non-covalent interactions that dictate a given DAT ligand's pharmacological profile (e.g., affinity, selectivity, potency, behavioral phenotype, etc.) have yet to be achieved. Answers to these research questions remain unknown principally due to the absence of human DAT x-ray crystal structures and incomplete structure-function characterization of proposed ligand-binding sites within the DAT. In turn, this lack of 3-D DAT structural knowledge significantly compromises our understanding of the neuronal mechanisms underlying numerous disease states associated with the DAT (reviewed in Vaughan and Foster, 2013 and Mash, 2008), which include Parkinson's disease, Alzheimer's disease, normal aging, schizophrenia, Tourette's syndrome, Lesch-Nyhan disease, attention deficit hyperactivity disorder (ADHD), obesity, depression, and stimulant abuse.

### 4.1.2. mGlu2 Structure-Function Knowledge Gap

Analogous to DAT ligands, positive allosteric modulators of mGlu2 represent promising drug candidates for a number of disease states including schizophrenia (Fell *et al.*, 2012), drug abuse (Moussawi and Kalivas, 2010), impaired cognition, and depression (Goeldner *et al.*, 2013). Likewise, there are a multitude of compounds known to modulate mGlu2 in a positive allosteric manner (reviewed in Trabanco *et al.*, 2011; Trabanco and Cid, 2013). However, very few studies have been disclosed with respect to structure-function characterization of allosteric sites within mGlu2 (Lundstrom *et al.*, 2011; Schaffhauser *et al.*, 2003). Furthermore, and in very sharp contrast to the DAT field where homology modeling is well established, currently there is only one recently disclosed low-resolution homology model of the transmembrane domain of mGlu2 (Radchenko *et al.*, 2014).

Collectively, challenges associated with developing mGlu2 PAMs for clinical use (e.g., biased signaling (Kenakin, 2012), molecular switches (Wood *et al.*, 2011), desired higher selectivity with durable pharmacological effects under repeated dosing (Trabanco and Cid, 2013) can be attributed to the affinity and / or cooperativity of mGlu2 PAMs, which are dictated by specific non-covalent interactions within distinct mGlu2 binding sites. However, our understanding of mechanistic and / or conformational mGlu2 structure-function relationships is grossly lacking when compared to other well-studied mGlu receptor subtypes such as mGlu5 (Dalton *et al.*, 2014). Additionally, experimental strategies that further refine and validate the recently disclosed mGlu2 homology model are sorely needed. In short, elucidation of the molecular determinants for mGlu2 allosteric modulator affinity, selectivity, potency, and cooperativity represents a key knowledge gap that must be resolved if we are to understand the inherent complexities of these compounds that hinder their rational development into

therapeutics. Furthermore, and much like the DAT inhibitor field, transition of the design and development of mGlu2 PAMs from a ligand- to a structure-based perspective would represent a major advance and no doubt spur further research.

### 4.1.3. nAChR Structure-Function Knowledge Gap

The implication of neuronal nAChRs in mediating reward, tolerance, dependence, and sensitization-producing effects associated with drugs of abuse (De Biasi and Dani, 2011; Hendrickson *et al.*, 2013; Rahman, 2013) has led to multiple drug discovery efforts in finding ligands targeting nAChRs for smoking cessation (Crooks *et al.*, 2014), alcohol abuse (Rhaman and Prendergast, 2012), and psychostimulant addiction (Pubill *et al.*, 2011). Bupropion's anti-depressant and smoking-cessation effects have been mainly attributed to its inhibition of the DAT and NET; however, there is increasing evidence that bupropion non-competitively inhibits several nAChR subtypes, particularly $\alpha4\beta2$ and $\alpha3\beta4$, and modulation of these targets may also contribute to the drug's therapeutic efficacy (Arias, 2009 and 2010; Carroll *et al.*, 2014). Additionally, varenicline (Chantix) is a $\alpha4\beta2$ nAChR partial agonist FDA approved for smoking cessation, thus providing additional substantial evidence of involvement of this receptor subtype in nicotine addiction (Coe *et al.*, 2005; Crunelle *et al.*, 2010). Despite its status as an FDA-approved drug for major depressive disorder, seasonal affective disorder, and aid to help people stop smoking by reducing cravings and other withdrawal effects, the molecular determinants of how bupropion interacts with its major drug targets, including the DAT and select nAChR subtypes, remains unknown. As a result, in order to identify improved therapeutics targeting these proteins, it is important to understand, in detail, how clinically approved ligands like bupropion interact with binding sites within the DAT and select nAChR subtypes. This

information is currently lacking in the nAChR field due to the unavailability of high-resolution x-ray crystal structures of human α4β2 and α3β4 nAChR subtypes. Despite predictions that bupropion binds near the middle of the nAChR ion channel between M2-6 and M2-13 from molecular dynamics and docking simulations (Arias *et al.*, 2009; Arias, 2010), currently there is a dearth of direct experimental evidence regarding the location of bupropion-binding sites within the DAT and select nAChR subtypes.

### 4.2. Long-Term Goal of This Research

The long-term goal of this research is to understand how the pharmacology profile (i.e., affinity, selectivity, potency, behavioral phenotype, etc.) of clinically relevant lead compounds (e.g., bupropion, BINA) is dictated by the three-dimensional interactions that occur when these compounds non-covalently interact with their major drug targets (e.g., the DAT, mGlu2, and select nAChR subtypes) at the molecular level. This information is expected to facilitate improved rational, structure-based manipulation and discovery of lead compounds in order to obtain improved therapeutics for numerous disease states associated with these proteins, including drug abuse and addiction.

### 4.3. Overall Objective of This Research Dissertation

The overall objective of this research dissertation was to rationally design and chemically synthesize irreversible chemical probes based on promising anti-addiction lead compounds (e.g., pyrovalerone, bupropion, BINA) in order to map the binding sites and poses of these compounds within their proposed major drug targets (i.e., the DAT, α4β2 nAChR, α3β4 nAChR, or mGlu2).

## 4.4. Central Hypothesis of This Research Dissertation

The central hypothesis of this research dissertation was that appropriate anti-addiction lead compounds (i.e., pyrovalerone, bupropion and BINA) could be rationally derivatized without significant alteration in their pharmacological activity to contain both a photoreactive group (PRG) and a tag for application of a "Binding Ensemble Profiling with (f)Photoaffinity Labeling (BEProFL)" experimental approach (He *et al.*, 2009). In particular, BEProFL sequentially and rationally couples photoaffinity labeling, chemical proteomics, and computational molecular modeling in order to map the binding poses and sites of lead compounds within a target protein (Scheme 4.1).

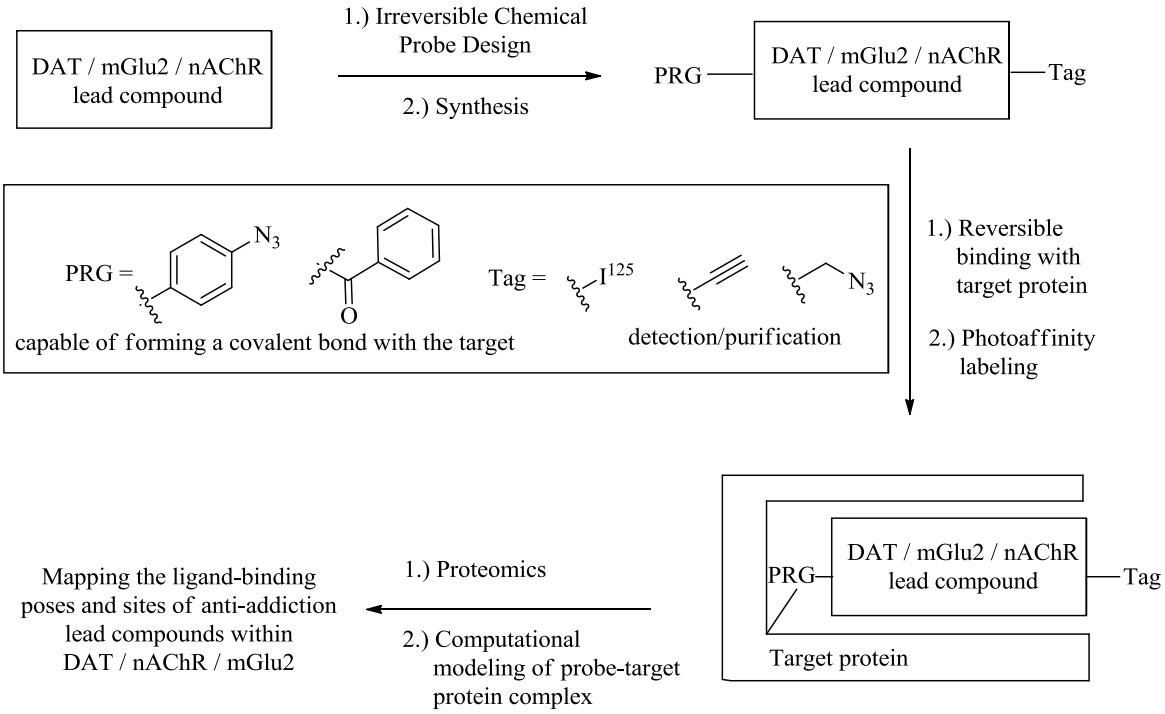


**Scheme 4.1.** Schematic representation of the BEProFL experimental approach in order to map the ligand-binding poses and sites of anti-addiction lead compounds within the human DAT, mGlu2, or a select nAChR subtype.

BEProFL has been successfully used to understand the binding modes of histone deacetylase (HDAC) inhibitors as epigenetic modulators (Abdelkarim *et al.*, 2013; Vaidya *et al.*, 2012; Neelarapu *et al.*, 2011, He *et al.*, 2009) and to probe the microenvironment of fatty acid

amide hydrolase (FAAH) as a drug target implicated for the development of pain therapeutics (Saario *et al.*, 2012). In general, the coupling of photoaffinity labeling, chemical proteomics, and computational molecular modeling *via* BEProFL has been proposed as a unique and powerful way to analyze the binding of ligands to their macromolecular drug targets (He *et al.*, 2009). In particular, BEProFL expands the data typically obtained in protein x-ray crystallography. Furthermore, this experimental approach serves as a viable alternative towards understanding protein structure-function relationships at the molecular level when co-crystallization of a target protein with a ligand of interest has failed, as is frequently the case with membrane-bound proteins such as transporters and GPCRs. Importantly, the ligand-binding poses determined by BEProFL are determined in solution, thus the "snapshots" generated by this experimental approach arguably reflect the dynamic nature of ligand-macromolecular drug target conformations in a more accurate manner. Finally, BEProFL has the potential to guide future ligand optimization and is poised to contribute to multiple disciplines including molecular modeling, validation, development, and application of computer-aided drug design methods, especially those for rapid prediction of ligand-protein interactions such as scoring and docking.

### 4.5. Rationale of This Research Dissertation

The rationale that underlies this research dissertation is that, once it is known how promising anti-addiction lead compounds (e.g., pyrovalerone, bupropion, BINA) interact with their major drug targets (i.e., the DAT, α4β2 nAChR, α3β4 nAChR, or mGlu2) in a three-dimensional manner at the molecular level, this information can then be rationally exploited to manipulate lead compounds into drug candidates *via* structure-based drug design in order to improve therapeutic outcomes associated with disease states linked to these proteins.

Additionally, detailed, 3-D structural information generated by application of the BEProFL approach to the DAT, α4β2 nAChR, α3β4 nAChR, or mGlu2 is also expected to aid in the building, refinement, and experimental validation of reliable computer-generated molecular models of these proteins, thus providing an improved template for powerful, structure-based *in silico* / virtual screening of millions of candidate therapeutic compounds for drug discovery and development (e.g., see Nolan *et al.*, 2011; Indarte *et al.*, 2010; Mahasenan *et al.*, 2011).

### 4.6. Rational Design of Pyrovalerone-Based Photoprobes for DAT Structure-Function Studies

As previously introduced in Section 1.4.2.2.3., pyrovalerone ((±)-**1.19**; PV; Scheme 4.2) is a high affinity and potent DAT inhibitor (DAT $K_i$ = 21.4 ± 4.6 nM; DA uptake $IC_{50}$ = 52.0 ± 20 nM) and NET inhibitor (NET $K_i$ = 195 ± 26 nM; NE uptake $IC_{50}$ = 28.3 ± 8.1 nM) with little effect on serotonin trafficking (SERT $K_i$ = 3770 ± 560 nM; SER uptake $IC_{50}$ = 2780 ± 590 nM) (pharmacology data from Meltzer *et al.*, 2006). Additionally, being structurally similar to rapidly emerging, highly abusive designer cathinones (also called "bath salts"; Simmler *et al.*, 2013; Zawilska and Wojcieszak, 2013; Bonano *et al.*, 2014; Glennon, 2014), pyrovalerone possesses significant abuse and addiction liability. In particular, pyrovalerone is known to produce psychostimulant effects similar to amphetamine in humans (Holliday *et al.*, 1964) and is a schedule V controlled substance in the United States.

As previously mentioned, the binding site(s) and conformational preference(s) for pyrovalerone in its major drug target, the DAT, are largely unknown, thus representing a significant knowledge gap in terms of understanding the molecular basis of addiction and abuse associated with this compound and related cathinones. This prompted rational design and

synthesis of photoprobes based on PV (Lapinsky *et al.*, 2009) in order to address this important knowledge gap *via* DAT structure-function studies.

It should be noted that the overwhelming majority of DAT irreversible ligands prior to this dissertation were designed such that the photoreactive aryl azide group was some distance away from the inhibitor pharmacophore *via* the employment of conformationally flexible, variable-length methylene linkers (e.g., see [$^{125}$I]-MFZ-2-24, **4.7** in Figure 4.1 where the azide functional group is predicted to be 10.5 Angstroms from the tropane pharmacophore nitrogen as calculated by molecular modeling (Zhou *et al*., 2001; Parnas *et al.*, 2008). In particular, the covalent point of photoprobe attachment to a protein is directly dictated by the location of the photoreactive functional group with respect to a ligand pharmacophore. As a result, when a photoreactive functional group is somewhat removed from a ligand's pharmacophore by means of a conformationally flexible, variable-length methylene linker, adduction to a target protein may occur at a residue near, but not at, a direct ligand pharmacophore-protein contact point. As a result, employment of conformationally flexible, variable-length methylene linkers in irreversible chemical probe design strategy creates distinct disadvantages when trying to definitively map the amino acids of a ligand-binding pocket or optimally model a photoprobe-protein complex *via* BEProFL. Furthermore, prior to this dissertation the overwhelming majority of known DAT irreversible ligands (see Figure 4.1 for examples) were based on tropane-containing compounds (e.g., see Carroll *et al.*, 1992; Agoston *et al.*, 1997; Lever *et al.*, 2005; Newman *et al.*, 2006; Vaughan *et al.*, 2007; Murthy *et al.*, 2008; Dahal *et al*., 2014) or their conformationally flexible piperidine- or piperazine-based analogues (e.g, see Grigoriadis *et al.*, 1989; Sallee *et al.*, 1989; Dutta, *et al.*, 2001; Cao *et al.*, 2004), whereas non-tropane DAT irreversible ligands had yet to be examined.

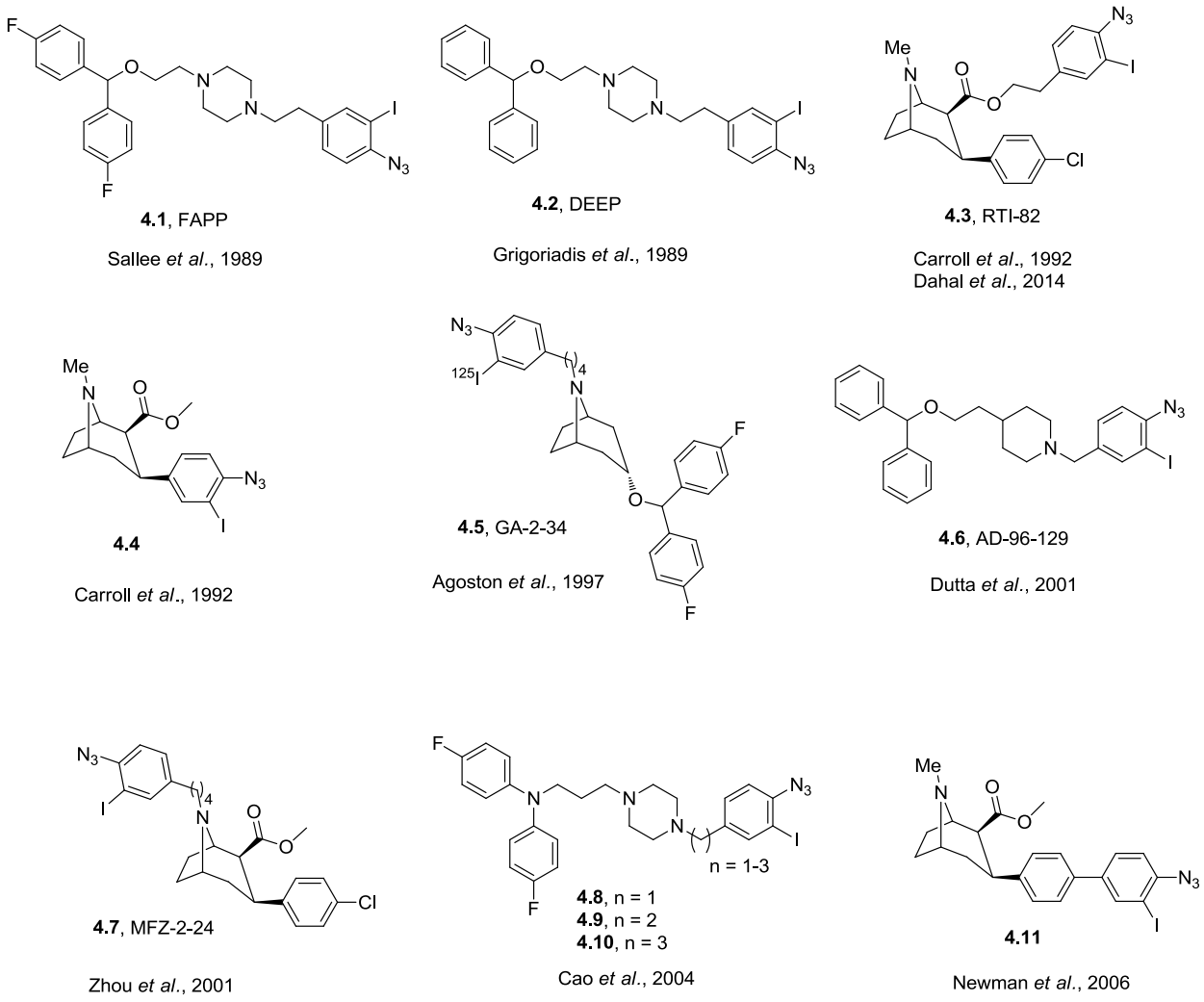


**Figure 4.1.** Photoaffinity probes based on tropane-, piperidine- and piperizine-containing DAT inhibitors featuring aromatic 4-azido-3-iodo ring substituted motif.

Given these previous literature observations, this research dissertation features the design and synthesis of three compact photoprobes (**(±)-4.16** – **(±)-4.18**) based on PV as a non-tropane DAT inhibitor (Scheme 4.2). These novel photoprobes were significantly unique at the time of their design and chemical synthesis given they represented the very first examples of compact non-tropane photoaffinity ligands for DAT structure-function studies wherein the photoreactive group was placed directly on the inhibitor pharmacophore (i.e., bearing no linker functionality). Such photoprobes are expected to covalently attach to an amino acid residue directly within the

pyrovalerone-binding pocket of the DAT and also result in a more conformationally restricted photoprobe-DAT complex in 3-D hDAT molecular modeling studies. In particular, PV photoprobes **(±)-4.16 – (±)-4.18** in Scheme 4.2 were rationally designed based on known DAT binding affinity data for a host of pyrovalerone analogs previously reported in the chemical literature.

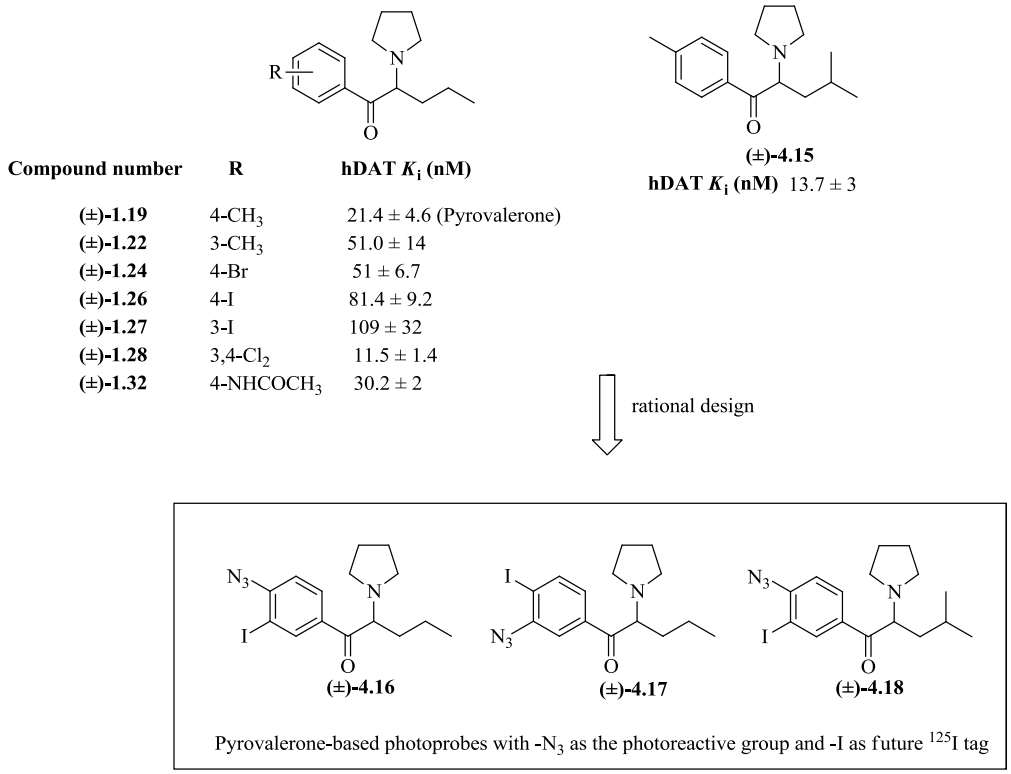


**Scheme 4.2.** Rational design of azido-iodo-PV photoprobes **(±)-4.16 – (±)-4.18** as photoaffinity ligands for DAT structure-function studies *via* isosteric replacement.

According to the DAT binding affinity SAR reported (Meltzer *et al.*, 2006), the 3- and 4-positions of the phenyl ring of PV appeared tolerable to a variety of functional groups in terms maintaining significant DAT binding affinity for potential photoprobe design (see Section 1.4.2.2.3 for more pyrovalerone SAR details). Initially, dichloro-substituted pyrovalerone analog **(±)-1.28** (Scheme 4.2) was chosen as an appropriate lead compound for DAT photoprobe design given this compound displayed the highest DAT binding affinity within a series of aromatic ring-

substituted analogs pharmacologically tested by Meltzer and coworkers (DAT $K_i$ for **(±)-1.28** = 11.5 ± 1.4 nM; Meltzer *et al.*, 2006). Target DAT photoprobes **(±)-4.16** to **(±)-4.18** were then rationally designed by systematic replacement of the chlorine atoms within lead compound **(±)-1.28** with a photoreactive azide and iodine atom at the 3- and 4-positions (Scheme 4.2). The iodine atom was viewed as a classical bioisostere of the chlorine atom (Brown, 2014) given both atoms are halogens and lipophilic. Additionally, the location of the iodine atoms within the target photoprobes were also viewed as natural positions for potential substitution with an $^{125}I$ radiotracer for detection during proteomic experiments. Furthermore, the photoreactive aryl azide functional group has been suggested as an isostere for aryl chlorine atoms given both functional groups display similar hydrophobic properties (He *et al.*, 2009).

Additionally, target pyrovalerone-based DAT photoprobe **(±)-4.16** features a photoreactive aryl azide functional group at the 4-position of the aromatic ring and an iodine atom at the 3-position, whereas these functional groups are flip-flopped in target photoprobe **(±)-4.17** (Scheme 4.2). The rational design behind these particular photoprobes is that each probe could potentially covalently react with a different amino acid within the DAT pyrovalerone-binding site given their aryl azides are located at different positions on the pyrovalerone scaffold. In turn, such photoprobes would then be expected to give finer details of the DAT pyrovalerone-binding site upon microlevel characterization. In particular, target DAT pyrovalerone-based photoprobe **(±)-4.18** was pursued as a potential higher DAT binding affinity, branched-side chain analog of target photoprobe **(±)-4.16** (Scheme 4.2) given the observation that branched-side chain PV analog **(±)-4.15** displays ~1.6-fold higher DAT binding affinity than pyrovalerone, which contains an *n*-propyl side chain (DAT $K_i$ for **(±)-4.15** = 13.7 ± 3 nM versus DAT $K_i$ for PV = 21.4 ± 4.6 nM; Meltzer *et al.*, 2006).

Target pyrovalerone-based DAT photoprobes **(±)-4.16** to **(±)-4.18** were synthesized as described in Section 5.1 and sent for pharmacological determination of their DAT binding affinities in N2A neuroblastoma cells. In particular, photoprobe **(±)-4.16** was characterized as a promising compound for DAT photoaffinity labeling studies given the DAT binding affinity of this compound was $\leq$100 nM and within 10-fold of parent compound **(±)-1.19** (DAT $K_i$ = 78 ± 18 nM for **(±)-4.16** versus DAT $K_i$ = 8 ± 2 nM for **(±)-1.19** represents an ~9.8-fold loss in DAT binding affinity; Lapinsky *et al.*, 2009). Finally, an $^{125}$I version of compound **(±)-4.16** was synthesized and shown to bind specifically and irreversibly to rDAT and hDAT upon UV irradiation in the absence or presence of cocaine as a competitor (Lapinsky *et al.*, 2009) (see Appendix, Section A.1).

## 4.7. Rational Design of Bupropion-Based Photoprobes for DAT and nAChR Structure-Function Studies

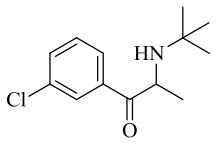


**(±)-1.20**

**Figure 4.2.** The chemical structure of bupropion (**(±)-1.20**, Wellbutrin, Zyban), a DAT, NET, and nAChR inhibitor.

Bupropion (**(±)-1.20**, Figure 4.2) is a well-known, FDA approved drug for the treatment of major depressive disorder and seasonal affective disorder (marketed as Wellbutrin; Dhillon *et al.*, 2008), and is also used to help people stop smoking by reducing cravings and other withdrawal effects (marketed as Zyban). It is well established that bupropion exerts its therapeutic effects mainly by binding to and inhibiting the DAT and NET as neurotransmitter reuptake transporters, thus increasing the synaptic concentrations of dopamine (DA) and

norepinephrine (NE), respectively, in key areas of the brain associated with these disease states (Sasse *et al.*, 2008). In addition, another widely accepted mechanism of action of bupropion is noncompetitive antagonism of select nAChR subtypes, mainly $\alpha4\beta2$ and $\alpha3\beta4$ (Arias, 2009).

It should be noted that at the initiation of this dissertation research, bupropion was disclosed as a clinically promising lead compound for potential development into a pharmacotherapeutic for cocaine and methamphetamine dependence (Elkashef *et al.*, 2008; Reichel *et al.*, 2009; Heinzerling *et al.*, 2014). As a result and concomitant to this dissertation research, a number of bupropion analogs were chemically synthesized and pharmacologically evaluated as potential treatments for cocaine and methamphetamine dependence in addition to smoking cessation (Carroll *et al.*, 2009, 2010, and 2014). However, despite its clinical success as a routinely prescribed antidepressant and smoking cessation agent, plus its significant promise as a lead compound for the development of cocaine and methamphetamine dependence therapeutics, the specific non-covalent interactions bupropion has with its major drug targets remain poorly understood. As a result, it is imperative to elucidate the high-resolution structural features of bupropion's binding sites within its major target proteins in order to improve health outcomes. In particular with respect to the DAT, high quality structure-function information would be expected to help our understanding of the molecular basis of how this protein discriminates high addiction liability compounds (e.g., methamphetamine, pyrovalerone, and cocaine) from therapeutic compounds (e.g., bupropion), despite these compounds having several shared structural features. With these thoughts in mind, bupropion-based photoprobes were rationally designed and chemically synthesized for mapping the binding sites and poses of bupropion within the DAT, the $\alpha4\beta2$ nAChR, and the $\alpha3\beta4$ nAChR (as the drug's major targets) *via* BEProFL.

### 4.7.1. Rational Design of 4-Azido-3-Iodo-Bupropion as a Photoprobe for DAT and nAChR Structure-Function Studies

As previously mentioned, Carroll and coworkers have prepared numerous bupropion analogs with various substituents on the phenyl ring, as well as side chain analogs (for detailed SAR studies of bupropion, see Section 1.4.2.2.4) (Carroll *et al.*, 2009, 2010, and 2014). Given dichloro-substituted compound **(±)-1.43** (Scheme 4.3) displayed 1.8-fold higher DAT binding affinity than bupropion, this particular bupropion analog was chosen as a lead compound for rational photoprobe design (hDAT $K_i$ = 472 ± 81 nM for **(±)-1.43**; hDAT $K_i$ = 871 ± 126 nM for bupropion; Carroll *et al.*, 2009). Once again and now based on previous DAT labeling success of structurally similar 4-azido-3-iodo-PV photoprobe **(±)-4.16** (Scheme 4.2) (Lapinsky *et al.*, 2009), which features an *n*-propyl side chain instead of a methyl side chain and a tertiary cyclic amine instead of secondary *tert*-butyl amine (when structurally compared to bupropion), target bupropion photoprobe **(±)-4.20** was rationally designed by isosteric replacement of chlorine atoms in lead compound **(±)-1.43** with a hydrophobic iodine at the 3-position and a hydrophobic, photoreactive azide at the 4-position of the aromatic ring (Scheme 4.3).

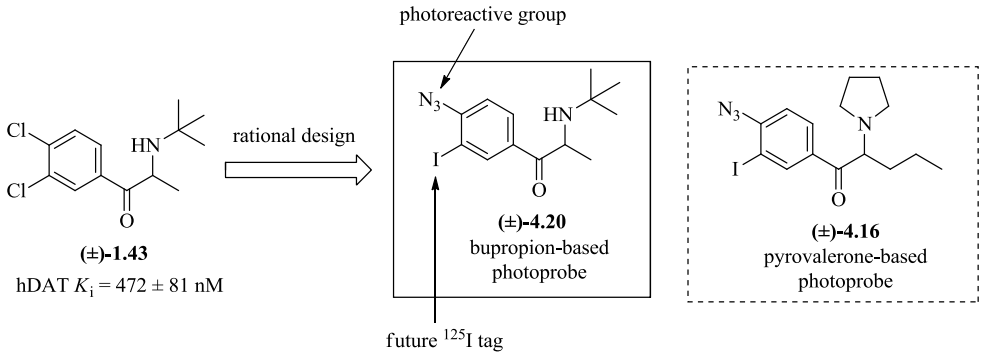


**Scheme 4.3.** Rational design of target bupropion-based photoprobe **(±)-4.20** for DAT and nAChR structure-function studies based on known analog **(±)-1.43** (Carroll *et al.*, 2009).

Target bupropion-based photoprobe **(±)-4.20** was synthesized as described in Section 5.2.1 and its hDAT and α4β2 nAChR binding affinity were determined (Lapinsky *et al.*, 2012). In particular, the DAT binding affinity of target compound **(±)-4.20** was found to be 7-fold lower than bupropion (hDAT $K_i$ = 3071 ± 497 nM for **(±)-4.20**; hDAT $K_i$ = 441 ± 174 nM for bupropion). Furthermore, (±)-bupropion inhibited **(±)-[$^{125}$I]-4.20** binding to human α4β2 nAChRs with an $IC_{50}$ value of 8.3 μM (Lapinsky *et al.*, 2012). Additionally, photoreactive bupropion analog **(±)-4.20** was characterized at different muscle nicotinic acetylcholine receptors and subjected to molecular docking studies (Arias *et al.*, 2012). In short, collected results from this work were consistent with a model where bupropion, photoreactive analog **(±)-4.20**, and thienycyclohexylpiperidine bind to overlapping sites within the lumen of muscle AChR ion channels. Furthermore, it was suggested that **(±)-4.20** represents a promising photoprobe for mapping the bupropion-binding site, especially within the resting AChR ion channel.

Even though target photoprobe **(±)-4.20** displayed modest DAT and α4β2 nAChR binding affinity when compared to bupropion, this compound still met one of our criteria for identifying candidates for preliminary photoaffinity labeling experiments; namely, no more than 10-fold lower binding affinity when compared to an appropriate parent compound. As a result, photoprobe **(±)-4.20** was advanced to preliminary DAT and nAChR photoaffinity labeling experiments. Photoprobe **(±)-[$^{125}$I]-4.20** was shown to bind covalently to hDAT expressed in cultured cells and affinity-purified, lipid-reincorporated human α4β2 neuronal nAChRs (Lapinsky *et al.*, 2012). Additionally, fragmentation studies of the **(±)-[$^{125}$I]-4.20**-nAChR binding site complex subsequently led to the identification of the exact point of covalent probe attachment to the *Torpedo* nAChR transmembrane domain (Pandhare *et al.*, 2012) (see Appendix, Section A.2 for more details).

### 4.7.2. Rational Design of 3-Iodo-Bupropion as a Potentially Photoreactive Acetophenone-Based Probe

Despite successful photoaffinity labeling results achieved with bupropion-based photoprobe **(±)-[$^{125}$I]-4.20** (Lapinsky *et al.*, 2012; Pandhare *et al.*, 2012), this compound raised a potential issue of concern. In particular, photoprobe **(±)-[$^{125}$I]-4.20** not only contains a photoreactive aryl azide group, but also is an example of an acetophenone derivative, which represents another potential photoreactive functional group (Lukac *et al.*, 2009). As a result, discrepancy could potentially arise in terms of discerning the exact point of covalent attachment of **(±)-[$^{125}$I]-4.20** to a protein after photoaffinity labeling. Therefore, in order to experimentally investigate this potential discrepancy, target compound **(±)-4.21** (Figure 4.3) was rationally designed to remove any ambiguity during proteomics after photoaffinity labeling, and also to test whether the iodo isostere of bupropion could function as a natural acetophenone-based photoprobe. Additionally, a tri-*n*-butyl stannyl version **(±)-4.22** was synthesized as described in Section 5.2.2 as a precursor to the $^{125}$I analog of **(±)-4.21** *via* radio-iodo destannylation. In short, **(±)-[$^{125}$I]-4.21** was unable to covalently label the *Torpedo* nAChR using identical photoreaction conditions to that previously described for **(±)-[$^{125}$I]-4.20** (Pandhare *et al.*, 2012), thus suggesting the aryl azide in **(±)-[$^{125}$I]-4.20** was the functional group responsible for covalent attachment of this probe to the *Torpedo* nAChR, not the acetophenone moiety (see Appendix, Section A.3).

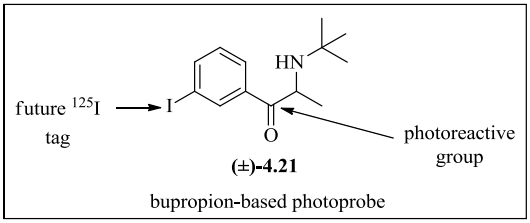


**Figure 4.3.** Compound **(±)-4.21** contains a potentially photoreactive acetophenone moiety and is the iodo isostere of bupropion.

### 4.7.3. Rational Design of 4-Azido-3-Iodo-Hydroxybupropion as a Potential DAT and nAChR Photoprobe for Structure-Function Studies

Hydroxybupropion, a major metabolite of bupropion, is believed to contribute to the antidepressant and smoking cessation activity of bupropion. In particular, it has been observed that the (2*S*,3*S*)-hydroxy enantiomer is significantly more pharmacologically active than other hydroxybupropion enantiomers in a number of behavioral-, monoamine-, and nAChR-based pharmacological assays (Damaj *et al.*, 2004 and 2010). Furthermore, hydroxybupropion displays higher potency and a longer elimination half-life than bupropion (Yeniceli *et al.*, 2011; Parekh *et al.*, 2012; Laib *et al.*, 2014). Due to its clinical significance, a number of hydroxybupropion analogs have also been pursued in the search for better drugs for treatment of nicotine addiction (Lukas *et al.*, 2010; Carroll *et al.*, 2011) (for detailed SAR studies of hydroxybupropion, see Section 1.6.4). As a result and given the previous photolabeling successes with pyrovalerone probe **(±)-[$^{125}$I]-4.16** (Lapinsky *et al.*, 2009) and bupropion probe **(±)-[$^{125}$I]-4.20** (Lapinsky *et al.*, 2012; Pandhare *et al.*, 2012), hydroxybupropion represented an additional logical scaffold for photoprobe development. In particular, it is known that racemic dichlorohydroxybupropion analog **(±)-(2*S*,3*S*)-1.62** (Scheme 4.4) is significantly more potent than (2*S*,3*S*)-hydroxybupropion in terms of dopamine uptake inhibition ($IC_{50}$ = 70 ± 20 nM for racemic **(±)-(2*S*,3*S*)-1.62**; $IC_{50}$ = 630 ± 50 nM for (2*S*,3*S*)-hydroxybupropion; binding affinities for these compounds, which are traditionally used for photoprobe design, were not reported; Lukas *et al.*, 2010) and inhibition of α3β4 nAChR function ($IC_{50}$ = 2.6 μM for racemic **(±)-(2*S*,3*S*)-1.62**; $IC_{50}$ = 11 μM for (2*S*,3*S*)-hydroxybupropion; once again, binding affinities for these compounds, which are traditionally used for photoprobe design, were not reported; Lukas *et al.*, 2010). Therefore, analogous to that previously described for rational design of pyrovalerone probe **(±)-**

**[$^{125}$I]-4.16** (Section 4.6) and bupropion probe **(±)-[$^{125}$I]-4.20** (Section 4.7.1), target bupropion metabolite photoprobe **(2*S*,3*S*)-4.23** was rationally designed using dichlorohydroxybupropion analog **(±)-(2*S*,3*S*)-1.62** as a lead compound and azido-iodo isosteric replacement (Scheme 4.4). The synthesis of target bupropion metabolite photoprobe **(2*S*,3*S*)-4.23** is described in Section 5.2.3.

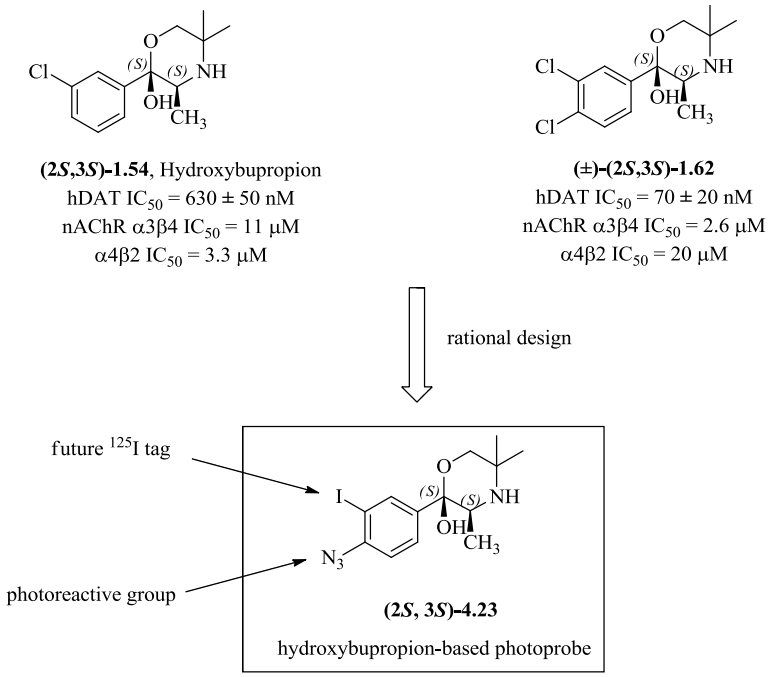


**Scheme 4.4.** Design of target photoaffinity probe **(2*S*, 3*S*)-4.23** based on known bupropion metabolites.

## 4.8. Rational Design of BINA-Based PAM Photoprobes for mGlu2 Structure-Function Studies

BINA (**(±)-1.71**, Figure 4.4) originated from extensive SAR efforts by Merck in an attempt to improve the physicochemical properties of an initial hit compound discovered *via* mGlu2 high-throughput screening (Pinkerton *et al.*, 2005). In particular, BINA is a selective, brain-penetrant, and potent mGlu2 PAM that produces long-lasting antipsychotic and anxiolytic effects in various behavioral animal models (Galici *et al.*, 2006). Furthermore, BINA has

garnered significant attention as a cocaine abuse therapeutic, wherein *in vivo* studies in rats showed that the reinforcing and rewarding effects of cocaine were inhibited by BINA (Jin *et al.*, 2010), and the compound also decreased cue-induced cocaine-seeking behavior without affecting food-seeking behavior (Dhanya *et al.*, 2011). These initial *in vivo* results strengthen BINA as a lead compound for potential development into a therapeutic entity.

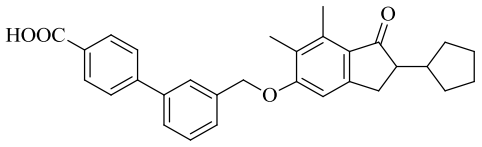


**(±)-1.71**

**Figure 4.4.** The chemical structure of BINA (**(±)-1.71**), a selective mGlu2 PAM (GTPγS binding $EC_{50}$ = 111 nM; % glutamate potentiation = 114; Bonnefous *et al.* 2005)

### 4.8.1. Rational Design of a Clickable BINA-Based mGlu2 PAM Photoprobe for Structure-Function Studies Containing an Inherent Acetophenone Photoreactive Group

In an effort to improve BINA's physicochemical properties, including bioavailability, a series of BINA analogs were reported featuring numerous substitutions on the terminal phenyl ring (Bonnefous *et al.*, 2005) (for a detailed discussion of BINA mGlu2 SAR studies, see Section 1.8.2.1.2). Analogous to bupropion, BINA contains an acetophenone moiety that could potentially represent a natural photoreactive compound analogous to other acetophenones (e.g., **4.26**; Scheme 4.5; van Scherpenzeel *et al.*, 2009 and 2010). As a result, we hypothesized that inclusion of a bioorthogonal / click chemistry handle into an appropriate BINA analog would result in a compact photoprobe for potential use in mGlu2 BEProFL studies. In this regard, BINA analog **(±)-1.74** (Scheme 4.5; mGlu2 PAM $EC_{50}$ = 111 nM) bearing a methyl ether at the 6-position was chosen as a lead compound for photoprobe design given the observation that this compound is 3-fold more potent than BINA as a mGlu2 PAM (hmGluR2 GTP-γS $EC_{50}$ = 111 nM with 114% potentiation for BINA; hmGluR2 GTP-γS $EC_{50}$ = 36 nM with 114% potentiation

for **(±)-1.74**; Bonnefous *et al.*, 2005). As a result and with the aim of retaining high mGlu2 functional potency (note: mGlu2 binding affinities are not reported for mGlu2 PAMs for rational photoprobe design, given the absence of an appropriate radioligand for competitive displacement), target photoprobe **(±)-4.25** was designed by slight extension of the 6-methoxy group within BINA analog **(±)-1.74** to a clickable propargyl ether terminal alkyne as a click chemistry handle (Scheme 4.5). In particular, target compound **(±)-4.25** bears a natural photoreactive acetophenone moiety and represents a compact photoprobe potentially capable of covalently reacting with an amino acid directly within the mGlu2 BINA-binding site. Target BINA photoprobe **(±)-4.25** was chemically synthesized as described in Section 5.3.2 and sent for pharmacological evaluation in a mGlu2 functional assay *via* the Gregory group. In turn, the mGlu2 PAM functional potency of target photprobe **(±)-4.25** measured *via* $Ca^{2+}$ mobilization assay (mGlu2 PAM $pEC_{50}$ = 6, % glutamate potentiation = 135) proved comparable to the lead compound **(±)-1.74** (mGlu2 PAM $pEC_{50}$ = 6, % glutamate potentiation = 114) in the pharmacological assay, thus representing a justifiable candidate for future photoaffinity labeling studies involving mGlu2 (for further pharmacological details, see Appendix Section A.4). In case if it is observed during photoaffinity labeling studies that the acetophenone moeity is not capable of crosslinking to the mGlu2 binding site due to steric hindrance, as an alternative, the ketone will be synthetically converted to a diazirine photoactivatable labeling group (Vervacke *et al*., 2014) which forms a more reactive carbene intermediate upon photoactivation by UV light.

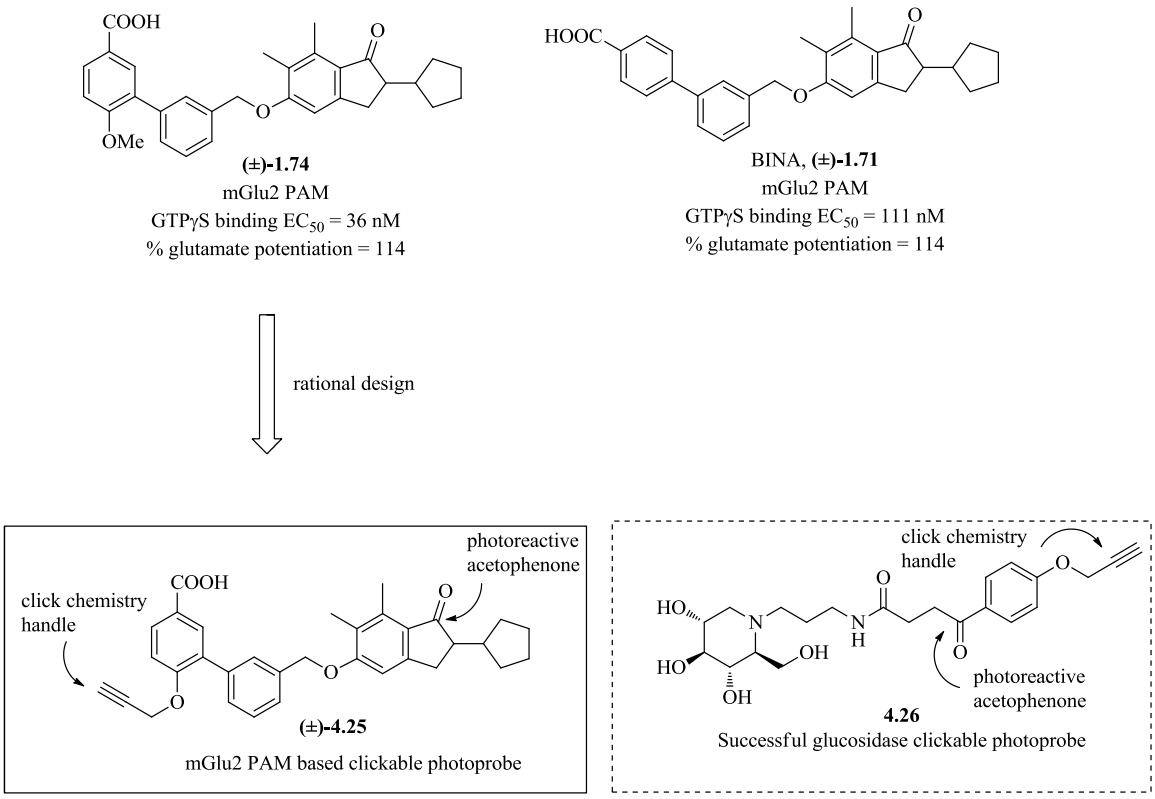


**Scheme 4.5.** Rational design of target BINA-based photoprobe **(±)-4.25** for mGlu2 structure-function studies based on known BINA analog **(±)-1.74** (Bonnefous *et al.*, 2005) and known acetophenone-alkyne clickable photoprobe **4.26** (van Scherpenzeel *et al.*, 2010).

### 4.8.2. Rational Design of a BINA-Based PAM Photoprobe for mGlu2 Structure-Function Studies That Contains an Aryl Azide as a Photoreactive Group

In an attempt to access an additional clickable compound featuring a photoreactive group at a different position on the BINA scaffold, target photoprobe **(±)-4.27** was rationally designed as a potential photoaffinity probe for mGlu2 structure-function studies (Scheme 4.6). Target photoprobe **(±)-4.27** features isosteric replacement of the hydrophobic chlorine atom in functionally potent BINA analog **(±)-1.75** with a hydrophobic aryl azide (He *et al.*, 2009). In particular, support for the design of target photoprobe **(±)-4.27** stems from the observation that BINA analog **(±)-1.75** is 4.6-fold more potent than BINA as a mGlu2 PAM (hmGluR2 GTP-γS $EC_{50}$ = 24 nM with 109% potentiation for compound **(±)-1.75**; hmGluR2 GTP-γS $EC_{50}$ = 111

nM with 114% potentiation for BINA; Bonnefous *et al.*, 2005). Furthermore, the underlying rationale for pursuit of target photoprobe **(±)-4.27** is two-fold: 1.) the aryl azide is expected to have higher probability for successful covalent attachment to mGlu2 versus the acetophenone based on previous work with bupropion-based photoprobes (see Section 4.7.1); 2.) the aryl azide photoreactive group is present at the opposite end of the molecule versus alkyne compound **(±)-4.25**, thus allowing one to potentially obtain additional information regarding the BINA-binding site in mGlu2 when these compounds are used in photoaffinity labeling studies (i.e., given the anticipated different points of covalent attachment to mGlu2 with compounds **(±)-4.25** and **(±)-4.27**). Last but not least, another unique feature in the rational design of **(±)-4.27** is the potential utilization of the ketone in the probe as a chemical reporter for attachment of detection and purification tags *via* bioorthogonal chemistry. In particular, Kiyonaka and coworkers have successfully demonstrated the use of a ketone as a bioorthogonal chemistry handle within a diazirine-based photoprobe, wherein attachment of a biotin tag to the probe was accomplished by oxime formation after photoaffinity labeling (Kiyonaka *et al.*, 2009). However, in case the ketone in **(±)-4.27**, due to steric hindrance, is inaccessible for attachment of a biotin tag during the tandem photoaffinity labeling experiment, an alternative strategy will be employed. The ketone will be converted to a diazirine photoreactive group *via* known synthetic methodology (Vervacke *et al*., 2014) and the aryl azide will instead be used as a clickable handle for attachment of a tag. The synthesis of target photoprobe **(±)-4.27** is described in Section 5.3.2.

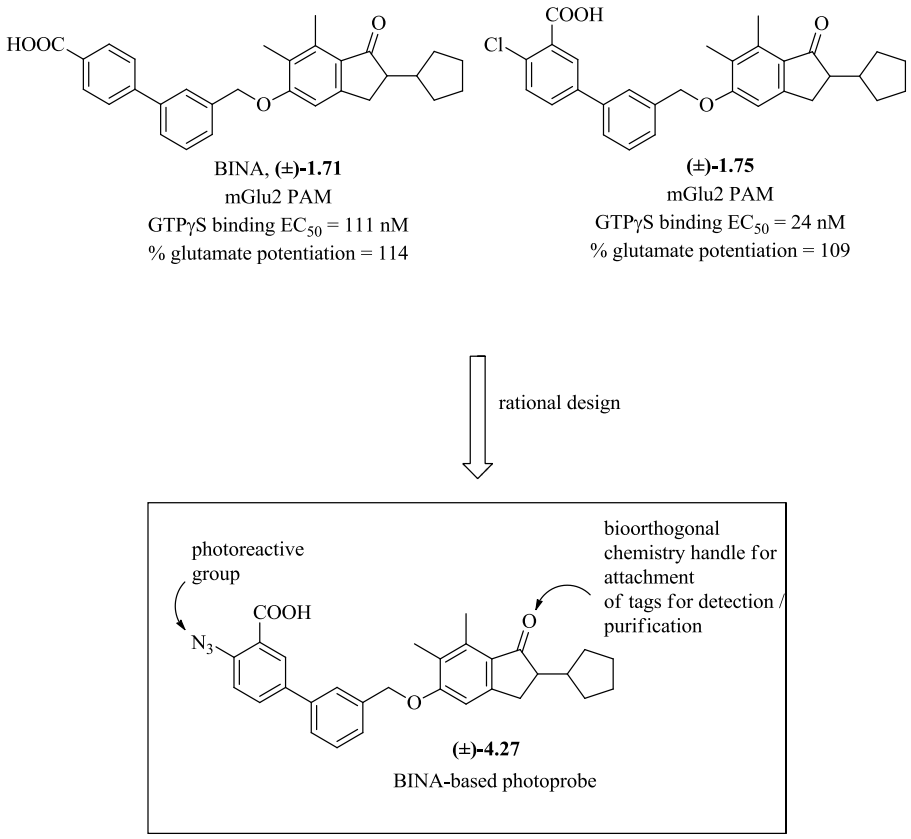


**Scheme 4.6.** Rational design of target photoaffinity probe **(±)-4.27** for mGlu2 structure-function studies based on known BINA-analog **(±)-1.75** (Bonnefous *et al.*, 2005).

## 4.9. Rational Design of Clickable Pyridone-Based PAM Photoprobes for mGlu2 Structure-Function Studies

1,5-Substituted pyridones emerged as a promising class of potent and selective mGlu2 PAMs *via* high throughput screening (HTS) efforts at Addex Pharmaceuticals using a mGluR2 PAM FLIPR (fluorometric imaging plate reader) assay (Cid *et al.*, 2010). The initial hits from screening of the Addex compound collection were selected as lead compounds for further exploration of SAR (for discussion, see Section 1.8.2.1.3). In particular, a variety of substituents explored on the *N*-benzyl ring suggested that this ring is tolerable to hydrophobic substituents at positions 2 and 4. From this series of analogs, compound **1.89** (Scheme 4.7) emerged as a lead compound for photoprobe design given its high mGlu2 potency and selectivity.

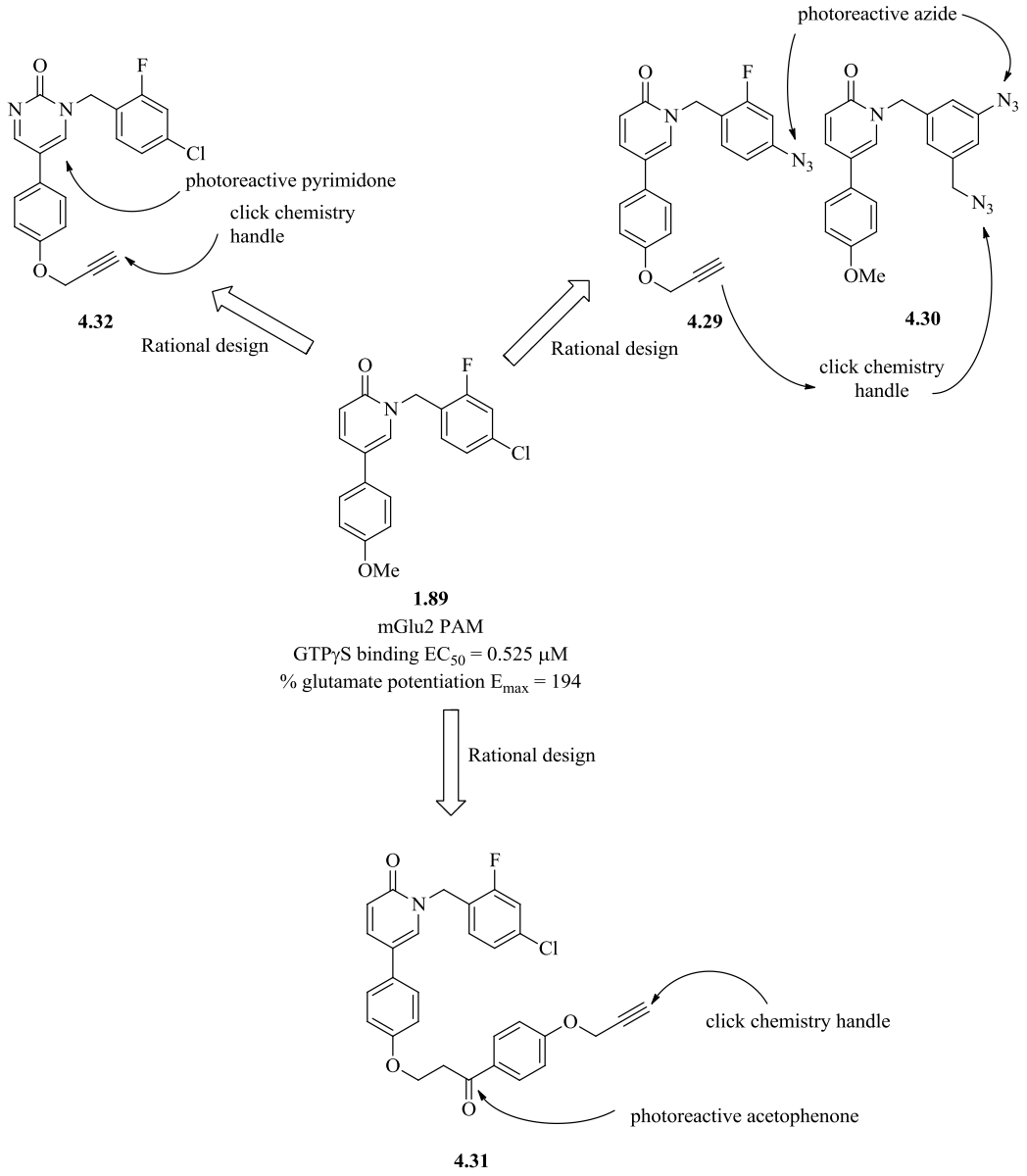


**Scheme 4.7.** Chemical structures of target clickable photoprobes for mGlu2 structure-function studies based on mGlu2 PAM **1.89** (Cid *et al.*, 2010).

The rationally designed photoprobes in Scheme 4.7 (discussed in detail *vide infra*) feature incorporation of different photoreactive functional groups at different parts on the 1,5-pyridone mGlu2 PAM scaffold, thus allowing potential systematic mapping of the PAM-binding site within mGlu2 *via* BEProFL. Furthermore, the absence of a stereocenter in the 1,5-pyridone

series represents a distinct advantage in terms of chemical simplification versus the BINA-based photoprobes previously discussed in Section 4.8.

### 4.9.1. Rational Design of a Pyridone-Based PAM Photoprobe for mGlu2 Structure-Function Studies Featuring an Aryl Azide as a Photoreactive Group

Target pyridone-based mGlu2 PAM photoprobe **4.29** was rationally designed by isosteric replacement of the chlorine atom in lead compound **1.89** with a hydrophobic, photoreactive aryl azide and extension of the methoxy ether into a clickable propargyl ether (Scheme 4.8). Support for the tolerability of these proposed structural changes stems from lead compounds **1.90** and **1.94**, which retain appreciable mGlu2 PAM selectivity and potency by containing a 4-trifluoro methyl group and a 4-methylnitrile group, respectively. In addition, target photoprobe **4.29** features a fluorine atom *meta* to the photoreactive aryl azide group, which as an electron-withdrawing group that could potentially stabilize the *in situ* generated highly reactive nitrene formed during photoirradation. In turn, this chemical strategy could potentially prevent undesirable 7-membered ketenimine ring formation, which is traditionally associated with non-specific protein labeling (Schrock and Schuster, 1984; Poe *et al.*, 1992; Schnapp *et al.*, 1993; see Section 2.2.1.1. for discussion). The synthesis of target photoprobe **(±)-4.29** is described in Section 5.3.6.

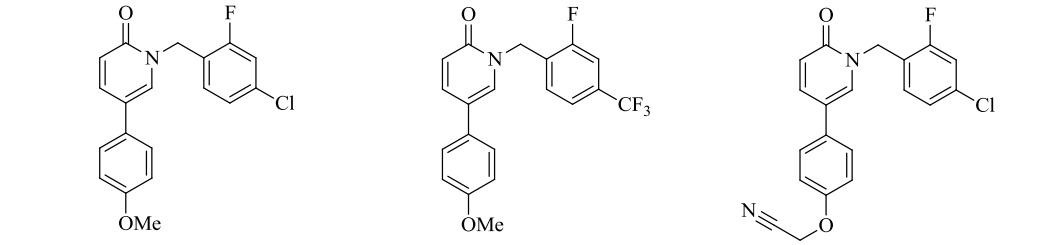


**1.89**
mGlu2 PAM
GTPγS binding $EC_{50}$ = 0.525 μM
% glutamate potentiation $E_{max}$ = 194

**1.90**
mGlu2 PAM
GTPγS binding $EC_{50}$ = 3.16 μM
% glutamate potentiation $E_{max}$ = 124

**1.94**
mGlu2 PAM
GTPγS binding $EC_{50}$ = 3.39 μM
% glutamate potentiation $E_{max}$ = 184

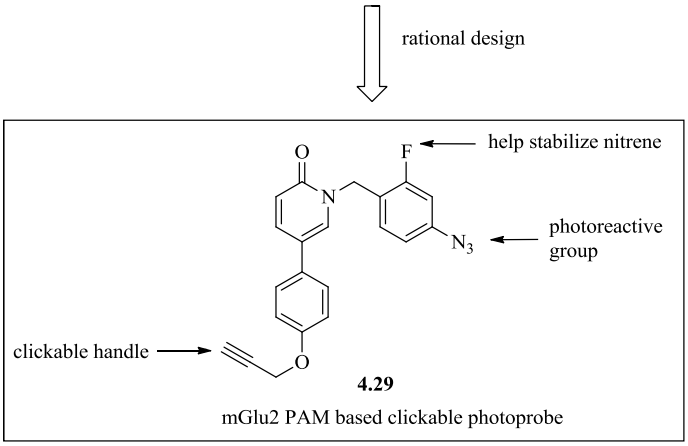


**4.29**
mGlu2 PAM based clickable photoprobe

**Scheme 4.8.** Rational design of target mGlu2 PAM photoaffinity probe **4.29** based on known pyridone-containing mGlu2 PAMs (Cid *et al.*, 2010).

### 4.9.2. Rational Design of a Pyridone-Based PAM Photoprobe for mGlu2 Structure-Function Studies That Contains a Diazido Structural Motif Common to Clickable Photoprobes

A number of clickable photoprobes have been disclosed featuring a parent ligand conjugated to a phenyl ring bearing an aryl azide photoreactive group and an aliphatic alkyl azide chemical reporter that survives photolysis (e.g., see **4.33** in Figure 4.5; Hosoya *et al.*, 2004, 2005, and 2009; He *et al.*, 2009; Neelarapu *et al.*, 2011; Gandy *et al.*, 2011). In particular, these probes tend to possess a common structural motif wherein the three substituents are spatially oriented in a 1,3,5-fashion around an aromatic phenyl ring. Additionally, parameters for this

routinely employed diazido structural motif have been reported for application of designed photoaffinity ligands in molecular dynamics studies (Pieffet and Petukhov, 2009). Given the *N*-benzyl ring of lead mGlu2 PAM **1.89** is tolerable to a wide variety of hydrophobic groups at different positions (see Section 1.8.2.1.3 for discussion of detailed SAR), target photoprobe **4.30** was rationally designed to include the common diazido structural motif as an *N*-benzyl substituent (Figure 4.5). The synthesis of target photoprobe **4.30** is described in Section 5.3.7.

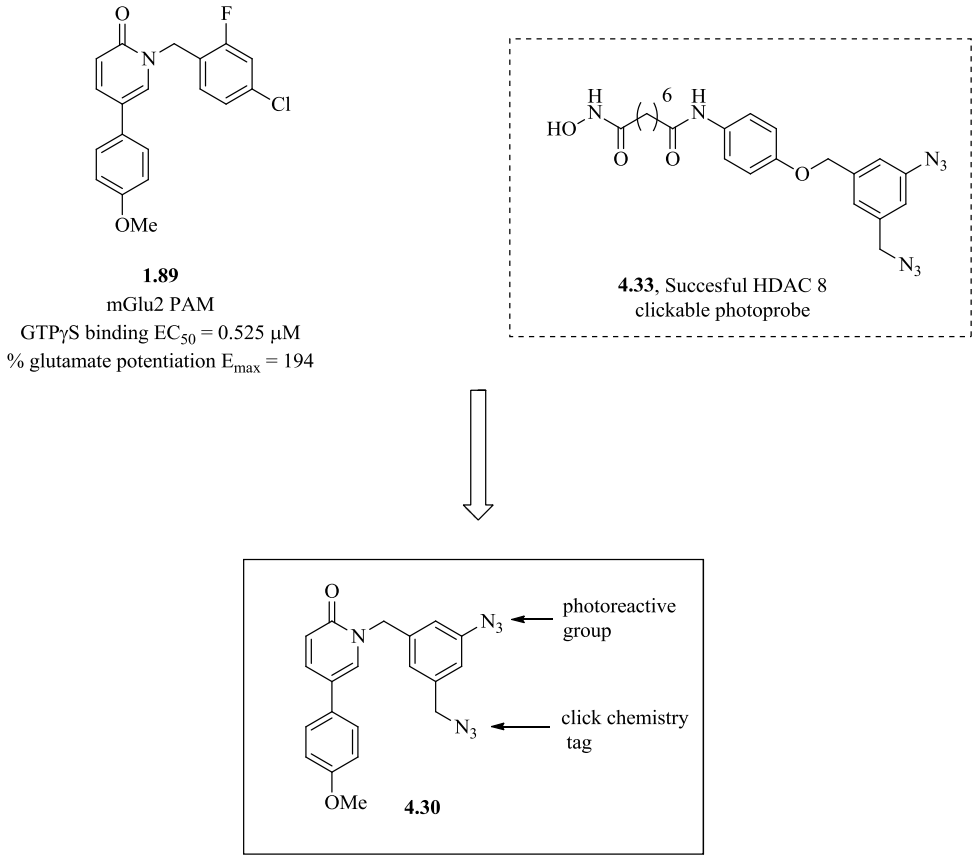


**Figure 4.5.** Structure of target mGlu2 PAM pyridone-based photoprobe **4.30**, that contains a common diazido structural motif common to many clickable photoprobes.

### 4.9.3. Rational Design of a Pyridone-Based Clickable PAM Photoprobe for mGlu2 Structure-Function Studies That Contains an Acetophenone Photoreactive Group

Lead compound **1.93** (Scheme 4.9) represents another potent and selective mGlu2 PAM from the 1,5-pyridone series (Cid *et al.*, 2010). In particular, this lead compound contains an

acetophenone as a potential photoreactive functional group. As a result, target photoprobe **4.31** was rationally designed by adding a propargyl ether *para* to the photoreactive carbonyl in order to enable click chemistry proteomic applications after photoaffinity labeling.

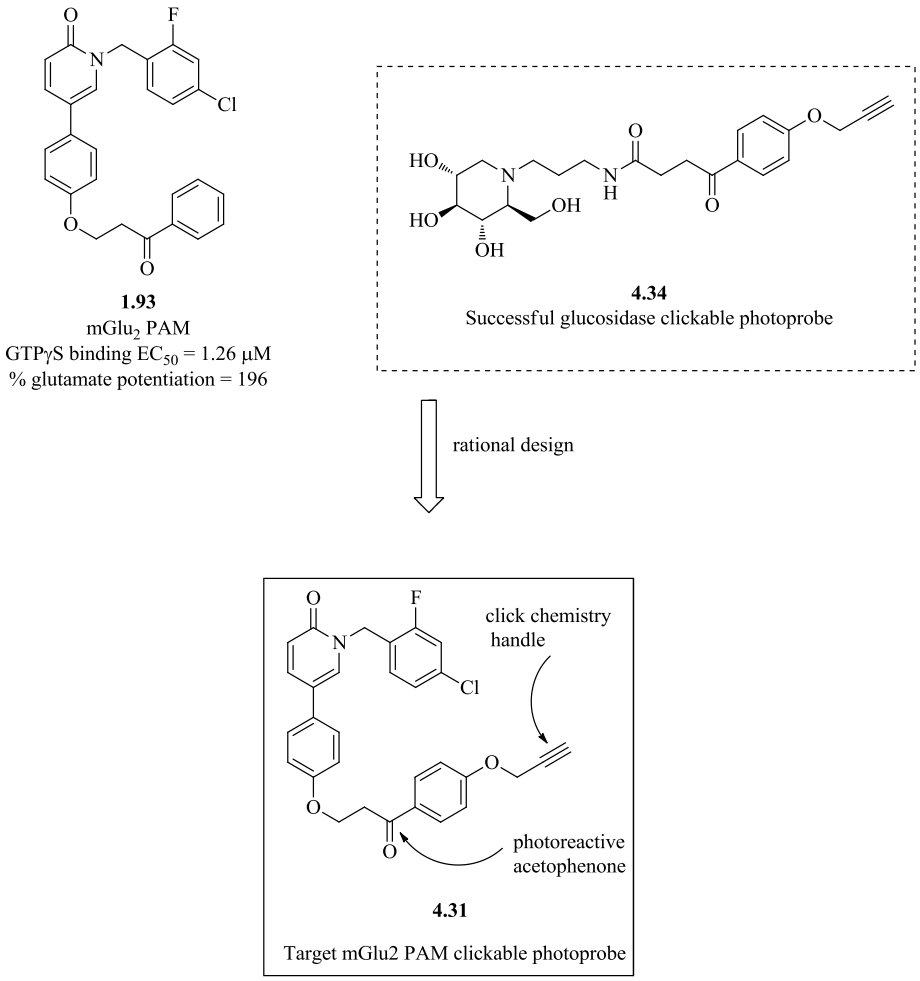


**Scheme 4.9.** Rational design of target PAM photoprobe **4.31** for mGlu2 structure-function studies based on mGlu2 PAM lead pyridone **1.93** (Cid *et al.*, 2010) and known acetophenone-alkyne clickable photoprobe **4.34** (van Scherpenzeel *et al.*, 2010).

In particular, support for the rational design of target photoprobe **4.31** stems from compound **4.34**, which possesses a similar acetophenone-*para*-propargyl ether structural motif. Compound **4.34** was shown to label a glycosidase enzyme after UV irradiation and click chemistry visualization with a fluoroscein-azide (van Scherpenzeel *et al.*, 2010). Furthermore, the presence of the labeling moiety two-carbon atoms removed from the substituted pyridone

scaffold could potentially lead to better labeling efficiency due to less steric hindrance from the surrounding aromatic groups and conformational flexibility. The synthesis of target photoprobe **4.31** is described in Section 5.3.8.

### 4.9.4. Rational Design of a Photo-masked mGlu2 PAM Affinity Labeling Probe for mGlu2 Structure-Function Studies

Pyrimidones are common moieties found in numerous bioactive compounds and natural products. In particular, pyrimidones display photochemistry capable of generating latent electrophiles that can react with nucleophilic amino acids in proteins *via* photo-masked affinity labeling. For example, pyrimidone **4.37** (Scheme 4.10) was successfully employed by the Battenberg group for protein profiling in crude cell lysates (Battenberg *et al.*, 2011). Specifically upon UV irradiation, pyrimidones undergo a Norrish type 1 reaction leading to the formation reactive intermediates capable of forming covalent bonds with proximal nucleophiles in the ligand-binding site (see Section 2.2.1.3). During this work, labeled proteins were visualized by click chemistry attachment of a rhodamine-azide dye to the heteroaryl alkyne moiety. Furthermore, labeling results of a vancomycin-based probe containing a pyrimidone were compared with a vancomycin-based probe containing a benzophenone as a photoreactive group. In particular, the labeling patterns of both probes were identical and indicated selective labeling of autolysin (ATLam) and an ABC transporter protein (pABC) in *S. aureus* and *E. faecalis*, respectively. These results have provided proof-of-concept that pyrimidones are capable of acting as efficient photo-masked affinity labeling groups similar to benzophenones traditionally employed in photoaffinity labeling.

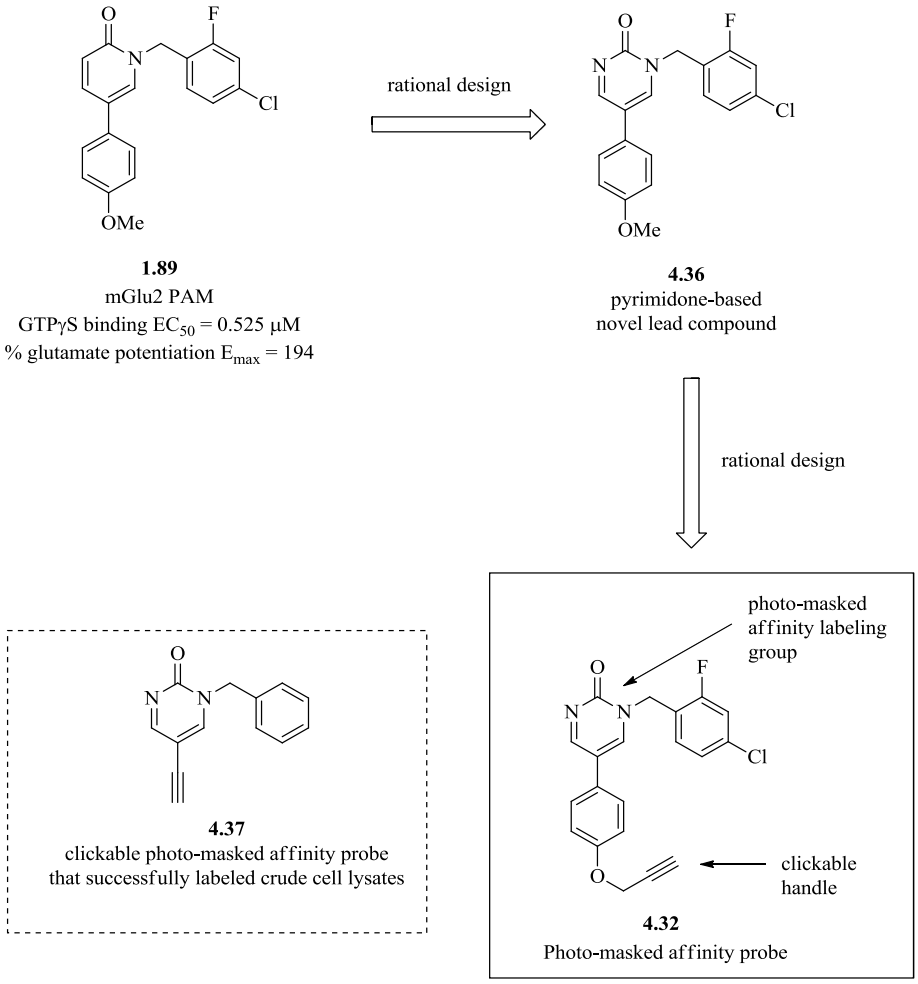


**Scheme 4.10.** Rational design of pyrimidone-containing lead compound **4.36** and target photo-masked affinity probe **4.32** from mGlu2 PAM **1.89** and known affinity probe **4.37**.

With this acquired knowledge in hand, target probe **4.32** (Scheme 4.10), which features a photoreactive pyrimidone moiety instead of a pyridone moiety found in lead mGlu2 PAM compound **1.89**, was rationally designed for future mGlu2 structure-function studies. This target probes also features slight extension of the methyl ether in lead mGlu2 PAM compound **1.89** to a propargyl ether for click chemistry applications after photo-unmasking affinity labeling. Furthermore, in order to compare the mGlu2 pharmacology profile of target probe **4.32** versus an appropriate analog, compound **4.36** was also synthesized featuring a –CH versus –N= isosteric replacement when structurally compared to lead mGlu2 PAM compound **1.89**. In particular,

compounds **4.32** and **4.36** were synthesized as described in Section 5.3.9 and are currently the subject of mGlu2 pharmacology and photoaffinity labeling studies *via* an established research collaboration with Dr. Karen Gregory.

# CHAPTER FIVE

## 5. Chemical Discussion

### 5.1. Synthesis of Pyrovalerone-Based Photoprobes for DAT Structure-Function Studies

As previously discussed in Section 4.6., our interest in pyrovalerone-based photoaffinity probes for DAT structure-function studies emerged from its structural resemblance to the marketed antidepressant and smoking cessation agent, bupropion (Wellbutrin, Zyban), as well as highly abused designer cathinones (e.g., MDPV). Additionally, high DAT binding affinities were reported for a number of pyrovalerone analogs as a promising class of monoamine uptake inhibitors (Meltzer *et al.*, 2006), thus aiding in rational photoprobe design from a ligand-based perspective.

#### 5.1.1. Synthesis of Racemic 1-(4-Azido-3-Iodophenyl)-2-(Pyrrolidin-1-yl)Pentan-1-one as a Photoaffinity Ligand for DAT Structure-Function Studies

As previously described in Section 4.6, racemic *p*-azido-*m*-iodo pyrovalerone (**(±)-4.16**) was desired as a compact photoaffinity labeling probe featuring a photoreactive aryl azide placed directly on the pyrovalerone pharmacophore. The synthesis of target probe **(±)-4.16** was envisioned from known acetamide pyrovalerone analog **(±)-1.32** (Meltzer *et al.*, 2006) utilizing three steps: amide hydrolysis, electrophilic aromatic iodination of the resulting aniline, then conversion of the aniline to the azide *via* diazotization and azide displacement (Scheme 5.1). In turn, acetamide pyrovalerone analog **(±)-1.32** was envisioned from commercially available acetanilide (**5.1**) using methodology previously reported (i.e., Friedel-Crafts acylation, α-bromination, and pyrrolidine *N*-alkylation; Meltzer *et al.*, 2006). In particular, the vision behind this proposed retrosynthesis features incorporation of the photoreactive aryl azide as the last step

in the synthesis given the potential inherent instability traditionally associated with this functional group over multiple synthetic steps.

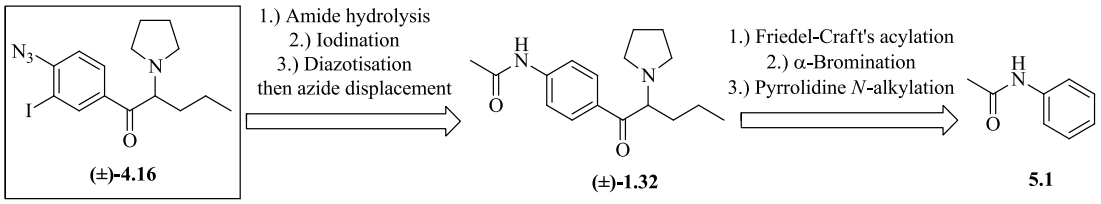


**Scheme 5.1.** Proposed retrosynthesis of target pyrovalerone-based photoprobe **(±)-4.16** from acetanilide (**5.1**).

For the forward synthesis, acetanilide (**5.1**) was initially subjected to Friedel-Craft's acylation using 1,2-dichloroethane (1,2-DCE), $AlCl_3$, and valeryl chloride (**5.2**) (reaction conditions adapted from Ogawa *et al.*, 1988 and Ianni and Waldvogel, 2006) in order to obtain known ketone **5.3** (Meltzer *et al.*, 2006) in bulk quantities. However, this particular Friedel-Craft's acylation suffered from several practical problems in the lab (Table 5.1). Initially, the reaction resulted in no product formation due to the insolubility of acetanilide in 1,2-DCE (Entry 1, Table 5.1). Even though changing the solvent to dichloromethane (DCM) resulted in improved solubility of the starting materials, monitoring of the reaction for completion *via* TLC was difficult because acetanilide **5.1** and ketone **5.3** have the same $R_f$ values ($R_f$ = 0.42 in hexanes:EtOAc, 1:1) (Entry 2, Table 5.1). As a result, target ketone **5.3** was obtained alongside acetanilide as a major impurity because separation by silica gel flash column chromatography could not be readily achieved. Even with increasing equivalents of valeryl chloride and $AlCl_3$, complete consumption of acetanilide was not observed (Entry 3, Table 5.1).

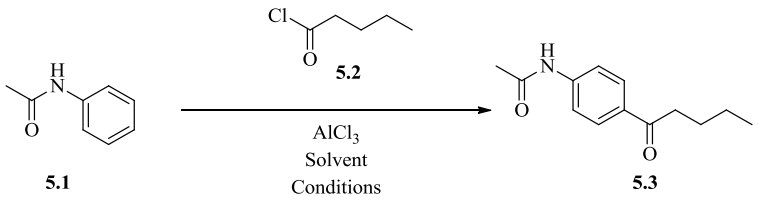


| Entry | Acetanilide | Valeryl Chloride | $AlCl_3$ | Solvent | Reaction Conditions | Result |
|---|---|---|---|---|---|---|
| **1** | 1 eq. | 2 eq. | 2.5 eq. | 1,2-DCE | 0˚C to rt, 2 hr | No reaction; solubility problems |
| **2** | 1 eq. | 1.8 eq. | 1.8 eq. | DCM | 0˚C to rt, 3 hr | Incomplete reaction |
| **3** | 1 eq. | 5 eq. | 5 eq. | DCM | 0˚C to reflux, O/N | Incomplete reaction |

**Table 5.1.** Optimization efforts with respect to Friedel-Craft's acylation of acetanilide with valeryl chloride.

In order to overcome this previously noted problem, the inseparable mixture of target ketone **5.3** and acetanilide (**5.1**) (after silica gel chromatography) was subjected to reduction with $NaBH_4$ in MeOH (Scheme 5.2).

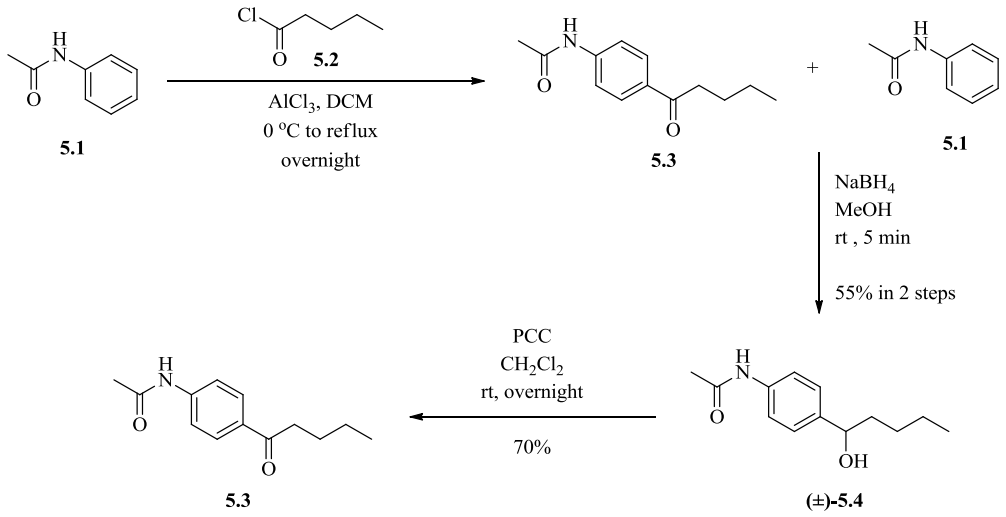


**Scheme 5.2.** Synthesis of target ketone **5.3** *via* a Friedel-Crafts acylation, ketone reduction, alcohol oxidation sequence.

This reaction selectively reduced ketone **5.3** to benzyl alcohol derivative **(±)-5.4** and did not reduce the amide in acetanilide. As a result, benzyl alcohol **(±)-5.4** could then be readily separated from acetanilide *via* silica gel flash chromatography due to the significant difference in $R_f$ values for the two compounds. In turn, benzyl alcohol **(±)-5.4** was then oxidized back to pure target ketone **5.3** in 70% yield using PCC in dichloromethane. With ketone **5.3** in hand, the next synthetic step, α-bromination of the ketone, was optimized using the conditions listed in Table 5.2. When ketone **5.3** was treated with liquid bromine and $AlCl_3$ in a mixture of $Et_2O$ and dichloromethane, incomplete formation of target product **(±)-5.5** was observed (Entry 1, Table 5.2). Changing the solvent to chloroform resulted in no product formation (Entry 2, Table 5.2). However, subsequent increase in the number of equivalents of $AlCl_3$ provided better yields of target bromide **(±)-5.5**. In particular, the best reaction conditions that provided quantitative yield of alkyl bromide **(±)-5.5** were utilization of 0.5 equivalents of $AlCl_3$ and $CHCl_3$ as the reaction solvent (Entry 5, Table 5.2).

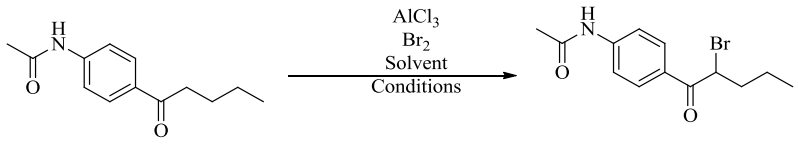


**5.3** **(±)-5.5**

| Entry | $AlCl_3$ | $Br_2$ | Solvent | Conditions | Result |
|---|---|---|---|---|---|
| **1** | 0.05 eq. | 1 eq. | $Et_2O$, DCM | 0˚C, O/N | Target Bromide + Starting material |
| **2** | 0.05 eq. | 1 eq. | $CHCl_3$ | 0˚C, O/N | No reaction |
| **3** | 0.2 eq. | 1 eq. | $CHCl_3$ | 0˚C, 1 hr then rt, 1.5 hr | 73% yield of **(±)-5.5** |
| **4** | 0.2 eq. | 1 eq. | $CHCl_3$ | 0˚C, 30 min then rt, O/N | 96% yield of **(±)-5.5** |
| **5** | 0.5 eq. | 1 eq. | $CHCl_3$ | 0˚C, 1 hr then rt, O/N | 100% yield of **(±)-5.5** |

**Table 5.2.** Optimization of bromination of ketone **5.3** to provide α-bromide **(±)-5.5**.

Using Entry 5 from Table 5.2, α-bromoketone **(±)-5.5** was then taken ahead without purification to nucleophilic displacement with pyrrolidine to provide known pyrovalerone acetamide analog **(±)-1.32** (Meltzer *et al.*, 2006) in 59% yield (Scheme 5.3). The amide in compound **(±)-1.32** was then subjected to acid hydrolysis (conditions adapated from Ianni and Waldvogel, 2006) followed by basification with aqueous $K_2CO_3$ to provide aniline **(±)-5.6** in 58% yield. Subsequently, electrophilic iodination of aniline **(±)-5.6** (conditions adapted from Newman *et al.*, 2006), followed by aniline diazotization and displacement with $NaN_3$ provided target pyrovalerone-based probe **(±)-4.16** for DAT photoaffinity labeling (Lapinsky *et al.*, 2009).

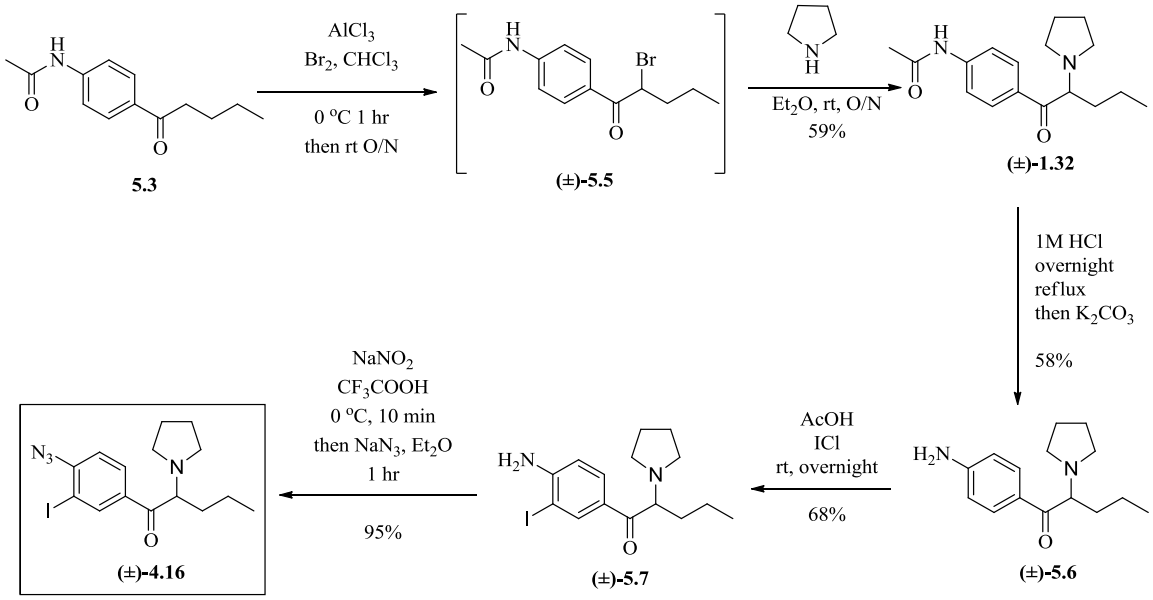


**Scheme 5.3.** Synthesis of target pyrovalerone-based photoprobe **(±)-4.16** for DAT structure-function studies starting from acetamide **5.3**.

### 5.1.2. Synthesis of Racemic 1-(4-Azido-3-Iodophenyl)-4-Methyl-2-(Pyrrolidin-1-yl)Pentan-1-one as a Potential Photoaffinity Ligand for DAT Structure-Function Studies

According to pyrovalerone SAR reported by Meltzer and coworkers (Meltzer *et al.*, 2006), branched side chain analogs of pyrovalerone possess higher DAT binding affinity than pyrovalerone (see Section 4.6). As a result, target photoprobe **(±)-4.18** (Scheme 5.4) was

envisioned as a DAT photoaffinity ligand with potentially higher DAT binding affinity than previously described successful pyrovalerone DAT photoprobe **[$^{125}$I]-(±)-4.16** (Lapinsky *et al.*, 2009). In particular, a proposed retrosynthesis (Scheme 5.4) of branched side chain target probe **(±)-4.18** was naturally envisioned similar to straight chain analog **(±)-4.16** in Scheme 5.1. Once again, incorporation of the photoreactive aryl azide was envisioned as the last step in the synthesis given the potential inherent instability traditionally associated with this functional group over multiple synthetic steps.

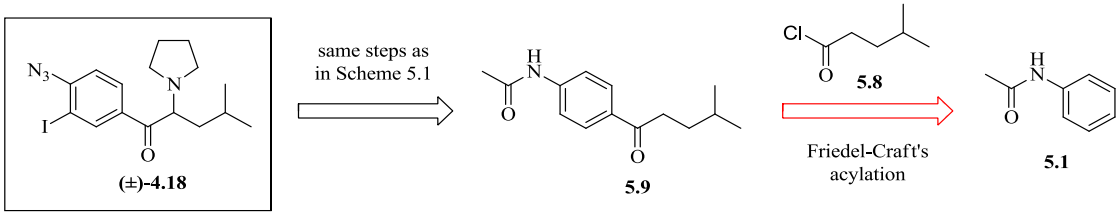


**Scheme 5.4.** Proposed retrosynthesis of target branched side chain pyrovalerone-based photoprobe **(±)-4.18** for DAT structure-function studies.

The synthesis of target pyrovalerone-based photoprobe **(±)-4.18** was initiated by Friedel-Craft's acylation of acetanilide (**5.1**) with 4-methylvaleryl chloride (**5.8**). However, once again, this Friedel-Craft's acylation provided an inseparable mixture of acetanilide (**5.1**) and target ketone *N*-(4-(4-methylpentanoyl)phenyl)acetamide (**5.9**). As a result, access to target ketone **5.9** was instead anticipated *via* its aniline precursor **5.11** *via* *N*-acetylation (Scheme 5.5). Aniline precursor **5.11** could then be obtained from commercially available 4-(trifluoromethyl)aniline (**5.10**) *via* a known synthetic route (Lin *et al.*, 1997).

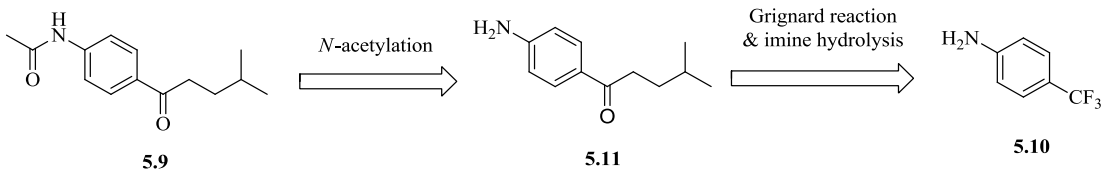


**Scheme 5.5.** An alternative synthetic strategy to access the target branched side chain ketone **5.9**.

This work began with the synthesis of isopentylmagnesium bromide from isopentyl bromide and magnesium turnings (Scheme 5.6). In particular, Grignard reagent formation was accelerated by adding a few drops of dibromoethane at 0˚C. After the mixture was stirred for 1 hour, the reaction was cooled to -78˚C and 4-(trifluoromethyl)aniline (**5.10**) was added followed by refluxing the reaction for 4 hours at 80˚C. Subsequent hydrolysis of the intermediate imine with 10% $H_2SO_4$ provided the branched side chain ketone **5.11** in 10% yield (Lin *et al.*, 1997). The low yield of target ketone formation was reflective of the incomplete formation of the *in situ* Grignard reagent.

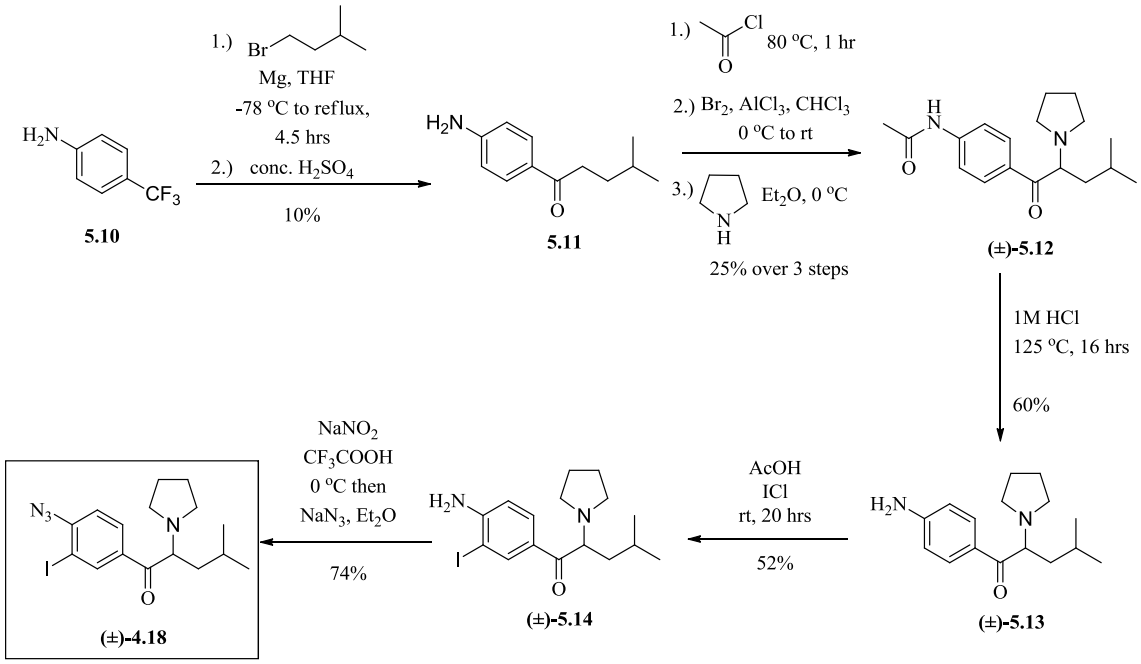


**Scheme 5.6.** Synthesis of branched side chain pyrovalerone-based photoprobe **(±)-4.18** for DAT structure-function studies.

Subsequently, aniline **5.11** was *N*-acetylated, followed by α-bromination and displacement with pyrrolidine to provide 4-acetamide-branched chain intermediate **(±)-5.12** (25% yield, 3 steps). The amide of compound **(±)-5.12** was then subjected to acid hydrolysis and electrophilic aromatic iodination to provide *p*-amino-*m*-iodo branched chain pyrovalerone analog

**(±)-5.14**. Finally, aniline **(±)-5.14** was subjected to diazotization and displacement with $NaN_3$ to provide the target photoprobe **(±)-4.18** in 74% yield. In turn, the free base of pyrovalerone analog **(±)-4.18** was converted to its hydrochloride salt by treatment with 2M HCl-ether solution to provide the HCl salt of target photoprobe **(±)-4.18** as a yellow solid.

### 5.1.3. Synthesis of Racemic 1-(3-Azido-4-Iodophenyl)-2-(Pyrrolidin-1-yl)Pentan-1-one as a Potential Photoaffinity Ligand for DAT Structure-Function Studies

Alongside branched side chain pyrovalerone-based photoprobe **(±)-4.18**, the synthesis of *meta*-azido-*para*-iodo pyrovalerone probe **(±)-4.17** was pursued simultaneously. From a retrosynthesis perspective (Scheme 5.7), target azide **(±)-4.17** was envisioned from acetamide derivative **(±)-5.20** *via* acid hydrolysis and conversion of the requisite aniline to the azide *via* the corresponding diazonium salt. In turn, the synthesis of acetamide **(±)-5.20** was anticipated by subjecting *p*-iodo valerophenone (**5.16**; Meltzer *et al.*, 2006) to a sequence of electrophilic aromatic nitration, nitro reduction, and aniline acylation, then α-bromination and pyrrolidine *N*-alkylation. Once again, incorporation of the photoreactive aryl azide was envisioned as the last step in the synthesis given the potential inherent instability traditionally associated with this functional group over multiple synthetic steps.

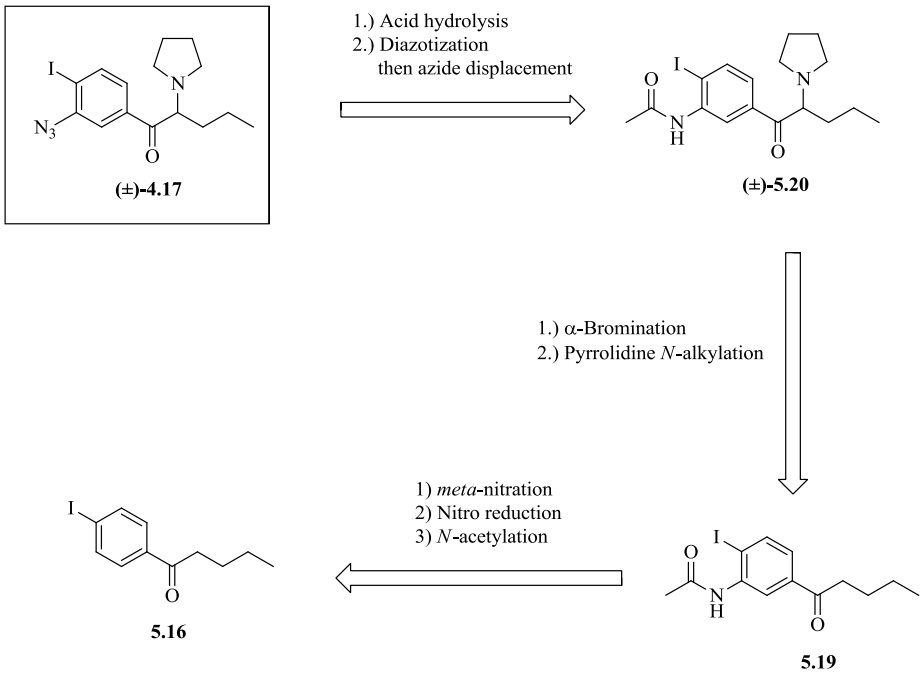


**Scheme 5.7.** Proposed retrosynthesis of target pyrovalerone-based photoprobe **(±)-4.17** featuring the azide and iodo functional groups reversed versus the traditional 3-iodo-4-azido photoaffinity labeling motif.

Therefore, according to this proposed retrosynthesis, *p*-iodovalerophenone (**5.16**), obtained from *p*-aminovalerophenone *via* aprotic diazotization and iodide displacement (see Krasnokutskaya *et al.*, 2007), was subjected to electrophilic aromatic nitration (conditions adapted from Chang *et al.*, 1995) by treatment with fuming nitric acid to yield *p*-iodo-*m*-nitro valerophenone (**5.17**) in 58% yield (Scheme 5.8). It was observed that valerophenone derivative **5.17** was rather unstable at room temperature and completely degraded within 24 hours according to TLC experiments. As a result, nitro valerophenone derivative **5.17** was immediately reduced (Fe powder and sonication; conditions adapted from Gamble *et al.*, 2007) after chromatography to provide aniline **5.18** in 83% yield and requiring no purification. Aniline **5.18** was then subjected to *N*-acetylation, α-bromination, and displacement with pyrrolidine to provide pyrovalerone analog **(±)-5.20** in 43% yield from **(±)-5.19**. However, subsequent acid hydrolysis of amide **(±)-5.20** proved unsuccessful. In particular, refluxing amide **(±)-5.20** in

aqueous HCl resulted in a mixture of several inseparable compounds. The only compound isolated from this reaction in a very small amount was the des-iodo derivative of the target (**(±)-5.21**) (confirmed from $^1$H-NMR and HRMS results), which was formed *via* an unidentified mechanism.

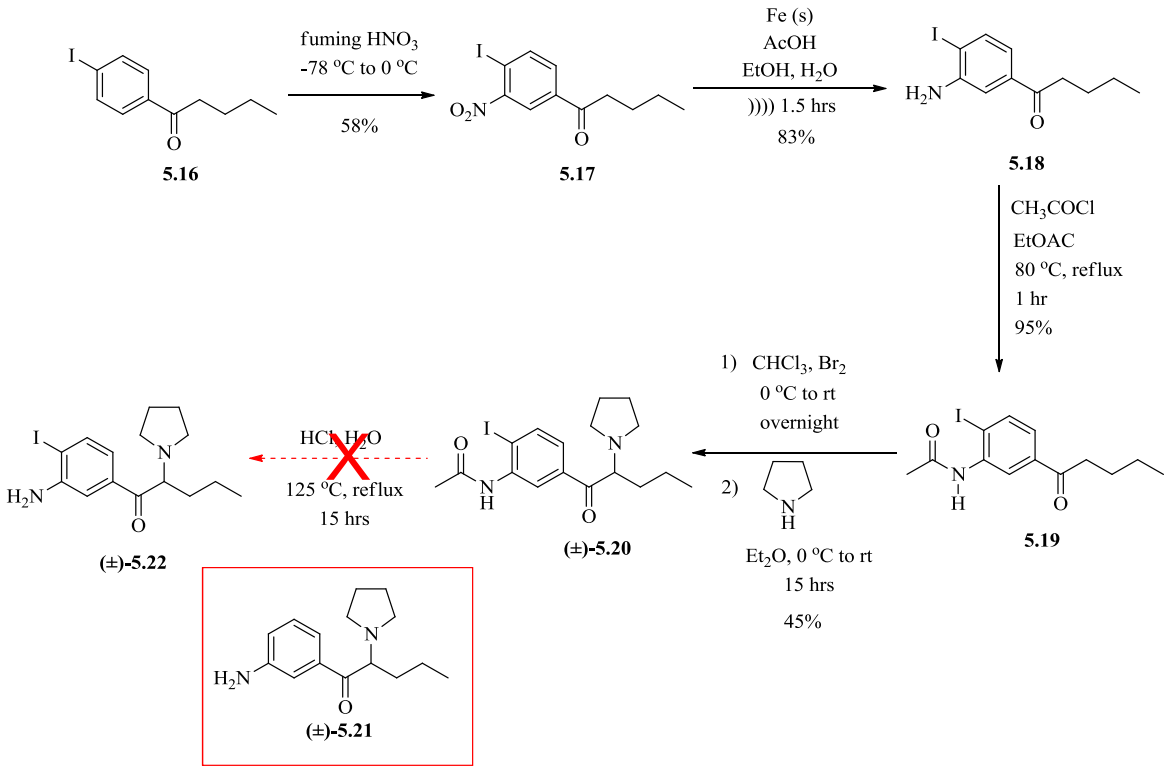


**Scheme 5.8.** Attempted synthesis of pyrovalerone aniline analog **(±)-5.22** towards generation of target pyrovalerone-based probe **(±)-4.17** for DAT structure-function studies.

In order to overcome the roadblock encountered upon amide hydrolysis, a new strategy towards target photoprobe **(±)-4.17** was envisioned featuring incorporation of the photoreactive azide moiety earlier in the synthesis (Scheme 5.9). In particular, target photoprobe **(±)-4.17** was now envisioned from *m*-azido-*p*-iodo valerophenone (**5.23**) *via* α-bromination and displacement with pyrrolidine, and the synthesis of ketone **5.23** was envisioned from previously mentioned *m*-amino-*p*-iodo valerophenone (**5.18**) *via* diazotization and displacement with $NaN_3$.

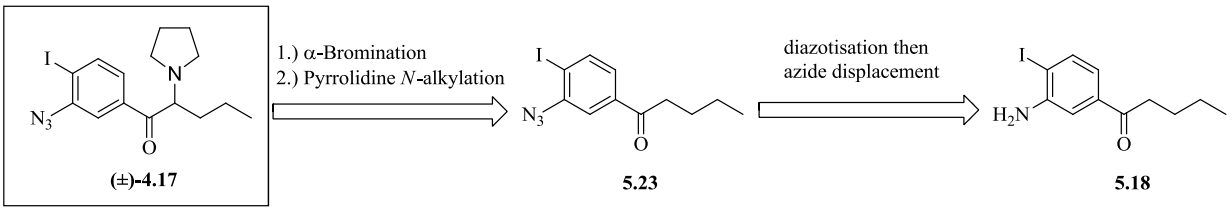


**Scheme 5.9.** Alternative retrosynthesis of target pyrovalerone-based photoprobe **(±)-4.17** for DAT structure-function studies *via* incorporation of the azide moiety earlier in the synthesis.

With this strategy in mind, *m*-amino-*p*-iodovalerophenone (**5.18**) was converted to its corresponding diazonium salt then treated with $NaN_3$ to provide target azide **5.23** in nearly quantitative yield (conditions adapted from Kym *et al.*, 1993) (Scheme 5.10). Azide **5.23** was found to degrade upon storage for prolonged periods, thus α-bromination was pursued immediately (using conditions adapted from Habeeb *et al.*, 2001). Finally, displacement of α-bromide **(±)-5.24** with pyrrolidine provided target pyrovalerone-based photoprobe **(±)-4.17** in 20% yield from ketone **5.23**. In particular, the success of the chemistry in Scheme 5.10 indicates pyrovalerone-based photoprobes for DAT structure-function studies can be accessed by introducing the photoreactive aryl azide group either earlier in the synthesis, or as the last step (e.g., see Scheme 5.6).

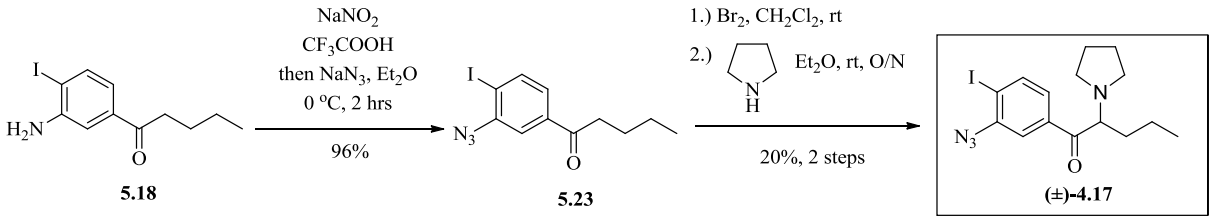


**Scheme 5.10.** Synthesis of target photoprobe **(±)-4.17** for DAT structure-function studies featuring the azide and iodo groups reversed versus the traditional 4-azido-3-iodo photoaffinity labeling motif.

## 5.2. Synthesis of Bupropion-Based Photoprobes for DAT and Select nAChR Subtypes Structure-Function Studies

### 5.2.1. Synthesis of Racemic 1-(4-Azido-3-Iodophenyl)-2-(*tert*-Butylamino)Propan-1-one as a Potential Photoaffinity Ligand for DAT and nAChR Structure-Function Studies

As previously described in Section 4.7.1 and given the DAT labeling success of structurally similar 4-azido-3-iodo-PV photoprobe **(±)-4.16** (Section 4.6), racemic *p*-azido-*m*-iodo bupropion (**(±)-4.20**) was desired as a compact photoaffinity labeling probe featuring a photoreactive aryl azide placed directly on the bupropion pharmacophore. In this regard, a proposed retrosynthesis of target probe **(±)-4.20** (Scheme 5.11) was envisioned using similar methodology employed earlier to synthesize pyrovalerone-based photoprobe **(±)-4.16** (in Scheme 5.3) featuring incorporation of the photoreactive aryl azide as the last step in the synthesis. This strategy was pursued in order to also allow the formation of aniline intermediate **(±)-5.31** (Scheme 5.12) as a synthetic precursor to access the radio-iodinated version of **(±)-4.20** by our collaborator, Dr. John Lever (see Appendix, Section A.2).

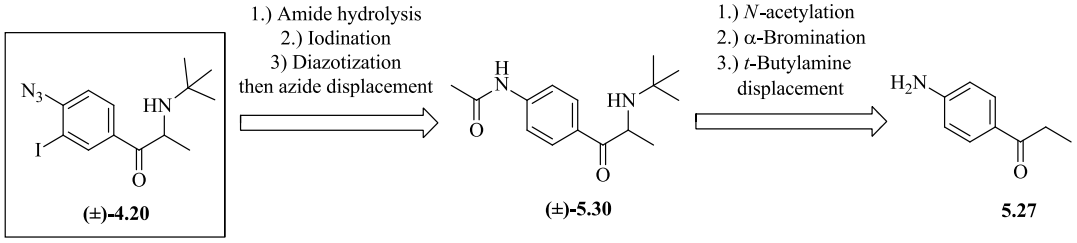


**Scheme 5.11.** Proposed retrosynthesis of bupropion-based photoprobe **(±)-4.20** featuring the traditional 4-azido-3-iodo photoaffinity labeling motif starting from 4-aminopropiophenone (**5.27**).

The synthesis of target bupropion-based photoprobe **(±)-4.20** was initiated by *N*-acylation of commercially available 4-aminophenylpropanone (**5.27**) to obtain *p*-acetamidephenylpropanone (**5.28**) in quantitative yield (Scheme 5.12). Acetamide **5.28** was then subjected to α-bromination and displacement with *t*-butylamine to provide amide analog **(±)-**

**5.30**, which upon acid hydrolysis provided aniline **(±)-5.31** in 20% yield over 4 steps. Subsequently, electrophilic iodination of aniline **(±)-5.31** with iodine monochloride in the presence of glacial acetic acid provided *p*-amino-*m*-iodo **(±)-5.32** in low yield (23%). The low yield of **(±)-5.32** was a result of difficult monitoring of the reaction for completion *via* TLC because the aniline and its *p*-amino-*m*-iodo derivative **(±)-5.32** have the same $R_f$ values ($R_f$ = 0.27 in hexanes:EtOAc:$Et_3N$, 10:88:2). As a result, *p*-amino-*m*-iodo derivative **(±)-5.32** was obtained alongside aniline **(±)-5.31** as a major impurity and separation by silica gel flash column chromatography could not be achieved efficiently. Furthermore, increasing the number of equivalents of ICl to facilitate the completion of the reaction resulted in a mixture of aniline **(±)-5.31**, target **(±)-5.32** and di-iodinated side product **(±)-5.33**, all having the same $R_f$ value and proved practically inseparable by silica gel flash column chromatography (Scheme 5.12).

The resulting small quantities of *p*-amino-*m*-iodo derivative **(±)-5.32**, due to the previously mentioned problems of incomplete reaction and poor chromatographic separation, was subsequently subjected to diazotization conditions and displacement with $NaN_3$ to provide the target photoprobe **(±)-4.20**. However, this final reaction resulted in multiple spots on TLC. The isolation of clean *p*-azido-*m*-iodo derivative **(±)-4.20** proved unsuccessful due to decomposition of the labile azide functional group during the silica gel flash column chromatography upon elution with $CHCl_3$:MeOH:$Et_3N$ mobile phase. Furthermore, attempted purification of target **(±)-4.20** *via* HCl salt formation by treatment with 1N HCl in diethyl ether solution, followed by trituration of the salt in diethyl ether did not provide sufficiently clean product.

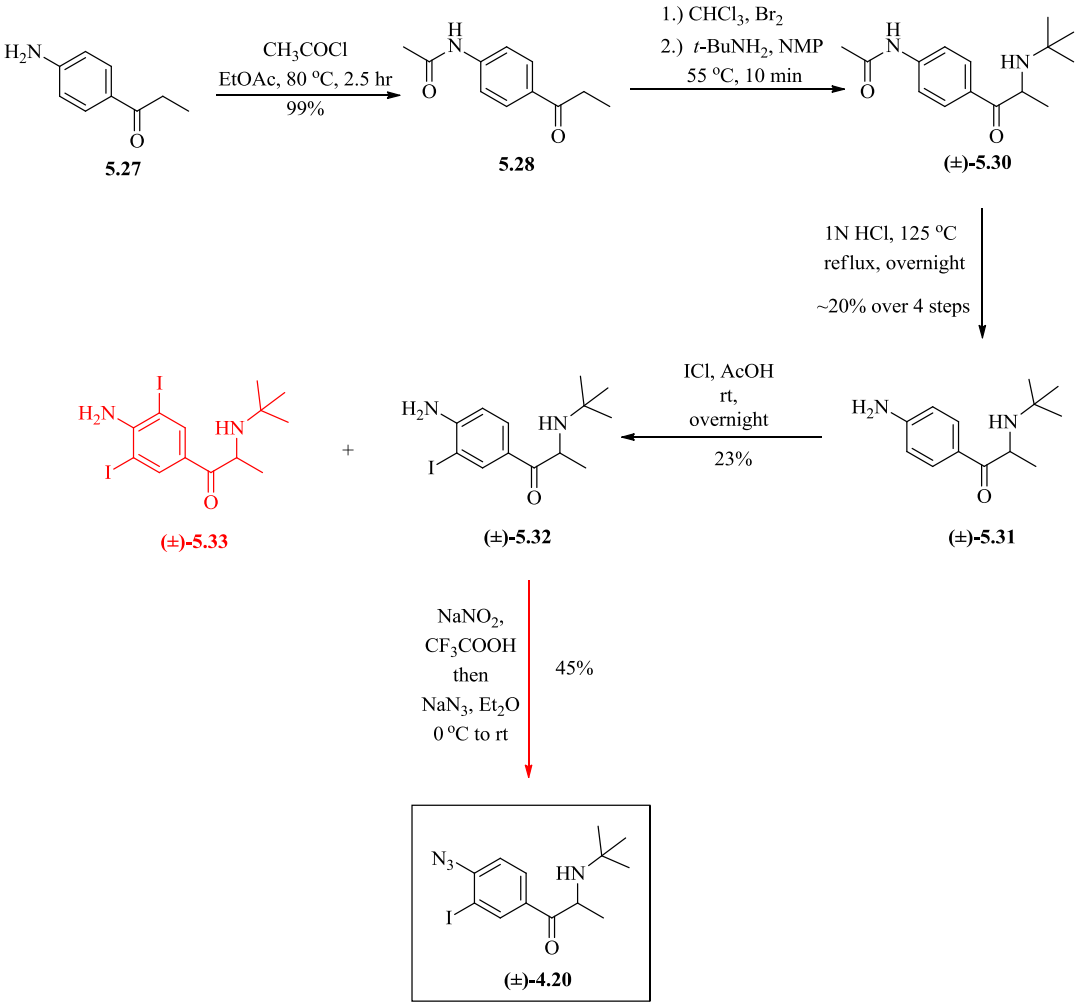


**Scheme 5.12.** Attempted synthesis of bupropion-based photoprobe **(±)-4.20** starting from 4-aminopropiophenone (**5.27**).

As a result, an alternative strategy towards target photoprobe **(±)-4.20** was envisioned featuring incorporation of the photoreactive azide moiety earlier in the synthesis (Scheme 5.13). According to this strategy, target photoprobe **(±)-4.20** was now envisioned from *p*-azido-*m*-iodopropiophenone (**5.36**) *via* α-bromination and displacement with *tert*-butylamine, and the synthesis of ketone **5.36** was envisioned from previously mentioned *p*-aminopropiophenone (**5.27**) in two steps *via* iodination followed by diazotization and displacement with $NaN_3$ (Scheme 5.13).

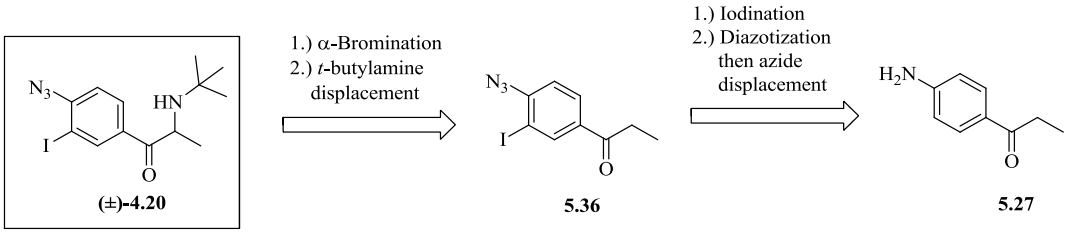


**Scheme 5.13.** Alternate retrosynthesis of target bupropion-based photoprobe **(±)-4.20** for DAT and nAChR structure-function studies *via* incorporation of the azide moiety earlier in the synthesis.

With this strategy in mind, commercially available *p*-aminopropiophenone (**5.27**) was subjected to electrophilic iodination with ICl in presence of $CaCO_3$, MeOH, and water to obtain *p*-amino-*m*-iodo ketone **5.35** in 47% yield (Scheme 5.14). *p*-Amino-*m*-iodopropiophenone (**5.35**) was then converted to its corresponding diazonium salt, and treated with $NaN_3$ to provide azide **5.36** in nearly quantitative yield. With *p*-azido-*m*-iodopropiophenone (**5.36**) in hand, α-bromination was carried out with liquid bromine in the presence of $CHCl_3$. The reaction was concentrated and the α-bromo ketone **(±)-5.37**, without isolation, was directly subjected to displacement with *t*-butylamine. The resulting crude product was treated directly with 2M HCl in diethyl ether solution to obtain the HCl salt of target **(±)-4.20** (11% yield over 3 steps) (see Lapinsky *et al.*, 2012).

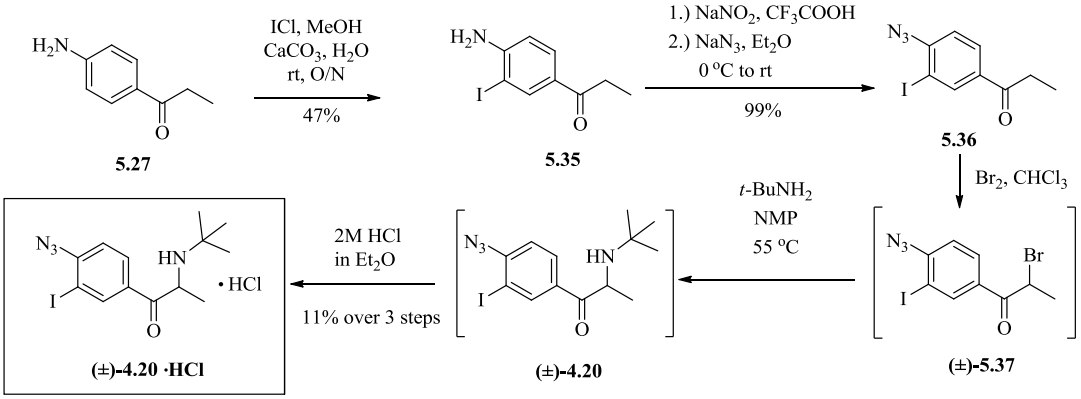


**Scheme 5.14.** Synthesis of target bupropion-based photoprobe **(±)-4.20** for DAT and nAChR structure-function studies featuring the traditional 4-azido-3-iodo photoaffinity labeling motif (Lapinsky *et al.*, 2012).

### 5.2.2. Synthesis of Racemic 2-(*tert*-Butylamino)-1-(3-Iodophenyl)Propan-1-one as a Photoaffinity Ligand Featuring an Intrinsic Acetophenone Moeity for DAT and nAChR Structure-Function Studies

Bupropion-based photoprobe **(±)-4.20** (Section 5.2.1) not only contains a photoreactive aryl azide group, but also is an example of an acetophenone derivative, which represents another potential photoreactive functional group (Lukac *et al.*, 2009). As a result, discrepancy could potentially arise in terms of discerning the exact point of covalent attachment of **(±)-4.20** to a protein after photoaffinity labeling. In order to experimentally investigate whether the nitrene from the azide or the diradical from the intrinsic acetophenone was acting as the photoreactive center, the des-azido probe **(±)-4.21** was rationally designed to remove any ambiguity during proteomics after photoaffinity labeling.

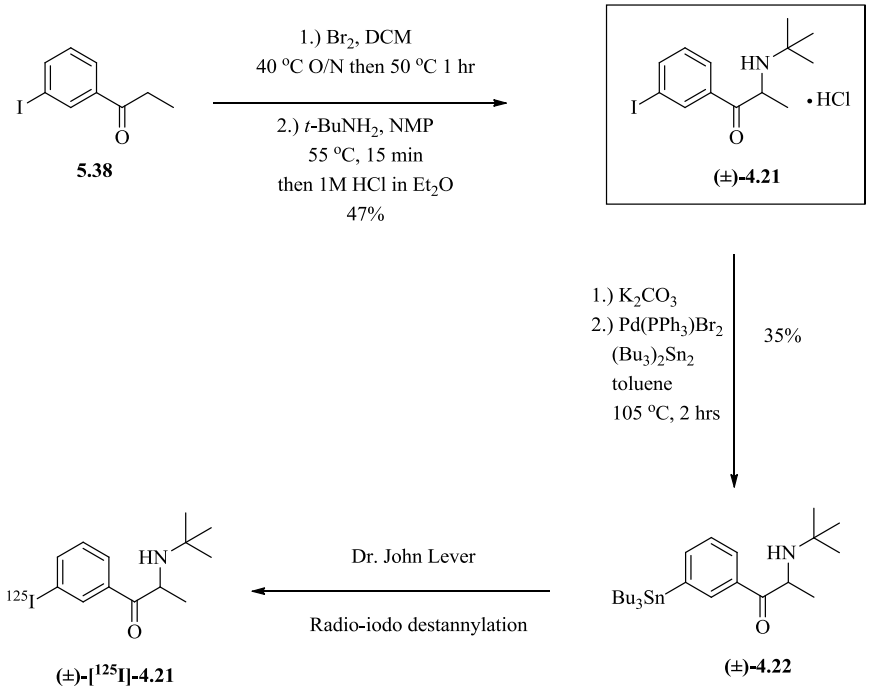


**Scheme 5.15.** Synthesis of des-azido probe **(±)-4.21** featuring an intrinsic acetophenone as a potential photoreactive moiety, and tri-*n*-butyl stannyl analog **(±)-4.22** as a precursor to radio-iodinated photoprobe **(±)-[$^{125}$I]-4.21** for DAT and nAChR structure-function studies.

Target **(±)-4.21** was obtained in 47% overall yield starting with α-bromination of 3-iodophenylpropiophenone (**5.38**) with bromine, followed by displacement of the α-bromide with *tert*-butylamine, and subsequent isolation of the target as the hydrochloride salt by stirring in 1M HCl in diethyl ether (Scheme 5.15). Tri-*n*-butyl stannyl analog **(±)-4.22** was also synthesized as a precursor to the $^{125}$I analog of **(±)-4.21**. In this regard, the HCl salt of **(±)-4.21** was basified using aqueous $K_2CO_3$, then subjected to Pd-catalyzed Stille coupling with bis(tributyltin) to provide tri-*n*-butyl stannyl derivative **(±)-4.22** in 35% yield. Synthesis of the $^{125}$I analog of **(±)-4.21** *via* radio-iodo destannylation was subsequently performed by Dr. John Lever to enable photoaffinity labeling studies with nAChRs by Dr. Michael Blanton's group (see Appendix, Section A.3).

### 5.2.3. Synthesis of (2*S*,3*S*)-2-(4-Azido-3-Iodophenyl)-3,5,5-Trimethylmorpholin-2-ol as a Photoaffinity Ligand for DAT and nAChR Structure-Function Studies

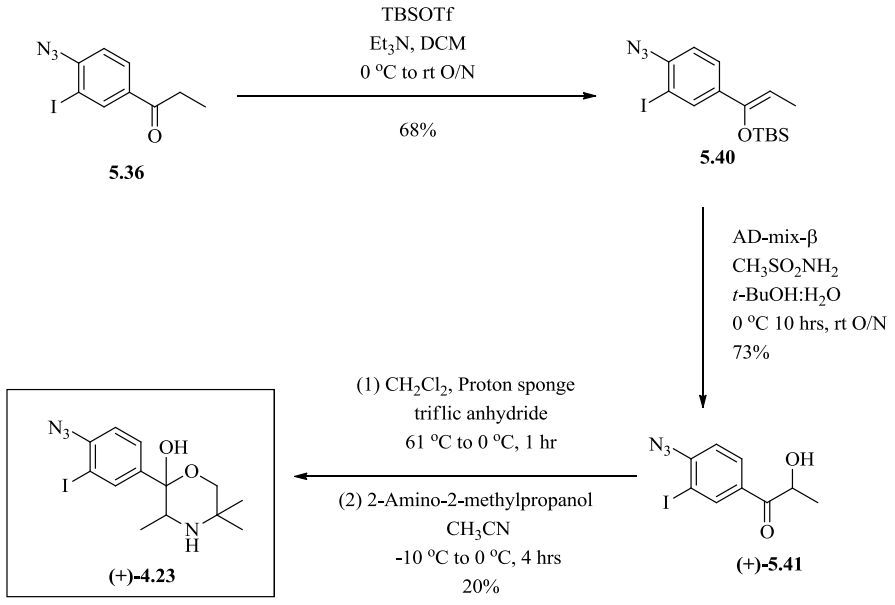


**Scheme 5.16.** Synthesis of hydroxybupropion-based photoaffinity probe **(+)-4.23** featuring the classical azido-iodo motif.

As previously described in Section 4.7.3, synthesis of target azido-iodo probe **(2*S*,3*S*)-4.23** based on bupropion's active metabolite, (2*S*,3*S*)-hydroxybupropion (**(2*S*,3*S*)-1.54**), was desired for DAT and nAChR structure-function studies. In particular, the synthesis of target photoprobe **(2*S*,3*S*)-1.54** was adapted using the synthetic strategy reported by Lukas and coworkers (Lukas *et al.*, 2010) to prepare several analogs of (2*S*,3*S*)-hydroxybupropion. Briefly, *p*-azido-*m*-iodophenyl propanone (**5.36**) (prepared in Scheme 5.14) was treated with $Et_3N$ and TBSOTf to provide silyl enol ether **5.40** in 68% yield after silica gel flash column chromatography (Scheme 5.16). α-Hydroxylation of silyl enol ether **5.40** under Sharpless asymmetric dihydroxylation conditions using AD-mix-β and $CH_3SO_2NH_2$ in *t*-BuOH and $H_2O$ (conditions adapted from Lukas *et al*., 2010) subsequently provided α-hydroxyphenylketone **(+)-5.41** in 73% yield. Treatment of alcohol **(+)-5.41** with triflic anhydride, followed by displacement of the *in situ* formed α-OTf group with 2-amino-2-methylpropanol and subsequent intramolecular cyclization, provided photoprobe (+)-**4.23**, which was isolated as an oxalate salt in 20% yield. The absolute stereochemistry of **(+)-4.23** was not determined *via* x-ray crystallography.

## 5.3. Synthesis of mGlu2 PAM Control Compounds and Irreversible Chemical Probes Suitable for mGlu2 Structure-Function Studies

### 5.3.1. Synthesis of a Lead Biphenylindanone-Based mGlu2 PAM as a Control Compound for mGlu2 Pharmacological Evaluation

Given known lead mGlu2 PAM **(±)-1.71** was required as a positive control for pharmacological comparison to our novel BINA-based photoprobes, **(±)-1.71** was synthesized according to the known chemical literature (Bonnefous *et al*., 2005). In this regard, synthesis of

required intermediate phenol **(±)-3.40** was initiated (Scheme 5.17) according to conditions reported in the literature (Woltersdorf *et al.*, 1977; DeSolms *et al.*, 1978).

As shown in Scheme 5.17, Friedel-Craft's acylation of **5.45** with acetyl chloride derivative **5.46** first provided ketone **5.47** in 82% yield. Next, the synthesis of α,β-unstaurated ketone **5.48** *via* Mannich base formation (following previously reported conditions; i.e., paraformaldehyde, dimethylamine, AcOH, 80 ºC; DeSolms *et al*., 1978) provided **5.48** in only 30% yield. Reducing the number of equivalents of dimethylamine hydrochloride from 4.5 to 3 equivalents, and stirring the reaction at 100 ºC in DMF with paraformaldehyde and AcOH, led to significant improvements in product yield of the reaction (69% from modified procedure versus 30% from the literature procedure). Subsequent intra-molecular cyclization of the resulting α,β-unsaturated ketone **5.48** under strong acidic conditions (i.e. conc. $H_2SO_4$) provided with cyclized ketone **(±)-5.49** in 81% yield without the need for chromatography. For methyl ether deprotection of **(±)-5.49**, $BBr_3$ was employed instead of stirring in hot 30-48% HBr as reported in the literature. This $BBr_3$ deprotection proceeded with excellent yield (90%) to directly provide known hydroxyl indanone **(±)-3.40** as a white solid.

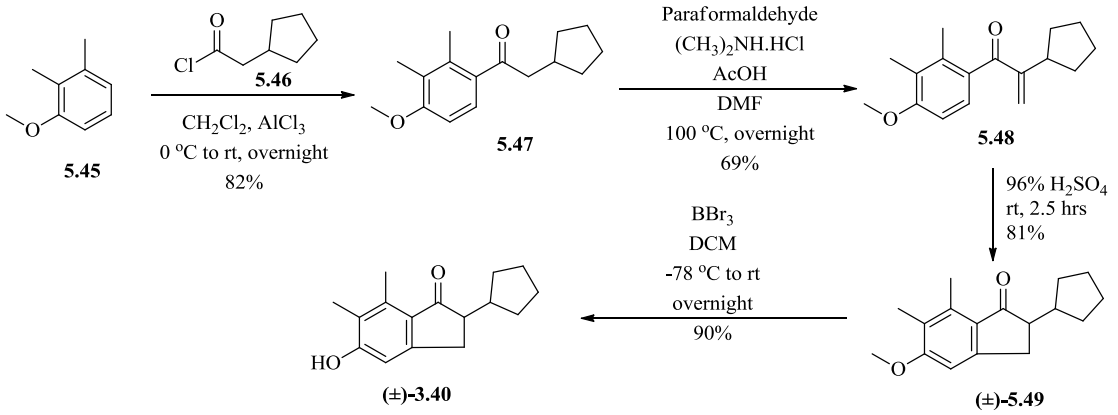


**Scheme 5.17.** Synthesis of intermediate hydroxyl indanone **(±)-3.40** with reaction conditions modified from DeSolms *et al*., 1978 and Woltersdorf *et al*., 1977.

For the forward synthesis, biphenyl **5.52** (Scheme 5.18) was obtained in 90% yield *via* Suzuki coupling (conditions adapted from Bonnefous *et al.*, 2005; Pinkerton *et al.*, 2006) of 3-bromo-4-methoxyphenyl methyl ester (**5.50**) with 3-boronic acid benzyl alcohol (**5.51**). The resulting biphenyl **5.52** was then subjected to Mitsunobu coupling (conditions adapted from Pinkerton *et al.*, 2006) with phenol **(±)-3.40** to provide the ester **(±)-3.44**. This ester **(±)-3.44** was obtained in extremely low yield (16%) with the majority of starting phenol recovered back *via* chromatography. Hydrolysis of ester **(±)-3.44** under basic conditions (LiOH) then provided target acid **(±)-1.74** (Bonnefous *et al*., 2005) in 65% yield. With control compound **(±)-1.74** in hand, synthesis of novel mGlu2 irreversible PAMs as chemical probes for mGlu2 structure-function studies were subsequently initiated.

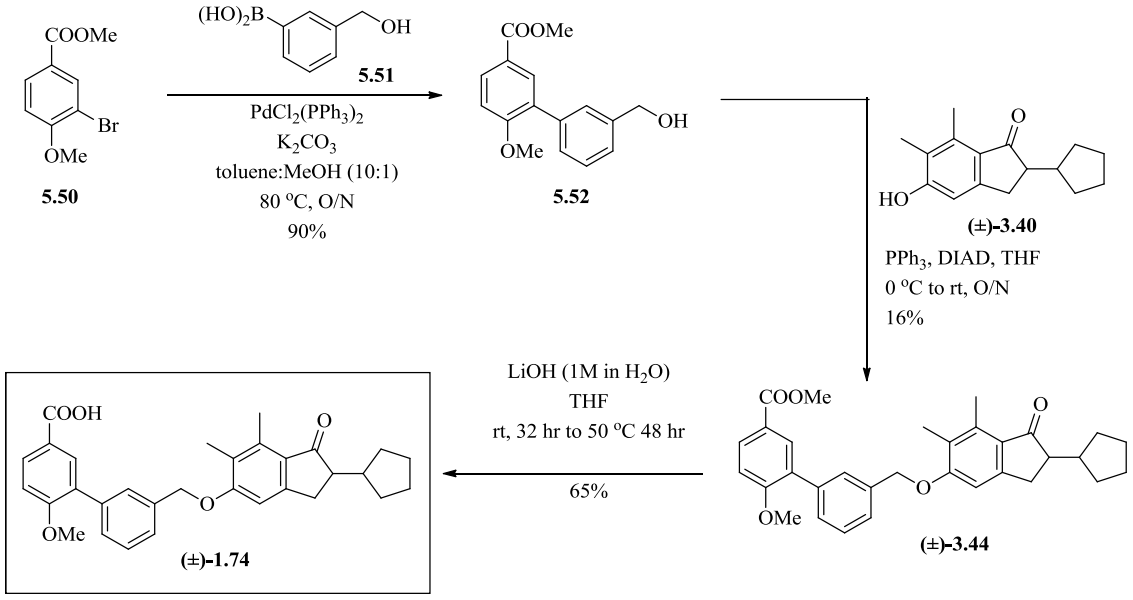


**Scheme 5.18.** Synthesis of lead biphenylindanone-based mGlu2 PAM **(±)-1.74** as a control for mGlu2 pharmacological evaluation (Bonnefous *et al*., 2005).

### 5.3.2. Synthesis of a Racemic Clickable BINA-based mGlu2 PAM Photoprobe for mGlu2 Structure-Function Studies Containing an Inherent Acetophenone Photoreactive Group

As previously described in Section 4.8.1, we desired clickable mGlu2 PAM **(±)-4.25** as a potential photoprobe suitable for mGlu2 structure-function studies. The synthesis of target photoprobe **(±)-4.25** was envisioned *via* Mitsunobu coupling of benzyl alcohol **5.58** with phenol **(±)-3.40** (synthesized in Section 5.3.1.1.) followed by ester hydrolysis. Benzyl alcohol **5.58**, in turn, could then be potentially accessed *via* Suzuki coupling between boronic acid **5.51** and aryl bromide **5.54**, followed by subsequent terminal alkyne deprotection of the silyl-protected propargyl ether (Scheme 5.19).

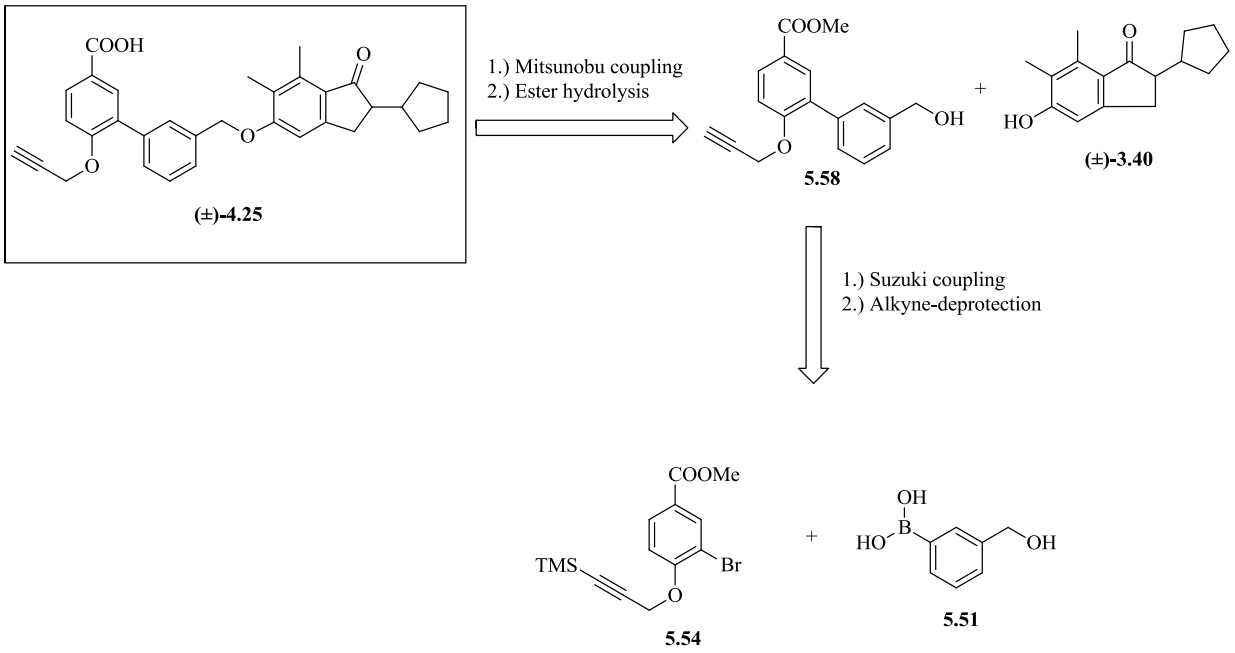


**Scheme 5.19.** Proposed retrosynthesis of clickable alkyne-acetophenone mGlu2 PAM photoprobe **(±)-4.25** for mGlu2 structure-function studies.

With this retrosynthesis in mind, Suzuki coupling of TMS-protected propargyl ether **5.54** (synthesized *via* *O*-alkylation of phenol **5.53** with TMS-protected propargyl bromide) with

commercially available boronic acid **5.51** proved unsuccessful due to the *in situ* deprotection of the TMS-protected propargyl group (Scheme 5.20).

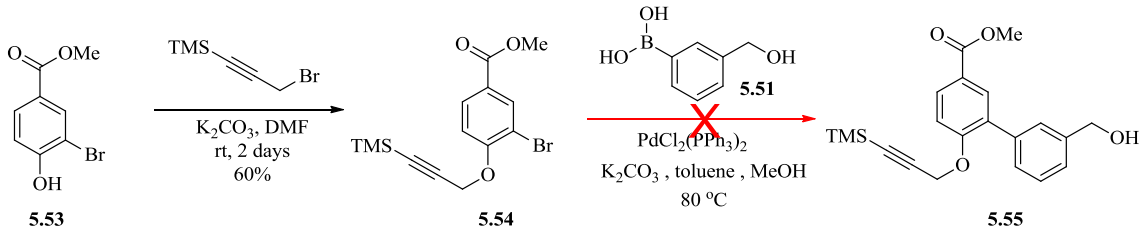


**Scheme 5.20.** Attempted synthesis of biphenyl intermediate **5.55** *via O*-alkylation and Suzuki coupling sequence.

In order to overcome this problem, the Suzuki coupling was instead carried out directly with commercially available phenol **5.53** to obtain biphenyl compound **5.57** in moderate yield (60%). Subsequent *O*-alkylation of phenol **5.57** with propargyl bromide then provided benzyl alcohol **5.58**, which was subjected to Mitsunobu coupling conditions with phenol **(±)-3.40** to obtain ester **(±)-5.59** in 46% yield. Final ester hydrolysis in aqueous LiOH then provided target acid **(±)-4.25** in 90% yield (Scheme 5.21).

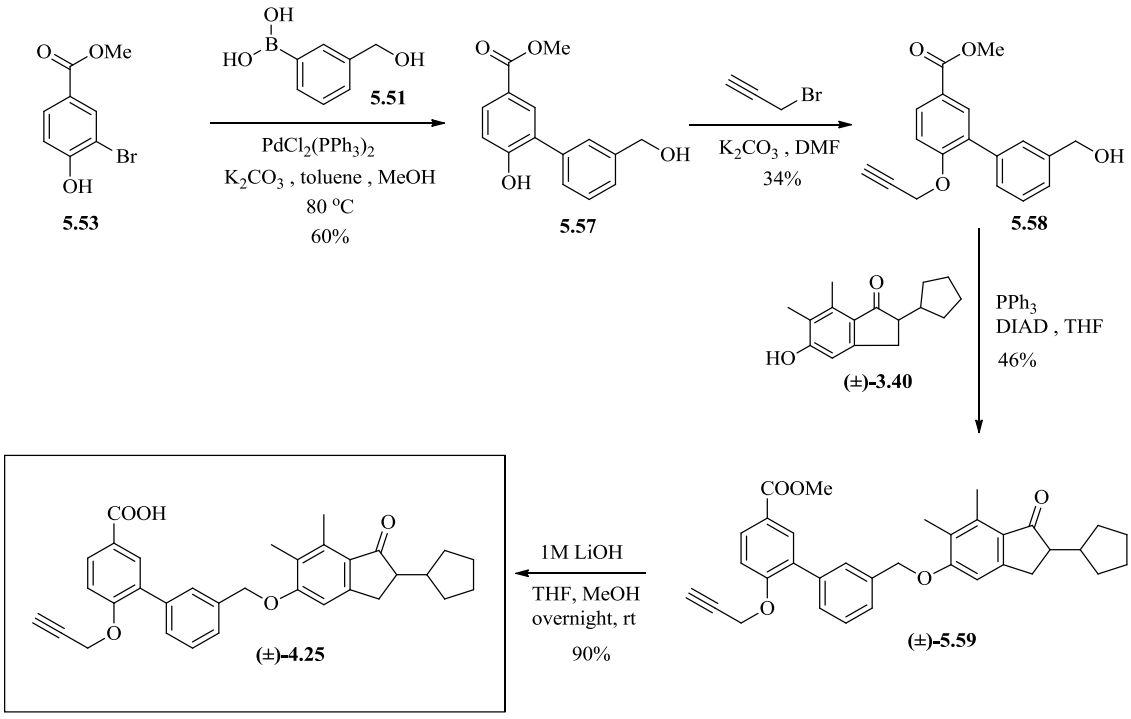


**Scheme 5.21.** Synthesis of clickable alkynyl-acetophenone mGlu2 PAM photoprobe **(±)-4.25** suitable for mGlu2 structure-function studies.

### 5.3.3. Synthesis of a Racemic BINA-Based mGlu2 PAM Photoprobe for mGlu2 Structure-Function Studies That Contains an Aryl Azide as a Photoreactive Group

As previously described in Section 4.8.2, mGlu2 PAM **(±)-4.27** was desired as a photoprobe for mGlu2 structure-function studies. The synthesis of aryl azido photoprobe **(±)-4.27** was envisioned in 3 steps *via O*-alkylation, Suzuki coupling and ester hydrolysis, starting with commercially available 3-bromomethylphenyl boronic acid (**5.61**) and previously synthesized phenol **(±)-3.40**. This retrosynthesis strategy (Scheme 5.22) was adapted from the existing chemical literature known for BINA-based analogs (Bonnefous *et al*., 2005).

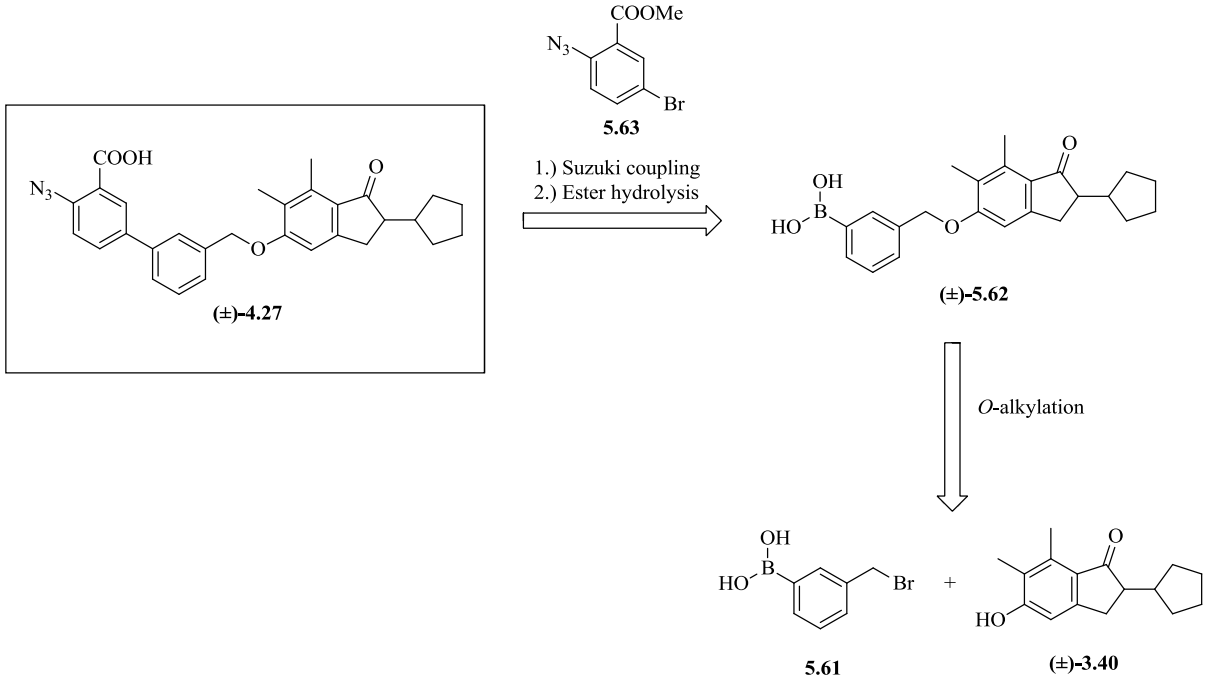


**Scheme 5.22.** Proposed retrosynthesis of racemic mGlu2 PAM photoprobe **(±)-4.27** featuring an aryl azide as a photoreactive group and an acetophenone as a chemical handle for the attachment of reporter tags.

With this synthetic strategy in mind, *O*-alkylation of phenol **(±)-3.40** with commercially available benzyl bromide **5.61** (under previously reported conditions; $Cs_2CO_3$, DMF; Van de Bittner *et al.*, 2013) provided ether **(±)-5.62** in only 10% yield after chromatography. In order to improve the yields of this transformation, conditions were modified by increasing the number of

equivalents of $K_2CO_3$ (from 3 to 4.5) and further addition of KI (0.2 equivalents) to the reaction mixture. The final outcome of the reaction improved drastically with aryl boronic acid derivative **(±)-5.62** obtained in nearly quantitative yields with sufficient purity without any need for purification *via* chromatography (Scheme 5.23). Boronic acid intermediate **(±)-5.62** was subsequently subjected to Suzuki coupling (conditions adapted from Pudlo *et al.*, 2007) with known methyl 2-azido-5-bromobenzoate **5.63** (Pokhodylo and Matiychuk, 2010), which provided ester **(±)-5.65** in 55% yield. Final ester hydrolysis with aqueous LiOH successfully gave target photoprobe **(±)-4.27** in 90% yield.

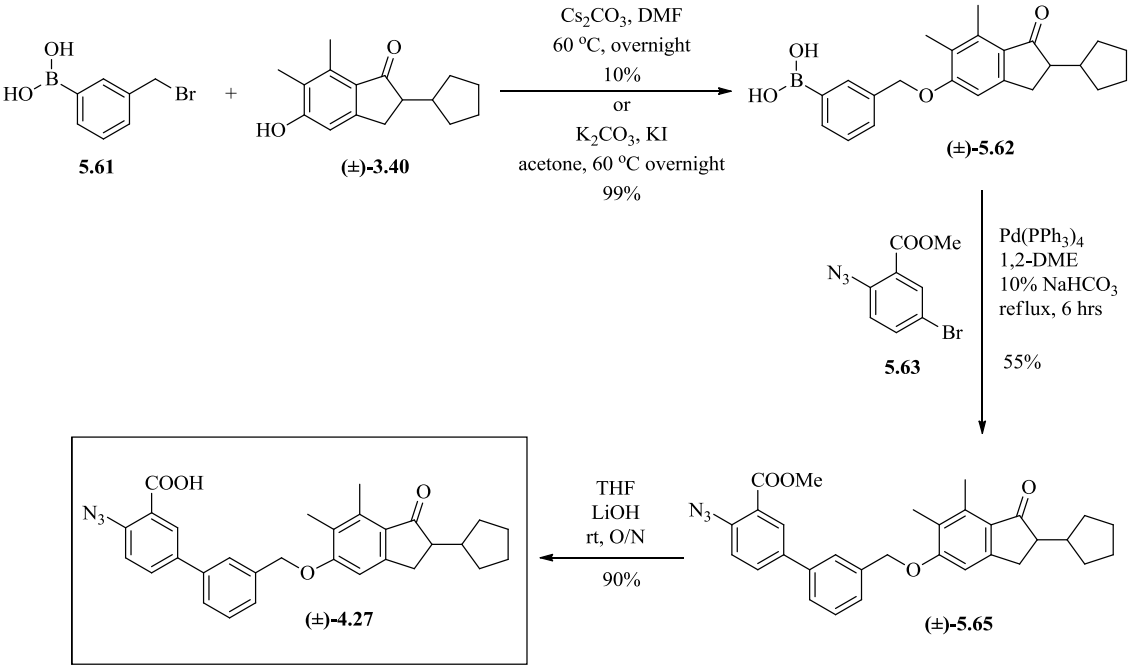


**Scheme 5.23.** Synthesis of racemic mGlu2 PAM photoprobe **(±)-4.27** for mGlu2 structure-function studies *via O*-alkylation, Suzuki coupling, ester hydrolysis sequence.

### 5.3.4. Synthesis of a Lead Pyridone-Based mGlu2 PAM as a Control Compound for mGlu2 Pharmacological Evaluation

Given known lead mGlu2 PAM **1.89** was required as positive control for pharmacological comparison to novel probe compounds, **1.89** was synthesized according to the known chemical literature (Imogai *et al.*, 2006).

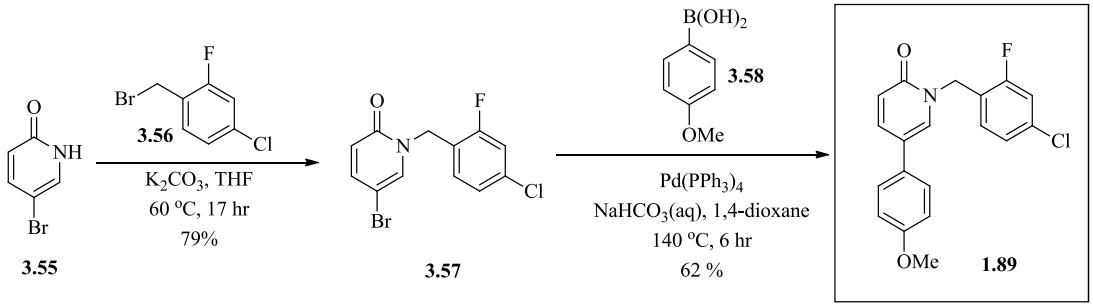


**Scheme 5.24.** Synthesis of lead pyridone-based mGlu2 PAM **1.89** as a control for mGlu2 pharmacological studies *via N*-alkylation and Suzuki coupling (Cid *et al*., 2010).

In this regard, *N*-alkylation of commercially available 5-bromo-2-pyridone (**3.55**) with 2-fluoro-4-chlorobenzyl bromide (**3.56**) first provided *N*-benzylated pyridone **3.57** in 79 % yield (Scheme 5.24). Subsequent Suzuki coupling of bromide **3.57** with 4-methoxy phenylboronic acid (**3.58**) under bench-top refluxing conditions instead of microwave-assisted heating (reported in Cid *et al.*, 2010), provided lead mGlu2 PAM **1.89** in 62% yield. Lead compound **1.89** was used as a standard control compound in the pharmacological evaluations of pyridone-based probes.

### 5.3.5. Synthesis of a Lead Pyridone-Based Acetophenone-Containing mGlu2 PAM as a Control Compound for mGlu2 Pharmacological Evaluation

The synthesis of known pyridone-based acetophenone-containing lead **1.93** was initially attempted *via* synthetic methodology reported in the literature (Cid *et al.*, 2010; Section 3.5). When phenol **3.59** was heated in a microwave with alkyl chloride **5.67** and $K_2CO_3$ in THF at

100ºC, no product (i.e., ether **1.93**) formation was observed (Entry 1, Table 5.3). Even with an increase in the number of equivalents of chloride **5.67** and addition of catalytic amounts of KI, no product was observed (Entry 2, Table 5.3). Furthermore, heating the reaction with traditional bench-top conditions upon changing the solvent to DMF (Entry 3, Table 5.3) or replacing $K_2CO_3$ with $Cs_2CO_3$ as the base still resulted in no reaction (Entry 4, Table 5.3). TLC of the reaction indicated the presence of only the starting phenol **3.59** with no spots indicative of target ether **1.93** upon separation *via* flash column chromatography and $^1$H NMR analysis.

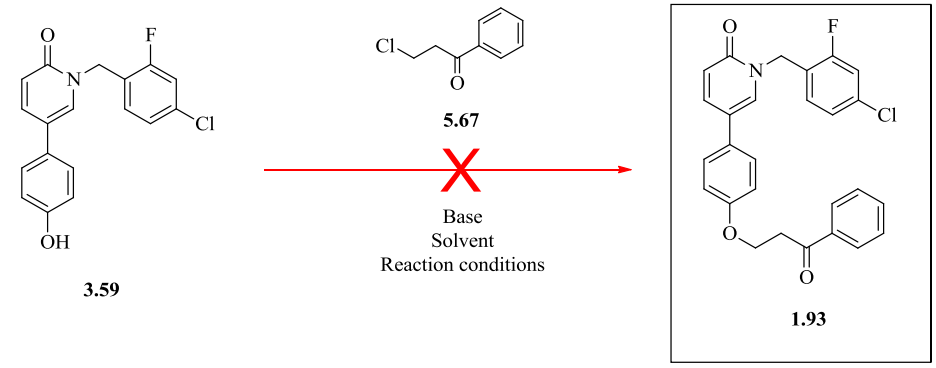


| Entry | Phenol 3.59 | Alkyl chloride 5.67 | Base | KI | Solvent | Reaction conditions | Result |
|---|---|---|---|---|---|---|---|
| **1** | 1 eq. | 1.1 eq. | $K_2CO_3$ | 0 eq. | THF | Microwave, 80ºC, 10 min | No observed target ether **1.93** formed |
| **2** | 1 eq. | 1.5 eq. | $K_2CO_3$ | 0.02 eq. | THF | Microwave, 100ºC, 10 min | No observed target ether **1.93** formed |
| **3** | 1 eq. | 2 eq. | $K_2CO_3$ | 0.5 eq. | DMF | Bench-top, 100ºC, overnight | No observed target ether **1.93** formed |
| **4** | 1 eq. | 2 eq. | $Cs_2CO_3$ | 0.5 eq. | DMF | Bench-top, 80ºC, overnight | No observed target ether **1.93** formed |

**Table 5.3.** Optimization efforts with respect to *O*-alkylation of phenol **3.59** with alkyl chloride **5.67** to provide mGlu2 PAM **1.93** as a control compound.

The previously noted problem of unsuccessful *O*-alkylation of phenol **3.59** was attributed mainly to the possibility that phenol **3.59** facilitated elimination of alkyl chloride **5.67** rather than

nucleophilic substitution. As a result, instead of using phenol **3.59**, synthesis of the target acetophenone **1.93** was attempted *via* an alternate strategy shown in Scheme 5.25 starting with commercially available 4-hydroxyphenyl pinacol boronate ester **5.70**.

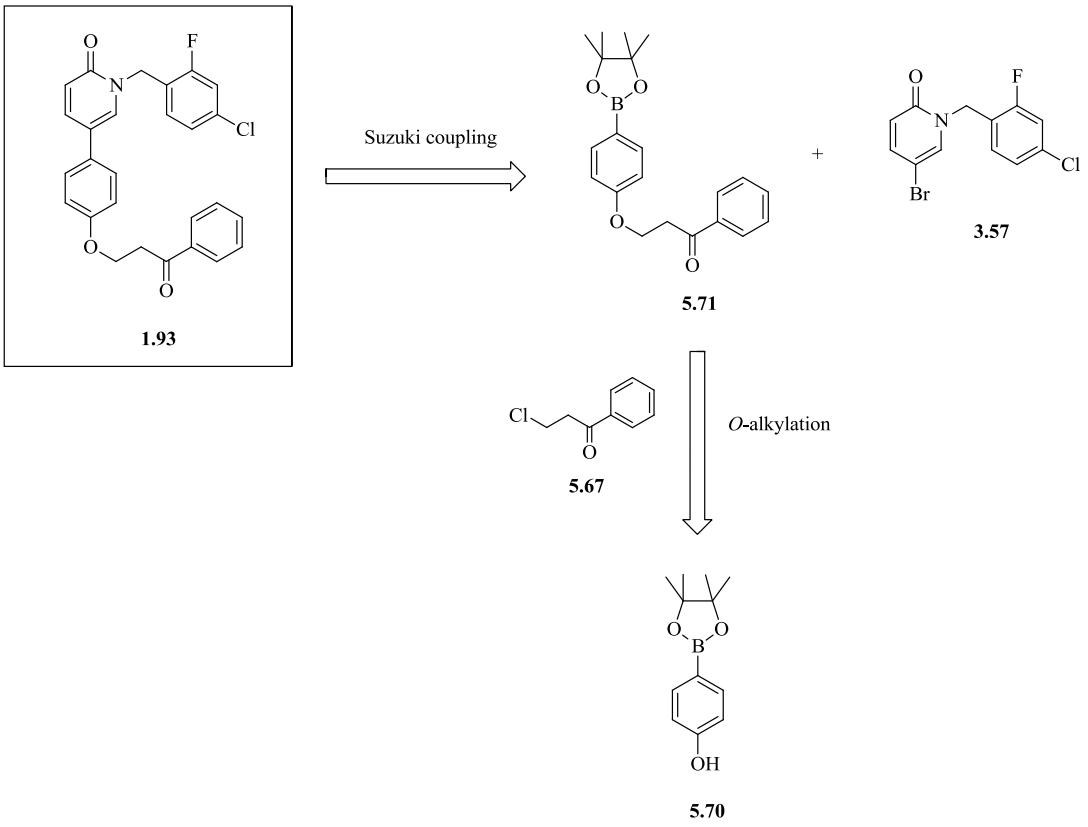


**Scheme 5.25.** Proposed alternate retrosynthesis for synthesis of lead mGlu2 PAM **1.93** starting with *O*-alkylation of commercially available phenol **5.70**.

As previously noted, attempts to *N*-alkylate 4-hydroxyphenyl boronate ester **5.70** with alkyl chloride **5.67** failed (Scheme 5.26). In particular, $^{1}$H NMR analysis of isolated reaction components indicated that β-chloroketone **5.67** converted to an unidentified side product, as the major product isolated from the reaction was the starting phenol **5.70**. Due to the susceptibility of β-haloketones to undergo β-elimination under basic conditions at high temperature, benzyl alcohol **5.72** (Onishi *et al.*, 2011; Park *et al.*, 2011; Coric *et al.*, 2013) was instead used as the more stable alkylating agent (Scheme 5.26).

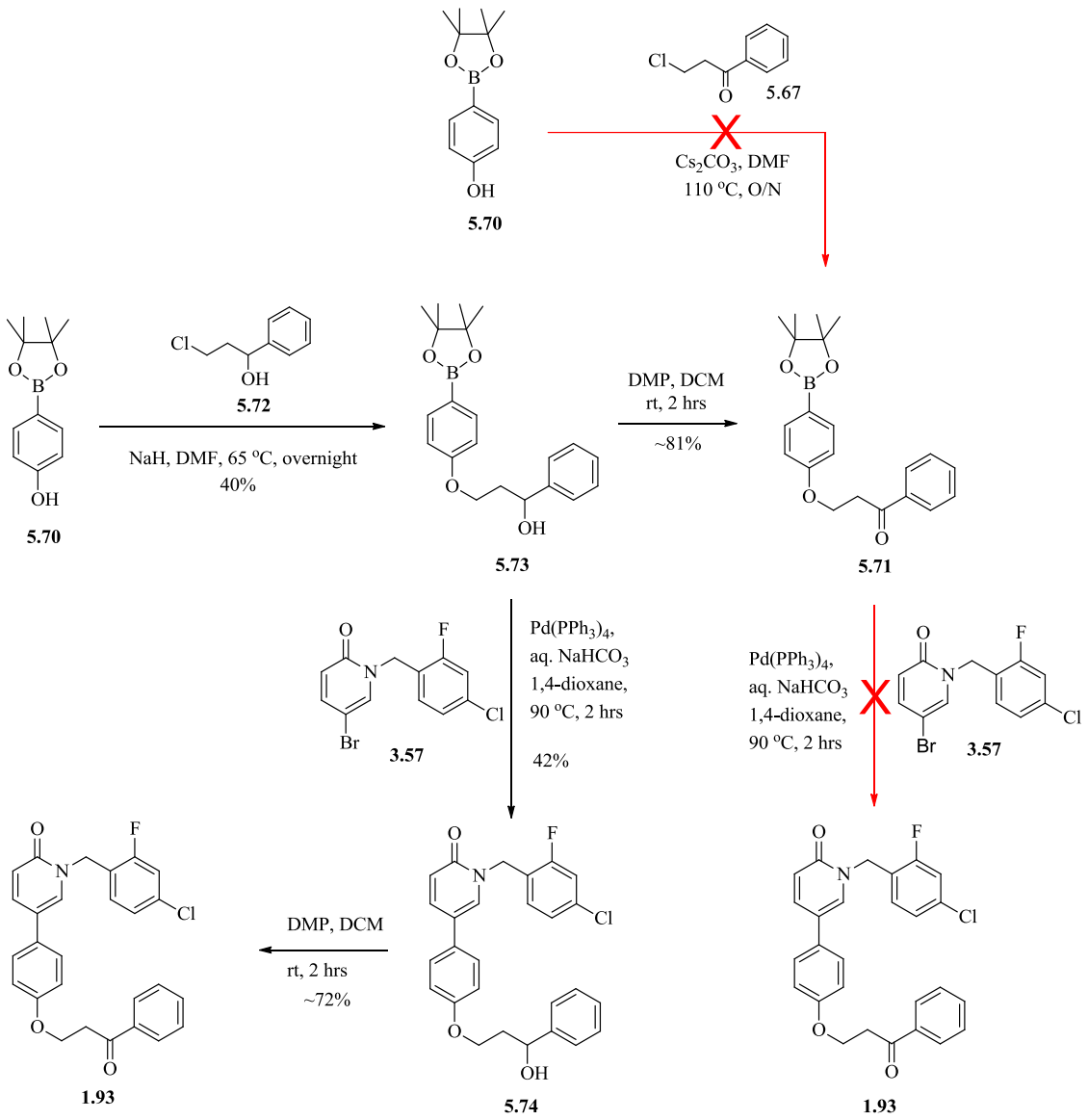


**Scheme 5.26.** Synthesis of lead mGlu2 PAM **1.93** as a control compound for mGlu2 pharmacological evaluations *via O*-alkylation of phenol **5.70** with thermally stable alkyl chloride **5.72**.

The phenoxide of 4-hydroxyphenyl boronate (**5.70**), generated *in situ* by treatment with NaH (conditions adapted from Mahale *et al.*, 2012 and Kolkhof *et al.*, 2009), was trapped with 3-chloro-1-phenylpropan-1-ol (**(±)-5.72**) to successfully provide ether **5.73** in 40% yield. Benzyl alcohol **(±)-5.73** was then subjected to Dess-Martin Periodinane oxidation (conditions adapted from Jin *et al.*, 2005) to provide ketone **5.71** in 81% yield. However, the reaction of boronate

ester **5.71** with bromide **3.57**, by implementing traditional Suzuki coupling conditions, did not result in the desired acetophenone **1.93**. Instead, phenol **3.59** was isolated from this reaction, which indicated that the β-substituted phenyl ketones could not be subjected to high temperature during basic reaction conditions due to competing β-elimination. In order to circumvent this problem, Suzuki reaction between the benzyl alcohol **5.73** and aryl bromide **3.57** was employed first to obtain benzyl alcohol **5.74** in 42% yield, followed by DMP-oxidation conditions at room temperature for 2 hours to obtain target ketone **1.93** in 72% yield (Scheme 5.26).

With pyridone based mGlu2 PAM control compounds **1.89** and **1.93** in hand, synthesis of novel mGlu2 irreversible PAMs as chemical probes for mGlu2 structure-function studies were subsequently initiated.

### 5.3.6. Synthesis of a Clickable Pyridone-Based mGlu2 PAM Photoprobe for mGlu2 Structure-Function Studies Featuring an Aryl Azide as a Photoreactive Group

The synthesis of azido-alkyne pyridone-based mGlu2 PAM photoprobe **4.29** was envisioned in 5 steps starting with known 2-fluoro-4-nitro benzyl bromide (**5.77**) (Scheme 5.27). Briefly, *N*-alkylation of 5-bromo-(1*H*)-*N*-pyridone with 2-fluoro-4-nitro benzyl bromide (**5.77**), followed by Suzuki coupling of *N*-benzyl pyridone derivative **5.78**, *O*-propargylation, nitro-reduction to aniline **5.81**, and aniline to azide conversion *via* diazotization and azide displacement was envisioned to efficiently provide target photoprobe **4.29**.

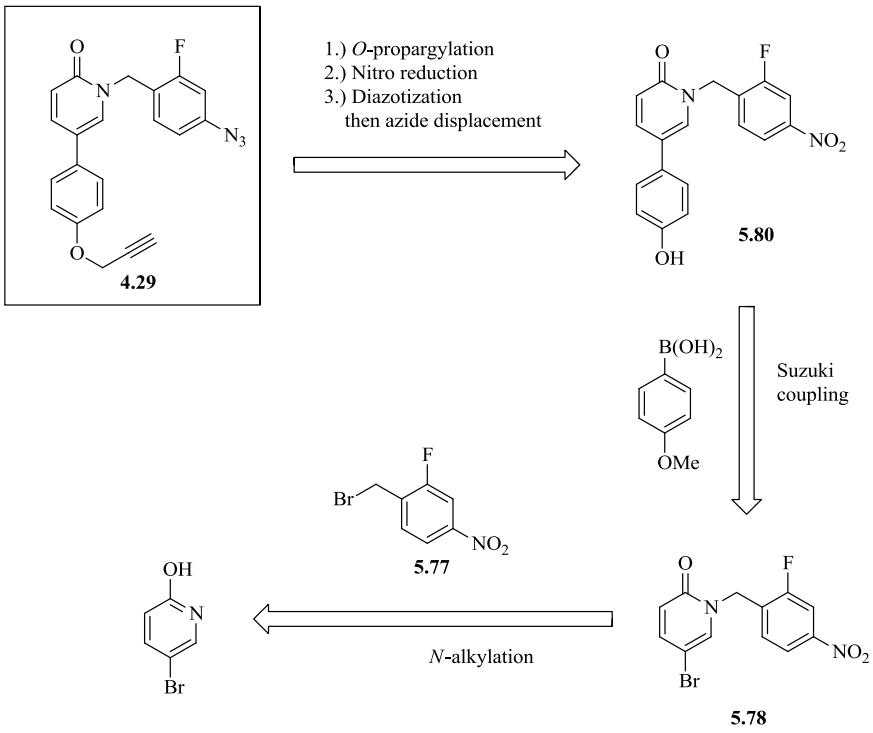


**Scheme 5.27.** Proposed retrosynthesis of clickable azide-alkyne mGlu2 photoprobe **4.29** for mGlu2 structure-function studies.

For the forward synthesis, 2-fluoro-4-nitro toluene (**5.76**) was initially subjected to radical-mediated benzyl bromination conditions (using N-bromosuccinamide (NBS) as a brominating agent and AIBN as a radical initiator; reaction conditions adapted from Ortuno *et al.*, 2011 and Frank *et al.*, 2013) in order to obtain 2-fluoro-4-nitrobenzyl bromide (**5.77**) in bulk quantities. However, this benzyl bromination reaction provided extremely low yields due to incomplete formation of target product **5.77** (Entry 1 and 2, Table 5.4). Even with an increase in the equivalents of NBS and using benzoyl peroxide as the radical initiator, a majority of target **5.77** was lost due to the formation of a mixture of target **5.77**, starting material **5.76**, and a possible dibromominated side product. All the three components appeared as close spots on TLC and were practically inseparable by silica gel flash column chromatography. In addition,

benzyl bromide **5.77** appeared to be a highly reactive compound that degraded when stored for a prolonged period.

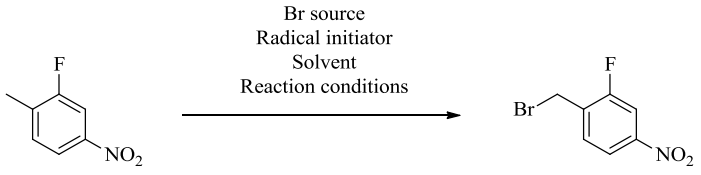


**5.76** **5.77**

| Entry | 2-Fluoro-4-nitrotoluene (5.76) | Br source | Radical initiator | Solvent | Reaction conditions | Result |
|---|---|---|---|---|---|---|
| **1** | 1 eq. | NBS (1.1 eq.) | AIBN (0.1 eq.) | Benzene | 80 ºC, 4 hrs | 8% yield of **5.77** |
| **2** | 1 eq. | NBS (1.05 eq.) | AIBN (0.02 eq.) | $CCl_4$ | 85 ºC, 7 hrs | 15% yield of **5.77** |
| **3** | 1 eq. | NBS (3 eq.) | $(PhCO_2)_2$ (0.3 eq.) | Chlorobenzene | 140 ºC, 2 hrs | Target Bromide + Starting material + Dibromination |

**Table 5.4**. Optimization efforts of radical bromination of **5.76** to provide benzyl bromide **5.77**.

Nevertheless, obtained benzyl bromide **5.77** (from Entry 2, Table 5.4) was sequentially subjected to *N*-alkylation with 5-bromo-2-pyridone, Suzuki coupling with 4-methoxy phenyl boronic acid, then methyl ether cleavage using $BBr_3$ to obtain phenol **5.80** in 5% yield over 4 steps (Scheme 5.28). The obtained phenol **5.80**, a highly polar compound, was practically insoluble in most organic solvents and required long, tedious silica gel flash column chromatography for its purification. Phenol **5.80** was subsequently treated with propargyl bromide followed by reduction of the *p*-nitro group to provide aniline **5.81**. The final conversion of aniline **5.81** to azide **4.29** *via* diazotization and displacement with azide completely failed and did not result in the formation of desired azide target **4.29**.

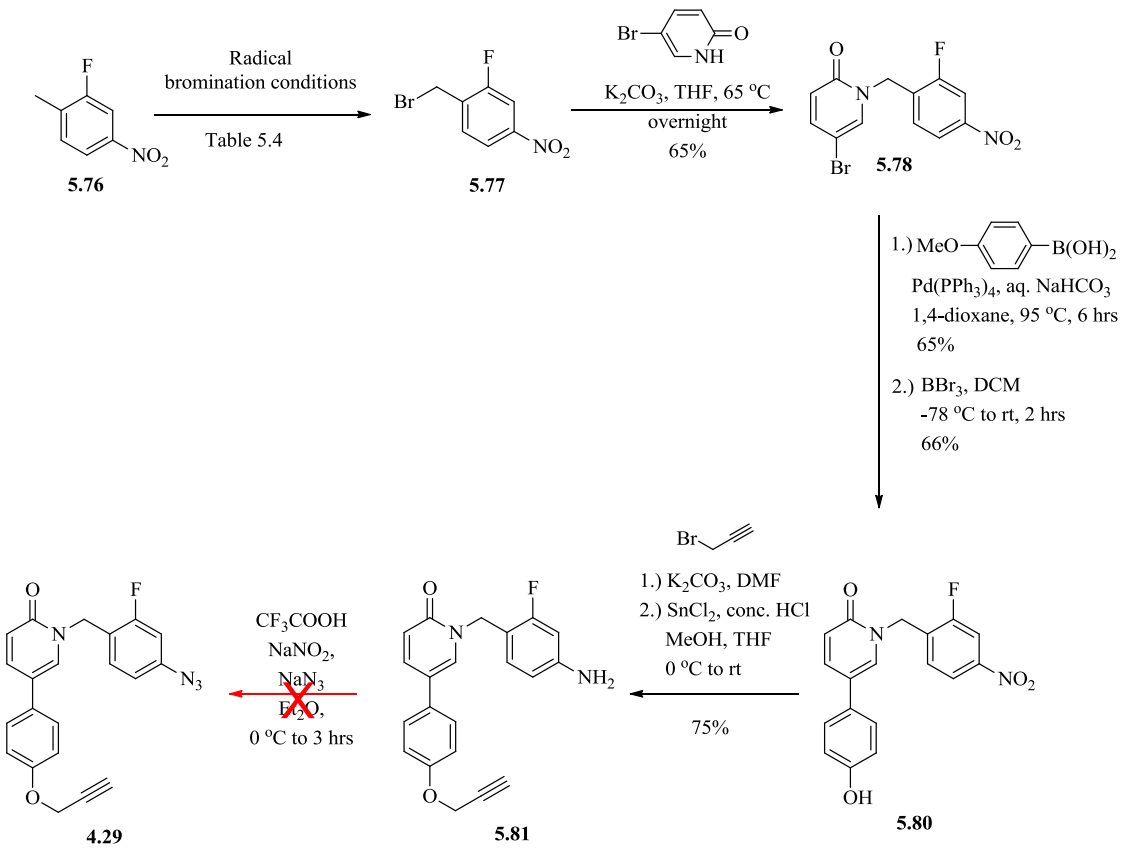


**Scheme 5.28.** Attempted synthesis of clickable mGlu2 PAM photoprobe **4.29** *via* a radical bromination, *N*-alkylation, Suzuki coupling, methyl ether deprotection, *O*-alkylation, nitro reduction, diazotization and azide displacement sequence.

Given the problems encountered in the previous synthetic scheme, this chemical strategy towards the target probe **4.29** was dropped in favor of pursuit of alternative synthetic routes. In particular, target **4.29** was envisioned *via* *N*-alkylation of key intermediate 2-methoxy pyridine (**5.85**) with 4-azido-2-fluoro benzyl chloride (**5.89**) (Scheme 5.29). The key synthetic intermediate 2-methoxypyridine **5.85** could potentially be accessed in three steps from commercially available 4-hydroxyphenyl boronate pinacol ester (**5.70**). Briefly, sequential *O*-propargylation of phenol **5.70** with propargyl bromide followed by Suzuki coupling with 2-methoxy-5-bromo pyridine (**5.83**) and then terminal alkyne deprotection of the protected propargyl ether was envisioned to provide pyridine derivative **5.85**. The synthesis of key

intermediate 4-azide-2-fluoro benzyl chloride (**5.89**) was envisioned starting with aniline to azide conversion of 4-amino-2-fluorobenzoic acid (**5.86**) *via* diazotization and azide displacement. Subsequent carboxylic acid (**5.87**) to benzyl alcohol (**5.88**) conversion was envisioned *via* mixed anhydride formation and then reduction, followed by the conversion of the resulting benzyl alcohol (**5.88**) to benzyl chloride **5.89**.

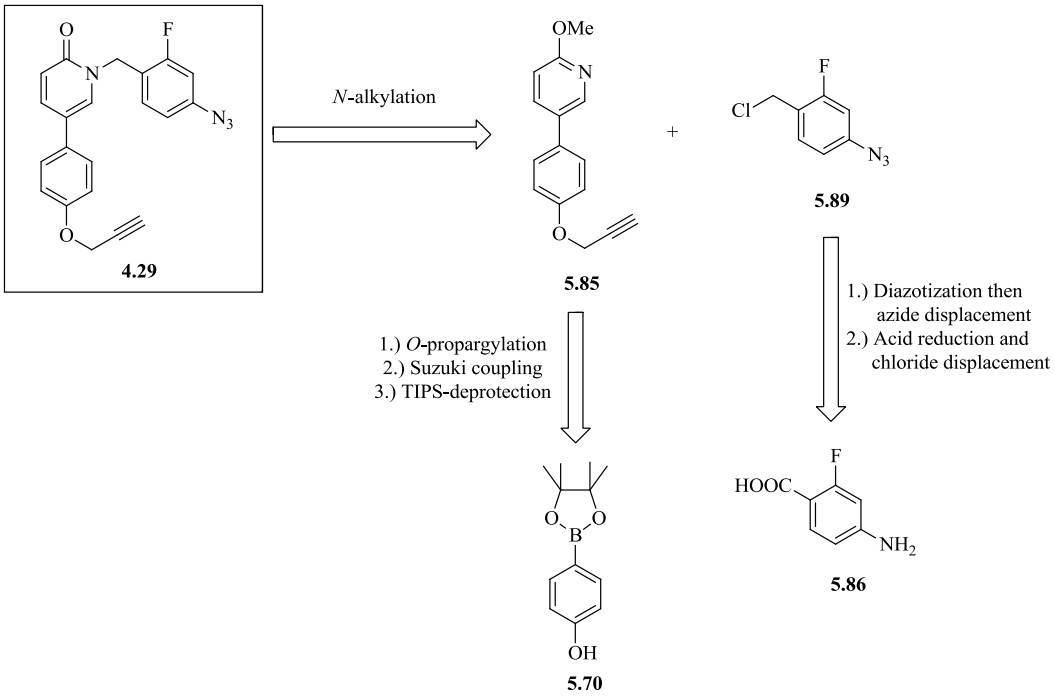


**Scheme 5.29.** Proposed alternate retrosynthesis of clickable azide-alkynyl mGlu2 PAM photoprobe **4.29** *via N*-alkylation reaction between synthetic intermediates **5.85** and **5.89**.

With this retrosynthesis in mind, commercially available 4-hydroxy boronate pinacol ester (**5.70**) was first treated with TIPS-protected propargyl bromide (Hoogboom and Swager, 2006) to obtain the *O*-alkylated phenyl boronate ester **5.82** in 62% yield (Scheme 5.30). The boronate ester **5.82** was then subsequently subjected to palladium-catalyzed Suzuki coupling conditions with 5-bromo-2-methoxypyridine (**5.83**) to provide biaryl **5.84** in excellent yield (99%). Subsequent TIPS-group deprotection of the terminal alkyne using *tert*-butyl ammonium fluoride (TBAF) provided pyridine intermediate **5.85** in 45% yield.

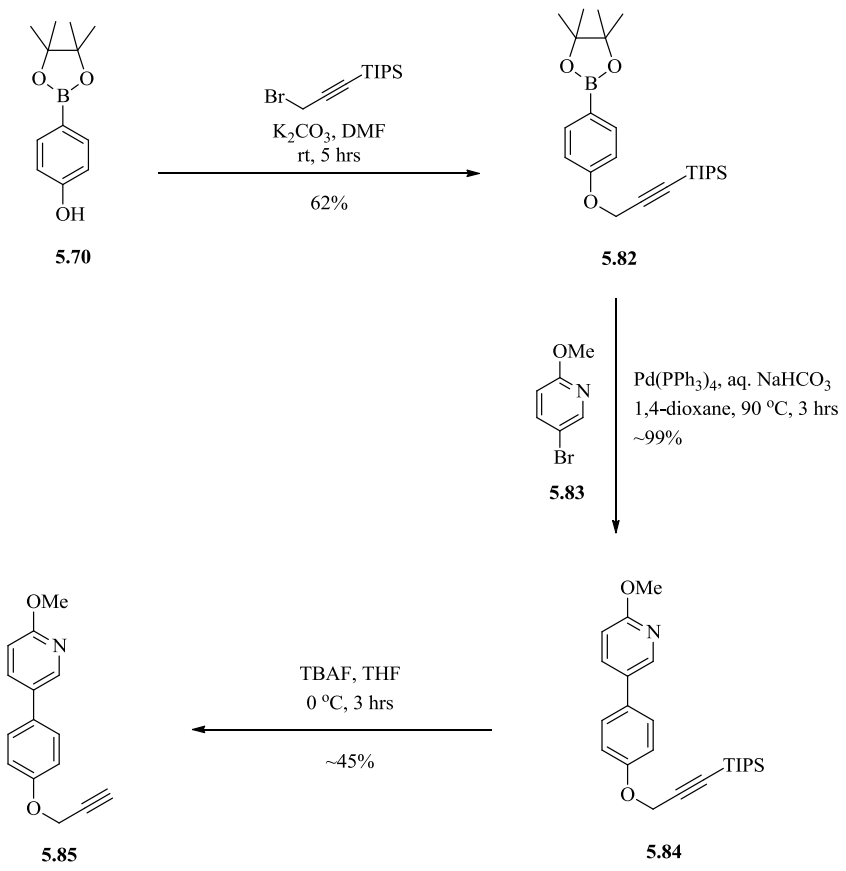


**Scheme 5.30.** Synthesis of pyridine derivative **5.85** *via O*-alkylation, Suzuki coupling, and silyl-group deprotection.

The synthesis of 4-azido-2-fluoro benzyl chloride (**5.89**) for *N*-alkylation of pyridone **5.85** was initiated by conversion of aniline **5.86** to azide **5.87** *via* diazotization and azide displacement (Scheme 5.31). Acid **5.87** was then subsequently converted into a mixed anhydride *in situ* by treatment with isopropyl chloroformate, followed by reduction with $NaBH_4$ in EtOH to form benzyl alcohol **5.88** in 30% yield. To convert primary alcohol **5.88** into a methanesulfonyl leaving group, benzyl alcohol **5.88** was treated with 1.5 equivalents of methane sulfonylchloride in the presence of $Et_3N$ at 0 °C for 1 hour. However, instead of the mesylate derivative, only benzyl chloride **5.89** was obtained in 15% yield *via* displacement of *in situ* generated benzylic mesylate by chloride ion. Nevertheless, the obtained benzyl chloride **5.89** was taken ahead for *N*-alkylation of **5.85** (Scheme 5.31) to obtain the final target **4.29** in 30% yield.

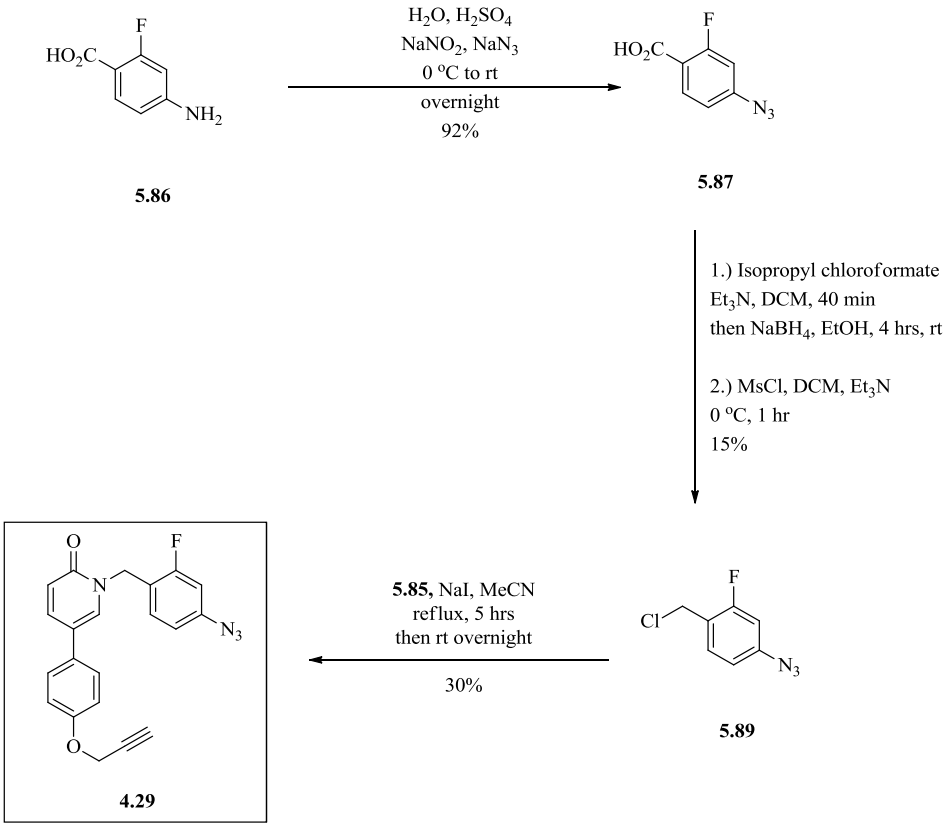


**Scheme 5.31.** Synthesis of clickable mGlu2 PAM photoprobe **4.29** featuring an azide and a propargyl ether for mGlu2 structure-function studies.

### 5.3.7. Synthesis of a Clickable Pyridone-Based mGlu2 PAM Photoprobe for mGlu2 Structure-Function Studies That Contains a Diazido Structural Motif Common to Clickable Photoprobes

The synthesis of probe **4.30** was accomplished by *N*-alkylation of known pyridone **5.90** with diazido benzyl mesylate **5.91** (Hosoya *et al.*, 2005) (provided by Dr. Ranganadh Velagaleti) to provide di-azido photoprobe **4.30** in 25% yield (Scheme 5.32).

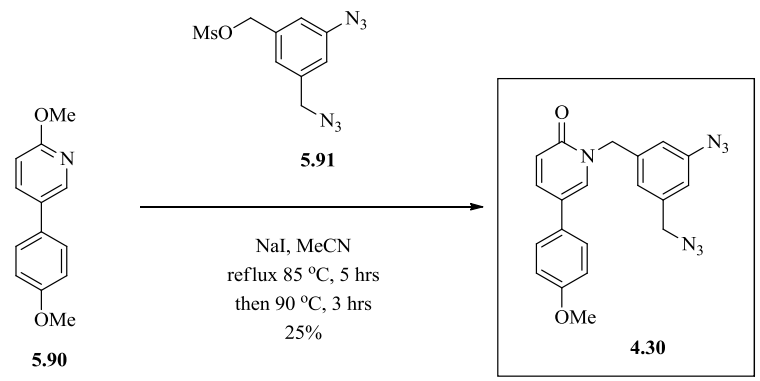


**Scheme 5.32.** Synthesis of diazido clickable mGlu2 PAM photoprobe **4.30** for mGlu2 structure-function studies.

## 5.3.8. Synthesis of a Clickable Pyridone-Based mGlu2 PAM Photoprobe for mGlu2 Structure-Function Studies That Contains an Acetophenone Photoreactive Group

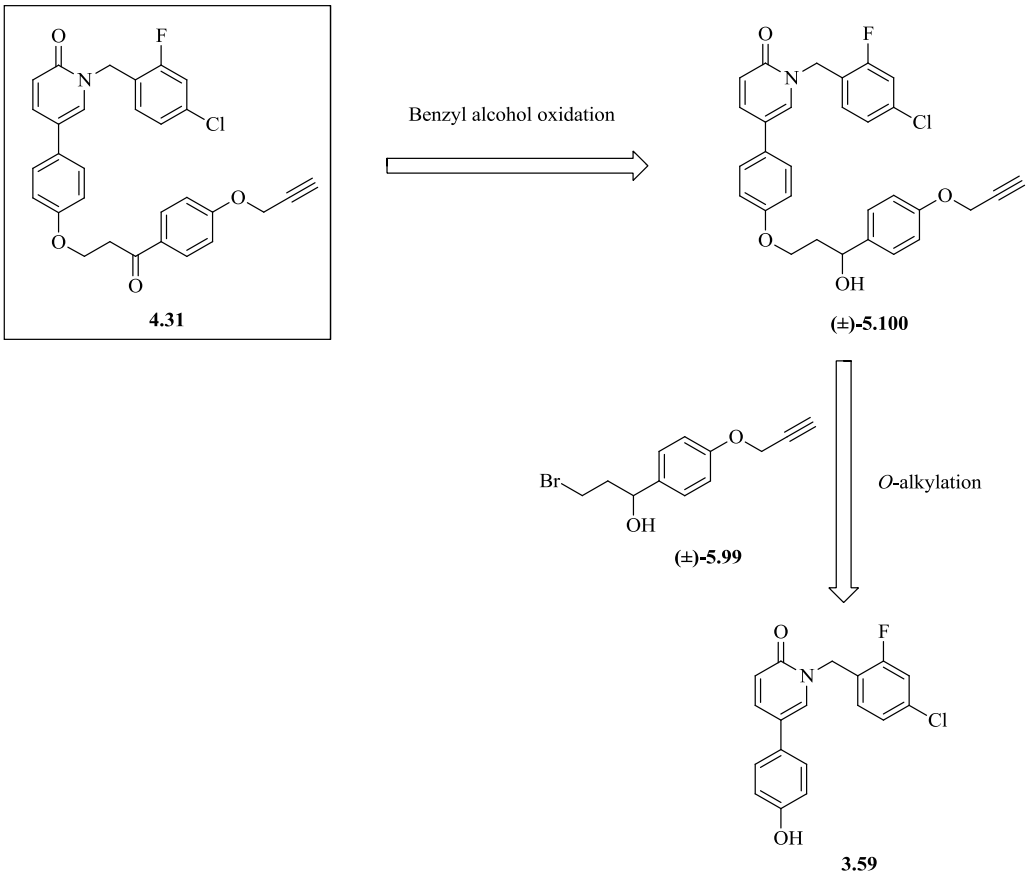


**Scheme 5.33.** Proposed retrosynthesis of clickable mGlu2 PAM photoprobe **4.31** featuring acetophenone and propargyl ether group for mGlu2 structure-function studies.

The synthesis of target photoprobe **4.31** was envisioned *via* direct alkylation of phenol **3.59** with alkyl bromide **(±)-5.99** followed by oxidation of resulting benzyl alcohol **(±)-5.100** to provide the target phenyl ketone **4.31** (Scheme 5.33).

With this plan in mind, the forward synthesis was initiated *via* Friedel-Craft's acylation of propargyl phenol (**5.95**) with 3-bromopropionyl chloride (**5.96**) (conditions adapted from Rueping and Hubener, 2011) to provide ketone **5.97** in 57% yield after silica gel flash column chromatography (Scheme 5.34). It was observed that β-bromophenylketone **5.97** was rather unstable at room temperature and completely degraded within 24 hours according to TLC experiments. As a result, ketone **5.97** was immediately taken ahead to the next reaction. Initial attempts to reduce ketone **5.97** to benzyl alcohol **(±)-5.99** using $NaBH_4$ (2 equivalents) at room temperature for 5 hours resulted in an inseparable mixture of target bromide **(±)-5.99** and 1-phenyl-1-hydroxy-propane derivative **5.98** in a 4:1 ratio. In order to favor ketone reduction more than undesirable bromide displacement, the reaction was attempted using $NaBH_4$ (1 equivalent) at 0 $^oC$ for 3 hours followed by stirring at room temperature for 1 hour. Using these conditions, target alcohol **5.99** was obtained in 57% yield after silica gel flash column chromatography without any indication of side product formation. With hydroxyl bromide **(±)-5.99** in hand, alkylation of phenol **3.59** was attempted by treatment with NaH and overnight heating at 70 $^oC$. The reaction proceeded with multiple spots observed on TLC, which upon separation resulted in the isolation of only 5% of ether **(±)-5.100**. The low yield of the reaction was attributed to side reactions associated with the of unprotected terminal alkyne of **(±)-5.99** under highly basic conditions. Since key intermediate **(±)-5.100** was obtained in less than 1% yield over 3 steps using this chemistry, this strategy was discontinued and an alternate reaction scheme was pursued thereafter.

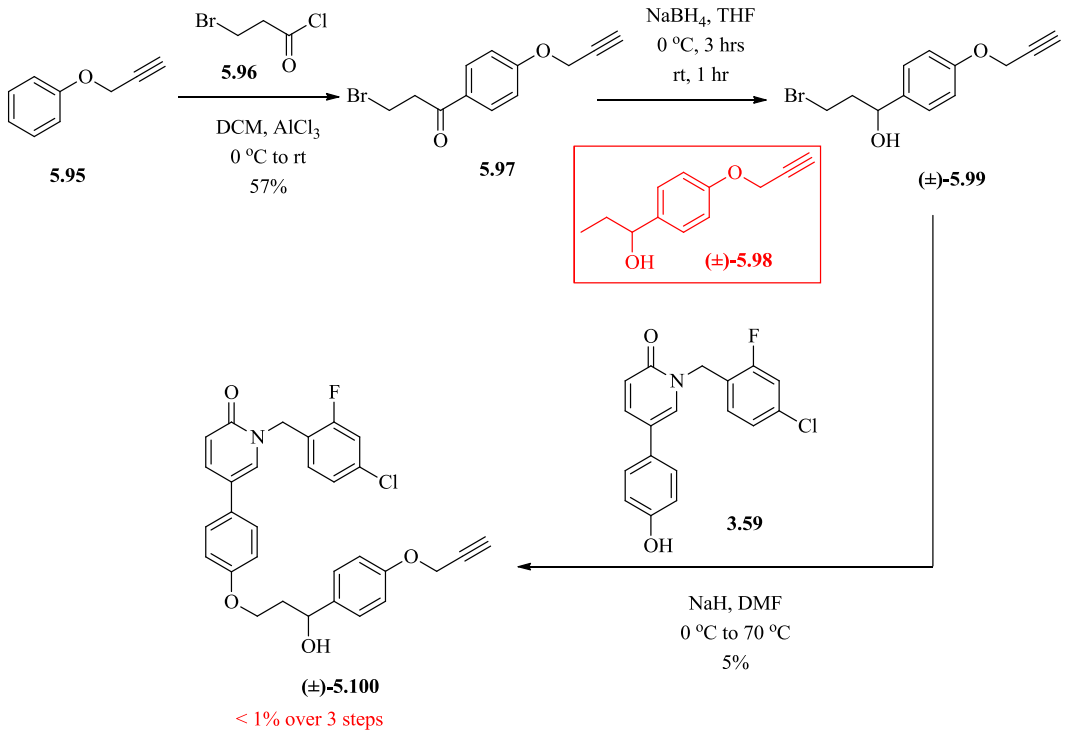


**Scheme 5.34.** Attempted synthesis of intermediate **(±)-5.100** *via* a Friedel-Craft's acylation, ketone reduction, phenol *O*-alkylation sequence.

In order to overcome the problem of undesirable reactivity of the unprotected terminal alkyne during the *O*-alkylation step, an alternate method involving the use of TIPS-protected propargyl phenol was employed (Scheme 5.35). This synthesis was initiated with the treatment of phenol **5.101** with known TIPS-protected propargyl bromide **5.102** (Hoogboom and Swager, 2006) to obtain TIPS-protected propargyl phenol ether **5.103** in excellent yield. Ether **5.103** was then treated with 3-bromopropionyl chloride **5.96** under Friedel-Craft's acylation conditions. This reaction, after work-up resulted in multiple spots on TLC which upon chromatographic separation followed by $^{1}$HNMR analysis, revealed the formation of target ketone **5.106** in 35% yield alongside formation of TIPS-deprotected ketone **5.104** and cleaved propargyl ether **5.105** as side products. Sequential ketone reduction of **5.106**, followed by phenol alkylation, provided ether intermediate **5.108** in 50% yield. This benzyl alcohol (**5.108**), although contaminated with

aliphatic impurities according to $^{1}$HNMR, was sufficiently clean enough for TIPS-deprotection by treatment with TBAF (Liu *et al.*, 2012).

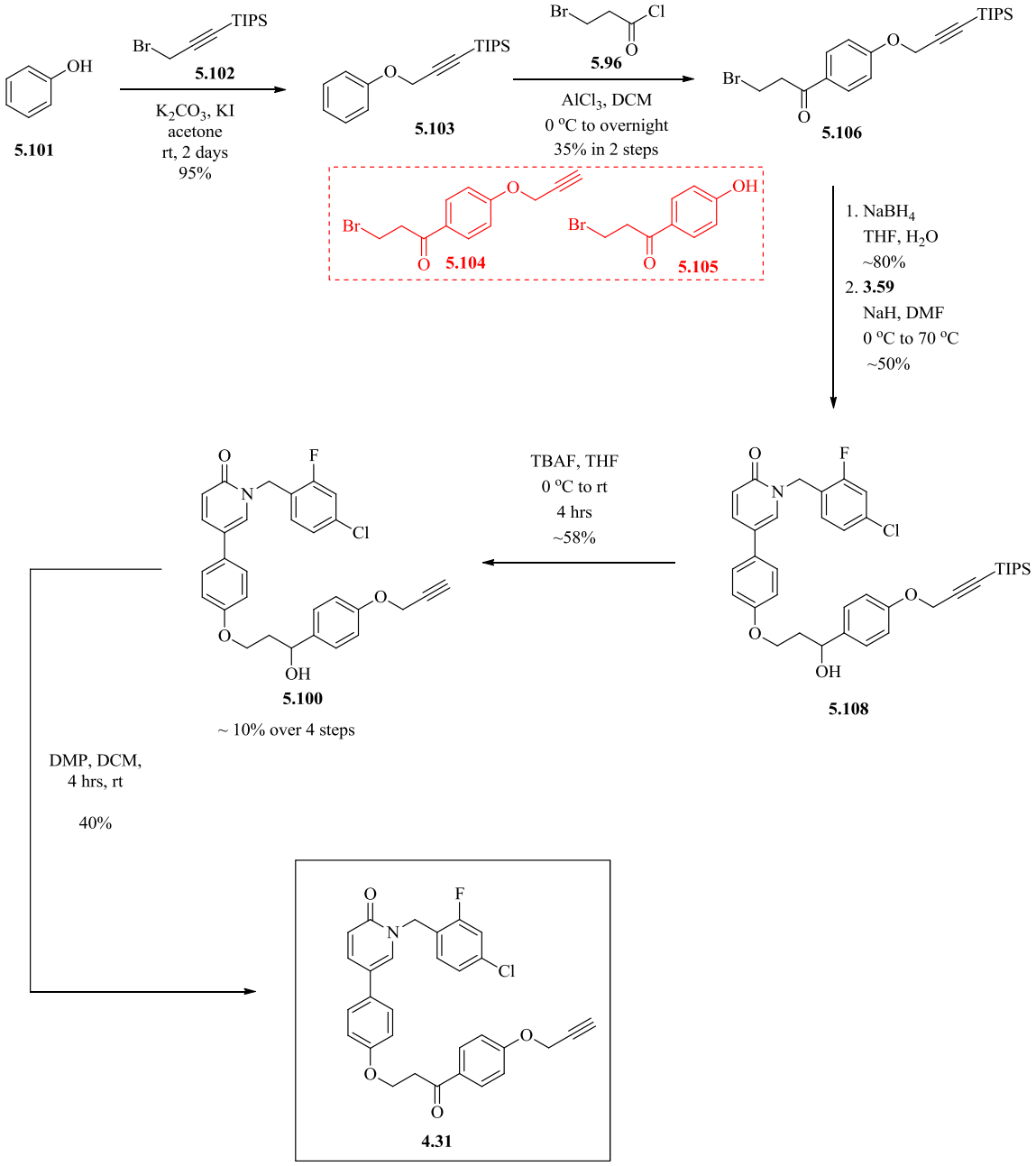


**Scheme 5.35.** Synthesis of target mGlu2 clickable photoprobe **4.31** featuring an acetophenone and a propargyl ether for mGlu2 structure-function studies.

The final intermediate alcohol **5.100**, although produced by a lengthier synthetic route (5 steps, Scheme 5.35) versus Scheme 5.34 (3 steps), gave yields that were drastically improved

(~10% over 5 steps in Scheme 5.35 versus <1% over 3 steps in Scheme 5.34). The resulting benzyl alcohol **5.100** was then subjected to Dess-Martin Periodinane oxidation to provide the final acetophenone containing target probe **4.31** in 40% yield.

### 5.3.9. Synthesis of a Photo-Masked mGlu2 PAM Affinity Labeling Probe for mGlu2 Structure-Function Studies

Pyrimidone lead compound **4.36** was obtained in 2 steps starting with known 5-iodo pyrimidone **5.110** (Efange *et al.*, 1985) *via N*-alkylation with benzyl bromide **3.56** and Suzuki coupling with methyl ether **3.58** (Scheme 5.36). The initial *N*-alkylation reaction was carried out in DMFin the presence of $K_2CO_3$ with overnight stirring at room temperature to provide target iodide **5.111** in low yield (30%). In order to improve the yield, the workup of this reaction was modified by diluting the reaction with $H_2O$ after completion until a white precipitate ceased to exist, then target iodide **5.111** was isolated *via* filtration. The resulting solid was purified *via* silica gel flash column chromatography to obtain *N*-alkylated pyrimidone **5.111** in 73% yield. Subsequent Suzuki coupling of aryl iodo **5.111** with commercially available 4-methoxy phenyl boronic acid (**3.58**) provided the pyrimidone lead compound **4.36** in 16% yield. This compound would be subsequently used as a standard control compound in the pharmacological evaluations of pyrimidone-based photo-masked affinity probe **4.32**.

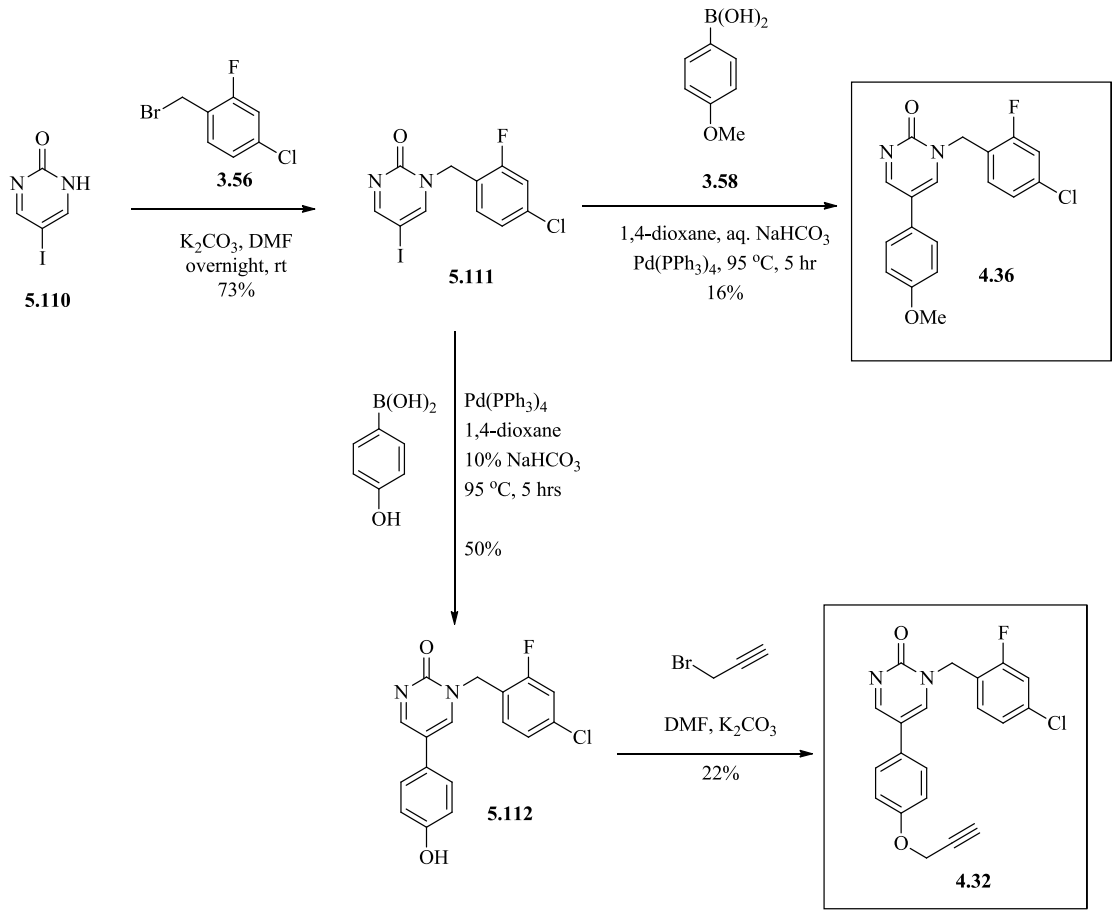


**Scheme 5.36.** Synthesis of novel pyrimidone-based mGlu2 PAM **4.36** as a control compound and pyrimidone-alkyne photo-masked affinity probe **4.32** for mGlu2 structure-function studies.

In order to synthesize propargyl ether photoprobe **4.32**, aryl iodo **5.111** was subjected to Suzuki coupling reaction with 4-hydroxyphenylboronic acid to obtain phenol **5.112** in 50% yield. Subsequet *O*-alkylation of phenol derivative **5.112** with propargyl bromide provided target photoprobe **4.32** in 22% yield.

## 5.4. Summary of Significance, Innovation, and Synthetic Accomplishments Associated With This Dissertation Work

Despite many years of research towards understanding the biological basis of substance abuse and addiction, there are currently no FDA-approved pharmacotherapies for the treatment of cocaine and methamphetamine addiction. Furthermore, FDA-approved treatments for tobacco smoking and nicotine addiction, such as nicotine replacement products, varencline (Chantix®), and bupropion (Zyban®), are inadequate in maintaining long-term abstinence as 80% of tobacco smokers relapse within the first month of treatment. This warrants a need for more efficacious and effective treatments for nicotine addiction. The lack of progress in the discovery and development of novel and effective pharmacotherapies to treat psychostimulant abuse is, in part, attributed to the absence of high quality 3-D structure and function information regarding significant proteins such as DAT, α4β2 nAChR, α3β4 nAChR and mGlu2 that are implicated in reinforcing and reward actions of psychostimulant drugs of abuse. As a result, a detailed understanding of the structure of binding sites of ligands within these proteins is imperative in order to develop new therapeutics to treat drug abuse and addiction. In this regard, the research objective of this dissertation was to provide chemical probes to facilitate understanding of how the pharmacology profile (i.e., affinity, selectivity, potency, behavioral phenotype, etc.) of anti-addiction lead compounds (e.g., pyrovalerone, bupropion, BINA) is dictated by the three-dimensional interactions that occur when these compounds non-covalently interact with their major drug targets (e.g., the DAT, mGlu2, and select nAChR subtypes) at the molecular level. In particular, this objective was accomplished *via* the rational design and chemical synthesis of photoaffinity probes based on promising anti-addiction lead compounds (e.g., pyrovalerone,

bupropion, BINA) in order to map the binding sites and poses of these compounds within their proposed major drug targets (i.e., the DAT, α4β2 nAChR, α3β4 nAChR, or mGlu2).

Despite the emergence of several LeuT-based DAT homology models and the identification of a plethora of DAT interactive compounds, it is still not clear how the DAT discriminates substrates (e.g., dopamine, amphetamines), inhibitors (e.g., cocaine, bupropion, methylphenidate, GBR-12909, pyrovalerone), highly abused compounds (e.g., cocaine, amphetamines, cathinones), and therapeutic compounds (e.g., bupropion, methylphenidate) at the molecular level. In this regard, photoaffinity probes based on DAT ligands remain important tools in determining their corresponding binding site(s) and conformational preference(s) within the DAT. Prior to this dissertation, the overwhelming majority of known DAT irreversible ligands were based on tropane-containing inhibitors (e.g., cocaine, benztropine) or their conformationally flexible piperidine- or piperazine-based analogues. One of the goals of this dissertation was to develop potent non-tropane irreversible ligands for mapping drug-binding sites within DAT. In particular, structurally-related DAT inhibitors pyrovalerone and bupropion, with disparate behavioral properties, were chosen as lead compounds for the design of chemical probes guided by their existing structure-activity relationship studies in the literature. Specifically, PV and BP were derivatized with a photoreactive functional group (i.e. aryl azide or acetophenone) and a chemical reporter group (i.e., $^{125}$I) placed directly on the inhibitor pharmacophore. The synthesized probes were then pharmacologically evaluated for DAT affinity and dopamine reuptake inhibition activity by Dr. Christopher Surratt's group. Probes with DAT activity comparable to lead compounds were then subjected to photoaffinity labeling experiments within the DAT by Dr. Roxanne Vaughan's lab. This portion of research is significant as the identification of structural elements and conformational preferences of PV and

BP binding sites within DAT could provide an experimental evidence for the mechanism of their different behavioral profiles despite having structural similarities. In this regard and as previously described in Sections 5.1 and 5.2, synthesis of pyrovalerone-based photoprobes **(±)-4.16 - (±)-4.18** and bupropion-based photoprobe **(±)-4.20** (Figure 5.1) represent the first successful examples of DAT photoaffinity ligands based on non-tropane DAT interactive compounds wherein the photoreactive azide and iodine tag are present directly on the inhibitor pharmacophore.

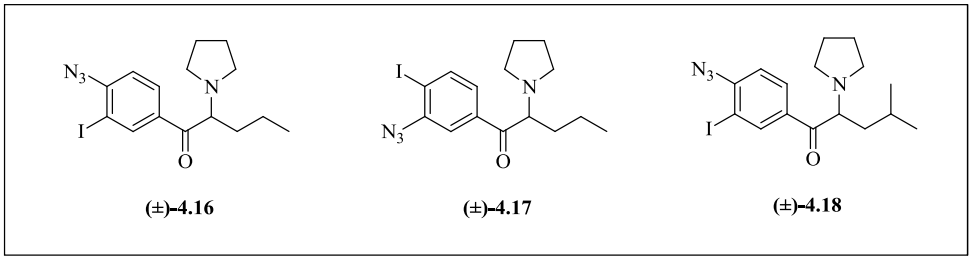


**Figure 5.1.** Photoprobes **(±)-4.16 - (±)-4.18** represent the first successful examples of non-tropane DAT irreversible compounds based on pyrovalerone with the photoreactive azide group and iodine tag present directly on the pharmacophore.

In terms of practical organic synthesis troubleshooting and as previously described in Section 5.1.1, an optimized synthesis of racemic 4-azido-3-iodo-pyrovalerone (**(±)-4.16**) (Scheme 5.3) was developed featuring the incorporation of the photoreactive aryl azide as the last step in the synthesis given the potential inherent instability traditionally associated with this functional group over multiple synthetic step. The synthesis of target probe **(±)-4.16** was envisioned from known acetanilide **5.1** utilizing six steps: Friedel-Craft's acylation with valeryl chloride **5.2**, α-bromination, pyrrolidine *N*-alkylation, *p*-amide hydrolysis, electrophilic iodination, diazotization and then azide displacement. However, the initial Friedel-Craft's acylation of acetanilide **5.1** with valeryl chloride under various conditions consistently resulted in an incomplete reaction (Scheme 5.2). As a result, target ketone **5.3** was obtained alongside

acetanilide as a major impurity because separation by silica gel flash column chromatography could not be readily achieved due to their same $R_f$ values ($R_f$ = 0.42 in hexanes:EtOAc, 1:1). This problem was overcome by subjecting the inseparable mixture to reduction with $NaBH_4$ in MeOH, then separating benzyl alcohol **(±)-5.4** from acetanilide *via* silica gel flash chromatography due to the significant difference in $R_f$ values for the two compounds. In turn, benzyl alcohol **(±)-5.4** was then oxidized back to ketone **5.3** in 70% yield using PCC in dichloromethane (Scheme 5.2). The next step, α-bromination of ketone **5.3** was optimized to obtain α-bromoketone **(±)-5.5** in 100% yield which was further subjected to a sequence of pyrrolidine *N*-alkylation, *p*-amide hydrolysis, electrophilic iodination, diazotization and then azide displacement. Overall, this route utilized 8 steps and produced target photoprobe 4-azido-3-iodo-pyrovalerone (**(±)-4.16**) in 23% yield (Scheme 5.3). The branched side chain analog of racemic 4-azido-3-iodo-pyrovalerone (**(±)-4.18**) was also envisioned similar to the straight chain analog **(±)-4.16** as described in Scheme 5.4. However, once again, the initial Friedel-Craft's acylation provided an inseparable mixture of acetanilide (**5.1**) and target ketone *N*-(4-(4-methylpentanoyl)phenyl)acetamide (**5.9**) (Scheme 5.4). As a result, ketone **5.9** was instead synthesized in 3 steps starting from commercially available 4-(trifluoromethyl)aniline (**5.10**) *via* Grignard reaction, then imine hydrolysis followed by *N*-acetylation. The desired photoprobe **(±)-4.18** was obtained from ketone **5.9** following same steps as in Scheme 5.4. Alongside the branched side chain pyrovalerone-based photoprobe **(±)-4.18**, the synthesis of *meta*-azido-*para*-iodo pyrovalerone probe **(±)-4.17** was pursued simultaneously. However, synthesis of its precursor *p*-iodo-*m*-amino pyrovalerone was problematic wherein acid hydrolysis of *meta*-amide-*para*-iodo pyrovalerone derivative **(±)-5.20** in refluxing aqueous HCl did not provide the desired aniline **(±)-5.22** (Scheme 5.8). In order to overcome this roadblock, target photoprobe

**(±)-4.17** was envisioned featuring incorporation of the photoreactive azide moiety earlier in the synthesis, and was subsequently synthesized from *m*-azido-*p*-iodo valerophenone (**5.23**) *via* α-bromination and displacement with pyrrolidine (Scheme 5.10).

Additionally and as previously described in Section 5.2.1, synthesis of racemic *p*-azido-*m*-iodo-bupropion (**(±)-4.20**) was needed as a potential photoprobe for DAT structure-function studies. In this regard, synthesis of racemic *p*-amino-*m*-iodo derivative **(±)-5.32** was required as the synthetic precursor to obtain target photoprobe **(±)-4.20** *via* diazotization and azide displacement. However, the synthesis of racemic *p*-amino-*m*-iodo derivative **(±)-5.32** was problematic wherein electrophilic iodination of aniline **(±)-5.31** with iodine monochloride in the presence of glacial acetic acid provided *p*-amino-*m*-iodo **(±)-5.32** in low yields (23%, Scheme 5.12). The low yield was a result of difficult monitoring of the reaction for completion *via* TLC because the aniline and its *p*-amino-*m*-iodo derivative **(±)-5.32** had the same $R_f$ values ($R_f$ = 0.27 in hexanes: EtOAc: $Et_3N$, 10:88:2). As a result, *p*-amino-*m*-iodo derivative **(±)-5.32** was obtained alongside aniline **(±)-5.31** as a major impurity and separation by silica gel flash column chromatography could not be achieved efficiently. Furthermore, the conversion of *p*-amine-*m*-iodo derivative **(±)-5.32** to azide **(±)-4.20**, and its subsequent purification *via* silica gel flash column chromatography or HCl salt formation, resulted in decomposition of the aryl azide functional group. As a result, an alternate synthetic strategy towards target photoprobe **(±)-4.20** was employed featuring incorporation of the photoreactive azide moiety earlier in the synthesis (Scheme 5.13). In particular, target photoprobe **(±)-4.20** was obtained from *p*-azido-*m*-iodopropiophenone (**5.36**) *via* α-bromination and displacement with *tert*-butylamine in 11% overall yield over 3 steps (Scheme 5.14).

Bupropion's anti-depressant and smoking-cessation effects have been mainly attributed to its inhibition of the DAT and NET; however, there is increasing evidence that bupropion non-competitively inhibits several nAChR subtypes, particularly α4β2 and α3β4, and modulation of these targets may also contribute to the drug's therapeutic efficacy. Despite its status as an FDA-approved drug for major depressive disorder, seasonal affective disorder, and aid to help people stop smoking by reducing cravings and other withdrawal effects, the molecular determinants of how bupropion interacts with select nAChR subtypes remains unknown. In particular, this information is currently lacking due to the unavailability of high-resolution x-ray crystal structures of human α4β2 and α3β4 nAChR subtypes. In addition, (2*S*,3*S*)-hydroxybupropion, a major active and potent metabolite of bupropion is believed to contribute to the antidepressant and smoking cessation activity of bupropion. The overall objective of the second portion of this dissertation work was to develop α4β2 and α3β4 nAChR irreversible ligands based on bupropion to allow nAChR structure-function studies. In this regard and as previously described in Sections 4.7 and 5.2, irreversible chemical probes based on bupropion (i.e. *p*-azido-*m*-iodo analog **(±)-4.20** and *m*-iodo analog **(±)-4.21**) and (2*S*,3*S*)-hydroxybupropion (i.e. *p*-azido-*m*-iodo analog **(±)-4.23**) were rationally designed and chemically synthesized in order to map the binding sites and poses of these compounds within the α4β2 nAChR and α3β4 nAChR.

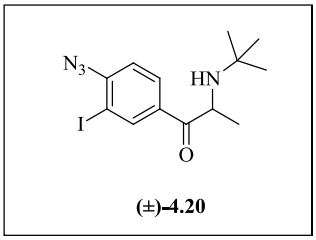


**(±)-4.20**

**Figure 5.2.** Photoprobe **(±)-4.20** represents the first example of bupropion based irreversible ligand successfully utilized towards application of the "BEProFL" approach to understand its binding modes with α4β2 nAChR and α3β4 nAChR.

Among the synthesized probes, *p*-azido-*m*-iodo BP photoprobe **(±)-4.20** (Figure 5.2), previously developed as a photoprobe for DAT structure-function studies, was successfully utilized towards application of the "BEProFL" approach to understand the binding modes of bupropion within α4β2 nAChR and α3β4 nAChR. Given that *p*-azido-*m*-iodo BP photoprobe **(±)-4.20** displayed modest pharmacological activity as compared to lead bupropion within select nAChRs as evaluated by Dr. Hugo Arias, its radio-iodinated analog **(±)-[$^{125}$I]-4.20**, synthesized by Dr. John Lever, was subjected to irreversible photo-crosslinking within *Torpedo* nAChRs by Dr. Michael Blanton's group, followed by proteolytic degradation and amino-acid mapping which led to the successful identification of the exact point of covalent probe attachment to the *Torpedo* nAChR transmembrane domain. The collected results from pharmacology and proteomic experiments of **(±)-[$^{125}$I]-4.20** were consistent with a computational molecular model wherein bupropion, photoreactive analog **(±)-4.20**, and TCP (a nAChR noncompetitive antagonist) bind to overlapping sites within the lumen of muscle-type nAChR ion channels.

Analogous to DAT and nAChR ligands, numerous pharmacological and behavioral studies indicate positive allosteric modulation of mGlu2 as a promising pharmacological approach for treating drug abuse. In particular, mGlu2 PAMs are currently being pursued as drug abuse therapeutics given their ability to reduce conditioned reward, self-administration, and reinstatement of drug seeking which are behavioral hallmarks of drug abuse and addiction. Nevertheless, discovery and optimization of mGlu2 positive allosteric modulators is associated with numerous challenges due to the problem of ligand-biased pharmacology, "flat" and difficult SAR, and molecular switches. These problems that currently represent a major impediment in developing mGlu2 PAMs as potential therapeutics can be attributed to a lack of understanding of mechanistic and / or conformational mGlu2 structure-function relationships that dictate the

affinity and cooperativity of mGlu2 PAMs. This is principally due to lack of 3-D structural knowledge and understanding of mGlu2 when compared to other well-studied mGlu receptor subtypes such as mGlu5. Moreover, experimental strategies that further refine and validate the recently disclosed mGlu2 homology model are sorely needed. Consequently, the overall objective of the third portion of this research was to develop mGlu2 PAM irreversible ligands as chemical probes to map their corresponding binding sites and poses within mGlu2 *via* affinity or photoaffinity labeling to be performed by Dr. Karen Gregory's group. The hypothesis was that chemically distinct mGlu2 PAMs could be derivatized with a functional group capable of forming a covalent bond to mGlu2 and, if necessary, a tag functional group. It should be noted that, instead of radioisotopes (i.e., $^{125}$I) previously used in the design of DAT and nAChRs photoaffinity ligands, mGlu2 PAM-based chemical probes in this section of dissertation work were developed bearing "clickable handles" (e.g., aliphatic azides, terminal alkynes) or other chemical reporter groups (such as ketones) to allow the attachment of detection and purification tags *via* bioorthogonal chemistry. Such chemical probes, upon photo-irradiation and covalent ligation within a mGlu2 allosteric binding site, are expected to allow derivatization of the probe by the attachment of tags such as biotin for easy enrichment, isolation, and detection, or fluorophores for detection and imaging applications. This tandem photoaffinity labeling-bioorthogonal conjugation approach is expected to aid in microlevel analysis *via* purification, proteolysis, and mass spectrometric (MS) studies in order to identify specific sites of photoprobe crosslinking within mGlu2. This contribution is expected to vertically advance the field towards elucidation of molecular determinants for mGlu2 allosteric modulator affinity *versus* cooperativity, and further help in understanding the inherent complexities of these compounds that hinder their rational development into therapeutics.

In particular, BINA (**(±)-1.71**), a known clinically relevant mGlu2 PAM, was modified to contain a tag (i.e., terminal alkyne or an acetophenone) and a photoreactive functional group (i.e. an aryl azide or an acetophenone). In this regard, the design and synthesis of BINA-based probes **(±)-4.25** and **(±)-4.27** (see Section 5.3) featuring an intrinsic acetophenone or an aryl azide as photoreactive groups, respectively, represent the first successful examples of mGlu2 photoaffinity ligands for mGlu2 structure-function studies (Figure 5.3). In terms of practical organic synthesis and as previously described in Scheme 5.17, racemic hydroxyl indanone **(±)-3.40** was obtained in 70% yield over 4 steps *via* modified and optimized reaction conditions with a significant improvement in product yield when compared to the previously known conditions (DeSolms *et al*., 1978; 4 steps, 30% overall yield, Scheme 5.17). The synthesized phenol derivative **(±)-3.40** was subsequently utilized as an intermediate in the synthesis of target BINA-based mGlu2 PAM photoprobes **(±)-4.25** (Scheme 5.21) and **(±)-4.27** (Scheme 5.23). Additionally, a 1,5-substituted pyridone class of mGlu2 PAMs discovered *via* HTS efforts at Addex Pharmaceuticals was selected as a scaffold for further development of mGlu2 irreversible chemical photoprobes. More specifically, compound **1.89** was selected as a lead compound for rational photoprobe design featuring incorporation of different photoreactive functional groups at different parts on the 1,5-pyridone mGlu2 PAM scaffold (Scheme 4.7). In this regard and as previously described in Section 5.3, pyridone-based photoaffinity ligands **4.29** – **4.32** (Figure 5.3) were synthesized *via* optimized synthetic methodology as potential candidates for mGlu2 structure-function studies. In particular, the initial synthetic methodology to synthesize clickable alkyne-azido mGlu2 PAM photoprobe **4.29** was problematic wherein aniline to azide conversion failed to provide the desired target due to the presence of a reactive unprotected terminal alkyne group. In order to overcome this problem, the target photoprobe was successfully synthesized

*via* an alternate route featuring *N*-alkylation of 2-methoxypyridine derivative **5.85** (3 steps, 35% overall yield, Scheme 5.30) with 4-azido-2-fluoro benzyl chloride **5.89** (3 steps, 15% overall yield, Scheme 5.31) in 30% yield (Scheme 5.31). Additionally and as previously described in Section 5.3.8, in order to synthesize clickable alkyne acetophenone mGlu2 PAM photoprobe **4.31**, the initial route to obtain benzyl alcohol precursor **5.100** was not optimal as it provided **5.100** in <<1% overall yield in 3 steps *via* a Friedel-Craft's acylation, ketone reduction, and phenol *O*-alkylation sequence (Scheme 5.34). In turn, the new efficient route featuring a TIPS-protected terminal alkynyl starting material provided the benzyl alcohol **5.100** in 4 steps, (10% overall yield), which then provided access to target clickable alkyne acetophenone mGlu2 PAM photoprobe **4.31** *via* oxidation in 40% yield. Finally, the synthesis of clickable alkyne pyrimidone **4.32** represents another mGlu2 PAM clickable photoprobe rationally designed based on lead **1.89**. This photoprobe features a unique photo-masked affinity labeling pyrimidone moiety, which upon UV irradiation undergoes a Norrish type 1 reaction leading to the formation of reactive intermediates capable of forming covalent linkage with nucleophilic residues within a mGlu2 PAM binding site.

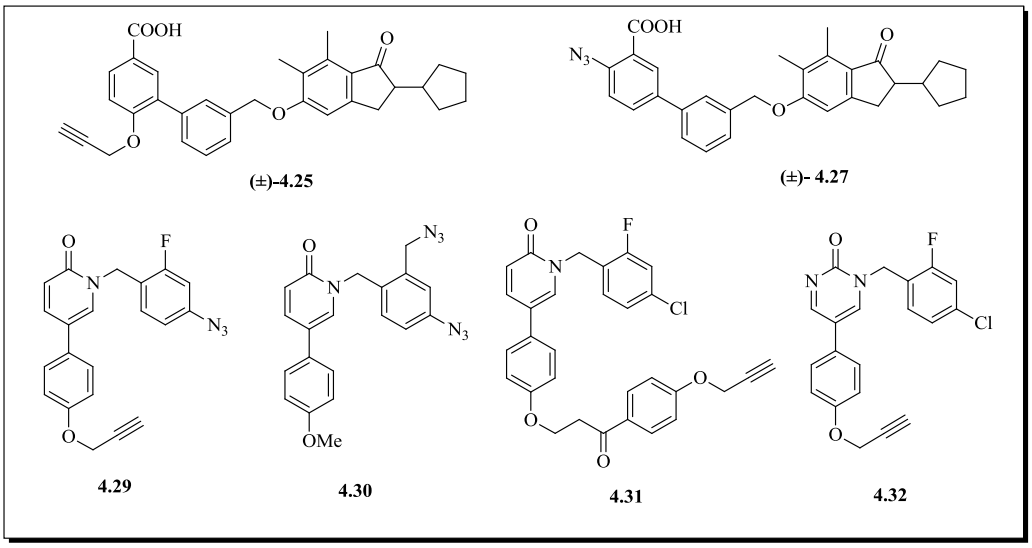


**Figure 5.3.** First successful examples of mGlu2 photoaffinity ligands for mGlu2 structure-function studies.

In conclusion, the synthesis and utilization of the irreversible chemical probes described in this dissertation are ultimately expected to facilitate improved rational, structure-based manipulation and discovery of lead compounds in order to develop therapeutics for numerous disease states associated with the DAT, α4β2 nAChR, α3β4 nAChR, and mGlu2, including drug abuse and addiction.

## 5.5. Summary of Final Compounds Synthesized During This Dissertation Work

| **Compound Name** | **Novel / Known** |
|---|---|
| (±)-1-(4-Azido-3-iodophenyl)-2-(pyrrolidin-1-yl)pentan-1-one (**(±)-4.16**) | Novel |
| (±)-1-(3-Azido-4-iodophenyl)-2-(pyrrolidin-1-yl)pentan-1-one (**(±)-4.17**) | Novel |
| (±)-1-(4-Azido-3-iodophenyl)-4-methyl-2-(pyrrolidin-1-yl)pentan-1-one (**(±)-4.18**) | Novel |
| (±)-1-(4-Azido-3-iodophenyl)-2-(*tert*-butylamino)propan-1-one hydrochloride (**(±)-4.20**) | Novel |
| (±)-2-(*tert*-Butylamino)-1-(3-iodophenyl)propan-1-one (**(±)-4.21**) | Novel |
| (±)-2-(*tert*-Butylamino)-1-(3-(tri-*n*-butylstannyl)phenyl)propan-1-one (**(±)-4.22**) | Novel |
| (+)-2-(4-Azido-3-iodophenyl)-2-hydroxy-3,5,5-trimethylmorpholin-4-ium 3-carboxy-2,3-dihydroxypropanoate (**(+)-4.23**) | Novel |
| 3'-(((2-Cyclopentyl-6,7-dimethyl-1-oxo-2,3-dihydro-1*H*-inden-5-yl)oxy)methyl)-6-methoxy-[1,1'-biphenyl]-3-carboxylic acid (**(±)-1.74)** | Known |
| (±)-3'-(((2-Cyclopentyl-6,7-dimethyl-1-oxo-2,3-dihydro-1*H*-inden-5-yl)oxy)methyl)-6-(prop-2-yn-1-yloxy)-[1,1'-biphenyl]-3-carboxylic acid (**(±)-4.25**) | Novel |
| (±)-4-Azido-3'-(((2-cyclopentyl-6,7-dimethyl-1-oxo-2,3-dihydro-1*H*-inden-5-yl)oxy)methyl)-[1,1'-biphenyl]-3-carboxylic acid (**(±)-4.27**) | Novel |
| 1-(4-Chloro-2-fluorobenzyl)-5-(4-methoxyphenyl)pyridin-2(1*H*)-one (**1.89**) | Known |
| 1-(4-Chloro-2-fluorobenzyl)-5-(4-(3-oxo-3-phenylpropoxy)phenyl)pyridin-2(1*H*)-one (**1.93**) | Known |
| 1-(4-Chloro-2-fluorobenzyl)-5-(4-(3-oxo-3-(4-(prop-2-yn-1-yloxy)phenyl)propoxy) | Novel |

| | |
|---|---|
| phenyl)pyridin-2(1*H*)-one (**4.31**) | |
| 1-(4-Chloro-2-fluorobenzyl)-5-(4-methoxyphenyl)pyrimidin-2(1*H*)-one (**4.36**) | Novel |
| 1-(4-Chloro-2-fluorobenzyl)-5-(4-(prop-2-yn-1-yloxy)phenyl)pyrimidin-2(1*H*)-one (**4.32**) | Novel |
| 1-(3-Azido-5-(azidomethyl)benzyl)-5-(4-methoxyphenyl)pyridin-2(1*H*)-one (**4.30**) | Novel |
| 1-(4-Azido-2-fluorobenzyl)-5-(4-(prop-2-yn-1-yloxy)phenyl)pyridin-2(1*H*)-one (**4.29**) | Novel |

**Table 5.5.** Final compounds synthesized for this dissertation work.

**EXPERIMENTAL**

All reactions were performed using flame-dried glassware under an inert atmosphere of argon unless otherwise noted. All solvents and chemicals were purchased from Aldrich Chemical Co. or Fisher Scientific and used without further purification unless otherwise noted. Flash column chromatography was performed using Fisher S826-25 silica gel sorbent (70–230 mesh) and eluting solvent mixtures as specified. Thin-layer chromatography (TLC) was performed using TLC Silica Gel 60 F254 plates obtained from EMD Chemicals, Inc. and compounds were visualized under UV light and/or $I_2$ stain. Proportions of solvents used for TLC are by volume. $^1H$ and $^{13}C$ NMR spectra were recorded on either a Bruker 400 or 500 MHz spectrometer. Chemical shifts for $^1H$ and $^{13}C$ NMR spectra are reported as parts per million ($\delta$ ppm) relative to tetramethylsilane (0.00 ppm) as an internal standard. Coupling constants are measured in hertz (Hz). HRMS samples were analyzed at Old Dominion University (Norfolk, VA) by positive ion electrospray on a Bruker 12 Tesla APEX-Qe FTICR-MS with an Apollo II ion source. Combustion analyses of selected solid compounds were performed by Atlantic Microlab, Inc. (Norcross, GA) and are in agreement within 0.4% of calculated values. Infrared spectra were recorded using a Perkin–Elmer Spectrum RZ I FT-IR spectrophotometer. Optical rotation was recorded using an AutoPol IV, Automatic Polarimeter. On the basis of NMR, all compounds were $\geq$ 95% pure.

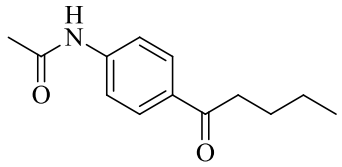

**5.3**

***N*-(4-pentanoylphenyl)acetamide (5.3)**

A mixture of valeryl chloride **5.2** (23.88 mL, 200 mmol) and acetanilide **5.1** (5.5 g, 40 mmol) in $CH_2Cl_2$ (60 mL) was added dropwise to $AlCl_3$ (26.60 g, 200 mmol) at 0ºC. The reaction was then allowed to reflux overnight, then cooled to room temperature, followed by quenching with crushed ice. The mixture was then diluted with $H_2O$ and $CH_2Cl_2$ with vigorous stirring. The organic layer was then separated, washed with brine, dried ($MgSO_4$), filtered, concentrated to obtain a crude mixture of ketone **5.3** and starting acetanilide **5.1**. The crude (9.0 g, 41.04 mmol) in MeOH (20 mL) was treated with $NaBH_4$ (7.70 g, 205.2 mmol) in three portions at 0ºC. The reaction was then stirred at room temperature for 1 hour, then quenched with brine and extracted with EtOAc. The organic layer was separated, dried with $MgSO_4$, filtered, concentrated, and chromatographed ($CHCl_3$:MeOH, 9:1) to provide 4.2 g of benzyl alcohol **(±)-5.4** in 2 steps. The resulting benzyl alcohol (4.2 g, 18.08 mmol) in $CH_2Cl_2$ (32 mL) at 0ºC was treated with PCC (5.84 g, 27.11 mmol) in four portions. The resulting reaction mixture was stirred at room temperature overnight, then filtered through Celite®, concentrated, and chromatographed (hexane:EtOAc, 7:3) to provide 2.8 g of ketone **5.3** as a yellow solid (70%). $R_f$ = 0.33 (hexane:EtOAc, 8:2). $^1$H NMR proved identical to that previously reported (Meltzer *et al*., 2006). $^1$H NMR ($CDCl_3$, 400 MHz): $\delta$ 8.18 (s, 1H), 7.92 (d, 2H, $J$ = 8.7 Hz), 7.64 (d, 2H, $J$ = 8.5 Hz), 2.93 (m, 2H), 2.21 (s, 3H), 1.70 (td, 2H, $J$ = 7.5, 15.1 Hz), 1.40 (dd, 2H, $J$ = 7.5, 15.0 Hz), 0.94 (t, 3H, $J$ = 7.3 Hz).

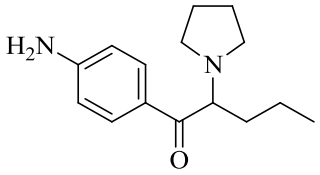

**(±)-5.6**

**(±)-1-(4-Aminophenyl)-2-(pyrrolidin-1-yl)pentan-1-one ((±)-5.6)**

A solution of *N*-[4-(2-pyrrolidin-1-yl-pentanoyl)phenyl]acetamide (**(±)-1.32**; Meltzer *et al.*, 2006) (183 mg, 0.63 mmol) in 1M aq. HCl (7 mL) was refluxed for 15 hours. The mixture was then cooled to room temperature, diluted with $H_2O$, carefully alkalinized with $K_2CO_3$, and extracted with EtOAc. The organic layer was then washed with brine, dried ($MgSO_4$), filtered, concentrated, and chromatographed (hexanes:EtOAc:$Et_3N$, 60:38:2) to provide 67 mg of aniline **(±)-5.6** as a yellow oil (58%). $R_f$ = 0.24 (hexanes:EtOAc:$Et_3N$, 60:38:2). $^1$H NMR ($CDCl_3$, 400 MHz): $\delta$ 7.89 (d, 2H, $J$ = 8.7 Hz), 6.56 (d, 2H, $J$ = 8.8 Hz), 4.53 (br s, 2H), 3.78 (m, 1H), 2.60 (m, 2H), 2.48 (m, 2H), 1.82 (m, 1H), 1.67 (m, 5H), 1.17 (m, 2H), 0.77 (t, 3H, $J$ = 7.3 Hz). $^{13}$C NMR ($CDCl_3$, 100 MHz): $\delta$ 199.3, 151.9, 131.1, 126.9, 113.5, 68.1, 51.3, 33.9, 23.2, 19.3, 14.3. HRMS calcd for $C_{15}H_{23}N_2O^+$ 247.1805, found 247.1804.

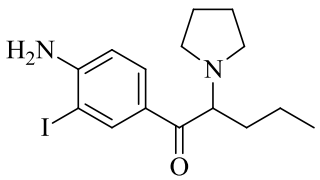

**(±)-5.7**

**(±)-1-(4-Amino-3-iodophenyl)-2-(pyrrolidin-1-yl)pentan-1-one ((±)-5.7)**

ICl (426 mg, 2.62 mmol) was added to a solution of 1-(4-aminophenyl)-2-(pyrrolidin-1-yl)pentan-1-one (**(±)-5.6**) (577 mg, 2.34 mmol) in glacial AcOH (41.5 mL). The resulting mixture was stirred for 16 hours at room temperature then concentrated to dryness. The residue

obtained was then partitioned between $H_2O$ and $CHCl_3$, and then the aqueous layer was alkalinized to pH 9 using a sat. aq. $NaHCO_3$ solution. This aqueous layer was then extracted with $CHCl_3$ (X3). The combined organic layers were dried ($MgSO_4$), filtered, and concentrated to provide 620 mg of iodide **(±)-5.7** as a colorless oil (70%). $R_f$ = 0.2 (hexanes:EtOAc:$Et_3N$, 80:18:2). $^1H$ NMR ($CDCl_3$, 400 MHz): $\delta$ 8.47 (d, 1H, $J$ = 1.9 Hz), 7.98 (dd, 1H, $J$ = 1.9, 8.5 Hz), 6.71 (d, 1H, $J$ = 8.5 Hz), 4.65 (br s, 2H), 3.75 (m, 1H), 2.66 (m, 2H), 2.55 (m, 2H), 1.91-1.84 (m, 1H), 1.78-1.70 (m, 5H), 1.29-1.20 (m, 2H), 0.87 (t, 3H, $J$ = 7.3 Hz). $^{13}C$ NMR ($CDCl_3$, 100 MHz): $\delta$ 198.0, 150.9, 140.7, 130.7, 128.8, 113.0, 82.8, 68.8, 51.3, 33.5, 23.4, 19.3, 14.3. HRMS calcd for $C_{15}H_{21}IN_2ONa^+$ 395.0591, found 395.0582.

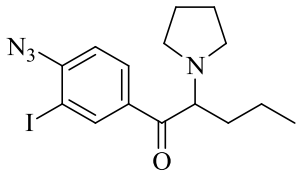


**(±)-4.16**

**(±)-1-(4-Azido-3-iodophenyl)-2-(pyrrolidin-1-yl)pentan-1-one ((±)-4.16)**

A 0˚C solution of 1-(4-amino-3-iodophenyl)-2-(pyrrolidin-1-yl)pentan-1-one (**(±)-5.7**) (248 mg, 0.67 mmol) in trifluoroacetic acid (3.3 mL) was treated with $NaNO_2$ (113 mg, 1.64 mmol). The mixture was then stirred in the dark for 45 minutes at 0˚C then carefully treated with $NaN_3$ (532 mg, 8.18 mmol) and $Et_2O$ (3.3 mL). The resulting reaction was allowed stirred in the dark at 0˚C for 2 hours, and then was diluted with $H_2O$ and $Et_2O$. The organic layer was separated, washed with brine, dried ($MgSO_4$), filtered, and concentrated. Chromatography (hexanes:EtOAc:$Et_3N$, 80:18:2) provided 247 mg of azide **(±)-4.16** (93%) as a yellow oil. $R_f$ = 0.37 (hexanes:EtOAc:$Et_3N$, 80:18:2). $^1H$ NMR ($CDCl_3$, 400 MHz): $\delta$ 8.59 (d, 1H, $J$ = 1.9 Hz), 8.27 (dd, 1H, $J$ = 1.9, 8.4 Hz), 7.18 (d, 1H, $J$ = 8.4 Hz), 3.73 (m, 1H), 2.67 (m, 2H), 2.54 (m, 2H),

1.92-1.82 (m, 1H), 1.80-1.70 (m, 5H), 1.28-1.17 (m, 2H), 0.88 (t, 3H, $J$ = 7.3 Hz). $^{13}$C NMR ($CDCl_3$, 100 MHz): $\delta$ 198.2, 146.0, 140.8, 134.4, 130.2, 117.9, 87.6, 69.9, 60.4, 51.1, 32.5, 23.4, 21.0, 19.4, 14.2. HRMS calcd for $C_{15}H_{20}IN_4O^+$ 399.0676, found 399.0669. IR: azide, 2100 cm$^{-1}$.

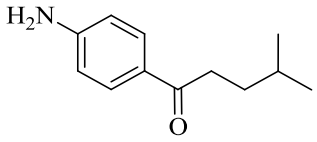


**5.11**

**1-(4-Aminophenyl)-4-methylpentan-1-one (5.11)**

1,2-Dibromoethane (4 drops) was added to a suspension of Mg turnings (4.860 g, 200 mmol) in dry THF (440 mL) at 0˚C, followed by dropwise addition of 1-bromo-3-methylbutane (25 mL, 200 mmol). When the boiling of THF ceased, the reaction mixture was cooled to -78˚C and 4-(trifluoromethyl)aniline (**5.10,** 5 mL, 40 mmol) was added dropwise. The reaction was then refluxed at 80˚C for 4 hrs, cooled to 0˚C, then carefully quenched with sat. aq. $NH_4Cl$ solution followed by extraction with $Et_2O$. The organic layer was then filtered over silica gel and the filtrate was concentrated. The resulting residue was then hydrolyzed by refluxing in 10% $H_2SO_4$ (20 mL) for 2 hours at 120˚C. The mixture was then cooled to room temperature, neutralized with $K_2CO_3$, then extracted with $Et_2O$. The organic layer was then dried ($MgSO_4$), filtered, concentrated, and chromatographed (hexanes:EtOAc, 8:2) to give 700 mg of ketone **5.11** as a colorless oil (10%). $R_f$ = 0.30 (7:3, hexanes:EtOAc). $^1$H NMR ($CDCl_3$, 400 MHz): $\delta$ 7.81 (d, 2H, $J$ = 8.6 Hz), 6.64 (d, 2H, $J$ = 8.5 Hz), 4.20 (s, 2H), 2.86 (m, 2H), 1.61 (m, 3H), 0.94 (d, 6H, $J$ = 6.2 Hz). $^{13}$C NMR ($CDCl_3$, 100 MHz): $\delta$ 199.2, 151.1, 130.5, 127.5, 113.7, 36.0, 33.8, 27.9, 22.5. HRMS calcd for $C_{12}H_{17}NONa^+$ 214.1202, found 214.1208.

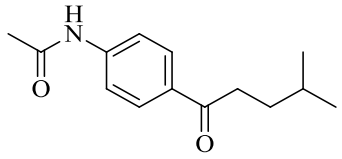

**5.9**

***N*-(4-(4-Methylpentanoyl)phenyl)acetamide (5.9)**

Aniline **5.11** (653 mg, 3.4 mmol) in EtOAc (6.7 mL) was treated dropwise with acetyl chloride (0.53 mL, 7.51 mmol) at 0˚C. The reaction was then refluxed at 80˚C for 1 hour, cooled to 0˚C, then quenched with $NaHCO_3$ and extracted with EtOAc. The organic layer was then dried ($MgSO_4$), filtered, and concentrated. Chromatography (hexanes:EtOAc, 7:3) provided 353 mg of acetamide **5.9** as a colorless oil (44%). $R_f$ = 0.42 (hexanes:EtOAc, 1:1). $^1$H NMR ($CDCl_3$, 400 MHz): $\delta$ 8.01 (s, 1H), 7.93 (d, 2H, $J$ = 8.7 Hz), 7.64 (d, 2H, $J$ = 8.6 Hz), 2.93 (m, 2H), 2.22 (s, 3H), 1.64 (m, 3H), 0.94 (d, 6H, $J$ = 6.3 Hz). $^{13}$C NMR ($CDCl_3$, 100 MHz): $\delta$ 199.9, 168.8, 142.3, 132.6, 129.4, 118.9, 36.5, 33.4, 27.9, 24.7, 22.4. HRMS calcd for $C_{14}H_{19}NO_2Na^+$ 256.1308, found 256.1312.

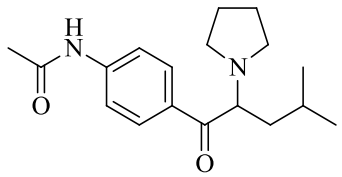

**(±)-5.12**

**(±)-*N*-(4-(4-Methyl-2-(pyrrolidin-1-yl)pentanoyl)phenyl)acetamide ((±)-5.12)**

A mixture of ketone **5.9** (1.25 g, 5.36 mmol) in $CH_2Cl_2$ (15 mL) was treated dropwise with liquid $Br_2$ (0.3 mL, 5.36 mmol) at 0˚C. The reaction was then warmed to room temperature, stirred for 3 hours, then concentrated to provide the resulting α-bromo ketone (1.67 g, 100%), which was used without further purification. A solution of α-bromide (1.67 g, 5.36 mmol) in $Et_2O$ (11 mL) was treated with pyrrolidine (0.97 mL) at 0˚C. The reaction was then stirred at room temperature

overnight, quenched with solid $NaHCO_3$, then extracted with $Et_2O$ (X2). The organic layer was washed with 1M aq. HCl, then dried ($MgSO_4$), filtered, and concentrated to provide 871 mg of pyrovalerone analog **(±)-5.12** as a yellow oil (54%). $R_f$ = 0.17 (hexanes:EtOAc:$Et_3N$, 40:58:2). $^1H$ NMR ($CDCl_3$, 400 MHz): $\delta$ 8.14 (d, 2H, $J$ = 8.8 Hz), 7.62 (br, m, 3H), 4.00 (q, 1H, $J$ = 4.7 Hz), 2.72 (m, 2H), 2.56 (m, 2H), 2.22 (s, 3H), 1.89 (m, 1H), 1.72 (m, 4H), 1.61-1.54 (m, 1H), 1.51-1.41 (m, 1H), 0.87 (dd, 6H, $J$ = 6.5, 14.9 Hz). $^{13}C$ NMR ($CDCl_3$, 100 MHz): $\delta$ 200.6, 169.3, 142.7, 132.5, 130.0, 119.0, 66.3, 50.6, 39.4, 25.3, 24.6, 23.6, 23.4, 22.2. HRMS calcd for $C_{18}H_{26}N_2O_2H^+$ 303.2067, found 303.2064.

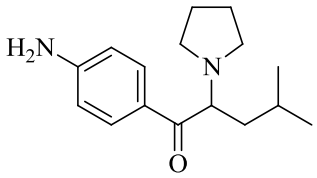


**(±)-5.13**

**1-(4-Aminophenyl)-4-methyl-2-(pyrrolidin-1-yl)pentan-1-one ((±)-5.13)**

*N*-(4-(4-methyl-2-(pyrrolidin-1-yl)pentanoyl)phenyl)acetamide (**(±)-5.12**; 628 mg, 2.08 mmol) was refluxed in 1M aq. HCl (22 mL) at 125˚C for 20 hours. The mixture was then cooled to room temperature, diluted with $H_2O$, carefully alkalinized with $K_2CO_3$ to pH 9, then extracted with EtOAc. The organic layer was washed with brine, dried ($MgSO_4$), filtered, and concentrated. Chromatography (hexanes:EtOAc:$Et_3N$, 80:18:2) provided 459 mg of aniline **(±)-5.13** as a yellow oil (60%). $R_f$ = 0.33 (hexanes:EtOAc:$Et_3N$, 40:58:2). $^1H$ NMR ($CDCl_3$, 400 MHz): $\delta$ 8.00 (d, 2H, $J$ = 8.8 Hz), 6.64 (d, 2H, $J$ = 8.8 Hz), 4.16 (s, 2H), 3.99 (dd, 1H, $J$ = 4.6, 9.5 Hz), 2.71 (m, 2H), 2.56 (m, 2H), 1.90 (m, 1H), 1.72 (p, 4H, $J$ = 7.5 Hz), 1.59-1.42 (m, 2H), 0.88 (dd, 6H, $J$ = 6.4, 14.8 Hz). $^{13}C$ NMR ($CDCl_3$, 100 MHz): $\delta$ 199.5, 151.1, 131.1, 127.9,

113.7, 65.3, 50.7, 40.0, 25.3, 23.4, 22.3. HRMS calcd for $C_{16}H_{24}N_2ONa^+$ 283.1781, found 283.1779.

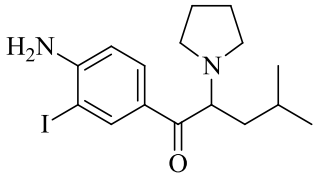


**(±)-5.14**

**(±)-1-(4-Amino-3-iodophenyl)-4-methyl-2-(pyrrolidin-1-yl)pentan-1-one ((±)-5.14)**

A mixture of 1-(4-aminophenyl)-4-methyl-2-(pyrrolidin-1-yl)pentan-1-one (**(±)-5.13**; 310 mg, 1.19 mmol), glacial AcOH (21 mL), and ICl (216 mg, 1.33 mmol) was stirred at room temperature for 20 hours. The mixture was then concentrated to dryness and the resulting residue was dissolved with $H_2O$ and extracted with $CHCl_3$. The aqueous layer was then basified with solid $NaHCO_3$ and extracted with $CHCl_3$. The combined organic layers were then washed with brine, dried ($MgSO_4$), filtered, concentrated and chromatographed (hexanes:EtOAc:$Et_3N$, 60:38:2) to provide 200 mg of target **(±)-5.14** (52%). $R_f$ = 0.34 (hexanes:EtOAc:$Et_3N$, 40:68:2). $^1$H NMR ($CDCl_3$, 400 MHz): $\delta$ 8.47 (d, 1H, $J$ = 1.9 Hz), 7.99 (dd, 1H, $J$ = 1.9, 8.5 Hz), 6.70 (d, 1H, $J$ = 8.5 Hz), 4.67 (s, 2H), 3.89 (dd, 1H, $J$ = 4.6, 9.5 Hz), 2.68 (q, 2H, $J$ = 7.2 Hz), 2.52 (dd, 2H, $J$ = 9.5, 11.9 Hz), 1.86 (m, 1H), 1.71 (m, 4H), 1.58-1.40 (m, 2H), 0.87 (dd, 6H, $J$ = 6.5, 15.2 Hz). $^{13}$C NMR ($CDCl_3$, 100 MHz): $\delta$ 198.1, 150.9, 140.7, 130.7, 129.0, 113.0, 82.9, 65.9, 50.7, 39.7, 25.4, 23.7, 23.4, 22.3. HRMS calcd for $C_{16}H_{23}IN_2OH^+$ 387.0928, found 387.0924. MP: 240-241 ºC.

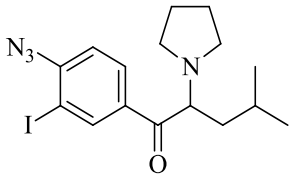

**(±)-4.18**

**(±)-1-(4-Azido-3-iodophenyl)-4-methyl-2-(pyrrolidin-1-yl)pentan-1-one ((±)-4.18)**

A solution of 1-(4-amino-3-iodophenyl)-4-methyl-2-(pyrrolidin-1-yl)pentan-1-one (**(±)-5.14**; 96 mg, 0.25 mmol) in trifluoroacetic acid (1 mL) was treated at 0˚C with $NaNO_2$ (34 mg, 0.50 mmol). The mixture was then stirred in the dark for 45 minutes at 0˚C, then carefully treated with $NaN_3$ (162 mg, 2.5 mmol) and $Et_2O$ (1 mL). The reaction was then stirred in the dark at 0˚C for 2 hours then diluted with $H_2O$ and $Et_2O$. The organic layer was then separated and washed with brine, then dried ($MgSO_4$), filtered, and concentrated. Chromatography (hexanes:EtOAc:$Et_3N$, 60:38:2) provided 76 mg of azide **(±)-4.18** as a yellow oil (75%). $R_f$ = 0.66 (hexanes:EtOAc:$Et_3N$, 60:38:2). $^1H$ NMR ($CDCl_3$, 400 MHz): $\delta$ 8.58 (d, 1H, $J$ = 1.9 Hz), 8.27 (dd, 1H, $J$ = 1.9, 8.4 Hz), 7.17 (d, 1H, $J$ = 8.4 Hz), 3.84 (dd, 1H, $J$ = 4.7, 9.5 Hz), 2.67 (m, 2H), 2.52 (dd, 2H, $J$ = 5.6, 16.1 Hz), 1.85 (ddd, 1H, $J$ = 5.1, 9.6, 13.5 Hz), 1.72 (m, 4H), 1.56 (ddd, 1H, $J$ = 4.7, 8.8, 13.4 Hz), 1.48-1.38 (m, 1H), 0.87 (dd, 6H, $J$ = 6.5, 15.7 Hz). $^{13}C$ NMR ($CDCl_3$, 100 MHz): $\delta$ 198.1, 145.9, 140.8, 134.5, 130.2, 117.9, 87.6, 67.3, 50.5, 38.5, 25.4, 23.6, 23.5, 22.1. HRMS calcd for $C_{16}H_{21}IN_4OH^+$ 413.0833, found 413.0839. The hydochloride salt of **(±)-4.18** was synthesized by stirring the free base in 2M ethereal HCl (3 mL) overnight followed by concentration to provide 30 mg of a yellow semi-solid (36%). $^1H$ NMR (DMSO-$d_6$, 400 MHz): $\delta$ 10.54 (br, s, 1H), 8.54 (d, 1H, $J$ = 1.3 Hz), 8.15 (d, 1H, $J$ = 8.3 Hz), 7.56 (d, 1H, $J$ = 8.4 Hz), 5.40 (m, 1H), 3.63-3.02 (m, 4H), 2.01-1.70 (m, 6H), 0.81 (dd, 6H, $J$ = 2.2, 6.3 Hz). $^{13}C$ NMR (DMSO-$d_6$, 100 MHz): $\delta$ 195.8, 148.5, 140.5, 133.0, 130.7, 120.4, 89.4, 65.2, 53.6, 52.8,

52.7, 24.7, 23.8, 23.3, 21.9. Anal Calcd for $C_{16}H_{22}ClIN_4O$: C, 42.83; H, 4.94; N, 12.49; I, 28.28; Cl, 7.90. Found C, 43.16; H, 5.02; N, 12.27; I, 28.50; Cl, 7.52. IR: azide, 2072 $cm^{-1}$. MP: 211 ºC.

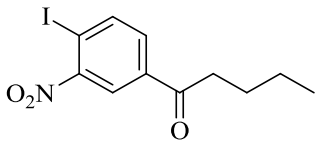


**5.17**

**1-(4-Iodo-3-nitrophenyl)pentan-1-one (5.17)**

Fuming nitric acid (2.03 mL, 48.6 mmol) was added dropwise to *p*-iodovalerophenone (**5.16**; Meltzer *et al.*, 2006) (297 mg, 1.03 mmol) at -78˚C. After the addition, the reaction was warmed to 0˚C, stirred for 1 hour, then poured over ice cold $H_2O$. The aqueous layer was then extracted with $Et_2O$. The organic layer was dried and concentrated. Chromatography (hexanes:EtOAc, 95:5) yielded 200mg of nitro ketone **5.17** (58%) as a yellow solid. $R_f$ = 0.13 (hexanes:EtOAc, 95:5). $^1$H NMR ($CDCl_3$, 400 MHz): $\delta$ 8.36 (d, 1H, $J$ = 2.0 Hz), 8.17 (d, 1H, $J$ = 8.2 Hz), 7.80 (dd, 1H, $J$ = 2.0, 8.2 Hz), 2.97 (m, 2H), 1.73 (td, 2H, $J$ = 7.4, 15.0 Hz), 1.41 (qd, 2H, $J$ = 7.4, 14.7 Hz), 0.96 (t, 3H, $J$ = 7.3 Hz). $^{13}$C NMR ($CDCl_3$, 100 MHz): $\delta$ 197.4, 153.3, 142.5, 137.8, 131.8, 124.5, 92.0, 38.4, 26.0, 22.3, 13.9. HRMS analysis of this compound was not obtained due to sample degradation (i.e., this compound is relatively unstable and should be used immediately in the next reaction).

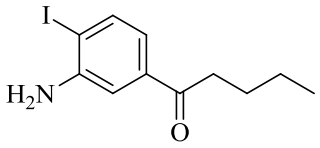

**5.18**

**1-(3-Amino-4-iodophenyl)pentan-1-one (5.18)**

Fe(s) (174.2 mg, 3.12 mmol) was added to a solution of 1-(4-iodo-3-nitrophenyl)pentan-1-one (**5.17**) (200 mg, 0.60 mmol) dissolved in $H_2O$ (0.62 mL), EtOH (1.25 mL), and glacial AcOH (1.25 mL). The reaction was then sonicated for 1.5 hours then filtered. 2M aq. KOH (50 mL) was then added to the filtrate followed by dilution with EtOAc. The organic layer was then washed with $H_2O$ and brine, dried ($MgSO_4$), filtered, and concentrated to give 151 mg of amine **5.18** as a yellow solid (83%). $R_f$ = 0.67 (hexanes:EtOAc, 7:3). $^1$H NMR ($CDCl_3$, 400 MHz): $\delta$ 7.70 (d, 1H, $J$ = 8.2 Hz), 7.30 (d, 1H, $J$ = 1.9 Hz), 6.99 (dd, 1H, $J$ = 1.9, 8.2Hz), 4.32 (s, 2H), 2.86 (t, 2H, $J$ = 7.4 Hz), 1.67 (m, 2H), 1.37 (m, 2H), 0.93 (t, 3H, $J$ = 7.3 Hz). $^{13}$C NMR ($CDCl_3$, 100 MHz): $\delta$200.3, 147.2, 139.2, 138.2, 119.0, 113.3, 89.9, 38.3, 26.4, 22.4, 13.9. HRMS calcd for $C_{11}H_{14}INONa^+$ 326.0012, found 326.0015.

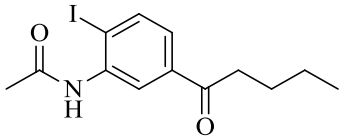

**5.19**

***N*-(2-Iodo-5-pentanoylphenyl)acetamide (5.19)**

Acetyl chloride (0.43 mL, 6.12 mmol) was added dropwise to a mixture of amine **5.18** (841.5 mg, 2.77 mmol) in EtOAc (5.44 mL) at 0˚C. The reaction was then refluxed at 80˚C for 1 hour, cooled to room temperature, basified with $NaHCO_3$ to pH 9, then extracted with EtOAc (X2). The combined organic layers were washed with brine, dried ($MgSO_4$), filtered, and concentrated

to provide 912 mg of acetamide **5.19** as a brown solid (95%). $R_f$ = 0.34 (hexanes:EtOAc, 6:4). $^1$H NMR ($CDCl_3$, 500 MHz): $\delta$ 8.70 (s, 1H), 7.85 (d, 1H, $J$ = 8.3 Hz), 7.60 (s, 1H), 7.40 (dd, 1H, $J$ = 1.8, 8.3 Hz), 2.93 (t, 2H, $J$ = 7.4 Hz), 2.27 (s, 3H), 1.69 (m, 2H), 1.38 (m, 2H), 0.93 (t, 3H, $J$ = 7.4 Hz). $^{13}$C NMR ($CDCl_3$, 100 MHz): $\delta$ 199.7, 168.6, 139.1, 138.6, 137.8, 124.8, 121.7, 96.1, 38.3, 26.3, 22.3, 13.9. HRMS calcd for $C_{13}H_{16}INO_2Na^+$ 368.0118, found 368.0114.

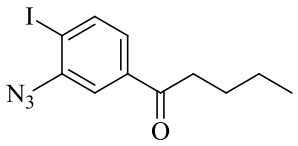


**5.23**

**1-(3-Azido-4-iodophenyl)pentan-1-one (5.23)**

A mixture of 1-(3-amino-4-iodophenyl)pentan-1-one (**5.18**) (135 mg, 0.44 mmol), trifluoroacetic acid (1.76 mL), and $NaNO_2$ (614 mg, 0.89 mmol) was stirred at 0˚C for 45 minutes in the dark, followed by careful addition of $NaN_3$ (289 mg, 4.45 mmol) and anhydrous $Et_2O$ (1.76 mL). The resulting reaction was then stirred in dark at 0˚C for 2 hours followed by dilution with $H_2O$ and $Et_2O$. The organic layer was separated, washed with brine, dried ($MgSO_4$), filtered, and concentrated to provide 141 mg of azide **5.23** as a brown oil (96%). $R_f$ = 0.67 (hexanes:EtOAc, 8:2). $^1$H NMR ($CDCl_3$, 400 MHz): $\delta$ 7.87 (d, 1H, $J$ = 8.2 Hz), 7.65 (d, 1H, $J$ = 1.8 Hz), 7.37 (dd, 1H, $J$ = 1.9, 8.2 Hz), 2.92 (m, 2H), 1.70 (td, 2H, $J$ = 7.5, 15.0 Hz), 1.39 (qd, 2H, $J$ = 7.4, 14.7 Hz), 0.94 (t, 3H, $J$ = 7.3 Hz). $^{13}$C NMR ($CDCl_3$, 100 MHz): $\delta$ 199.0, 142.6, 140.3, 138.2, 125.4, 117.1, 94.1, 38.3, 26.2, 22.4, 13.9. HRMS analysis of this compound was not obtained (i.e., this compound is relatively unstable at room temperature and should be used immediately in the next reaction).

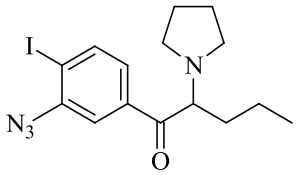

**(±)-4.17**

**(±)-1-(3-Azido-4-iodophenyl)-2-(pyrrolidin-1-yl)pentan-1-one ((±)-4.17)**

Liquid $Br_2$ (0.03 mL, 0.64 mmol) was added dropwise to a mixture of ketone **5.23** (210 mg, 0.64 mmol) in $CH_2Cl_2$ (2.74 mL) at 0˚C. The reaction was then warmed to room temperature, stirred for 2 hours, then concentrated to provide bromide **5.24**, which was used without further purification. To 265 mg (0.65 mmol) of bromide **5.24** was added $Et_2O$ (1.35 mL) at 0˚C, followed by the addition of pyrrolidine (0.165 mL, 2 mmol). The reaction was then stirred at room temperature for 20 hours, quenched with solid $NaHCO_3$, then extracted with $Et_2O$ (X2). The combined organic layers were then washed with 1M aq. HCl, dried ($MgSO_4$), filtered, concentrated, and chromatographed (hexanes:EtOAc:$Et_3N$, 80:18:2) to provide 30 mg of pyrovalerone analog **(±)-4.17** as an oil (20%). $R_f$ = 0.54 (hexanes:EtOAc:$Et_3N$, 50:48:2). $^1H$ NMR ($CDCl_3$, 500 MHz): $\delta$ 8.08 (d, 1H, $J$ = 1.8 Hz), 7.90 (d, 1H, $J$ = 8.2 Hz), 7.68 (dd, 1H, $J$ = 1.8, 8.2 Hz), 3.73 (m, 1H), 2.71 (s, 2H), 2.58 (s, 2H), 1.81 (m, 6H), 1.24 (m, 2H), 0.90 (t, 3H, $J$ = 7.3 Hz). $^{13}C$ NMR ($CDCl_3$, 100 MHz): $\delta$ 199.4, 142.5, 140.2, 137.8, 126.1, 118.2, 94.2, 70.4, 51.1, 32.3, 23.4, 19.5, 14.2. HRMS calcd for $C_{15}H_{19}IN_4OH^+$ 399.0676, found 399.0680. IR: azide, 2111.9 $cm^{-1}$.

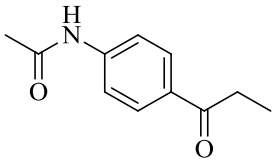

**5.28**

***N*-(4-Propionylphenyl)acetamide (5.28)**

4'-Aminopropiophenone (**5.27**; 3.0 g, 20 mmol) in EtOAc (40 mL) was treated dropwise with acetyl chloride (3.1 mL, 44 mmol) at 0˚C. The reaction was then refluxed at 80˚C for 2.5 hours, then cooled to room temperature and carefully quenched with sat. aq. $NaHCO_3$ solution followed by extraction with EtOAc. The organic layer was washed with brine, dried ($MgSO_4$), filtered, and concentrated to provide 3.8 g of amide **5.28** as a white solid that was used without further purification (99%). $R_f$ = 0.18 (hexanes:EtOAc, 1:1). $^1$H NMR ($CDCl_3$, 400 MHz): $\delta$ 7.96 (d, 2H, $J$ = 8.6 Hz), 7.64 (d, 2H, $J$ = 8.3 Hz), 7.58 (s, 1H), 3.00 (q, 2H, $J$ = 7.3 Hz), 2.24 (s, 3H), 1.24 (t, 3H, $J$ = 7.2 Hz). $^{13}$C NMR ($CDCl_3$, 100 MHz): $\delta$ 199.7, 168.5, 142.0, 132.6, 129.3, 118.8, 31.5, 24.7, 8.3. HRMS calcd for $(C_{11}H_{13}NO_2)Na^+$ 214.0839, found 214.0841. MP: 167ºC.

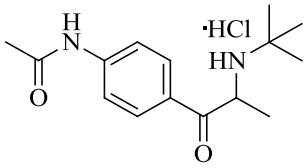

**(±)-5.30**

**(±)-*N*-(4-(2-(*tert*-Butylamino)propanoyl)phenyl)acetamide hydrochloride ((±)-5.30)**

A mixture of liquid bromine (0.26 mL, 5.2 mmol) in $CHCl_3$ (60 mL) was added dropwise to a solution of ketone **5.28** (898 mg, 4.7 mmol) in $CHCl_3$ (60 mL). The orange reaction mixture was then heated at 55˚C for 3 hours until it became yellow, cooled to room temperature, then

concentrated. The rsulting residue was dissolved in *N*-methylpyrrolidinone (2.7 mL) and *t*-$BuNH_2$ (0.95 mL, 9.0 mmol) was added dropwise. The mixture was then heated at 55˚C for 10 minutes, cooled to room temperature, then diluted with $Et_2O$ and $H_2O$. The organic layer was separated, washed with $H_2O$ and brine, dried ($MgSO_4$), filtered, and concentrated. The resulting solid was then dissolved in a minimum amount of $Et_2O$ and treated dropwise with 2M HCl in $Et_2O$ to produce a white solid, which was collected *via* filtration, washed with $Et_2O$, and dried to provide 120 mg of bupropion analog **(±)-5.30** as its HCl salt (23%, three steps). $^1$H NMR (MeOD, 500 MHz): $\delta$ 8.16 (d, 2H, $J$ = 8.9 Hz), 7.85 (d, 2H, $J$ = 8.9 Hz), 5.24 (q, 1H, $J$ = 7.1 Hz), 2.20 (s, 3H), 1.61 (d, 3H, $J$ = 7.1 Hz), 1.39 (s, 9H). $^{13}$C NMR (MeOD, 100 MHz): $\delta$ 193.9, 170.7, 145.2, 130.3, 126.9, 119.1, 58.4, 53.1, 25.0, 22.7, 17.5. HRMS calcd for $(C_{15}H_{22}N_2O_2)H^+$ 263.1754, found 263.1755. Anal. calcd for: $C_{15}H_{23}N_2O_2Cl$•0.3HCl: C, 58.16; H, 7.58; N, 9.04. Found C, 57.80; H, 7.41; N, 9.01.

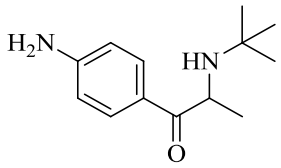


**(±)-5.31**

**(±)-1-(4-Aminophenyl)-2-(*tert*-butylamino)propan-1-one ((±)-5.31)**

A solution of amide **(±)-5.30** (701 mg, 2.7 mmol) in 1M aq. HCl (30 mL) was refluxed for 15 hours, cooled to room temperature, diluted with $H_2O$, carefully alkalinized with $K_2CO_3$ to pH 12, then extracted with EtOAc. The organic layer was washed with brine, dried ($MgSO_4$), filtered, concentrated, and chromatographed (hexanes:EtOAc:$Et_3N$, 30:68:2) to provide 488 mg of aniline **(±)-5.31** as a yellow solid (83%). $R_f$ = 0.2 (hexanes:EtOAc:$Et_3N$, 30:68:2). $^1$H NMR ($CDCl_3$, 500 MHz): $\delta$ 7.85 (d, 2H, $J$ = 8.7 Hz), 6.67 (d, 2H, $J$ = 8.7 Hz), 4.29 (s, 2H), 4.28 (q, 1H, $J$ = 7.1

Hz), 2.59 (s, 1H), 1.24 (d, 3H, $J$ = 7.1 Hz), 1.04 (s, 9H). $^{13}$C NMR ($CDCl_3$, 100 MHz): $\delta$ 202.9, 151.5, 130.8, 125.0, 113.9, 51.1, 50.7, 29.7, 23.1. HRMS calcd for $(C_{13}H_{20}N_2O)H^+$ 221.1648, found 221.1650. Anal. calcd for $C_{13}H_{20}N_2O \cdot 0.1EtOAc$: C, 70.24; H, 9.15; N, 12.22. Found C, 70.04; H, 9.09; N, 12.5. MP: 113 ˚C.

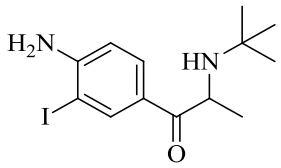


**(±)-5.32**

**(±)-1-(4-Amino-3-iodophenyl)-2-(*tert*-butylamino)propan-1-one ((±)-5.32)**

A mixture of aniline **(±)-5.31** (312 mg, 1.41 mmol), glacial AcOH (25 mL), and ICl (257 mg, 1.59 mmol) was stirred at room temperature overnight. The reaction was then concentrated and the resulting residue was partitioned between $CHCl_3$ and $H_2O$. The aqueous layer was then separated, alkalinized with solid $NaHCO_3$, and extracted with $CHCl_3$. The organic layer was then washed with brine, dried ($MgSO_4$), filtered, and concentrated. Chromatography (hexanes:EtOAc:$Et_3N$, 50:48:2) then provided 180 mg of iodide **(±)-5.32** as a white solid (23%). $R_f$ = 0.27 (hexanes: EtOAc: $Et_3N$, 10:88:2). $^1$H NMR ($CDCl_3$, 400 MHz): $\delta$ 8.30 (d, 1H, $J$ = 2.0 Hz), 7.78 (dd, 1H, $J$ = 2.0, 8.5 Hz), 6.73 (d, 1H, $J$ = 8.5 Hz), 4.81 (s, 2H), 4.20 (q, 1H, $J$ = 7.1 Hz), 2.56 (s, 1H), 1.22 (d, 3H, $J$ = 7.1 Hz), 1.01 (s, 9H). $^{13}$C-NMR ($CDCl_3$, 100 MHz): $\delta$ 201.7, 151.2, 140.3, 130.3, 126.5, 113.2, 83.0, 51.3, 50.8, 29.7, 22.9. HRMS calcd. for $(C_{13}H_{19}IN_2O)H^+$ 347.0615, found 347.0615. Anal. calcd for: $C_{13}H_{19}IN_2O$: C, 45.10; H, 5.53; I, 36.66; N, 8.09; O, 4.62. Found C, 44.81; H, 5.45; I, 36.39; N, 7.95. MP: 91 ˚C.

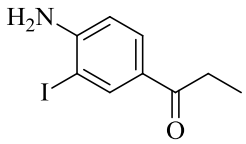

**5.35**

**1-(4-Amino-3-iodophenyl)propan-1-one (5.35)**

A mixture of 4'-aminopropiophenone **5.27** (597 mg, 4.0 mmol), $CaCO_3$ (628 mg, 6.3 mmol), $H_2O$ (1.6 mL), and MeOH (4 mL) was cooled to 0˚C and ICl (714 mg, 4.4 mmol) in MeOH (1.5 mL) was added. The reaction was stirred at room temperature for 16 hours, diluted with sat. aq. $Na_2S_2O_3$ solution, then extracted with $Et_2O$ (X2). The combined organic layers were washed with brine, dried ($MgSO_4$), filtered, concentrated, and chromatographed (hexanes:EtOAc, 8:2) to provide 514 mg of iodide **5.35** as a brown solid (47%). $R_f$ = 0.36 (hexanes:EtOAc, 7:3). $^1$H NMR ($CDCl_3$, 400 MHz): $\delta$ 8.28 (s, 1H), 7.76 (d, 1H, $J$ = 8.2 Hz), 6.72 (d, 1H, $J$ = 8.3 Hz), 4.69 (s, 2H), 2.88 (d, 2H, $J$ = 7.1 Hz), 1.19 (t, 3H, $J$ = 7.0 Hz). $^{13}$C NMR ($CDCl_3$, 100 MHz): $\delta$ 198.0, 150.9, 139.9, 129.9, 128.8, 113.2, 82.7, 31.1, 8.6. HRMS calcd for $(C_9H_{10}INO)_2Na^+$ 572.9506, found 572.9500.

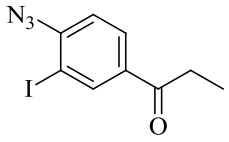

**5.36**

**1-(4-Azido-3-iodophenyl)propan-1-one (5.36)**

A 0˚C solution of aniline **5.35** (514 mg, 1.9 mmol) in trifluoroacetic acid (7.5 mL) was treated with $NaNO_2$ (258 mg, 3.7 mmol). The mixture was stirred in the dark for 45 minutes at 0˚C then carefully treated with $NaN_3$ (1.21 g, 18.6 mmol) and $Et_2O$ (7.5 mL). The reaction was then stirred in the dark at 0˚C for 1 hour then diluted with $H_2O$ and $Et_2O$. The organic layer was

separated, washed with brine, dried ($MgSO_4$), filtered, and concentrated to provide 554 mg of azide **5.36** (99%), which was used without further purification. $R_f$ = 0.75 (hexanes:EtOAc, 7:3). $^1H$ NMR ($CDCl_3$, 400 MHz): $\delta$ 8.33 (d, 1H, $J$ = 1.9 Hz), 7.96 (dd, 1H, $J$ = 1.9, 8.4 Hz), 7.15 (d, 1H, $J$ = 8.3 Hz), 2.94 (q, 2H, $J$ = 7.2 Hz), 1.19 (t, 3H, $J$ = 7.2 Hz). $^{13}C$ NMR ($CDCl_3$, 100 MHz): $\delta$ 198.0, 146.0, 139.9, 134.6, 129.3, 118.0, 87.7, 31.7, 8.1. HRMS calcd for $(C_9H_8IN_3O)_2Na^+$ 624.9316, found 624.9331. IR: azide, 2102 $cm^{-1}$.

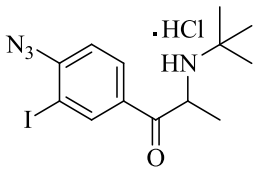


**(±)-4.20**

**(±)-1-(4-Azido-3-iodophenyl)-2-(*tert*-butylamino)propan-1-one hydrochloride ((±)-4.20)**

A solution of 1-(4-azido-3-iodophenyl)propan-1-one (**(±)-5.36**, 602 mg, 2.0 mmol) in $CHCl_3$ (12 mL) was treated with a mixture of liquid $Br_2$ (0.1 mL, 2.2 mmol) in $CHCl_3$ (12 mL). The reaction was then heated at 50˚C for 20 hours, cooled to room temperature, then concentrated. *N*-Methylpyrrolidinone (3 mL) was then added to the residue followed by *t*-$BuNH_2$ (0.5 mL, 4.7 mmol). The mixture was then heated at 55˚C for 10 minutes, cooled to room temperature, then diluted with $Et_2O$. The organic layer was then washed with $H_2O$, dried ($MgSO_4$), filtered, and concentrated. 2M HCl in $Et_2O$ was then added dropwise to the residue until a yellow solid ceased to precipitate. The resulting solid was collected *via* filtration, washed with $Et_2O$, then dried to provide 79 mg of bupropion analog **(±)-4.20** as the HCl salt (11%, 3 steps). $^1H$ NMR (MeOD, 400 MHz): $\delta$ 8.61 (d, 1H, $J$ = 2.0 Hz), 8.30 (dd, 1H, $J$ = 2.0, 8.5 Hz), 7.50 (d, 1H, $J$ = 8.5 Hz), 5.28 (q, 1H, $J$ = 7.1 Hz), 1.62 (d, 3H, $J$ = 7.1 Hz), 1.40 (s, 9H). $^{13}C$ NMR (MeOD, 100 MHz): $\delta$ 193.2, 148.9, 140.6, 130.4, 129.5, 118.8, 87.5, 58.5, 53.3, 26.3, 25.1, 17.4. HRMS

calcd for the free base as $(C_{13}H_{17}IN_4O)Na^+$ 395.0339, found 395.0344. Anal. calcd for: $C_{13}H_{18}ICIN_4O \cdot 0.4Et_2O \cdot 0.2HCl$: C, 39.35; H, 5.02; N, 12.57; I, 28.48. Found C, 39.32; H, 4.98; N, 12.78; I, 28.41. IR: azide, 2109 $cm^{-1}$. MP: 96 ˚C.

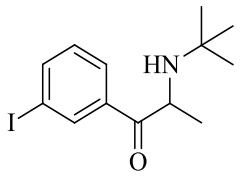


**(±)-4.21**

**(±)-2-(*tert*-Butylamino)-1-(3-iodophenyl)propan-1-one ((±)-4.21)**

3-Iodo-propiophenone (**5.38**, 388 mg, 1.49 mmol) was treated with a mixture of liquid $Br_2$ (0.83 mL) in $CH_2Cl_2$ (12 mL). The reaction was then heated at 40˚C for 20 hours followed by 50˚C for 1 hour. The reaction was then cooled to room temperature and concentrated to provide the resulting α-bromo ketone, which was used immediately without further purification. To the resulting bromide (522 mg) was added *N*-methylpyrrolidinone (2 mL) and *t*-$BuNH_2$ (0.7 mL). The mixture was then heated to 55˚C for 15 minutes. The reaction was then cooled, diluted with $Et_2O$, and washed with sat. aq. $NaHCO_3$ solution. The organic layer was then washed with brine, dried ($MgSO_4$), filtered, and concentrated. The resulting material was then treated dropwise with 1M HCl in $Et_2O$ (1.5 mL) to provide 257 mg of the hydrochloride salt of bupropion analog (**(±)-4.21** as a yellow solid after filtration and drying (47%). $^1H$ NMR (DMSO-$d_6$, 400 MHz): $\delta$ 9.54 (br, d, 1H, $J$ = 13.0 Hz), 8.61 (br, s, 1H), 8.52 (t, 1H, $J$ = 1.6 Hz), 8.23 (m, 1H), 8.15 (m, 1H), 7.44 (t, 1H, $J$ = 7.8 Hz), 5.29 (m, 1H), 1.52 (d, 3H, $J$ = 7.0 Hz), 1.32 (s, 9H). $^{13}C$ NMR (DMSO-$d_6$, 400 MHz): $\delta$ 195.9, 143.8, 137.4, 134.6, 131.8, 128.9, 96.5, 58.6, 53.2, 26.5, 18.5. HRMS calcd for the free base as $(C_{13}H_{18}INO)Na^+$ 354.0325, found 354.0331. Anal. calcd for

(C13H19ClNIO), C, 42.47; H, 5.21; N, 3.81; I, 34.52. Found, C, 42.64; H, 5.40; N, 3.94; I, 34.24.

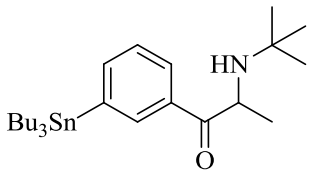


**(±)-4.22**

**(±)-2-(*tert*-Butylamino)-1-(3-(tri-*n*-butylstannyl)phenyl)propan-1-one ((±)-4.22)**

To 2-(*tert*-butylamino)-1-(3-iodophenyl)propan-1-one (**(±)-4.21**, 59 mg, 0.18 mmol) was sequentially added toluene (5 mL), $Pd(PPh_3)Br_2$ (5 mg, 0.01 mmol), and $(n\text{-}Bu_3)_2Sn_2$ (0.13 mL, 0.33 mmol). The resulting mixture was heated at 105˚C for 2 hours then cooled to room temperature. The mixture was then partitioned between sat. aq. $K_2CO_3$ solution and EtOAc. The EtOAc layer was then separated, washed with brine, dried ($MgSO_4$), filtered, and concentrated. Chromatography (hexanes:EtOAc:$Et_3N$, 100:0:0 to 80:18:2) provided 30 mg of organostannane **(±)-4.22** as a yellow oil (35%). $R_f$ = 0.43 (hexanes:EtOAc:$Et_3N$, 70:28:2). $^1H$ NMR ($CDCl_3$, 400 MHz): δ 8.10 (s, 1H), 7.92 (m, 1H), 7.70 (td, 1H, $J$ = 1.1, 7.2 Hz), 7.46 (t, 1H, $J$ = 7.5 Hz), 4.39 (q, 1H, $J$ = 7.1 Hz), 2.42 (br s, 1H), 1.58 (m, 6H), 1.36 (qd, 6H, $J$ = 7.3, 14.4 Hz), 1.29 (d, 3H, $J$ = 7.1 Hz), 1.13 (m, 6H), 1.08 (s, 9H), 0.91 (t, 9H, $J$ = 7.3 Hz). $^{13}C$ NMR ($CDCl_3$, 100 MHz): $\delta$ 205.7, 143.2, 141.4, 136.1, 134.2, 128.1, 127.9, 51.9, 50.8, 29.8, 29.1, 27.3, 22.7, 13.7, 9.7. HRMS calcd for $(C_{25}H_{45}NOSn)Na^+$ 518.2415, found 518.2415.

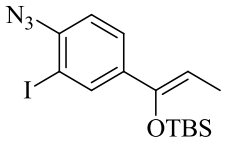


**5.40**

**((1-(4-Azido-3-iodophenyl)prop-1-en-1-yl)oxy)(*tert*-butyl)dimethylsilane (5.40)**

To a 0˚C mixture of 4-azido-3-iodopropiophenone (**5.36**, 164 mg, 0.54 mmol), $CH_2Cl_2$ (1.5 mL), and $Et_3N$ (0.12 mL, 0.87 mmol) was added TBSOTf (0.14 mL, 0.60 mmol) dropwise. The formation of white fumes ceased after 10 minutes and the mixture was allowed to stir at room temperature overnight. The reaction mixture was then diluted with $CH_2Cl_2$ and the organic layer was washed with sat. aq. $NaHCO_3$ solution. The organic layer was then separated, washed with brine, dried ($MgSO_4$), filtered, and concentrated. Chromatography (100% hexanes) provided 154 mg of silyl enol ether **5.40** as a pale yellow oil (68%). $R_f$ = 0.32 (hexanes:EtOAc, 99:1). $^1$H NMR ($CDCl_3$, 400 MHz): $\delta$ 7.90 (d, 1H, $J$ = 2.0 Hz), 7.47 (dd, 1H, $J$ = 2.0, 8.3 Hz), 7.07 (d, 1H, $J$ = 8.3 Hz), 5.24 (q, 1H, $J$ = 6.9 Hz), 1.75 (d, 3H, $J$ = 7.1 Hz), 1.02 (bs, 9H), 0.01 (s, 6H). $^{13}$C NMR ($CDCl_3$, 400 MHz): $\delta$ 147.8, 140.3, 138.1, 136.9, 126.6, 117.8, 106.9, 87.2, 25.8, 18.3, 11.8, -3.9. HRMS calcd for $(C_{15}H_{22}IN_3OSi)H^+$ 416.0649, found 416.0650. IR: azide, 2105.6 $cm^{-1}$.

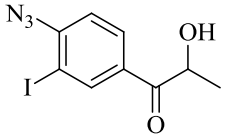


**(+)-5.41**

**(+)-1-(4-Azido-3-iodophenyl)-2-hydroxypropan-1-one ((+)-5.41)**

A bright orange mixture of AD-mix-β (478 mg), $CH_3SO_2NH_2$ (33 mg, 0.35 mmol) in *t*-BuOH:$H_2O$ (3.5 mL, 1:1.5) was cooled to 0˚C. Enol ether **5.40** (140 mg, 0.34 mmol) in *t*-BuOH

(0.5 mL) was then added to the mixture. The reaction was stirred at 0˚C for 10 hours followed by stirring at room temperature overnight. The reaction was then cooled to 0˚C and sodium sulfite (331 mg) was added to the mixture resulting in an instant color change from bright orange to a light brown color. The mixture was then stirred for 1.5 hours followed by partitioning between $H_2O$ and $Et_2O$. The organic layer was then separated, washed with brine, dried ($MgSO_4$), filtered, and concentrated. Chromatography (hexanes:EtOAc, 7:3) provided 79 mg of alcohol **(+)-5.41** as a yellow solid (73%). $R_f$ = 0.62 (hexanes:EtOAc, 6:4). $^1$H NMR ($CDCl_3$, 400 MHz): $\delta$ 8.37 (d, 1H, $J$ = 1.9 Hz), 7.96 (dd, 1H, $J$ = 2.0, 8.4 Hz), 7.24 (d, 1H, $J$ = 8.4 Hz), 5.10 (m, 1H, $J$ = 6.9 Hz), 3.68 (d, 1H, $J$ = 6.4 Hz), 1.46 (d, 3H, $J$ = 7.0 Hz). $^{13}$C NMR ($CDCl_3$, 100 MHz): $\delta$ 199.7, 147.2, 140.6, 130.9, 129.9, 118.2, 87.9, 69.2, 22.3. HRMS calcd for $(C_9H_8IN_3O_2)Na^+$ 339.9553, found 339.9554. IR: azide, 2103 cm$^{-1}$. Optical rotation $[\alpha]^{20.4}_D$ = +50.8˚ (c = 4.6, $CHCl_3$). The absolute stereochemistry of alcohol **(+)-5.41** was not determined *via* x-ray crystallography.

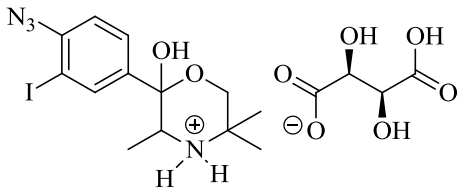


**(+)-4.23**

**(+)-2-(4-Azido-3-iodophenyl)-2-hydroxy-3,5,5-trimethylmorpholin-4-ium 3-carboxy-2,3-dihydroxypropanoate ((+)-4.23)**

To a solution of α-hydroxy ketone **(+)-5.41** (320 mg, 1.01 mmol) in $CH_2Cl_2$ (3 mL) was added proton sponge (257 mg, 1.20 mmol). The mixture was cooled to -61˚C and triflic anhydride (0.19 mL, 1.11 mmol) was added dropwise. The reaction was then allowed to warm to 0˚C and

stirred for 1 hour. In a separate round bottom flask was added $CH_3CN$ (3 mL) and 2-amino-2-methylpropanol (0.21 mL, 2.18 mmol), then the mixture was cooled to -10˚C. The 0˚C α-hydroxy ketone slurry was then transferred to the 2-amino-2-methylpropanol mixture at -10˚C resulting in a brown colored reaction that was stirred for 4 hours at 0˚C. The reaction mixtures was then concentrated and the residue was triturated in $Et_2O$. The resulting white precipitate was removed *via* filtration and the filtrate was concentrated and chromatographed (EtOAc:$Et_3N$, 95:5) to provide 77 mg of the bupropion metabolite analog **(+)-4.23** as a yellow solid (20%). $R_f$ = 0.33 (EtOAc:$Et_3N$, 95:5). $^1H$ NMR ($CDCl_3$, 500 MHz): $\delta$ 7.99 (s, 1H), 7.60 (d, 1H, $J$ = 8.3 Hz), 7.09 (d, 1H, $J$ = 8.3 Hz), 3.81 (d, 2H, $J$ = 11.3 Hz), 3.40 (d, 1H, $J$ = 11.3 Hz), 3.12 (m, 1H), 1.37 (s, 3H), 1.08 (s, 3H), 0.79 (d, 3H, $J$ = 6.4 Hz). HRMS calcd for $(C_{13}H_{17}IN_4O_2)Na^+$ 411.0288, found 411.0298. The free base of **(+)-4.23** was dissolved in MeOH (2.5 mL) and (*D*)-tartaric acid (14 mg) was added to the mixture. After 2 hours of stirring, the mixture was concentrated then triturated with $Et_2O$ to provide the tartarate salt of **(+)-4.23** as a yellow solid. $^1H$ NMR (MeOD, 400 MHz): $\delta$ 8.04 (d, 1H, $J$ = 1.9 Hz), 7.71 (dd, 1H, $J$ = 1.9, 8.4 Hz), 7.31 (d, 1H, $J$ = 8.4 Hz), 4.36 (s, 1H), 4.22 (d, 1H, $J$ = 12.4 Hz), 3.53 (m, 2H), 1.64 (s, 3H), 1.41 (s, 3H), 1.13 (d, 3H, $J$ = 6.5 Hz). $^{13}C$ NMR (MeOD, 100 MHz): $\delta$ 177.9, 143.9, 140.1, 139.3, 129.3, 119.3, 95.9, 87.8, 74.6, 66.9, 55.3, 54.6, 23.5, 20.8, 13.7. IR: azide, 2131 $cm^{-1}$. Optical rotation $[\alpha]^{24.1}_D$ = +59.27˚ (c = 1.1, $CHCl_3$). The absolute stereochemistry of bupropion metabolite analog **(+)-4.23** was not determined *via* x-ray crystallography.

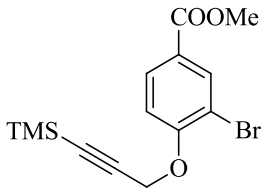


**5.54**

**Methyl 3-bromo-4-((3-(trimethylsilyl)prop-2-yn-1-yl)oxy)benzoate (5.54)**

DMF (38 mL) was added to a mixture of phenol derivative **5.53** (996 mg, 4.31 mmol) and $K_2CO_3$ (1.79 g, 12.93 mmol) followed by dropwise addition of TMS-protected propargyl bromide (0.98 mL, 6.04 mmol). The reaction was stirred at room temperature for 48 hours then diluted with $H_2O$ and extracted with EtOAc. The organic layer was washed with $H_2O$ and brine, then dried ($MgSO_4$), filtered, concentrated, and chromatographed (hexanes:EtOAc, 9:1) to provide 851 mg of silyl-protected propargyl ether **5.54** as a white solid (58%). $R_f$ = 0.43 (hexanes:EtOAc, 9:1). $^1$H NMR ($CDCl_3$, 400 MHz): $\delta$ 8.27 (d, 1H, $J$ = 2.1 Hz), 8.01 (dd, 1H, $J$ = 2.1, 8.6 Hz), 7.13 (d, 1H, $J$ = 8.7 Hz), 4.85 (s, 2H), 3.92 (s, 3H), 0.18 (s, 9H). $^{13}$C NMR ($CDCl_3$, 100 MHz): $\delta$ 165.4, 157.6, 134.8, 130.1, 124.3, 112.8, 111.8, 98.6, 94.2, 57.6, 52.1, 0.4. HRMS calcd for $(C_{14}H_{17}BrO_3Si)Na^+$ 363.0022, found 363.0020.

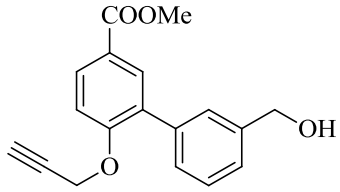


**5.58**

**Methyl 3'-(hydroxymethyl)-6-(prop-2-yn-1-yloxy)-[1,1'-biphenyl]-3-carboxylate (5.58)**

To aryl bromide derivative **5.53** (601 mg, 2.60 mmol) was sequentially added boronic acid **5.51** (474 mg, 3.12 mmol), toluene (7.6 mL), MeOH (1.3 mL), $K_2CO_3$ (719 mg, 5.19 mmol), and

$PdCl_2(PPh_3)_2$ (182 mg, 0.26 mmol). The reaction mixture was degassed then refluxed at 90˚C for 4 hours, then 70˚C overnight. The reaction was then cooled to room temperature and filtered over Celite® rinsing with EtOAc. The filtrate was then washed with $H_2O$ and brine, dried ($MgSO_4$), filtered, and concentrated to provide 333 mg of phenol derivative **5.57** (50%), which was used without further purification. $R_f$ = 0.12 (hexanes:EtOAc, 6:4). $^1$H NMR ($CDCl_3$ + $D_2O$, 400 MHz): $\delta$ 8.30 (s, 1H), 7.95 (d, 1H, $J$ = 2.1 Hz), 7.40 (m, 4H), 6.97 (d, 1H, $J$ = 8.5 Hz), 4.69 (s, 2H), 3.89 (s, 3H). To a suspension of phenol **5.57** (333 mg, 1.29 mmol) and $K_2CO_3$ (535 mg, 3.86 mmol) in DMF (11 mL) was added propargyl bromide (80% in toluene; 0.16 mL) dropwise. The resulting light-yellow colored reaction was then stirred at room temperature overnight followed by dilution with $H_2O$ and EtOAc. The organic layer was separated and washed with $H_2O$ and brine, then dried ($MgSO_4$), filtered, and concentrated. Chromatography (hexanes:EtOAc, 6:4) provided 129 mg of propargyl ether **5.58** as a colorless oil (34%). $R_f$ = 0.65 (hexanes:EtOAc, 1:1). $^1$H NMR ($CDCl_3$, 500 MHz): $\delta$ 8.05 (m, 1H), 7.54 (s, 2H), 7.43 (m, 3H), 7.17 (m, 1H), 4.76 (m, 4H), 3.92 (s, 3H), 2.55 (m, 1H), 2.03 (br s, 1H). $^{13}$C NMR ($CDCl_3$, 100 MHz): $\delta$ 166.8, 158.0, 140.9, 137.5, 132.6, 131.0, 130.6, 129.0, 128.3, 128.1, 126.1, 123.6, 112.4, 77.9, 76.3, 65.3, 56.1, 52.0. HRMS calcd for $(C_{18}H_{16}O_4)Na^+$ 319.0941, found 319.0943.

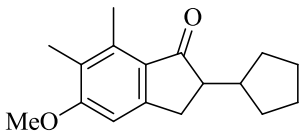


**(±)-5.49**

**2-Cyclopentyl-5-methoxy-6,7-dimethyl-2,3-dihydro-1H-inden-1-one ((±)-5.49)**

A mixture of cyclopentylphenyl ethanone derivative **(±)-5.47** (3.07 g, 12.48 mmol; DeSolms *et al*., 1978), paraformaldehyde (948 mg, 31.6 mmol), dimethylamine hydrochloride (3.05 g, 37.44

mmol) and glacial acetic acid (6.24 mmol, 0.36 mL) in DMF (15 mL) was heated at 100ºC overnight. The reaction was then cooled to room temperature, poured over dis. $H_2O$, extracted with EtOAc, washed with brine, and then concentrated to provide α,β-unsaturated phenyl ketone **5.48** as a colorless oil (2.2 g, 70%). $^1$H NMR ($CDCl_3$, 500 MHz): $\delta$ 7.14 (d, 1H, J = 8.5 Hz), 6.70 (d, 1H, J = 8.5 Hz), 5.81 (d, 2H, J = 1.3 Hz), 3.85 (s, 3H), 2.3 (m, 1H, J = 0.7 Hz), 2.26 (s, 3H), 2.19 (s, 3H), 2.00 (m, 2H), 1.71 (m, 4H), 1.46 (m, 2H). $^{13}$C NMR ($CDCl_3$, 100 MHz): $\delta$ 201.1, 158.7, 154.1, 136.8, 132.6, 127.3, 126.0, 124.7, 106.4, 55.4, 40.5, 31.8, 24.9, 17.1, 11.6. The ketone **5.48** (2.12 g, 8.6 mmol) was treated with 96% $H_2SO_4$ (10.1 mL) and stirred at room temperature for 2.5 hours, then quenched by pouring over dis. $H_2O$ (100 mL) and extracted with $CH_2Cl_2$ (3 times). The combined organic layers were washed with 1M NaOH, then brine, and concentrated to provide 1.8 g of cyclic ketone **(±)-5.49** as a yellow solid (81%) without further need for purification. $^1$H NMR ($CDCl_3$, 400 MHz): $\delta$ 6.72 (s, 1H), 3.90 (s, 3H), 3.09 (dd, 1H, J = 8.0, 17.2 Hz), 2.76 (m, 2H), 2.62 (s, 3H), 2.35 (m, 1H), 2.15 (s, 3H), 1.95 (m, 1H), 1.52 (m, 6H), 1.08 (td, 1H, J = 11.9, 18.4 Hz). $^{13}$C NMR ($CDCl_3$, 100 MHz): $\delta$ 208.4, 162.4, 155.0, 138.4, 127.8, 125.3, 104.2, 55.6, 51.2, 41.3, 30.8, 29.6, 28.1, 25.4, 25.2, 13.9, 10.9. HRMS calcd. for $(C_{17}H_{22}O_2)Na^+$ 281.3814, found 281.3819.

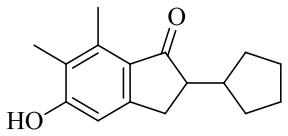


**(±)-3.40**

**2-Cyclopentyl-5-hydroxy-6,7-dimethyl-2,3-dihydro-1H-inden-1-one ((±)-3.40)**

A mixture of methyl ether **(±)-5.49** (128 mg, 0.50 mmol) in $CH_2Cl_2$ (3 mL) at -78ºC was carefully treated with dropwise addition of $BBr_3$ (0.12 mL, 1.23 mmol). The resulting mixture

was stirred overnight at room temperature, and then quenched by pouring over ice-cold $NaHCO_3$ (sat. solution). The aqueous mixture was extracted with EtOAc, the organic layer washed with brine, separated, and concentrated to provide 1.5 g of phenol **(±)-3.40** as a brown solid (95%) without further need for purification. $^1$H NMR (DMSO-$d_6$, 400 MHz): $\delta$ 10.31 (s, 1H), 6.73 (s, 1H), 3.35 (s, 1H), 2.99 (dd, 1H, J = 8.7, 18.0 Hz), 2.60 (m, 2H), 2.18 (s, 3H), 2.03 (s, 3H), 1.83 (m, 2H), 1.63 (m, 2H), 1.42 (m, 4H). $^{13}$C NMR (DMSO-$d_6$, 100 MHz): $\delta$ 207.2, 161.2, 154.8, 138.4, 126.5, 123.4, 109.3, 50.8, 41.3, 30.7, 29.1, 28.1, 25.4, 25.2, 13.9, 11.2. HRMS calcd. for $(C_{16}H_{20}O_2)Na^+$ 267.5224, found 267.5220.

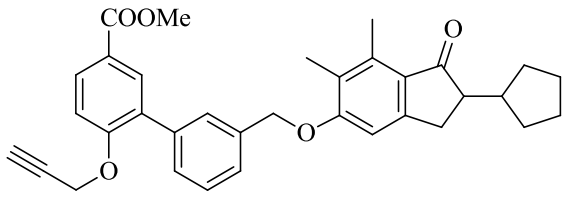


**(±)-5.59**

**(±)-Methyl 3'-(((2-cyclopentyl-6,7-dimethyl-1-oxo-2,3-dihydro-1H-inden-5-yl)oxy)methyl)-6-(prop-2-yn-1-yloxy)-[1,1'-biphenyl]-3-carboxylate ((±)-5.59)**

A mixture of DIAD (89.2 mg, 0.44 mmol) in THF (2 mL) was slowly added to a suspension of phenol **(±)-3.40** (90 mg, 0.37 mmol), $Ph_3P$ (116 mg, 0.44 mmol), and benzyl alcohol derivative **5.58** (131 mg, 0.44 mmol) in THF (2 mL) at -10˚C. The reaction was then stirred at room temperature overnight. The reaction mixture was then concentrated and chromatographed (100% $CH_2Cl_2$) to provide 90 mg of benzyl ether **(±)-5.59** as a colorless oil (47%). $R_f$ = 0.8 (100% $CH_2Cl_2$). $^1$H NMR ($CDCl_3$, 400 MHz): $\delta$ 8.08 (m, 2H), 7.65 (s, 1H), 7.50 (m, 3H), 7.19 (d, 1H, *J* = 8.5 Hz), 6.83 (s, 1H), 5.21 (s, 2H), 4.77 (d, 2H, *J* = 2. 4 Hz), 3.93 (s, 3H), 3.10 (m, 1H), 2.74 (m, 2H), 2.65 (s, 3H), 2.56 (t, 1H, *J* = 2.4 Hz), 2.35 (m, 1H), 2.24 (s, 3H), 1.94 (m, 1H), 1.67-

1.37 (m, 6H), 1.09 (m, 1H). $^{13}$C NMR ($CDCl_3$, 100 MHz): $\delta$ 208.5, 166.6, 161.5, 158.0, 154.9, 138.7, 137.6, 136.5, 132.7, 130.8, 130.6, 129.2, 128.5, 128.3, 128.1, 126.2, 125.7, 123.6, 112.4, 105.6, 77.9, 76.3, 70.0, 56.1, 52.0, 51.2, 41.3, 30.8, 29.7, 28.2, 25.4, 25.3, 14.0, 11.3. HRMS calcd. for $(C_{34}H_{34}O_5)Na^+$ 545.2298, found 545.2291.

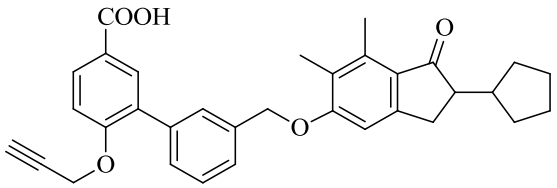


**(±)-4.25**

**(±)-3'-(((2-cyclopentyl-6,7-dimethyl-1-oxo-2,3-dihydro-1H-inden-5-yl)oxy)methyl)-6-(prop-2-yn-1-yloxy)-[1,1'-biphenyl]-3-carboxylic acid ((±)-4.25)**

A suspension of ester **(±)-5.59** (90 mg, 0.17 mmol) and LiOH (16.5 mg, 0.69 mmol) in THF (0.4 mL), MeOH (0.2 mL), and $H_2O$ (0.09 mL) was vigorously stirred at room temperature overnight. The resulting clear solution was then acidified with 1M aq. HCl to pH 1 then diluted with EtOAc. The EtOAc layer was then separated and washed with brine, then dried ($MgSO_4$), filtered, and concentrated to provide 77 mg of carboxylic acid **(±)-4.25** as a white solid (88%), which was used without further purification. $R_f$ = 0.33 (EtOAc:hexanes:MeOH:AcOH, 35:60:3:2). $^1$H NMR (DMSO-$d_6$, 400 MHz): $\delta$ 12.85 (s, 1H), 7.97 (dd, 1H, $J$ = 2.2, 8.6 Hz), 7.88 (d, 1H, $J$ = 2.2 Hz), 7.62 (s, 1H), 7.49 (m, 3H), 7.31 (d, 1H, $J$ = 8.7 Hz), 7.07 (s, 1H), 5.28 (s, 2H), 4.92 (s, 2H), 3.63 (t, 1H, $J$ = 2.3 Hz), 3.09 (dd, 1H, $J$ = 7.7, 17.2 Hz), 2.68 (m, 2H), 2.53 (s, 3H), 2.18 (m, 4H), 1.83 (m, 1H), 1.60-1.29 (m, 6H), 1.02 (m, 1H). $^{13}$C NMR (DMSO-$d_6$, 100 MHz): $\delta$ 207.7, 167.3, 161.4, 158.0, 155.2, 137.8, 137.7, 137.3, 132.3, 131.0, 130.3, 129.2, 128.9, 128.6, 127.7, 126.8, 125.2, 124.5, 113.5, 106.8, 79.25, 79.16, 69.9, 56.4, 51.0, 41.2, 30.7, 29.6, 28.2, 25.4, 25.2, 13.9, 11.5. HRMS calcd for $(C_{33}H_{32}O_5)Na^+$ 531.2142, found 531.2134.

Anal. calcd. for ($C_{33}H_{32}O_5 \cdot CH_3COOC_2H_5$) C, 74.47; H, 6.76; found C, 74.28; H, 6.54. MP: 192ºC.

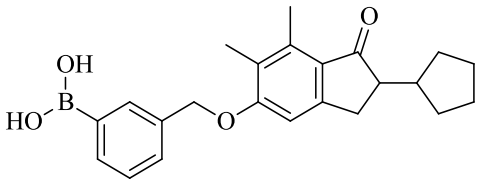


**(±)-5.62**

**(±)-(3-(((2-cyclopentyl-6,7-dimethyl-1-oxo-2,3-dihydro-1H-inden-5-yl)oxy)methyl) phenyl)boronic acid ((±)-5.62)**

A mixture of phenol **(±)-3.40** (500 mg, 2.05 mmol), $K_2CO_3$ (1.27 g, 9.21 mmol), KI (67.9 mg, 0.41 mmol), and 3-boronic acid benzyl bromide (**5.61**, 461 mg, 2.15 mmol) in acetone (36 mL) was heated at 60˚C overnight. The reaction was then cooled to room temperature and extracted with EtOAc. The EtOAc layer was then separated, washed with $H_2O$ and brine, then dried ($MgSO_4$), filtered, concentrated, and chromatographed (hexanes:EtOAc, 9:1 to 7:3) to provide 774 mg of benzyl ether **(±)-5.62** as a white solid (99%). $R_f$ = 0.17 (hexanes:EtOAc, 7:3). $^1$H NMR ($CDCl_3$, 400 MHz): $\delta$ 8.30 (m, 1H), 8.18 (d, 1H, $J$ = 7.1 Hz), 7.66 (m, 1H), 7.55 (t, 1H, $J$ = 7.3 Hz), 6.78 (m, 1H), 5.14 (s, 2H), 3.07 (m, 1H), 2.76-2.59 (m, 5H), 2.34-2.18 (m, 4H), 1.95 (m, 1H), 1.61 (m, 5H), 1.40 (m, 1H), 1.08 (m, 1H). $^{13}$C NMR ($CDCl_3$, 100 MHz): $\delta$ 208.7, 161.4, 155.1, 138.8, 136.3, 135.2, 134.1, 131.52, 131.51, 128.4, 128.1, 125.5, 105.4, 69.8, 51.3, 41.3, 30.8, 29.7, 28.2, 25.4, 25.3, 14.0, 11.2. HRMS calcd for $(C_{23}H_{27}BO_4)Na^+$ 401.1895, found 401.1898. MP: 112 ºC.

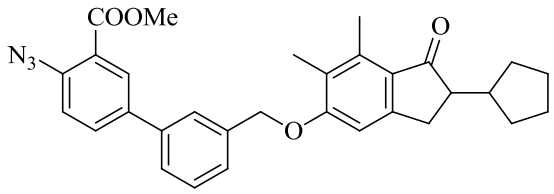


**(±)-5.65**

**(±)-Methyl 4-azido-3'-(((2-cyclopentyl-6,7-dimethyl-1-oxo-2,3-dihydro-1*H*-inden-5-yl)oxy)methyl)-[1,1'-biphenyl]-3-carboxylate ((±)-5.65)**

A mixture of boronic acid **(±)-5.62** (74 mg, 0.20 mmol) in 1,2-DME (2 mL) and DMF (1 mL) was added to a solution of aryl bromide **5.63** (42 mg, 0.16 mmol) in 1,2-DME (2 mL) containing $Pd(PPh_3)_4$ (37.9 mg, 0.03 mmol) and 10% aq. $NaHCO_3$ solution (0.32 mL). The resulting reaction was then refluxed for 6 hours in the dark, cooled to room temperature, then filtered through Celite® rinsing with EtOAc. The EtOAc filtrate was then washed with brine, dried ($MgSO_4$), filtered, concentrated, and chromatographed (hexanes:EtOAc, 10:1 to 9:1) to provide 20 mg of biphenyl compound **(±)-5.65** as a yellow oil (24%). $R_f$ = 0.39 (hexanes:EtOAc, 8:2). $^1$H NMR ($CDCl_3$, 500 MHz): $\delta$ 8.14 (d, 1H, $J$ = 2.2 Hz), 7.79 (dd, 1H, $J$ = 2.3, 8.4 Hz), 7.68 (s, 1H), 7.59 (td, 1H, $J$ = 1.6, 7.5 Hz), 7.54-7.48 (m, 2H), 7.35 (d, 1H, $J$ = 8.4 Hz), 6.82 (s, 1H), 5.23 (m, 2H), 3.97 (m, 3H), 3.12-3.07 (m, 1H), 2.74 (m, 2H), 2.65 (s, 3H), 2.40-2.32 (m, 1H), 2.24 (s, 3H), 1.98-1.92 (m, 1H), 1.68-1.51 (m, 6H), 1.46-1.38 (m, 1H), 1.28 (m, 1H), 1.09 (m, 1H). $^{13}$C NMR ($CDCl_3$, 100 MHz): $\delta$ 208.5, 165.7, 161.4, 154.9, 139.5, 139.3, 138.8, 137.6, 137.2, 131.6, 130.4, 129.4, 128.2, 126.6, 126.57, 125.6, 125.6, 122.9, 120.5, 105.5, 70.0, 52.5, 51.2, 41.3, 30.8, 29.7, 28.2, 25.4, 25.3, 14.0, 11.3. HRMS calcd for $(C_{31}H_{31}N_3O_4)Na^+$ 532.2207, found 532.2210. IR: azide, 2121.2 cm$^{-1}$.

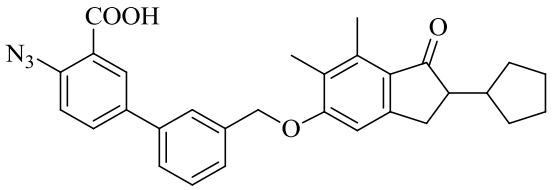


**(±)-4.27**

**(±)-4-Azido-3'-(((2-cyclopentyl-6,7-dimethyl-1-oxo-2,3-dihydro-1*H*-inden-5-yl)oxy)methyl)-[1,1'-biphenyl]-3-carboxylic acid ((±)-4.27)**

A suspension of ester **(±)-5.65** (20 mg, 0.04 mmol) and LiOH (6 mg, 0.24 mmol) in MeOH (1 mL), THF (2 mL), and $H_2O$ (0.5 mL) was stirred at room temperature overnight in the dark. The reaction was then acidified with 1M aq. HCl and extracted with EtOAc. The organic layer was then separated and washed with brine, then dried ($MgSO_4$), filtered, concentrated, and chromatographed (hexanes:EtOAc:MeOH:AcOH, 65:30:3:2) to afford 16 mg of carboxylic acid **(±)-4.27** as a light yellow oil (84%). $R_f$ = 0.2 (hexanes:EtOAc:MeOH:AcOH, 60:35:3:2). $^1$H NMR ($CDCl_3$, 400 MHz): $\delta$ 8.41 (d, 1H, $J$ = 1.9 Hz), 7.86 (d, 1H, $J$ = 8.4 Hz), 7.69 (s, 1H), 7.60 (d, 1H, $J$ = 7.3 Hz), 7.51 (m, 2H), 7.38 (d, 1H, $J$ = 8.4 Hz), 6.82 (s, 1H), 5.22 (m, 2H), 3.10 (m, 1H), 2.76 (m, 2H), 2.65 (s, 3H), 2.37 (m, 1H), 2.24 (s, 3H), 1.95 (m, 1H), 1.60 (m, 6H), 1.42 (m, 1H), 1.07 (m, 1H). $^{13}$C NMR ($CDCl_3$, 100 MHz): $\delta$ 208.6, 161.4, 155.0, 139.1, 138.9, 137.9, 137.7, 132.7, 131.9, 129.4, 128.2, 126.8, 126.6, 125.6, 125.6, 119.9, 105.5, 69.9, 51.2, 41.3, 30.8, 29.7, 28.1, 25.4, 25.3, 14.0, 11.3. HRMS calcd for $(C_{30}H_{29}N_3O_4)Na^+$ 518.2050, found 518.2053. IR: azide, 2118.4 cm$^{-1}$. MP: 180 ºC.

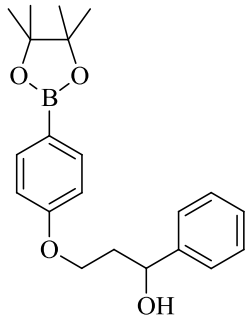

**5.73**

**(±)-1-Phenyl-3-(4-(4,4,5,5-tetramethyl-1,3,2-dioxaborolan-2-yl)phenoxy)propan-1-ol ((±)-5.73)**

A solution of 4-hydroxyphenyl boronic acid pinacol ester (**5.70**, 200 mg, 0.91 mmol) in DMF (0.5 mL) was added dropwise to a suspension of NaH (26 mg, 1.09 mmol) in DMF (1 mL) at 0˚C. After the effervescence ceased, the reaction was then stirred at room temperature for 30 minutes. 3-Chloro-1-phenylpropan-1-ol (**(±)-5.72**, 155 mg, 0.91 mmol) in DMF (0.5 mL) was then added dropwise to the reaction mixture followed by heating at 65˚C for 18 hours. The reaction was then cooled to room temperature, quenched with $H_2O$, and extracted with EtOAc. The organic layer was then separated, washed with brine, dried ($MgSO_4$), filtered, concentrated, and chromatographed (hexanes:EtOAc, 7:3) to provide 111 mg of ether **(±)-5.73** as a colorless oil (35%). $R_f$ = 0.36 (hexanes:EtOAc, 7:3). $^1$H NMR ($CDCl_3$, 400 MHz): $\delta$ 7.78 (d, 2H, $J$ = 8.6 Hz), 7.42-7.28 (m, 5H), 6.93 (d, 2H, $J$ = 8.7 Hz), 5.02 (m, 1H), 4.24-4.19 (m, 1H), 4.11-4.05 (m, 1H), 2.64 (br s, 1H), 2.32-2.15 (m, 2H), 1.36 (s, 12H). $^{13}$C NMR ($CDCl_3$, 100 MHz): $\delta$ 161.3, 144.2, 136.6, 128.6, 127.6, 125.8, 113.9, 83.6, 71.9, 65.1, 38.4, 24.9. HRMS calcd for $(C_{21}H_{27}BO_4)Na^+$ 377.1895, found 377.1894.

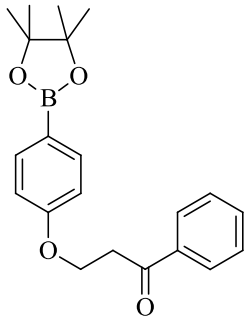

**5.71**

**1-Phenyl-3-(4-(4,4,5,5-tetramethyl-1,3,2-dioxaborolan-2-yl)phenoxy)propan-1-one (5.71)**

A mixture of benzyl alcohol **(±)-5.73** (111 mg, 0.31 mmol) and Dess-Martin periodinane (159 mg, 0.38 mmol) in $CH_2Cl_2$ (1 mL) was stirred at room temperature for 2 hours. The reaction was then filtered through Celite® and the filtrate was washed with 1M aq. NaOH, followed by extraction with $CH_2Cl_2$. The organic layer was then washed with brine, dried ($MgSO_4$), filtered, and concentrated to provide 91 mg of ketone **5.71** (81%), which was used without further purification. $R_f$ = 0.67 (hexanes:EtOAc, 7:3). $^1$H NMR ($CDCl_3$, 400 MHz): $\delta$ 8.03 (dd, 2H, $J$ = 1.2, 8.4 Hz), 7.78 (d, 2H, $J$ = 8.7 Hz), 7.61 (m, 1H), 7.51 (t, 2H, $J$ = 7.6 Hz), 6.95 (d, 2H, $J$ = 8.7 Hz), 4.48 (t, 2H, $J$ = 6.7 Hz), 3.50 (t, 2H, $J$ = 6.7 Hz), 1.36 (s, 12H). $^{13}$C NMR ($CDCl_3$, 100 MHz): $\delta$ 197.6, 161.2, 136.8, 136.6, 133.4, 128.7, 128.2, 113.9, 83.6, 63.0, 38.1, 24.9. HRMS calcd for $(C_{21}H_{25}BO_4)Na^+$ 375.1738, found 375.1739.

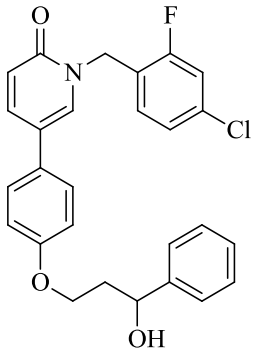


**(±)-5.74**

**(±)-1-(4-Chloro-2-fluorobenzyl)-5-(4-(3-hydroxy-3-phenylpropoxy)phenyl)pyridin-2(1*H*)-one ((±)-5.74)**

To a suspension of aryl bromide **3.57** (65 mg, 0.21 mmol) and boronate ester **(±)-5.73** (110 mg, 0.31 mmol) in 1,4-dioxane (2 mL) and sat. aq. $NaHCO_3$ solution (2 mL) was added $Pd(PPh_3)_4$ (35 mg, 0.03 mmol). The mixture was then degassed followed by heating at 90˚C for 6 hours. The reaction was then cooled to room temperature and filtered through Celite® rinsing with EtOAc. The organic filtrate was then washed with brine, dried ($MgSO_4$), filtered, concentrated, and chromatographed (hexanes:EtOAc, 7:3 to 1:1) to provide 37 mg of aryl-substituted pyridone **5.74** as an oil (39%), which was used without further purification. $R_f$ = 0.07 (hexanes:EtOAc, 1:1). $^1$H NMR ($CDCl_3$, 500 MHz): $\delta$ 7.58 (dd, 1H, $J$ = 2.7, 9.4 Hz), 7.52 (s, 1H), 7.48 (t, 1H, $J$ = 8.2 Hz), 7.39 (m, 5H), 7.31 (m, 2H), 7.13 (m, 2H), 6.96 (m, 2H), 6.65 (d, 1H, $J$ = 9.4 Hz), 5.18 (s, 2H), 5.02 (td, 1H, $J$ = 4.8, 9.4 Hz), 4.22 (ddd, 1H, $J$ = 5.2, 7.2, 9.3 Hz), 4.08 (m, 1H), 2.88 (s, 1H), 2.24 (m, 2H). HRMS calcd for $(C_{27}H_{23}ClFNO_3)Na^+$ 486.12427, found 486.12457.

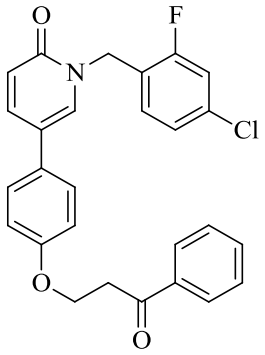

**1.93**

**1-(4-Chloro-2-fluorobenzyl)-5-(4-(3-oxo-3-phenylpropoxy)phenyl)pyridin-2(1*H*)-one (1.93)**

A suspension of benzyl alcohol derivative **5.74** (36 mg, 0.08 mmol) and Dess-Martin periodinane (39 mg, 0.09 mmol) in $CH_2Cl_2$ (3 mL) was stirred at room temperature for 4 hours. The reaction mixture was then filtered through Celite®. The clear filtrate was then diluted with sat. aq. $NaHCO_3$ solution and extracted with$CH_2Cl_2$. The $CH_2Cl_2$ layer was then separated, washed with brine, dried ($MgSO_4$), filtered, concentrated, and chromatographed (hexanes:EtOAc, 1:1) to provide 26 mg of ketone **1.93** (Cid *et al*., 2010) as a white solid (72%). $R_f$ = 0.64 (hexanes:EtOAc, 4:6). $^1$H NMR ($CDCl_3$, 400 MHz): $\delta$ 8.04 (d, 2H, $J$ = 7.1 Hz), 7.64-7.58 (m, 2H), 7.54-7.47 (m, 4H), 7.32 (d, 2H, $J$ = 8.8 Hz), 7.14 (td, 2H, $J$ = 2.2, 5.3 Hz), 6.99 (d, 2H, $J$ = 8.8 Hz), 6.68 (d, 1H, $J$ = 9.4 Hz), 5.20 (s, 2H), 4.48 (t, 2H, $J$ = 6.5 Hz), 3.52 (t, 2H, $J$ = 6.5 Hz). $^{13}$C NMR ($CDCl_3$, 100 MHz): $\delta$ 197.5, 162.0, 161.8, 159.5, 158.3, 139.7, 136.7, 135.1, 135.0, 134.1, 133.5, 132.4, 132.3, 129.0, 128.7, 128.1, 127.0, 125.1, 125.0, 122.0, 121.9, 121.1, 120.5, 116.4, 116.2, 115.2, 63.4, 46.2, 38.1. HRMS calcd for $(C_{27}H_{21}ClFNO_3)Na^+$ 484.1086, found 484.1089. Anal calcd for ($C_{27}H_{21}ClFNO_3 \cdot 0.14CH_3COOC_2H_5 \cdot 0.15HCl$): C, 69.03; H, 4.68; N, 2.92; Cl, 8.48; F, 3.96; Found C, 69.00; H, 4.59; N, 2.94; Cl, 8.46; F, 3.99. MP: 170 ºC.

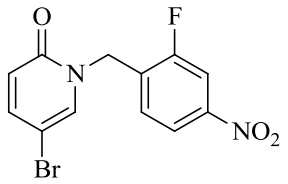

**5.78**

**5-Bromo-1-(2-fluoro-4-nitrobenzyl)pyridin-2(1*H*)-one (5.78)**

A mixture of 5-bromopyridone (120 mg, 0.69 mmol), $K_2CO_3$ (958 mg, 6.93 mmol), THF (10 mL), and 2-flouro-4-nitrobenzyl bromide (Frank *et al.*, 2013; 243 mg, 1.04 mmol) was heated at 65˚C for 17 hours followed by stirring at room temperature for 6 hours. The reaction was then quenched with $H_2O$ and diluted with EtOAc. The organic layer was separated, dried ($MgSO_4$), filtered, concentrated, and chromatographed (hexanes:EtOAc, 8:2) to obtain 148 mg of *N*-benzylated derivative **5.78** as a yellow solid (65%). $R_f$ = 0.13 (hexanes:EtOAc, 7:3). $^1$H NMR ($CDCl_3$, 500 MHz): $\delta$ 8.05-7.98 (ddd, 2H, $J$ = 2.1, 9.0, 11.7 Hz), 7.67 (t, 1H, $J$ = 7.9 Hz), 7.54 (m, 1H), 7.40 (dd, 1H, $J$ = 2.6, 9.7 Hz), 6.54 (d, 1H, $J$ = 9.7 Hz), 5.19 (s, 2H). $^{13}$C NMR ($CDCl_3$, 100 MHz): $\delta$ 161.5, 160.9, 159.0, 148.7, 148.6, 143.2, 137.3, 132.1, 129.7, 122.5, 119.7, 111.6, 111.3, 98.6, 46.6. HRMS calcd for $C_{12}H_8BrFN_2O_3Na^+$ 348.9594, found 348.9592.

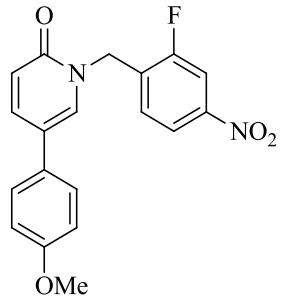

**5.79**

**1-(2-Fluoro-4-nitrobenzyl)-5-(4-methoxyphenyl)pyridin-2(1*H*)-one (5.79)**

A degassed suspension containing aryl bromide **5.78** (148 mg, 0.45 mmol), 4-methoxyphenyl boronic acid (104 mg, 0.69 mmol), 1,4-dioxane (4.1 mL), sat. aq. $NaHCO_3$ solution (4.1 mL),

and $Pd(PPh_3)_4$ (78 mg, 0.068 mmol) was heated at 95˚C for 5 hours. The reaction was then cooled to room temperature and filtered over Celite®. The filtrate was then diluted with $H_2O$ and extracted with EtOAc. The organic extract was washed with brine, dried ($MgSO_4$), filtered, concentrated, and chromatographed (hexanes:EtOAc, 1:1) to yield 103 mg of the anisole-substituted pyridinone derivative **5.79** as a yellow solid (65%). $R_f$ = 0.62 (hexanes:EtOAc, 4:6). $^1$H NMR ($CDCl_3$, 400 MHz): $\delta$ 8.02-7.94 (m, 2H), 7.68-7.62 (m, 2H), 7.55 (s, 1H), 7.33 (d, 2H, $J$ = 8.8 Hz), 6.95 (d, 2H, $J$ = 8.8 Hz), 6.68 (d, 1H, $J$ = 9.4 Hz), 5.29 (s, 2H), 3.84 (s, 3H). $^{13}$C NMR ($CDCl_3$, 100 MHz): $\delta$ 161.7, 161.5, 159.3, 159.0, 148.4, 148.36, 140.2, 134.0, 131.8, 131.76, 130.7, 130.6, 128.5, 127.0, 121.2, 120.8, 119.65, 119.62, 114.6, 111.5, 111.2, 55.4, 46.8. HRMS calcd as $C_{19}H_{15}FN_2O_4Na^+$ 377.0908, found 377.0905.

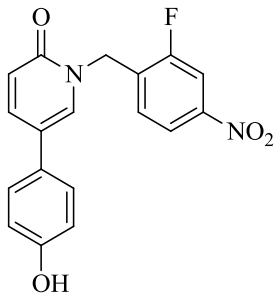


**5.80**

**1-(2-Fluoro-4-nitrobenzyl)-5-(4-hydroxyphenyl)pyridin-2(1*H*)-one (5.80)**

A mixture of methyl ether **5.79** (103 mg, 0.29 mmol) in $CH_2Cl_2$ (3.1 mL) was treated dropwise with $BBr_3$ (1M in $CH_2Cl_2$, 1.2 mL) at -78˚C. The reaction was then stirred at -78˚C for 1 hour followed by stirring at room temperature for 2 hours. The mixture was then carefully quenched by slow addition of MeOH (30 mL) at -78˚C followed by stirring at room temperature for 30 minutes. The mixture was then concentrated and chromatographed (hexanes:EtOAc, 40:60 to 0:100) to provide 66 mg of phenol **5.80** as a yellow solid (66%). $R_f$ = 0.48 (hexanes:EtOAc, 4:6). $^1$H NMR (DMSO-$d_6$, 400 MHz): $\delta$ 9.54 (br s, 1H), 8.15 (m, 2H), 8.07 (dd, 1H, $J$ = 2.0, 8.6

Hz), 7.84 (dd, 1H, $J$ = 2.7, 9.5 Hz), 7.39 (d, 3H, $J$ = 8.7 Hz), 6.82 (d, 2H, $J$ = 8.6 Hz), 6.52 (d, 1H, $J$ = 9.5 Hz), 5.30 (s, 2H). $^{13}$C NMR (DMSO-$d_6$, 100 MHz): $\delta$ 161.0, 160.9, 158.5, 157.2, 148.1, 148.0, 140.3, 135.9, 132.5, 132.3, 130.7, 130.6, 127.1, 126.9, 120.3, 120.2, 120.17, 119.4, 116.2, 111.8, 111.5, 47.0. HRMS calcd for $C_{18}H_{13}FN_2O_4Na^+$ 363.0751, found 363.0748.

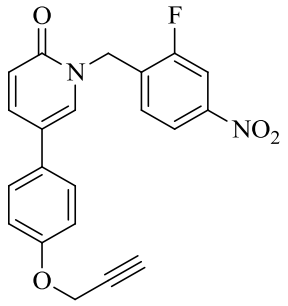


**5.94**

**1-(2-Fluoro-4-nitrobenzyl)-5-(4-(prop-2-yn-1-yloxy)phenyl)pyridin-2(1*H*)-one (5.94)**

Propargyl bromide (80% in toluene; 0.03 mL, 0.20 mmol) was added dropwise to a suspension of phenol **5.80** (63 mg, 0.19 mmol) and $K_2CO_3$ (77 mg, 0.56 mmol) in DMF (1.6 mL). The resulting mixture was then stirred at room temperature overnight followed by dilution with EtOAc and $H_2O$. The organic layer was then separated, washed with brine, dried ($MgSO_4$), filtered, and concentrated to provide 66 mg of propargyl ether **5.94** (94%). $R_f$ = 0.36 (hexanes: EtOAc, 4:6). $^1$H NMR ($CDCl_3$, 400 MHz): $\delta$ 7.99 (m, 2H), 7.65 (m, 2H), 7.56 (s, 1H), 7.34 (d, 2H, $J$ = 8.8 Hz), 7.04 (d, 2H, $J$ = 8.8 Hz), 6.68 (d, 1H, $J$ = 9.5 Hz), 5.29 (s, 2H), 4.73 (d, 2H, $J$ = 2.4 Hz), 2.56 (t, 1H, $J$ = 2.4 Hz). $^{13}$C NMR ($CDCl_3$, 100 MHz): $\delta$ 161.7, 161.5, 159.0, 157.2, 148.5, 148.4, 140.1, 134.2, 131.9, 131.8, 130.6, 130.5, 129.4, 127.1, 121.2, 120.7, 119.7, 119.6, 115.6, 111.5, 111.2, 78.3, 75.8, 55.9, 46.8. HRMS calcd for $(C_{21}H_{15}FN_2O_4)Na^+$ 401.0908, found 401.0906.

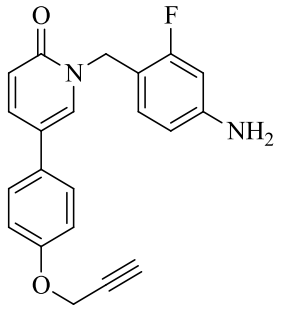

**5.81**

**1-(4-Amino-2-fluorobenzyl)-5-(4-(prop-2-yn-1-yloxy)phenyl)pyridin-2(1*H*)-one (5.81)**

A mixture of nitro-alkyne derivative **5.94** (63 mg, 0.17 mmol) in MeOH (1.3 mL), THF (1 mL), and conc. HCl (0.68 mL) was treated with $SnCl_2$ (123 mg, 0.65 mmol) at 0˚C then stirred at room temperature for 18 hours. The reaction was then neutralized with sat. aq. $K_2CO_3$ solution and extracted with EtOAc. The organic layer was then washed with brine, dried ($MgSO_4$), filtered, concentrated, and chromatographed ($CHCl_3$:MeOH:$Et_3N$, 90:8:2) to obtain 46 mg of amine **5.81** as a brown oil (84%). $R_f$ = 0.36 ($CHCl_3$:MeOH:$Et_3N$, 90:8:2). $^1$H NMR ($CDCl_3$, 400 MHz): $\delta$ 7.56 (m, 2H), 7.30 (m, 3H), 7.02 (dd, 2H, $J$ = 1.5, 8.8 Hz), 6.65 (m, 1H), 6.41 (m, 2H), 5.11 (s, 2H), 4.73 (s, 2H), 3.89 (br, s, 2H), 2.56 (m, 1H). $^{13}$C NMR ($CDCl_3$, 100 MHz): $\delta$ 162.0, 160.8, 156.9, 148.6, 139.2, 134.25, 134.23, 132.8, 132.7, 130.0, 127.0, 120.8, 120.0, 115.5, 112.3, 112.1, 111.1, 111.0, 101.7, 101.5, 78.4, 75.8, 55.9, 46.0. HRMS calcd for $(C_{21}H_{17}FN_2O_2)Na^+$ 371.11627, found 371.11646.

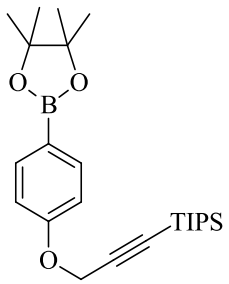


**5.82**

**Tri-isopropyl(3-(4-(4,4,5,5-tetramethyl-1,3,2-dioxaborolan-2-yl)phenoxy)prop-1-yn-1-yl)silane (5.82)**

A mixture of phenol **5.70** (330 mg, 1.5 mmol), DMF (11 mL), $K_2CO_3$ (623 mg, 4.5 mmol) and TIPS-protected propargyl bromide (Hoogboom and Swager, 2006; 578 mg, 2.10 mmol) was stirred at room temperature for 5 hours then diluted with $H_2O$ and extracted with EtOAc. The organic layer was then separated, washed with brine, concentrated, and chromatographed (hexanes:EtOAc, 100:0 to 95:5) to afford 388 mg of propargyl ether **5.82** as a colorless oil (62%). $R_f$ = 0.41 (hexanes:EtOAc, 9:1). $^1$H NMR ($CDCl_3$, 500 MHz): $\delta$ 7.77 (d, 2H, $J$ = 8.6 Hz), 7.02 (d, 2H, $J$ = 8.5 Hz), 4.76 (s, 2H), 1.36 (s, 12H), 1.06 (s, 21H). $^{13}$C NMR ($CDCl_3$, 100 MHz): $\delta$ 160.4, 136.3, 114.4, 101.8, 83.6, 77.2, 56.6, 24.9, 18.5, 11.1. HRMS calcd for $(C_{24}H_{39}BO_3Si)Na^+$ 437.26537, found 437.2657.

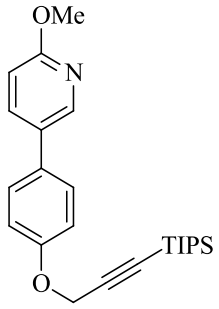


**5.84**

**2-Methoxy-5-(4-((3-(triisopropylsilyl)prop-2-yn-1-yl)oxy)phenyl)pyridine (5.84)**

A mixture of 2-methoxy-5-bromopyridine (0.023 mL, 0.18 mmol), boronic pinacol ester **5.82** (110 mg, 0.27 mmol), $Pd(PPh_3)_4$ (30 mg, 0.026 mmol), 1,4-dioxane (4 mL), and sat. aq. $NaHCO_3$ solution (1.6 mL) was degassed then heated at 90˚C for 3 hours. After cooling to room temperature, the mixture was filtered through Celite® and washed with $H_2O$ and brine, then dried ($MgSO_4$), filtered, concentrated, and chromatographed (hexanes:EtOAc, 8:2) to yield 70 mg of diaryl product **5.84** as a brown oil (90%). $R_f$ = 0.47 (hexanes:EtOAc, 9:1). $^1$H NMR ($CDCl_3$, 400 MHz): $\delta$ 8.36 (d, 1H, $J$ = 2.5 Hz), 7.76 (dd, 1H, $J$ = 2.6, 8.6 Hz), 7.46 (d, 2H, $J$ = 8.8 Hz), 7.11 (d, 2H, $J$ = 8.8 Hz), 6.82 (dd, 1H, $J$ = 0.5, 8.6 Hz), 4.79 (s, 2H), 4.00 (s, 3H), 1.06 (s, 21H). $^{13}$C NMR ($CDCl_3$, 100 MHz): $\delta$ 163.2, 157.2, 144.6, 137.2, 131.1, 130.0, 127.6, 115.9, 110.7, 101.8, 89.5, 56.9, 53.5, 18.5, 11.1. HRMS calcd for $(C_{24}H_{33}NO_2Si)Na^+$ 418.2173, found 418.2176.

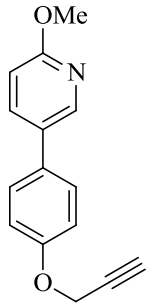


**5.85**

**2-Methoxy-5-(4-(prop-2-yn-1-yloxy)phenyl)pyridine (5.85)**

TBAF (1M in THF, 0.3 mL, 0.3 mmol) was added to a 0˚C mixture of TIPS-protected alkyne **5.84** (76 mg, 0.19 mmol) in THF (3.5 mL). The reaction was then stirred at room temperature for 2 hours followed by cooling again to 0˚C again and treatment with TBAF (1M in THF, 0.1 mL, 0.09 mmol). The reaction was then stirred at room temperature for 1 hour then concentrated and chromatographed (hexanes:EtOAc, 9.5:0.5) to obtain 20 mg of deprotected alkyne **5.84** as a white solid (43%). $R_f$ = 0.23 (hexanes:EtOAc, 9:1). $^1$H NMR ($CDCl_3$, 400 MHz): $\delta$ 8.37 (d, 1H, $J$ = 2.3 Hz), 7.76 (dd, 1H, $J$ = 2.6, 8.6 Hz), 7.48 (d, 2H, $J$ = 8.8 Hz), 7.08 (d, 2H, $J$ = 8.8 Hz), 6.82 (d, 1H, $J$ = 8.6 Hz), 4.76 (d, 2H, $J$ = 2.4 Hz), 4.00 (s, 3H), 2.58 (t, 1H, $J$ = 2.4 Hz). $^{13}$C NMR ($CDCl_3$, 100 MHz): $\delta$ 163.3, 157.1, 144.6, 137.2, 131.4, 129.6, 127.8, 115.4, 110.8, 78.5, 75.7, 55.9, 53.5. HRMS calcd for $(C_{15}H_{13}NO_2)Na^+$ 262.0838, found 262.0841.

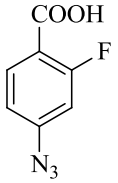


**5.87**

**4-Azido-2-fluorobenzoic acid (5.87)**

To a 0˚C suspension of aniline **5.86** (200 mg, 1.29 mmol) in $H_2O$ (7 mL) was carefully added conc. $H_2SO_4$ (1 mL) resulting in a clear, brown solution. $NaNO_2$ (110 mg, 1.6 mmol) was then

added to the mixture as a solid resulting in the evolution of brown gas. The mixture was then stirred for 20 minutes in the dark at 0˚C followed by dropwise addition of $NaN_3$ (151 mg, 2.32 mmol) dissolved in $H_2O$ (2 mL) resulting in a thick, white suspension. $H_2O$ (15 mL) was then added to this mixture and the reaction was stirred vigorously at room temperature overnight in the dark. The suspension was then filtered to obtain a white solid that was dissolved in EtOAc, dried ($MgSO_4$), filtered, and concentrated to provide 215 mg of aryl azide **5.87** as a white solid (92%), which was used without further purification. $R_f$ = 0.47 ($CHCl_3$:MeOH, 7:3). $^1$H NMR (DMSO-$d_6$, 400 MHz): $\delta$ 13.22 (s, 1H), 7.90 (t, 1H, $J$ = 8.3 Hz), 7.13 (dd, 1H, $J$ = 2.2, 11.7 Hz), 7.07 (dd, 1H, $J$ = 2.2, 8.5 Hz). $^{13}$C NMR (DMSO-$d_6$, 100 MHz): $\delta$ 164.8, 164.8, 163.8, 161.2, 146.2, 134.05, 134.03, 115.75, 115.72, 108.6, 108.3. IR: azide, 2133.8 cm$^{-1}$. HRMS analysis of this compound was not performed due to its relative instability at room temperature.

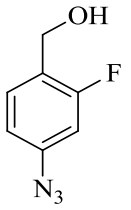


**5.88**

**(4-Azido-2-fluorophenyl)methanol (5.88)**

Triethylamine (0.2 mL, 1.44 mmol) was added to a suspension of carboxylic acid **5.87** (206 mg, 1.14 mmol) in $CH_2Cl_2$ (4 mL) resulting in a clear, yellow solution. Chloroformate (478 mg, 3.5 mmol) was then added dropwise to the mixture followed by stirring at room temperature for 45 minutes. A suspension of $NaBH_4$ (344 mg, 9.09 mmol) in EtOH (5 mL) was then added slowly to the reaction resulting in vigorous effervescence being observed. The resulting reaction was stirred at room temperature for 10 minutes then quenched with pH = 7 buffer. The mixture was then diluted with $H_2O$ and extracted with EtOAc. The organic extract was washed with brine,

then dried ($MgSO_4$), filtered, concentrated, and chromatographed (hexanes:EtOAc, 8:2) to give 50 mg of benzyl alcohol **5.88** as a colorless oil (30%). $R_f$ = 0.24 (hexanes:EtOAc, 8:2). $^1H$ NMR ($CDCl_3$, 400 MHz): $\delta$ 7.43 (t, 1H, $J$ = 8.1 Hz), 6.86 (dd, 1H, $J$ = 2.3, 8.4 Hz), 6.76 (dd, 1H, $J$ = 2.2, 10.6 Hz), 4.74 (s, 2H), 1.90 (s, 1H). $^{13}C$ NMR ($CDCl_3$, 100 MHz): $\delta$ 159.8, 141.3, 130.5, 130.47, 124.5, 114.8, 114.76, 106.7, 106.5, 58.9. IR: azide, 2109.7 $cm^{-1}$. HRMS analysis of this compound was not performed due to its relative instability at room temperature.

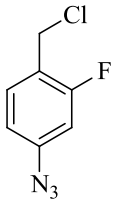


**5.89**

**4-Azido-1-(chloromethyl)-2-fluorobenzene (5.89)**

To a 0˚C mixture of 4-azido-2-fluorobenzyl alcohol (**5.88**, 50 mg, 0.31 mmol) in $CH_2Cl_2$ (2 mL) was added triethylamine (0.1 mL, 46.5 mmol) followed by MsCl (0.03 mL, 0.46 mmol). The resulting reaction was then stirred at 0˚C for 1 hour followed by quenching with sat. aq. $NaHCO_3$ solution and $H_2O$. The mixture was then extracted with $CH_2Cl_2$, followed by washing with brine then concentrated. Chromatography (hexanes:EtOAc, 10:1) provided 20 mg of benzyl chloride **5.89** (35%). $R_f$ = 0.86 ($CHCl_3$:MeOH, 9:1). $^1H$ NMR ($CDCl_3$, 400 MHz): $\delta$ 7.42 (t, 1H, $J$ = 8.2 Hz), 6.86 (dd, 1H, $J$ = 2.2, 8.3 Hz), 6.79 (dd, 1H, $J$ = 2.1, 10.4 Hz), 4.63 (s, 2H). $^{13}C$ NMR ($CDCl_3$, 100 MHz): $\delta$ 159.9, 142.4, 142.3, 132.0, 131.99, 121.3, 115.1, 115.0, 107.0, 106.7, 39.0. IR: azide, 2115.9 $cm^{-1}$. HRMS analysis of this compound was not performed due to its relative instability at room temperature.

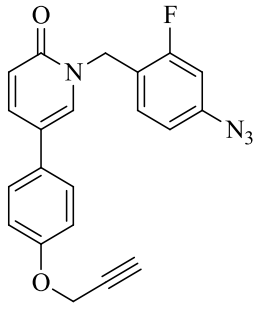

**4.29**

**1-(4-Azido-2-fluorobenzyl)-5-(4-(prop-2-yn-1-yloxy)phenyl)pyridin-2(1*H*)-one (4.29)**

A mixture containing pyridone **5.85** (25 mg, 0.10 mmol), $CH_3CN$ (3 mL), NaI (39 mg, 0.26 mmol), 4-azido-2-fluorobenzyl chloride (**5.89**, 19 mg, 0.10 mmol), and DMF (0.5 mL) was refluxed at 85˚C for 5 hours followed by stirring at room temperature overnight. The reaction mixture was then concentrated and the resulting residue was partitioned between EtOAc and $H_2O$. The EtOAc layer was washed with $H_2O$ and brine, then dried ($MgSO_4$), filtered, concentrated, and chromatographed (hexanes:EtOAc, 10:1 to 9:1). The resulting compound was then further purified by passing through a short silica gel plug eluting with hexanes:EtOAc (6:4) to afford 12 mg of azido-alkyne probe **4.29** as a yellow oil (31%). $R_f$ = 0.69 (hexanes:EtOAc, 4:6). $^1$H NMR ($CDCl_3$, 400 MHz): $\delta$ 7.61-7.54 (m, 3H), 7.34 (d, 2H, $J$ = 8.9 Hz), 7.05 (d, 2H, $J$ = 8.8 Hz), 6.85 (dd, 1H, $J$ = 2.2, 8.3 Hz), 6.78 (dd, 1H, $J$ = 2.2, 10.7 Hz), 6.68 (dd, 1H, $J$ = 0.5, 9.4 Hz), 5.20 (m, 2H), 4.75 (d, 2H, $J$ = 2.4 Hz), 2.56 (t, 1H, $J$ = 2.4 Hz). $^{13}$C NMR ($CDCl_3$, 100 MHz): $\delta$ 162.8, 161.8, 160.3, 157.0, 144.1, 142.0, 141.9, 139.6, 134.2, 132.9, 132.9, 127.0, 121.1, 120.2, 119.9, 119.7, 115.5, 115.2, 115.2, 78.3, 77.2, 75.8, 55.9. HRMS calcd for $(C_{21}H_{15}FN_4O_2)Na^+$ 397.1071, found 397.1073. IR: azide, 2117.8 cm$^{-1}$.

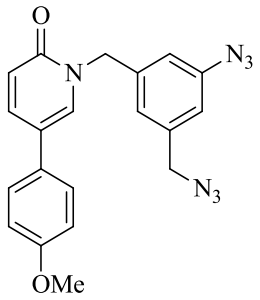

**4.30**

**1-(3-Azido-5-(azidomethyl)benzyl)-5-(4-methoxyphenyl)pyridin-2(1*H*)-one (4.30)**

To 2-methoxypyridinone derivative **5.90** (17 mg, 0.08 mmol) and NaI (24 mg, 0.16 mmol) was added a mixture of 3-azido-5-(azidomethyl)benzyl methanesulfonate (**5.91**, Hosoya *et al.*, 2005) (45 mg, 0.16 mmol) in $CH_3CN$ (3 mL). The reaction was then refluxed at 90˚C for 5 hours then stirred at room temperature overnight. $CH_3CN$ (1.5 mL) was then added to the reaction followed by reflux at 90˚C for another 3 hours. The reaction was then cooled to room temperature, concentrated, and chromatographed (hexanes:EtOAc, 6:4) to give 11 mg of *N*-benzylated derivative **4.30** as a yellow oil (23%). $R_f$ = 0.33 (hexanes:EtOAc, 6:4). $^1$H NMR ($CDCl_3$, 400 MHz): $\delta$ 7.63 (s, 1H), 7.41 (d, 1H, $J$ = 2.2 Hz), 7.32 (d, 2H, $J$ = 8.8 Hz), 7.06 (s, 1H), 6.96 (m, 4H), 6.73 (d, 1H, $J$ = 9.5 Hz), 5.21 (s, 2H), 4.36 (s, 2H), 3.85 (s, 3H). $^{13}$C NMR ($CDCl_3$, 100 MHz): $\delta$ 161.7, 159.2, 141.4, 139.8, 139.1, 138.2, 133.6, 128.7, 127.1, 123.8, 121.3, 120.7, 118.4, 118.0, 114.5, 55.4, 54.1, 51.9. HRMS calcd. for $(C_{20}H_{17}N_7O_2)Na^+$ 410.1336, found 410.1332. IR: azide, 2108 cm$^{-1}$.

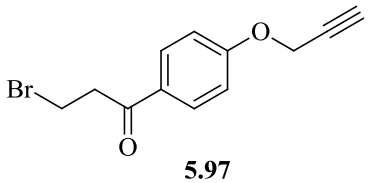

**5.97**

**3-Bromo-1-(4-(prop-2-yn-1-yloxy)phenyl)propan-1-one (5.97)**

A mixture of acid chloride **5.96** (0.39 mL, 3.90 mmol) and propargyl ether **5.95** (0.5 mL, 3.90 mmol) in $CH_2Cl_2$ (5 mL) was added dropwise to $AlCl_3$ (701 mg, 5.26 mmol) in $CH_2Cl_2$ (5 mL) at 0˚C. The reaction was then allowed to warm to room temperature and stirred overnight, followed by quenching with crushed ice. The mixture was then diluted with $H_2O$ and $CH_2Cl_2$ with vigorous stirring. The organic layer was then separated, washed with brine, dried ($MgSO_4$), filtered, concentrated and chromatographed (hexanes:EtOAc, 9:1 to 8:2) to provide 589 mg of ketone **5.97** as a white solid (57%). $R_f$ = 0.22 (hexanes:EtOAc, 9:1). $^1$H NMR ($CDCl_3$, 500 MHz): $\delta$ 7.97 (d, 2H, $J$ = 8.9 Hz), 7.05 (d, 2H, $J$ = 8.9 Hz), 4.79 (m, 2H), 3.76 (t, 2H, $J$ = 6.9 Hz), 3.55 (t, 2H, $J$ = 7.0 Hz), 2.58 (m, 1H). $^{13}$C NMR ($CDCl_3$, 100 MHz): $\delta$ 195.5, 161.6, 130.3, 130.1, 114.8, 77.6, 76.3, 55.9, 41.2, 26.0. HRMS calcd for $(C_{12}H_{11}BrO_2)Na^+$ 288.9835, found 288.9838.

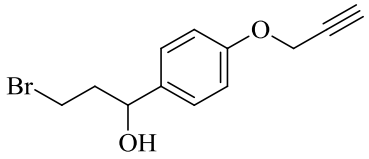

**(±)-5.99**

**(±)-3-Bromo-1-(4-(prop-2-yn-1-yloxy)phenyl)propan-1-ol ((±)-5.99)**

A suspension of ketone **5.97** (271 mg, 1.01 mmol) in THF (2 mL) and $H_2O$ (1 mL) was treated with $NaBH_4$ (38 mg, 1.01 mmol) at 0˚C. The reaction was then stirred at 0˚C for 3 hours followed by stirring for 1 hour at room temperature. The reaction mixture was then concentrated and the residue was partitioned between EtOAc and $H_2O$. The organic layer was then separated,

washed with brine, dried ($MgSO_4$), filtered, concentrated, and chromatographed (100% $CH_2Cl_2$) to obtain 150 mg of benzyl alcohol **(±)-5.99** as a colorless oil (55%). $R_f$ = 0.28 (100%$CH_2Cl_2$). $^1H$ NMR ($CDCl_3$, 400 MHz): $\delta$ 7.34 (d, 2H, $J$ = 8.6 Hz), 7.00 (d, 2H, $J$ = 8.8 Hz), 4.91 (m, 1H), 4.72 (d, 2H, $J$ = 2.4 Hz), 3.62-3.56 (m, 1H), 3.45-3.39 (m, 1H), 2.55 (t, 1H, $J$ = 2.4 Hz), 2.39-2.30 (m, 1H), 2.21-2.13 (m, 1H), 1.92 (m, 1H). $^{13}C$ NMR ($CDCl_3$, 100 MHz): $\delta$ 157.3, 136.6, 127.1, 115.0, 78.4, 75.6, 71.9, 55.8, 41.5, 30.3. HRMS calcd for $(C_{12}H_{13}BrO_2)Na^+$ 290.9991, found 290.9994.

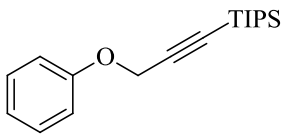


**5.103**

**Tri-isopropyl(3-phenoxyprop-1-yn-1-yl)silane (5.103)**

Phenol (142 mg, 1.50 mmol) was sequentially treated with acetone (1 mL, reagent grade, dried with molecular sieves), $K_2CO_3$ (518 mg, 3.75 mmol), and TIPS-protected propargyl bromide (Hoogboom and Swager, 2006; 495 mg, 1.8 mmol, dissolved in 3 mL acetone). NaI (100 mg, 0.67 mmol) was then added to the reaction mixture followed by stirring at room temperature overnight. The reaction mixture was then concentrated and the residue was partitioned between EtOAc and $H_2O$. The organic layer was separated, washed with 1M aq. NaOH and brine, then dried ($MgSO_4$), filtered, and concentrated to provide 410 mg of TIPS-protected propargyl ether **5.103** as a clear, yellow oil (95%), which was used without further purification. $R_f$ = 0.67 (hexanes:EtOAc, 95:5). $^1H$ NMR ($CDCl_3$, 400 MHz): $\delta$ 7.31 (m, 2H), 7.02 (m, 3H), 4.75 (s, 2H), 1.06 (s, 21H). $^{13}C$ NMR ($CDCl_3$, 100 MHz): $\delta$ 157.7, 129.3, 121.3, 115.3, 102.0, 89.1, 56.7, 18.5, 11.1. HRMS calcd for $(C_{18}H_{28}OSi)Na^+$ 311.1802, found 311.1803.

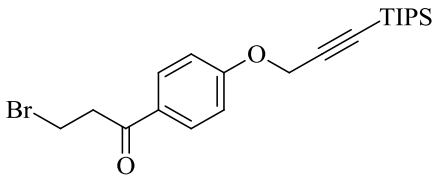


**5.106**

**3-Bromo-1-(4-((3-(triisopropylsilyl)prop-2-yn-1-yl)oxy)phenyl)propan-1-one (5.106)**

A mixture of TIPS-protected propargyl ether **5.103** (410 mg, 1.42 mmol) and 4-bromopropionyl chloride (0.15 mL, 1.56 mmol) in $CH_2Cl_2$ (1 mL) was slowly added to a mixture of $AlCl_3$ (282 mg, 2.12 mmol) in $CH_2Cl_2$ (2 mL) at 0˚C. The resulting brown-black reaction was then warmed to room temperature and stirred overnight. The reaction was then cooled to 0˚C, quenched with ice, and diluted with $H_2O$ and $CH_2Cl_2$ . Potassium sodium tartarate (500 mg) was then added to the mixture followed by vigorous stirring for 30 minutes. The organic layer was separated, washed with brine, then dried ($MgSO_4$), filtered, concentrated, and chromatographed (hexanes:EtOAc, 95:5) to provide 190 mg of ketone **5.106** as a brown solid (32%). $R_f$ = 0.6 (hexanes:EtOAc, 9:1). $^1$H NMR ($CDCl_3$, 500 MHz): $\delta$ 7.96 (d, 2H, $J$ = 9.0 Hz), 6.99 (d, 2H, $J$ = 9.0 Hz), 4.64 (s, 2H), 3.75 (t, 2H, $J$ = 6.9 Hz), 3.54 (t, 2H, $J$ = 6.9 Hz), 1.14 (s, 3H), 1.08 (d, 18H, $J$ = 6.7 Hz). $^{13}$C NMR ($CDCl_3$, 100 MHz): $\delta$ 195.5, 162.5, 140.4, 130.5, 114.6, 77.2, 71.5, 49.3, 26.0, 18.6, 11.9, 10.6. HRMS calcd. for $(C_{21}H_{31}BrO_2Si)Na^+$ 445.1169, found 445.1172.

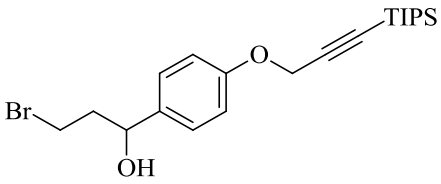


**(±)-5.107**

**(±)-3-Bromo-1-(4-((3-(triisopropylsilyl)prop-2-yn-1-yl)oxy)phenyl)propan-1-ol ((±)-5.107)**

A suspension of ketone **5.106** (175 mg, 0.42 mmol) in THF (3 mL) and $H_2O$ (1mL) was treated with $NaBH_4$ (15 mg, 0.42 mmol) at 0˚C. The reaction was then stirred at 0˚C for 1 hour followed by stirring at room temperature for 2 hours. The reaction mixture was then concentrated and the residue was partitioned between EtOAc and brine. The organic layer was then separated, dried ($MgSO_4$), filtered, concentrated, and chromatographed (hexanes:EtOAc, 9:1) to provide 141 mg of benzyl alcohol **(±)-5.107** as a colorless oil (80%). $R_f$ = 0.25 (hexanes:EtOAc, 9:1). $^1$H NMR ($CDCl_3$, 400 MHz): $\delta$ 7.32 (d, 2H, $J$ = 8.7 Hz), 6.94 (d, 2H, $J$ = 8.7 Hz), 4.89 (m, 1H), 4.58 (s, 2H), 3.58 (m, 1H), 3.41 (m, 1H), 2.33 (m, 1H), 2.18 (m, 1H), 2.11 (br s, 1H), 1.11 (m, 21H). HRMS calcd for $(C_{21}H_{33}BrO_2Si)Na^+$ 447.1325, found 447.1329.

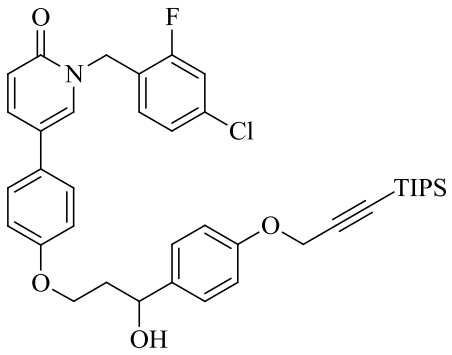


**(±)-5.108**

**(±)-1-(4-Chloro-2-fluorobenzyl)-5-(4-(3-hydroxy-3-(4-((3-(triisopropylsilyl)prop-2-yn-1-yl)oxy)phenyl)propoxy)phenyl)pyridin-2(1H)-one ((±)-5.108)**

A mixture of phenol **3.59** (110 mg, 0.33 mmol) in DMF (3mL) was added to a suspension of NaH (9.6 mg, 0.4 mmol) in DMF (3 mL) at 0˚C, followed by addition of more NaH (4.8 mg, 0.2 mmol). The mixture was then stirred at room temperature for 1 hour followed by dropwise addition of bromide **5.107** (142 mg, 0.33 mmol) in DMF (10 mL). The resulting reaction was then stirred at 70˚C for 5 hours, cooled to room temperature, then acidified with 1M aq. HCl and extracted with EtOAc. The organic layer was then separated, washed with brine, then dried ($MgSO_4$), filtered, concentrated, and chromatographed (hexanes:EtOAc, 4:6) to give 119 mg of ether **(±)-5.108** as a yellow oil (50%). $R_f$ = 0.38 (hexanes:EtOAc, 4:6). $^1$H NMR ($CDCl_3$, 400 MHz): $\delta$ 7.53 (dd, 1H, $J$ = 2.4, 9.4 Hz), 7.49 (s, 1H), 7.43 (t, 1H, $J$ = 8.0 Hz), 7.29 (m, 4H), 7.10 (d, 2H, $J$ = 8.8 Hz), 6.98 (d, 1H, $J$ = 8.7 Hz), 6.92 (d, 3H, $J$ = 8.8 Hz), 6.60 (d, 1H, $J$ = 9.4 Hz), 5.13 (s, 2H), 4.95 (s, 1H), 4.71 (s, 2H), 4.15 (m, 1H), 4.01 (m, 1H), 2.19 (m, 2H), 1.06 (m, 21H). HRMS calcd for $(C_{39}H_{45}ClFNO_4Si)Na^+$ 696.2683, found 696.2686.

.

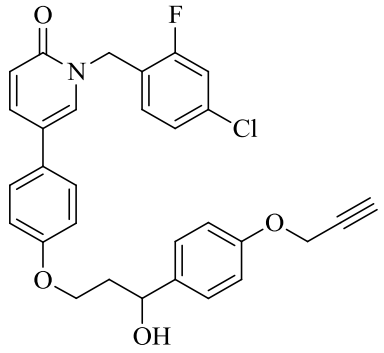


**5.100**

**(±)-1-(4-Chloro-2-fluorobenzyl)-5-(4-(3-hydroxy-3-(4-(prop-2-yn-1-yloxy)phenyl) propoxy)phenyl) pyridin-2(1H)-one ((±)-5.100)**

A solution of TIPS-protected alkyne **(±)-5.108** (100 mg, 0.15 mmol) in THF (3 mL) was treated with TBAF (1M in THF, 0.25 mL, 0.22 mmol) at 0˚C. The resulting mixture was then stirred for 1 hour at room temperature. The reaction was then cooled again to 0˚C and TBAF (1M in THF, 0.08 mL, 0.075 mL) was added. After stirring for 3 hours at room temperature, the the resulting mixture was concentrated and the residue was chromatographed (hexanes:EtOAc, 1:1) to provide 40 mg of deprotected alkyne **5.100** as a white semi-solid (58%). $R_f$ = 0.27 (hexanes:EtOAc, 4:6). $^1$H NMR ($CDCl_3$, 400 MHz): $\delta$ 7.59 (dd, 1H, $J$ = 2.6, 9.4 Hz), 7.50 (m, 2H), 7.32 (m, 4H), 7.14 (m, 2H), 6.98 (dd, 4H, $J$ = 8.6, 13.2 Hz), 6.67 (d, 1H, $J$ = 9.4 Hz), 5.19 (s, 2H), 4.99 (m, 1H), 4.72 (s, 2H), 4.13 (m, 2H), 2.55 (t, 1H, $J$ = 2.4 Hz), 2.47 (s, 1H), 2.23 (m, 2H). $^{13}$C NMR (CDCl3, 100 MHz): $\delta$ 162.0, 161.8, 158.3, 157.1, 139.7, 137.3, 132.4, 132.4, 129.0, 127.1, 127.0, 125.1, 125.0, 122.0, 121.9, 121.1, 120.4, 116.4, 116.2, 115.1, 115.0, 78.5, 75.6, 71.4, 65.5, 55.8, 46.3, 38.3. HRMS calcd for $(C_{30}H_{25}ClFNO_4)Na^+$ 540.1348, found 540.1351.

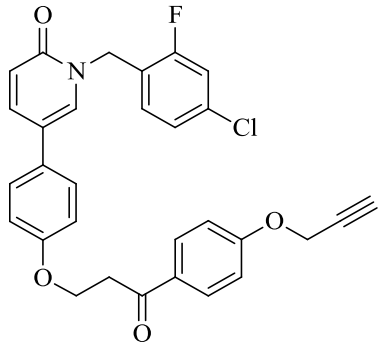

**4.31**

**1-(4-Chloro-2-fluorobenzyl)-5-(4-(3-oxo-3-(4-(prop-2-yn-1-yloxy)phenyl)propoxy) phenyl)pyridin-2(1*H*)-one (4.31)**

To a mixture of benzyl alcohol **(±)-5.100** (33 mg, 0.064 mmol) in $CH_2Cl_2$ (3 mL) was added DMP (32.6 mg, 0.077 mmol). The resulting reaction was then stirred at room temperature for 4 hours followed by dilution with $H_2O$. The organic layer was then separated, washed with brine, then dried ($MgSO_4$), filtered, concentrated, and chromatographed (hexanes:EtOAc, 7:3 to 1:1) to provide 12 mg of ketone **4.31** as a white solid (35%). $R_f$ = 0.46 (hexanes:EtOAc, 4:6). $^1$H NMR ($CDCl_3$, 400 MHz): $\delta$ 8.03 (d, 2H, $J$ = 9.0 Hz), 7.60 (dd, 1H, $J$ = 2.7, 9.4 Hz), 7.50 (m, 2H), 7.31 (d, 2H, $J$ = 8.8 Hz), 7.15 (m, 2H), 7.07 (d, 2H, $J$ = 9.0 Hz), 6.99 (d, 2H, $J$ = 8.8 Hz), 6.68 (d, 1H, $J$ = 9.4 Hz), 5.21 (s, 2H), 4.80 (s, 2H), 4.46 (t, 2H, $J$ = 6.6 Hz), 3.47 (t, 2H, $J$ = 6.6 Hz), 2.59 (t, 1H, $J$ = 2.4 Hz). $^{13}$C NMR (CDCl3, 100 MHz): $\delta$ 196.0, 162.0, 161.8, 161.5, 159.5, 158.3, 139.7, 135.1, 135.0, 134.1, 134.1, 132.4, 132.3, 130.6, 130.4, 129.0, 127.0, 125.1, 125.0, 122.0, 121.9, 121.1, 120.5, 116.4, 116.2, 115.2, 114.7, 77.7, 76.3, 63.5, 55.9, 46.2, 37.8. HRMS calcd. for $(C_{30}H_{23}ClFNO_4)Na^+$ 538.1192, found 538.1194. Anal. calcd. for $C_{30}H_{23}ClFNO_4 \cdot 0.96H_20$: C, 67.57; H, 4.71; N, 2.63; found C, 67.59; H, 4.92; N, 2.54. MP: 203 ºC.

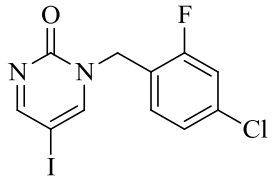

**5.111**

**1-(4-Chloro-2-fluorobenzyl)-5-iodopyrimidin-2(1*H*)-one (5.111)**

A mixture of 5-iodopyrimidin-2(1*H*)-one (**5.110**, 914 mg, 4.12 mmol), DMF (18 mL), 2-flouro-4-chlorobenzyl bromide (**3.56**, 1.1 g, 4.94 mmol), and $K_2CO_3$ (1.71 g, 12.36 mmol) was stirred at room temperature for 18 hours then diluted with $H_2O$. The resulting precipitate was then collected by filtration and dried to provide white solid. Chromatography ($CH_2Cl_2$:hexanes, 9:1 to 8:2) provided 1.1g of *N*-benzylated pyrimidin-2(1*H*)-one **5.111** as a white solid (73%). $R_f$ = 0.39 (hexanes:EtOAc, 1:1). $^1$H NMR ($CDCl_3$, 400 MHz): $\delta$ 8.62 (d, 1H, $J$ = 3.1 Hz), 7.94 (dd, 1H, $J$ = 1.4, 3.1 Hz), 7.59 (t, 1H, $J$ = 8.2 Hz), 7.19 (m, 2H), 5.05 (s, 2H). $^{13}$C NMR ($CDCl_3$, 100 MHz): $\delta$ 165.5, 162.2, 159.7, 154.0, 151.8, 136.1, 133.1, 125.3, 119.9, 116.6, 48.6. HRMS calcd. for $(C_{11}H_7ClFIN_2O)Na^+$ 386.9168, found 386.9164.

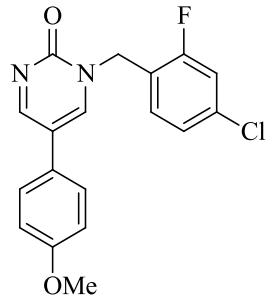

**4.36**

**1-(4-Chloro-2-fluorobenzyl)-5-(4-methoxyphenyl)pyrimidin-2(1*H*)-one (4.36)**

To aryl iodide **5.111** (290 mg, 0.80 mmol) was sequentially added 1,2-dioxane (8 mL), sat. aq. $NaHCO_3$ solution (8 mL), 4-methoxyphenyl boronic acid (204 mg, 1.34 mmol), and $Pd(PPh_3)_4$ (211 mg, 0.18 mmol). The reaction was then purged with argon and heated at 95˚C for 4.5

hours, followed by cooling to room temperature and filtering over Celite®. The filtrate was then diluted with EtOAc and sat. aq. $NH_4Cl$ solution. The organic layer was separated and washed with brine, then dried ($MgSO_4$), filtered, concentrated, and chromatographed (hexanes:EtOAc, 4:6 to 3:7) to provide 43 mg of pyrimidone **4.36** as a yellow solid (16%). $^1H$ NMR ($CDCl_3$, 400 MHz): $\delta$ 8.82 (d, 1H, $J$ = 3.3 Hz), 7.89 (dd, 1H, $J$ = 1.6, 3.2 Hz), 7.62 (t, 1H, $J$ = 8.2 Hz), 7.32 (d, 2H, $J$ = 8.8 Hz), 7.15 (m, 2H), 6.99 (d, 2H, $J$ = 8.8 Hz), 5.14 (s, 2H), 3.85 (s, 3H). $^{13}C$ NMR ($CDCl_3$, 100 MHz): $\delta$ 165.6, 162.2, 159.7, 155.6, 143.9, 135.8, 135.7, 133.2, 133.1, 127.1, 125.3, 125.26, 125.22, 120.6, 120.4, 118.7, 116.5, 116.3, 114.8, 55.4, 48.5. HRMS calcd for $(C_{18}H_{14}ClFN_2O_2)Na^+$ 367.0620, found 367.0618. Anal. calcd for $C_{18}H_{14}ClFN_2O_2 \cdot 0.2CH_3COOC_2H_5 \cdot 0.1HCl$ C, 61.89; H, 4.28; N, 7.74; Cl, 10.57; F, 5.25; found C, 62.02; H, 4.20; N, 7.63; Cl, 10.64; F, 5.00. MP: 210 ºC.

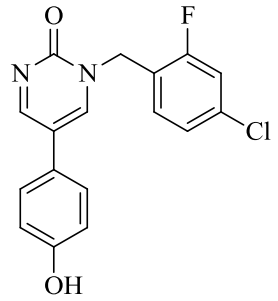


**5.112**

**1-(4-Chloro-2-fluorobenzyl)-5-(4-hydroxyphenyl)pyrimidin-2(1*H*)-one (5.112)**

A mixture of methyl ether **4.36** (394 mg, 1.08 mmol), 1,4-dioxane (10 mL), 4-hydroxyphenyl boronic acid (226 mg, 1.64 mmol), sat. aq. $NaHCO_3$ solution (10 mL), and $Pd(PPh_3)_4$ (250 mg, 0.22 mmol) was purged with argon then heated for 3 hours at 95˚C. The reaction mixture was then cooled to room temperature and filtered. The filtrate was then diluted with EtOAc and washed with sat. aq. $NH_4Cl$ solution. The organic layer was separated, washed with brine, dried ($MgSO_4$), filtered, and concentrated. The resulting material was then filtered through a short

plug of silica gel using $CH_2Cl_2$ followed by EtOAc, then concentrated. The resulting yellow solid was recrystallized in EtOAc to obtain 175 mg of phenol **5.112** (49%). $R_f$ = 0.33 ($CHCl_3$:MeOH, 9:1). $^1$H NMR (DMSO-$d_6$, 400 MHz): $\delta$ 9.64 (br, s, 1H), 8.93 (s, 1H), 8.59 (s, 1H), 7.49-7.28 (m, 5H), 6.85 (d, 2H, $J$ = 8.6 Hz), 5.14 (s, 2H). $^{13}$C NMR (DMSO-$d_6$, 100 MHz): $\delta$ 165.6, 161.9, 159.4, 157.6, 146.3, 133.9, 133.8, 132.0, 127.3, 125.23, 125.19, 124.1, 117.6, 116.7, 116.4, 116.3, 48.6. HRMS calcd for $(C_{17}H_{12}ClFN_2O_2)Na^+$ 353.0463, found 353.0463.

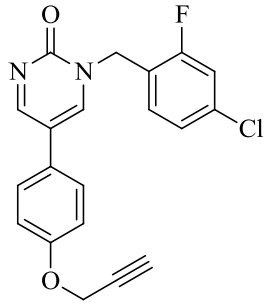


**4.32**

**1-(4-Chloro-2-fluorobenzyl)-5-(4-(prop-2-yn-1-yloxy)phenyl)pyrimidin-2(1*H*)-one (4.32)**

Propargyl bromide (80% in toluene, 0.07 mL) was added dropwise to a mixture of phenol **5.112** (144 mg, 0.44 mmol) and $K_2CO_3$ (180 mg, 1.31 mmol) in DMF (4 mL). The reaction was then stirred at room temperature overnight followed by dilution with EtOAc and $H_2O$. The organic layer was separated, washed with brine, dried ($MgSO_4$) filtered, concentrated and chromatographed (100% EtOAc) to provide 35 mg of propargyl ether **4.32** as a light yellow solid (22%). $R_f$ = 0.27 (100% EtOAc). $^1$H NMR ($CDCl_3$, 400 MHz): $\delta$ 8.83 (d, 1H, $J$ = 3.3 Hz), 7.89 (s, 1H), 7.63 (t, 1H, $J$ = 8.2 Hz), 7.34 (d, 2H, $J$ = 8.8 Hz), 7.17 (m, 2H), 7.08 (d, 2H, $J$ = 8.8 Hz), 5.15 (s, 2H), 4.75 (d, 2H, $J$ = 2.4 Hz), 2.57 (t, 1H, $J$ = 2.4 Hz). $^{13}$C NMR ($CDCl_3$, 100 MHz): $\delta$ 165.6, 159.7, 157.6, 155.6, 144.0, 135.9, 135.8, 133.3, 133.2, 127.2, 126.3, 125.3, 125.26, 120.5, 120.3, 118.5, 116.5, 116.3, 115.8, 78.1, 76.0, 55.9, 48.5. HRMS calcd for $(C_{20}H_{14}ClFN_2O_2)Na^+$ 391.0620, found 391.0619. Anal. calcd for

$C_{20}H_{14}ClFN_2O_2 \cdot 0.2CH_3COOC_2H_5$: C, 64.65; H, 4.07; N, 7.25; Cl, 9.17; F, 4.92. Found: C, 64.27; H, 4.13; N, 7.14; Cl, 9.44; F, 4.90.

**BIBLIOGRAPHY**


- Abdelkarim, H., Brunsteiner, M, Neelarapu, R., Bai, H., Madriaga, A., van Breemen, R.B., Blond, S.Y., Gaponenko, V., and Petukhov, P.A. Photoreactive "nanorulers" detect a novel conformation of full length HDAC3-SMRT complex in solution. *ACS Chem. Bio.* **2013**, *8*, 2538-2549.
- Adewale, A.S., Platt, D.M., and Spealman, R.D. Pharmacological stimulation of group II metabotropic glutamate receptors reduces cocaine self-administration and cocaine-induced reinstatement of drug seeking in squirrel monkeys. *J. Pharmacol. Exp. Ther.* **2006**, *318*, 922-931.
- Agoston, G.E., Vaughan, R., Lever, J.R., Izenwasser, S., Terry, P.D., and Newman, A.H. A novel photoaffinity label for the dopamine transporter based on *N*-substituted 3α-[bis(4'-fluorophenyl)methoxy]tropane. *Bioorg. Med. Chem. Lett.* **1997**, *7*, 3027-3032.
- Agoston, G.E., Wu, J.H., Izenwasser, S., George, C., Katz, J., Kline, R.H., and Newman, A.H. Novel *N*-substituted 3α-[bis(4'-fluorophenyl)methoxy]tropane analogues: Selective ligands for the dopamine transporter. *J. Med. Chem.* **1997**, *40*, 4329-4339.
- Al Suwaidi, J., Ali, W.M., and Aleryani, S.L. Cardiovascular complications of *khat*. *Clin. Chim. Acta* **2013**, *419*, 11-14.
- Al'Absi, M. and Grabowski, J. Concurrent use of tobacco and *khat*: Added burden on chronic disease epidemic. *Addiction* **2012**, *107*, 451-452.
- Albuquerque, E.X., Pereira, E.F., Alkondon, M., and Rogers, S.W. Mammalian nicotinic acetylcholine receptors: From structure to function. *Physiol. Rev.* **2009**, *89*, 73-120.

- Amarante, G., Cavallaro, M., and Coelho, F. Hyphenating the Curtius rearrangement with Morita-Baylis-Hillman adducts: Synthesis of biologically active acyloins and vicinal aminoalcohols. *J. Braz. Chem. Soc.* **2011**, *22*, 1568-1584.
- Amarante, G., Rezende, P., Cavallaro, M., and Coelho, F. Acyloins from Morita–Baylis–Hillman adducts: An alternative approach to the racemic total synthesis of bupropion. *Tetrahedron Lett.* **2008**, *49*, 3744-3748.
- Arias, H.R. Is the inhibition of nicotinic acetylcholine receptors by bupropion involved in its clinical actions? *Int. J. Biochem. Cell Biol.* **2009**, *41*, 2098-2108.
- Arias, H.R. Molecular interaction of bupropion with nicotinic acetylcholine receptors. *J. Pediatric Biochem.* **2010**, *1*, 185-197.
- Arias, H.R., Feuerbach, D., Targowska-Duda, K.M., Aggarwal, S., Lapinsky, D.J., and Jozwiak, K. Structural and functional interaction of (+/-)-2-(n-*tert*-butylamino)-3'-iodo-4'-azidopropiophenone, a photoreactive bupropion derivative, with nicotinic acetylcholine receptors. *Neurochem. Int.* **2012**, *61*, 1433-1441.
- Arias, H.R., Gumilar, F., Rosenberg, A., Targowska-Duda, K.M., Feuerbach, D., Jozwiak, K., Moaddel, R., Wainer, I.W., and Bouzat, C. Interaction of bupropion with muscle-type nicotinic acetylcholine receptors in different conformational states. *Biochemistry* **2009**, *48*, 4506-4518.
- Arias-Carrion, O., Stamelou, M., Murillo-Rodriguez, E., Menendez-Gonzalez, M., and Poppel, E. Dopaminergic reward system: A short integrative review. *Int. Arch. Med.* **2010**, *3*, 24.
- Atkinson, A., Graton, J., and Le Questel, J.Y. Insights into a highly conserved network of hydrogen bonds in the agonist binding site of nicotinic acetylcholine receptors: A structural

and theoretical study. *Proteins: Structure, Function, and Bioinformatics* **2014**, DOI: 10.1002/prot.24589.

- Banks, M.L., Worst, T.J., Rusyniak, D.E., and Sprague, J.E. Synthetic cathinones ("bath salts"). *J. Emerg. Med.* **2014**, *46*, 632-642.
- Baptista, M.A.S., Martin-Fardon, R., and Weiss, F. Preferential effects of the metabotropic glutamate 2/3 receptor agonist LY379268 on conditioned reinstatement versus primary reinforcement: Comparison between cocaine and a potent conventional reinforcer. *J. Neurosci.* **2004**, *24*, 4723-4727.
- Battenberg, O.A., Nodwell, M.B., and Sieber, S.A. Evaluation of α-pyrones and pyrimidones as photoaffinity probes for affinity-based protein profiling. *J. Org. Chem.* **2011**, *76*, 6075-6087.
- Baumann, M.H., Ayestas, M.A., Jr., Partilla, J.S., Sink, J.R., Shulgin, A.T., Daley, P.F., Brandt, S.D., Rothman, R.B., Ruoho, A.E., and Cozzi, N.V. The designer methcathinone analogs, mephedrone and methylone, are substrates for monoamine transporters in brain tissue. *Neuropsychopharmacology* **2012**, *37*, 1192-1203.
- Baumann, M.H., Partilla, J.S., Lehner, K.R., Thorndike, E.B., Hoffman, A.F., Holy, M., Rothman, R.B., Goldberg, S.R., Lupica, C.R., Sitte, H.H., Brandt, S.D., Tella, S.R., Cozzi, N.V., and Schindler, C.W. Powerful cocaine-like actions of 3,4-methylenedioxypyrovalerone (MDPV), a principal constituent of psychoactive 'bath salts' products. *Neuropsychopharmacology* **2013**, *38*, 552-562.
- Benarroch, E.E. Metabotropic glutamate receptors: Synaptic modulators and therapeutic targets for neurologic disease. *Neurology* **2008**, *70*, 964-968.

- Benowitz, N.L. Neurobiology of nicotine addiction: Implications for smoking cessation treatment. *Am. J. Med.* **2008**, *121*, S3-10.
- Benowitz, N.L. Pharmacology of nicotine: Addiction, smoking-induced disease, and therapeutics. *Annu. Rev. Pharmacol. Toxicol.* **2009**, *49*, 57-71.
- Benowitz, N.L., Zhu, A.Z., Tyndale, R.F., Dempsey, D., and Jacob, P. Influence of CYP2B6 genetic variants on plasma and urine concentrations of bupropion and metabolites at steady state. *Pharmacogenet. Genomics* **2013**, *23*, 135-141.
- Berger, M. and Steel, C. Photochemical and photophysical processes in acetophenone. *J. Am. Chem. Soc.* **1975**, *97*, 4817-4821.
- Berrang, B.D., Lewin, A.H., and Carroll, F.I. Enantiomeric α-aminopropiophenones (cathinone): Preparation and investigation. *J. Org. Chem.* **1982**, *47*, 2643-2647.
- Beuming, T., Kniazeff, J., Bergmann, M.L., Shi, L., Gracia, L., Raniszewska, K., Newman, A.H., Javitch, J.A., Weinstein, H., Gether, U., and Loland, C.J. The binding sites for cocaine and dopamine in the dopamine transporter overlap. *Nat. Neurosci.* **2008**, *11*, 780-789.
- Beuming, T., Shi, L., Javitch, J.A., and Weinstein, H. A comprehensive structure-based alignment of prokaryotic and eukaryotic neurotransmitter/$Na^+$ symporters (NSS) aids in the use of the LeuT structure to probe NSS structure and function. *Mol. Pharmacol.* **2006**, *70*, 1630-1642.
- Beveridge, T.J.R., Smith, H.R., Nader, M.A., and Porrino, L.J. Group II metabotropic glutamate receptors in the striatum of non-human primates: Dysregulation following chronic cocaine self-administration. *Neurosci. Lett.* **2011**, *496*, 15-19.

- Bill, R.M., Henderson, P.J., Iwata, S., Kunji, E.R., Michel, H., Neutze, R., Newstead, S., Poolman, B., Tate, C.G., and Vogel, H. Overcoming barriers to membrane protein structure determination. *Nat. Biotechnol.* **2011**, *29*, 335-340.
- Bisgaard, H., Larsen, M.A.B., Mazier, S., Beuming, T., Newman, A.H., Weinstein, H., Shi, L., Loland, C. J., and Gether, U. The binding sites for benztropines and dopamine in the dopamine transporter overlap. *Neuropharmacology* **2011**, *60*, 182-190.
- Bisson, W.H., Westera, G., Schubiger, P.A., and Scapozza, L. Homology modeling and dynamics of the extracellular domain of rat and human neuronal nicotinic acetylcholine receptor subtypes $\alpha4\beta2$ and $\alpha7$. *J. Mol. Model.* **2008**, *14*, 891-899.
- Bonano, J.S., Glennon, R.A., De Felice, L.J., Banks, M.L., and Negus, S.S. Abuse-related and abuse-limiting effects of methcathinone and the synthetic "bath salts" cathinone analogs methylenedioxypyrovalerone (MDPV), methylone and mephedrone on intracranial self-stimulation in rats. *Psychopharmacology* **2014**, *231*, 199-207.
- Bonnefous, C., Vernier, J.M., Hutchinson, J.H., Gardner, M.F., Cramer, M., James, J.K., Rowe, B.A., Daggett, L.P., Schaffhauser, H., and Kamenecka, T.M. Biphenyl-indanones: Allosteric potentiators of the metabotropic glutamate subtype 2 receptor. *Bioorg. Med. Chem. Lett.* **2005**, *15*, 4354-4358.
- Brejc, K., van Dijk, W.J., Klaassen, R.V., Schuurmans, M., van Der Oost, J., Smit, A.B., and Sixma, T.K. Crystal structure of an ACh-binding protein reveals the ligand-binding domain of nicotinic receptors. *Nature* **2001**, *411*, 269-276.
- Brown, N. Bioisosteres and scaffold hopping in medicinal chemistry. *Molecular Informatics* **2014**, *33*, 458-462.

- Calkins, R.F., Aktan, G.B., and Hussain, K.L. Methcathinone: The next illicit stimulant epidemic? *J. Psychoactive. Drugs* **1995**, *27*, 277-285.
- Cameron, K., Kolanos, R., Vekariya, R., De Felice, L., and Glennon, R.A. Mephedrone and methylenedioxypyrovalerone (MDPV), major constituents of "bath salts," produce opposite effects at the human dopamine transporter. *Psychopharmacology* **2013**, *227*, 493-499.
- Cameron, K.N., Kolanos, R., Solis, E., Jr., Glennon, R.A., and De Felice, L.J. Bath salts components mephedrone and methylenedioxypyrovalerone (MDPV) act synergistically at the human dopamine transporter. *Br. J. Pharmacol.* **2013**, *168*, 1750-1757.
- Cao, J., Lever, J.R., Kopajtic, T., Katz, J.L., Pham, A.T., Holmes, M.L., Justice, J.B., and Newman, A.H. Novel azido and isothiocyanato analogues of [3-(4-phenylalkylpiperazin-1-yl)propyl]bis(4-fluorophenyl)amines as potential irreversible ligands for the dopamine transporter. *J. Med. Chem.* **2004**, *47*, 6128-6136.
- Caron, M.G. Hyperlocomotion and indifference to cocaine and amphetamine in mice lacking the dopamine transporter. *Nature* **1996**, *379*, 15.
- Carroll, F.I., Blough, B.E., Abraham, P., Mills, A.C., Holleman, J.A., Wolckenhauer, S.A., Decker, A.M., Landavazo, A., McElroy, K.T., Navarro, H.A., Gatch, M.B., and Forster, M.J. Synthesis and biological evaluation of bupropion analogs as potential pharmacotherapies for cocaine addiction. *J. Med. Chem.* **2009**, *52*, 6768-6781.
- Carroll, F.I., Blough, B.E., Mascarella, S.W., Navarro, H.A., Eaton, J.B., Lukas, R.J., and Damaj, M.I. Synthesis and biological evaluation of bupropion analogs as potential pharmacotherapies for smoking cessation. *J. Med. Chem.* **2010**, *53*, 2204-2214.

- Carroll, F.I., Blough, B.E., Mascarella, S.W., Navarro, H.A., Lukas, R.J., and Damaj, M.I. Bupropion and bupropion analogs as treatments for CNS disorders. *Adv. Pharmacol.* **2014**, *69*, 177-216.
- Carroll, F.I., Blough, B.E., Navarro, H.A., Mascarella, S.W., Muresan, A.Z., Damaj, M.I., and Lukas, R.J. Preparation of hydroxybupropion analogs for treating drug dependence and other disorders responsive to monoamine reuptake inhibition or antagonism of nicotinic acetylcholine receptors. PCT Int. Appl. WO 2011146821 A2, **2011**.
- Carroll, F.I., Gao, Y., Abraham, P., Lewin, A.H., Lew, R., Patel, A., Boja, J.W., and Kuhar, M.J. Probes for the cocaine receptor: Potentially irreversible ligands for the dopamine transporter. *J. Med. Chem.* **1992**, *35*, 1813-1817.
- Carroll, F.I., Gao, Y.G., Rahman, M.A., Abraham, P., Parham, K., Lewin, A.H., Boja, J.W., and Kuhar, M.J. Synthesis, ligand binding, QSAR, and COMFA study of 3-β-(*p*-substituted phenyl)tropane-2 β-carboxylic acid methyl esters. *J. Med. Chem.* **1991**, *34*, 2719-2725.
- Carroll, F.I., Howell, L.L., and Kuhar, M.J. Pharmacotherapies for treatment of cocaine abuse: Preclinical aspects. *J. Med. Chem.* **1999**, *42*, 2721-2736.
- Carroll, F.I., Lewin, A.H., Boja, J.W., and Kuhar, M.J. Cocaine receptor: Biochemical characterization and structure-activity relationships of cocaine analogs at the dopamine transporter. *J. Med. Chem.* **1992**, *35*, 969-981.
- Carroll, F.I., Mascarella, S.W., Kuzemko, M.A., Gao, Y., Abraham, P., Lewin, A.H., Boja, J.W., and Kuhar, M.J. Synthesis, ligand binding, and QSAR (COMFA and classical) study of 3-beta-(3'-substituted phenyl)-, 3-beta-(4'-substituted phenyl)-, and 3-beta-(3',4'-

disubstituted phenyl)tropane-2 beta-carboxylic acid methyl esters. *J. Med. Chem.* **1994**, *37*, 2865-2873.

- Carroll, F.I., Muresan, A.Z., Blough, B.E., Navarro, H.A., Mascarella, S.W., Eaton, J.B., Huang, X., Damaj, M.I., and Lukas, R.J. Synthesis of 2-(substituted phenyl)-3,5,5-trimethylmorpholine analogues and their effects on monoamine uptake, nicotinic acetylcholine receptor function, and behavioral effects of nicotine. *J. Med. Chem.* **2011**, *54*, 1441-1448.
- Cartmell, J., and Schoepp, D.D. Regulation of neurotransmitter release by metabotropic glutamate receptors. *J. Neurochem.* **2000**, *75*, 889-907.
- Celie, P.H., Kasheverov, I.E., Mordvintsev, D.Y., Hogg, R.C., van Nierop, P., van Elk, R., van Rossum-Fikkert, S.E., Zhmak, M.N., Bertrand, D., and Tsetlin, V. Crystal structure of nicotinic acetylcholine receptor homolog AChBP in complex with an α-conotoxin PNIA variant. *Nat. Struct. Mol. Biol.* **2005**, *12*, 582-588.
- Chaki, S., Yoshikawa, R., Hirota, S., Shimazaki, T., Maeda, M., Kawashima, N., Yoshimizu, T., Yasuhara, A., Sakagami, K., Okuyama, S., Nakanishi, S., and Nakazato, A. MGS0039: A potent and selective group II metabotropic glutamate receptor antagonist with antidepressant-like activity. *Neuropharmacology* **2004**, *46*, 457-467.
- Chakrabarti, P. and Khorana, G. A new approach to the study of phospholipid-protein interactions in biological membranes. Synthesis of fatty acids and phospholipids containing photosensitive groups. *Biochemistry* **1975**, *14*, 5021-5033.
- Chang, L.L., Ashton, W.T., Flanagan, K.L., Chen, T.B., O'Malley, S.S., Zingaro, G.J., Kivlighn, S.D., Siegl, P.K.S., and Lotti, V.J. Potent and orally active angiotensin II

receptor antagonists with equal affinity for human AT1 and AT2 subtypes. *J. Med. Chem.* **1995**, *38*, 3741-3758.

- Changeux, J.P. Nicotine addiction and nicotinic receptors: Lessons from genetically modified mice. *Nat. Rev. Neurosci.* **2010**, *11*, 389-401.
- Changeux, J.P., and Edelstein, S.J. Allosteric receptors after 30 years. *Neuron* **1998**, *21*, 959-980.
- Chen, N. and Reith, M.E. Structure and function of the dopamine transporter. *Eur. J. Pharmacol.* **2000**, *405*, 329-339.
- Chen, N., Vaughan, R.A., and Reith, M.E. The role of conserved tryptophan and acidic residues in the human dopamine transporter as characterized by site-directed mutagenesis. *J. Neurochem.* **2001**, *77*, 1116-1127.
- Chen, N., Zhen, J., and Reith, M.E. Mutation of Trp84 and Asp313 of the dopamine transporter reveals similar mode of binding interaction for GBR12909 and benztropine as opposed to cocaine. *J. Neurochem.* **2004**, *89*, 853-864.
- Chiara, D.C., Hong, F.H., Arevalo, E., Husain, S.S., Miller, K.W., Forman, S.A., and Cohen, J.B. Time-resolved photolabeling of the nicotinic acetylcholine receptor by [$^3$H]-azietomidate, an open-state inhibitor. *Mol. Pharmacol.* **2009**, *75*, 1084-1095.
- Cid, J.M., Duvey, G., Cluzeau, P., Nhem, V., Macary, K., Raux, A., Poirier, N., Muller, J., Bolea, C., Finn, T., Poli, S., Epping-Jordan, M., Chamelot, E., Derouet, F., Girard, F., Macdonald, G.J., Vega, J.A., de Lucas, A.I., Matesanz, E., Lavreysen, H., Linares, M.L., Oehlrich, D., Oyarzabal, J., Tresadern, G., Trabanco, A.A., Andres, J.I., Le Poul, E., Imogai, H., Lutjens, R., and Rocher, J.P. Discovery of 1,5-disubstituted pyridones: A new

class of positive allosteric modulators of the metabotropic glutamate 2 receptor. *ACS. Chem. Neurosci.* **2010**, *1*, 788-795.

- Cid, J.M., Duvey, G., Tresadern, G., Nhem, V., Funary, R., Cluzeau, P., Vega, J.A., de Lucas, A.I., Matesanz, E., Alonso, J.M., Linares, M.L., Andres, J.I., Poli, S., Lutjens, R., Imogai, H., Rocher, J.P., MacDonald, G.J., Oehlrich, D., Lavreysen, H., Ahnaou, A., Drinkenburg, W., Mackie, C., and Trabanco, A. A. Discovery of 1,4-disubstituted 3-cyano-2-pyridones: a new class of positive allosteric modulators of the metabotropic glutamate 2 receptor. *J. Med. Chem.* **2012**, *55*, 2388−2405.
- Clarke, R.L., Daum, S.J., Gambino, A.J., Aceto, M.D., Pearl, J., Levitt, M., Cumiskey, W.R., and Bogado, E.F. Compounds affecting the central nervous system. 4. 3 beta-phenyltropane-2-carboxylic esters and analogs. *J. Med. Chem.* **1973**, *16*, 1260-1267.
- Claxton, D.P., Quick, M., Shi, L., de Carvalho, F.D., Weinstein, H., Javitch, J.A., and McHaourab, H.S. Ion/substrate-dependent conformational dynamics of a bacterial homolog of neurotransmitter:Sodium symporters. *Nat. Struct. Mol. Biol.* **2010**, *17*, 822-829.
- Coe, J.W., Brooks, P.R., Vetelino, M.G., Wirtz, M.C., Arnold, E.P., Huang, J., Sands, S.B., Davis, T.I., Lebel, L.A., and Fox, C.B. Varenicline: An α4β2 nicotinic receptor partial agonist for smoking cessation. *J. Med. Chem.* **2005**, *48*, 3474-3477.
- Colombo, S.F., Mazzo, F., Pistillo, F., and Gotti, C. Biogenesis, trafficking and up-regulation of nicotinic ACh receptors. *Biochem. Pharmacol.* **2013**, *86*, 1063-1073.
- Conn, P.J., and Pin, J.P. Pharmacology and functions of metabotropic glutamate receptors. *Annu. Rev. Pharmacol. Toxicol.* **1997**, *37*, 205-237.

- Conn, P.J., Christopoulos, A., and Lindsley, C.W. Allosteric modulators of GPCRs: A novel approach for the treatment of CNS disorders. *Nat. Rev. Drug Discov.* **2009**, *8*, 41-54.
- Coppola, M. and Mondola, R. Synthetic cathinones: Chemistry, pharmacology and toxicology of a new class of designer drugs of abuse marketed as "bath salts" or "plant food". *Toxicol. Lett.* **2012**, *211*, 144-149.
- Coric, I., Kim, J.H., Vlaar, T., Patil, M., Thiel, W., and List, B. Bronsted acid catalyzed asymmetric SN2-type *O*-alkylations. *Angew. Chem., Int. Ed.* **2013**, *52*, 3490-3493.
- Cornish, J.L., and Kalivas, P.W. Glutamate transmission in the nucleus accumbens mediates relapse in cocaine addiction. *J. Neurosci.* **2000**, *20*, RC89.
- Corringer, P.J., LeNovere, N., and Changeux, J.P. Nicotinic receptors at the amino acid level. *Annu. Rev. Pharmacol. Toxicol*. **2000**, *40*, 431–458.
- Crooks, P.A., Bardo, M.T., and Dwoskin, L.P. Nicotinic receptor antagonists as treatments for nicotine abuse. *Advances in Pharmacology* **2014**, *69*, 513-551.
- Cruickshank, C.C. and Dyer, K.R. A review of the clinical pharmacology of methamphetamine. *Addiction* **2009**, *104*, 1085-1099.
- Crunelle, C.L., Miller, M.L., Booij, J., and van den Brink, W. The nicotinic acetylcholine receptor partial agonist varenicline and the treatment of drug dependence: A review. *Eur. Neuropsychopharmacol.* **2010**, *20*, 69-79.
- Cryan, J.F., Bruijnzeel, A.W., Skjei, K.L., and Markou, A. Bupropion enhances brain reward function and reverses the affective and somatic aspects of nicotine withdrawal in the rat. *Psychopharmacology* **2003**, *168*, 347-358.

- Dabak, K., Keskin, H., Yurdakul, A., and Ridvanoglu, N. One-pot process for the preparation of bupropion hydrochloride from 3-chloropropiophenone and *tert*-butylamine in the presence of bromine. PCT Int. Appl. WO 2004024674 A1, **2004**.
- Dahal, R.A., Pramod, A.B., Sharma, B., Krout, D., Foster, J.D., Cha, J.H., Cao, J., Newman, A.H., Lever, J.R., Vaughan, R.A., Henry, K. Computational and biochemical docking of the irreversible cocaine analog RTI 82 directly demonstrates ligand positioning in the dopamine transporter central substrate binding site. *J. Bio. Chem.* **2014**, DOI 10.1074/jbc.M114.571521.
- Dalton, J.A.R., Gomez-Santacana, X., Llebaria, A., and Giraldo, J. Computational analysis of negative and positive allosteric modulator binding and function in metabotropic glutatmate receptor 5 (in)activation. *J. Chem. Inf. Model.* **2014**, *54*, 1476-1487.
- Damaj, M.I., Carroll, F.I., Eaton, J.B., Navarro, H.A., Blough, B.E., Mirza, S., Lukas, R.J., and Martin, B.R. Enantioselective effects of hydroxy metabolites of bupropion on behavior and on function of monoamine transporters and nicotinic receptors. *Mol. Pharmacol.* **2004**, *66*, 675-682.
- Damaj, M.I., Grabus, S.D., Navarro, H.A., Vann, R.E., Warner, J.A., King, L.S., Wiley, J.L., Blough, B.E., Lukas, R.J., and Carroll, F.I. Effects of hydroxymetabolites of bupropion on nicotine dependence behavior in mice. *J. Pharmacol. Exp. Ther.* **2010**, *334*, 1087-1095.
- Das, J. Aliphatic diazirines as photoaffinity probes for proteins: recent developments. *Chem. Rev.* **2011**, *111*, 4405-4417.

- Daws, L.C., Callaghan, P.D., Morón, J.A., Kahlig, K.M., Shippenberg, T.S., Javitch, J.A., and Galli, A. Cocaine increases dopamine uptake and cell surface expression of dopamine transporters. *Biochem. Biophys. Res. Commun.* **2002**, *290*, 1545-1550.
- De Biasi, M. and Dani, J.A. Reward, addiction, withdrawal to nicotine. *Annu. Rev. Neurosci.* **2011**, *34*, 105-130.
- Desai, R.I., Kopajtic, T.A., French, D., Newman, A.H., and Katz, J.L. Relationship between *in vivo* occupancy at the dopamine transporter and behavioral effects of cocaine, GBR 12909 [1-{2-[bis-(4-fluorophenyl) methoxy] ethyl}-4-(3-phenylpropyl) piperazine], and benztropine analogs. *J. Pharm. Exp. Ther.* **2005**, *315*, 397-404.
- Deshpande, P.B., Khan, R.A.R., Rathod, D.M., Katariya, L.K., and Mehta, H.M. An improved process for preparing bupropion hydrochloride. PCT Int. Appl. WO 2008099418 A2, **2008**.
- DeSolms, S.J., Woltersdorf, O.W., Cragoe, E.J., Watson, L.S., and Fanelli, G.M. (Acylaryloxy)acetic acid diuretics. 2. (2-Alkyl-2-aryl-1-oxo-5-indanyloxy)acetic acids. *J. Med. Chem.* **1978**, *21*, 437-443.
- Dhanya, R.P., Sidique, S., Sheffler, D.J., Nickols, H.H., Herath, A., Yang, L., Dahl, R., Ardecky, R., Semenova, S., Markou, A., Conn, P.J., and Cosford, N.D. Design and synthesis of an orally active metabotropic glutamate receptor subtype-2 (mGluR2) positive allosteric modulator (PAM) that decreases cocaine self-administration in rats. *J. Med. Chem.* **2011**, *54*, 342-353.
- Dhillon, S., Yang, L.P., and Curran, M.P. Bupropion: A review of its use in the management of major depressive disorder. *Drugs* **2008**, *68*, 653-689.

- Di Chiara, G. Role of dopamine in the behavioural actions of nicotine related to addiction. *Eur. J. Pharmacol.* **2000**, *393*, 295-314.
- Di Chiara, G. and Bassareo, V. Reward system and addiction: What dopamine does and doesn't do. *Curr. Opin. Pharmacol.* **2007**, *7*, 69-76.
- Doré, A.S., Okrasa, K., Patel, J.C., Serrano-Vega, M., Bennett, K., Cooke, R.M., Errey, J.C., Jazayeri, A., Khan, S., and Tehan, B. Structure of class c GPCR metabotropic glutamate receptor 5 transmembrane domain. *Nature* **2014**, *511*, 557-562.
- Dormán, G. and Prestwich, G.D. Benzophenone photophores in biochemistry. *Biochemistry* **1994**, *33*, 5661-5673.
- Dormán, G. and Prestwich, G.D. Using photolabile ligands in drug discovery and development. *Trends in Biotechnology* **2000**, *18*, 64-77.
- Dubinsky, L., Krom, B.P., and Meijler, M.M. Diazirine based photoaffinity labeling. *Bioorg. Med. Chem.* **2012**, *20*, 554-570.
- Dutta, A.K., Fei, X.S., Vaughan, R.A., Gaffaney, J.D., Wang, N., Lever, J.R., and Reith, M.E.A. Design, synthesis, and characterization of a novel, 4-[2-(diphenylmethoxy)ethyl]-1-benzylpiperidine-based, dopamine transporter photoaffinity label. *Life Sci.* **2001**, *68*, 1839-1849.
- Efange, S.M.N., Alessi, E.M., Shih, H.C., Cheng, Y.C., and Bardos, T.J. Synthesis and biological activities of 2-pyrimidinone nucleosides. 2. 5-Halo-2-pyrimidinone 2'-deoxyribosides. *J. Med. Chem.* **1985**, *28*, 904-910.
- Elkashef, A.M., Rawson, R.A., Anderson, A.L., Li, S.H., Holmes, T., Smith, E.V., Chiang, N., Kahn, R., Vocci, F., Ling, W., Pearce, V.J., McCann, M., Campbell, J., Gorodetzky, C.,

Haning, W., Carlton, B., Mawhinney, J., and Weis, D. Bupropion for the treatment of methamphetamine dependence. *Neuropsychopharmacology* **2008**, *33*, 1162-1170.

- Fang, Q.K., Han, Z., Grover, P., Kessler, D., Senanayake, C.H., and Wald, S.A. Rapid access to enantiopure bupropion and its major metabolite by stereospecific nucleophilic substitution on an α-ketotriflate. *Tetrahedron: Asymmetry* **2000**, *11*, 3659-3663.
- Fang, Q.K., Senanayake, C.H., and Grover, P. Bupropion metabolites, and preparation thereof, for treatment of sexual dysfunction. Patent US 6337328 B1, **2002**.
- Fang, Q.K., Senanayake, C.H., and Grover, P. Synthesis of bupropion metabolites and their use for treating disorders ameliorated by inhibition of neuronal monoamine reuptake. PCT Int. Appl. WO 2001062257 A2, **2001**.
- Fava, M., Rush, A.J., Thase, M.E., Clayton, A., Stahl, S.M., Pradko, J.F., and Johnston, J.A. 15 years of clinical experience with bupropion HCl: From bupropion to bupropion SR to bupropion XL. *Prim. Care Companion J. Clin. Psychiatry* **2005**, *7*, 106-113.
- Fell, M.J., McKinzie, D.L., Monn, J.A., and Svensson, K.A. Group II metabotropic glutamate receptor agonists and positive allosteric modulators as novel treatments for schizophrenia. *Neuropharmacology* **2012**, *62*, 1473-1483.
- Ferrer, J.V. and Javitch, J.A. Cocaine alters the accessibility of endogenous cysteines in putative extracellular and intracellular loops of the human dopamine transporter. *Proc. Natl. Acad. Sci. U.S.A* **1998**, *95*, 9238-9243.
- Fleming, S.A. Chemical reagents in photoaffinity labeling. *Tetrahedron* **1995**, *51*, 12479-12520.
- Forrest, L.R., Kramer, R., and Ziegler, C. The structural basis of secondary active transport mechanisms. *Biochim. Biophys. Acta* **2011**, *1807*, 167-188.

- Frank, R., Christoph, T., Damann, N., Lesch, B., Bahrenberg, G., Saunders, D.J., Stockhausen, H., Kim, Y.S., Kim, M.S., and Lee, J. Substituted pyrazolyl-based carboxamide and urea derivatives bearing a phenyl moiety substituted with an N-containing group as vanilloid receptor ligands and their preparation. PCT Int. Appl., WO 2013068462, **2013**.
- Freye, E. Pharmacology and abuse of cocaine, amphetamines, ecstasy and related designer drugs. Pharmacology of cocaine, Springer, **2010**, 49-60.
- Froimowitz, M., Wu, K.M., Moussa, A., Haidar, R.M., Jurayj, J., George, C., and Gardner, E.L. Slow-onset, long-duration 3-(3', 4'-dichlorophenyl)-1-indanamine monoamine reuptake blockers as potential medications to treat cocaine abuse. *J. Med. Chem.* **2000**, *43*, 4981-4992.
- Fundytus, M.E., and Coderre, T.J. Attenuation of precipitated morphine withdrawal symptoms by acute i.C.V. Administration of a group II mGluR agonist. *Br. J. Pharmacol.* **1997**, *121*, 511-514.
- Galici, R., Jones, C.K., Hemstapat, K., Nong, Y., Echemendia, N.G., Williams, L.C., de Paulis, T., and Conn, P.J. Biphenyl-indanone a, a positive allosteric modulator of the metabotropic glutamate receptor subtype 2, has antipsychotic- and anxiolytic-like effects in mice. *J. Pharmacol. Exp. Ther.* **2006**, *318*, 173-185.
- Gamble, A.B., Garner, J., Gordon, C.P., O'Conner, S.M.J., and Keller, P.A. Aryl nitro reduction with iron powder or stannous chloride under ultrasonic irradiation. *Syn. Commun.* **2007**, *37*, 2777-2786.
- Gandy, M.N., Debowski, A.W., and Stubbs, K.A. A general method for affinity-based proteomic profiling of exo-α-glycosidases. *Chem. Commun.* **2011**, *47*, 5037-5039.

- Garcia, G., Chiara, D.C., Nirthanan, S., Hamouda, A.K., Stewart, D.S., and Cohen, J.B. [$^3$H]Benzophenone photolabeling identifies state-dependent changes in nicotinic acetylcholine receptor structure. *Biochemistry* **2007**, *46*, 10296-10307.
- Garman, E.F. Developments in x-ray crystallographic structure determination of biological macromolecules. *Science* **2014**, *343*, 1102-1108.
- Gass, J.T., and Olive, M.F. Glutamatergic substrates of drug addiction and alcoholism. *Biochem. Pharmacol.* **2008**, *75*, 218-265.
- Gedeon, P.C., Indarte, M., Surratt, C.K., and Madura, J.D. Molecular dynamics of leucine and dopamine transporter proteins in a model cell membrane lipid bilayer. *Proteins: Structure, Function, and Bioinformatics* **2010**, *78*, 797-811.
- George, T.P. and O'Malley, S.S. Current pharmacological treatments for nicotine dependence. *Trends Pharmacol. Sci.* **2004**, *25*, 42-48.
- German, C.L., Fleckenstein, A.E., and Hanson, G.R. Bath salts and synthetic cathinones: An emerging designer drug phenomenon. *Life Sci.* **2014**, *97*, 2-8.
- Gether, U., Andersen, P.H., Larsson, O.M., and Schousboe, A. Neurotransmitter transporters: Molecular function of important drug targets. *Trends Pharmacol. Sci.* **2006**, *27*, 375-383.
- Gevaert, K., Impens, F., Ghesquiere, B., Van Damme, P., Lambrechts, A., and Vandekerckhove, J. Stable isotopic labeling in proteomics. *Proteomics* **2008**, *8*, 4873-4885.
- Glennon, R.A. Bath salts, mephedrone, and methylenedioxypyrovalerone as emerging illicit drugs that will need targeted therapeutic intervention. *Adv. Pharmacol.* **2014**, *69*, 581-620.

- Glennon, R.A., Yousif, M., Naiman, N., and Kalix, P. Methcathinone: A new and potent amphetamine-like agent. *Pharmacol. Biochem. Behav.* **1987**, *26*, 547-551.
- Goeldner, C., Ballard, T.M., Knoflach, F., Wichmann, J., Gatti, S., and Umbricht, D. Cognitive impairment in major depression and the mGlu2 receptor as a therapeutic target. *Neuropharmacology* **2013**, *64*, 337-346.
- Goldsmith, P., Golder, Z., Hunt, J., Berghmans, S., Jones, D., Stables, J.P., Murphree, L., Howden, D., Newton, P.E., and Richards, F.M. GBR12909 possesses anticonvulsant activity in zebrafish and rodent models of generalized epilepsy but cardiac ion channel effects limit its clinical utility. *Pharmacology* **2007**, *79*, 250-258.
- Goncalves, J., Baptista, S., and Silva, A.P. Psychostimulants and brain dysfunction: A review of the relevant neurotoxic effects. *Neuropharmacology* **2014**, DOI: 10.1016/j.neuropharm.2014.01.006.
- Green, A.R., Mechan, A.O., Elliott, J.M., O'Shea, E., and Colado, M.I. The pharmacology and clinical pharmacology of 3,4-methylenedioxymethamphetamine (MDMA, "ecstasy"). *Pharmacol. Rev.* **2003**, *55*, 463-508.
- Greenslade, R.G., and Mitchell, S.N. Selective action of (-)-2-oxa-4-aminobicyclo[3.1.0]hexane-4,6-dicarboxylate (LY379268), a group II metabotropic glutamate receptor agonist, on basal and phencyclidine-induced dopamine release in the nucleus accumbens shell. *Neuropharmacology* **2004**, *47*, 1-8.
- Grigoriadis, D.E., Wilson, A.A., Lew, R., Sharkey, J.S., and Kuhar, M.J. Dopamine transport sites selectively labeled by a novel photoaffinity probe: $^{125}$I-DEEP. *J. Neurosci.* **1989**, *9*, 2664-2670.

- Grishin, A.A., Cuny, H., Hung, A., Clark, R.J., Brust, A., Akondi, K., Alewood, P.F., Craik, D.J., and Adams, D.J. Identifying key amino acid residues that affect α-conotoxin AuIB inhibition of α3β4 nicotinic acetylcholine receptors. *J. Biol. Chem.* **2013**, *288*, 34428-34442.
- Gunderson, E.W., Kirkpatrick, M.G., Willing, L.M., and Holstege, C.P. Substituted cathinone products: A new trend in "bath salts" and other designer stimulant drug use. *J. Addict. Med.* **2013**, *7*, 153-162.
- Guptaroy, B., Fraser, R., Desai, A., Zhang, M., and Gnegy, M.E. Site-directed mutations near transmembrane domain 1 alter conformation and function of norepinephrine and dopamine transporters. *Mol. Pharmacol.* **2011**, *79*, 520-532.
- Habeeb, A.G., Praveen Rao, P.N., and Knaus, E.E. Design and synthesis of celecoxib and rofecoxib analogues as selective cyclooxygenase-2 (COX-2) inhibitors: Replacement of sulfonamide and methylsulfonyl pharmacophores by an azido bioisostere. *J. Med. Chem.* **2001**, *44*, 3039-3042.
- Hamad, M.O., Kiptoo, P.K., Stinchcomb, A.L., and Crooks, P.A. Synthesis and hydrolytic behavior of two novel tripartate codrugs of naltrexone and 6-β-naltrexol with hydroxybupropion as potential alcohol abuse and smoking cessation agents. *Bioorg. Med. Chem.* **2006**, *14*, 7051-7061.
- Hamouda, A.K., Jayakar, S.S., Chiara, D.C., and Cohen, J.B. Photoaffinity labeling of nicotinic receptors: Diversity of drug binding sites. *J. Mol. Neurosci.* **2014**, *53*, 480-486.
- Hamouda, A.K., Steward, D.S., Chiara, D.C., Savechenkov, P.Y., Bruzik, K.S., and Cohen, J.B. Identifying barbiturate binding sites in a nicotinic acetylcholine receptor with

[$^{3}$H]Allyl *m*-trifluoromethyldiazirine mephobarbital, a photoreactive barbiturate. *Mol. Pharmacol.* **2014**, *85*, 735-746.

- Hamouda, A.K., Jin, X., Sanghvi, M., Srivastava, S., Pandhare, A., Duddempudi, P.K., Steinbach, J.H., and Blanton, M.P. Photoaffinity lableing the agonist binding domain of α4β4 and α4β2 neuronal nicotinic acetylcholine receptors with [$^{125}$I]epibatidine and 5[$^{125}$I]A-85380. *Biochimica et Biophysica Acta, Biomembranes* **2009**, *1788*, 1987-1995.
- Hamouda, A.K., Stewart, D.S., Husain, S.S., and Cohen, J.B. Multiple transmembrane binding sites for p-trifluoromethyldiazirinyl-etomidate, a photoreactive *Torpedo* nicotinic acetylcholine receptor allosteric inhibitor. *J. Biol. Chem.* **2011**, *286*, 20466-20477.
- Hashimoto, M. and Hatanaka, Y. Recent progress in diazirine-based photoaffinity labeling. *Eur. J. Org. Chem.* **2008**, *15*, 2513-2523.
- He, B., Velaparthi, S., Pieffet, G., Pennington, C., Mahesh, A., Holzle, D.L., Brunsteiner, M., van Breemen, R., Blond, S.Y., and Petukhov, P.A. Binding ensemble profiling with photoaffinity labeling (BEProFL) approach: Mapping the binding poses of HDAC8 inhibitors. *J. Med. Chem.* **2009**, *52*, 7003-7013.
- Heal, D.J., Gosden, J., and Smith, S.L. Dopamine reuptake transporter (DAT) "inverse agonism" – A novel hypothesis to explain the enigmatic pharmacology of cocaine. *Neuropharmacology* **2014**, DOI: 10.1016/j.neuropharm.2014.06.012.
- Heffe, W. Stevens rearrangement of allylphenacylammonium salts. *Helv. Chim. Acta* **1964**, *47*, 1289-1292.
- Heinzerling, K.G., Swanson, A.N., Hall, T.M., Ba, Y.Y., Wu, Y., and Shoptaw, S.J. Randomized, placebo-controlled trial of bupropion in methamphetamine-dependent

participants with less than daily methamphetamine use. *Addiction* **2014**, DOI:10.111/add.12636.

- Hemstapat, K., Da Costa, H., Nong, Y., Brady, A.E., Luo, Q., Niswender, C.M., Tamagnan, G.D., and Conn, P.J. A novel family of potent negative allosteric modulators of group II metabotropic glutamate receptors. *J. Pharmacol. Exp. Ther.* **2007**, *322*, 254-264.
- Hendrickson, L.M., Guildford, M.J., and Tapper, A.R. Neuronal nicotinic acetylcholine receptors: Common molecular substrates of nicotine and alcohol dependence. *Front. Psychiatry* **2013**, *4*, 29-40.
- Herdener, M., Oppliger, R., Stohler, R., and Cafiisch, C. Treating cocaine addiction. *Praxis (Bern 1994)* **2012**, *101*, 1013-1019.
- Hiranita, T., Soto, P.L., Newman, A.H., and Katz, J.L. Assessment of reinforcing effects of benztropine analogs and their effects on cocaine self-administration in rats: Comparisons with monoamine uptake inhibitors. *J. Pharmacol. Exp. Ther.* **2009**, *329*, 677-686.
- Holladay, M.W., Dart, M.J., and Lynch, J.K. Neuronal nicotinic acetylcholine receptors as targets for drug discovery. *J. Med. Chem.* **1997**, *40*, 4169-4194.
- Holliday, A.R., Morris, R.B., and Sharpley, R.P. Compound 84/F 1983 compared with D-amphetamine and placebo in regard to effects on human performance. *Psychopharmacologia* **1964**, *6*, 192-200.
- Hoogboom, J. and Swager, T.M. Increased alignment of electronic polymers in liquid crystals *via* hydrogen bonding extension. *J. Am. Chem. Soc.* **2006**, *128*, 15058-15059.
- Hopkins, C.R. Is there a path forward for mGlu2 positive allosteric modulators for the treatment of schizophrenia? *ACS Chem. Neurosci.* **2013**, *4*, 211-213.

- Hosoya, T., Hiramatsu, T., Ikemoto, T., Aoyama, H., Ohmae, T., Endo, M., and Suzuki, M. Design of dantrolene-derived probes for radioisotope-free photoaffinity labeling of proteins involved in the physiological $Ca^{2+}$ release from sarcoplasmic reticulum of skeletal muscle. *Bioorg. Med. Chem. Lett.* **2005**, *15*, 1289-1294.
- Hosoya, T., Hiramatsu, T., Ikemoto, T., Nakanishi, M., Aoyama, H., Hosoya, A., Iwata, T., Maruyama, K., Endo, M., and Suzuki, M. Novel bifunctional probe for radioisotope-free photoaffinity labeling: compact structure comprised of photospecific ligand ligation and detectable tag anchoring units. *Org. Biomol. Chem.* **2004**, *2*, 637-641.
- Hosoya, T., Inoue, A., Hiramatsu, T., Aoyama, H., Ikemoto, T., and Suzuki, M. Facile synthesis of diazido-functionalized biaryl compounds as radioisotope-free photoaffinity probes by Suzuki-Miyaura coupling. *Bioorg. Med. Chem.* **2009**, *17*, 2490-2496.
- Hu, Z.J., Bai, L., Tizabi, Y., and Southerland, W. Computational modeling study of human nicotinic acetylcholine receptor for developing new drugs in the treatment of alcoholism. *Interdisciplinary Sciences: Computational Life Sciences* **2009**, *1*, 254-262.
- Huang, C.C., Yang, P.C., Lin, H.J., and Hsu, K.S. Repeated cocaine administration impairs group II metabotropic glutamate receptor-mediated long-term depression in rat medial prefrontal cortex. *J. Neurosci.* **2007**, *27*, 2958-2968.
- Huang, X. and Zhan, C.G. How dopamine transporter interacts with dopamine: Insights from molecular modeling and simulation. *Biophys. J.* **2007**, *93*, 3627-3639.
- Huang, X., Gu, H.H., and Zhan, C.G. Mechanism for cocaine blocking the transport of dopamine: Insights from molecular modeling and dynamics simulations. *J. Physical Chem. B* **2009**, *113*, 15057-15066.

- Huix-Rotllant, M., Siri, D., and Ferre, N. Theoretical study of the photochemical generation of triplet acetophenone. *Phys. Chem. Chem. Phys.* **2013**, *15*, 19293-19300.
- Hurst, R., Rollema, H., and Bertrand, D. Nicotinic acetylcholine receptors: From basic science to therapeutics. *Pharmacol. Ther.* **2013**, *137*, 22-54.
- Hyman, S.E., and Malenka, R.C. Addiction and the brain: The neurobiology of compulsion and its persistence. *Nat. Rev. Neurosci.* **2001**, *2*, 695-703.
- Hyman, S.E., Malenka, R.C., and Nestler, E.J. Neural mechanisms of addiction: The role of reward-related learning and memory. *Annu. Rev. Neurosci.* **2006**, *29*, 565-598.
- Ianni, A. and Waldvogel, S.R. Reliable and versatile synthesis of 2-aryl-substituted cinnamic acid esters. *Synthesis* **2006**, 2103-2112.
- Imogai, H.J., Cid-Nunez, J.M., Duvey, G.A.J., Bolea, C.M., Nhem, V., Finn, T.P., Le, P.E.C., Rocher, J.P., and Luetjens, R.J. Novel pyridinone derivatives and their preparation, pharmaceutical compositions, and use as positive allosteric modulators of mGluR2-receptors for treatment of various neurological and psychiatric disorders. PCT Int. Appl. WO 2006030032 A1, **2006**.
- Indarte, M., Liu, Y., Madura, J.D., and Surratt, C.K. Receptor-based discovery of a plasmalemmal monoamine transporter inhibitor *via* high-throughput docking and pharmacophore modeling. *ACS Chem. Neurosci.* **2010**, *1*, 223-233.
- Indarte, M., Madura, J.D., and Surratt, C.K. Dopamine transporter comparative molecular modeling and binding site prediction using the LeuT(aa) leucine transporter as a template. *Proteins* **2008**, *70*, 1033-1046.
- Iversen, L., White, M., and Treble, R. Designer psychostimulants: Pharmacology and differences. *Neuropharmacology* **2014**, DOI: 10.1016/j.neuropharm.2014.01.015.

- Jaber, M., Jones, S., Giros, B., and Caron, M.G. The dopamine transporter: A crucial component regulating dopamine transmission. *Mov. Disord.* **1997**, *12*, 629-633.
- Jackson, M.B. Spontaneous openings of the acetylcholine receptor channel. *Proc. Natl. Acad. Sci. U.S.A* **1984**, *81*, 3901-3904.
- Jackson, M.B., Imoto, K., Mishina, M., Konno, T., Numa, S., and Sakmann, B. Spontaneous and agonist-induced openings of an acetylcholine receptor channel composed of bovine muscle alpha-, beta- and delta-subunits. *Pflugers Arch.* **1990**, *417*, 129-135.
- Jardetzky, O. Simple allosteric model for membrane pumps. *Nature* **1966**, *211*, 969-970.
- Jensen, A.A., and Spalding, T.A. Allosteric modulation of G-protein coupled receptors. *Eur. J. Pharm. Sci.* **2004**, *21*, 407-420.
- Jensen, A.A., Frolund, B., Liljefors, T., and Krogsgaard-Larsen, P. Neuronal nicotinic acetylcholine receptors: Structural revelations, target identifications, and therapeutic inspirations. *J. Med. Chem.* **2005**, *48*, 4705-4745.
- Jerussi, T.P., McCullough, J.R., Senanayake, C.H., and Fang, Q.K. Bupropion metabolites and methods of their synthesis and therapeutic uses and compositions. PCT Int. Appl. WO 2000051546 A2, **2000**.
- Jin, B., Liu, Q., and Sulikowski, G.A. Development of an end-game strategy towards apoptolidin: a sequential Suzuki coupling approach. *Tetrahedron* **2005**, *61*, 401-408.
- Jin, X., Semenova, S., Yang, L., Ardecky, R., Sheffler, D.J., Dahl, R., Conn, P.J., Cosford, N.D., and Markou, A. The mGluR2 positive allosteric modulator bina decreases cocaine self-administration and cue-induced cocaine-seeking and counteracts cocaine-induced enhancement of brain reward function in rats. *Neuropsychopharmacology* **2010**, *35*, 2021-2036.

- Johnson, L.A., Johnson, R.L., and Portier, R.B. Current "legal highs". *J. Emerg. Med.* **2013**, *44*, 1108-1115.
- Johnston, A.J., Ascher, J., Leadbetter, R., Schmith, V.D., Patel, D.K., Durcan, M., and Bentley, B. Pharmacokinetic optimization of sustained-release bupropion for smoking cessation. *Drugs* **2002**, *62*, 11–24.
- Kahlig, K.M. and Galli, A. Regulation of dopamine transporter function and plasma membrane expression by dopamine, amphetamine, and cocaine. *Eur. J. Pharmacol.* **2003**, *479*, 153-158.
- Kahlig, K.M., Binda, F., Khoshbouei, H., Blakely, R.D., McMahon, D.G., Javitch, J.A., and Galli, A. Amphetamine induces dopamine efflux through a dopamine transporter channel. *Proc. Natl. Acad. Sci. USA* **2005**, *102*, 3495-3500.
- Kalivas, P.W., Pierce, R.C., Cornish, J., and Sorg, B.A. A role for sensitization in craving and relapse in cocaine addiction. *J. Psychopharmacol.* **1998**, *12*, 49-53.
- Kalivas, P.W., Lalumiere, R.T., Knackstedt, L., and Shen, H. Glutamate transmission in addiction. *Neuropharmacology* **2009**, *56*, 169-173.
- Katz, J.L., Agoston, G.E., Alling, K.L., Kline, R.H., Forster, M.J., Woolverton, W.L., Kopajtic, T.A., and Newman, A.H. Dopamine transporter binding without cocaine-like behavioral effects: Synthesis and evaluation of benztropine analogs alone and in combination with cocaine in rodents. *Psychopharmacology* **2001**, *154*, 362-374.
- Katz, J.L., Kopajtic, T.A., Agoston, G.E., and Newman, A.H. Effects of n-substituted analogs of benztropine: Diminished cocaine-like effects in dopamine transporter ligands. *J. Pharmacol. Exp. Ther.* **2004**, *309*, 650-660.

- Keiser, M.J., Irwin, J.J., and Shoichet, B.K. The chemical basis of pharmacology. *Biochemistry* **2010**, *49*, 10267-10276.
- Kenakin, T.P. Biased signalling and allosteric machines: New vistas and challenges for drug discovery. *Br. J. Pharmacol.* **2012**, *165*, 1659-1669.
- Kenny, P.J., and Markou, A. The ups and downs of addiction: Role of metabotropic glutamate receptors. *Trends Pharmacol. Sci.* **2004**, *25*, 265-272.
- Kew, J.N., and Kemp, J.A. Ionotropic and metabotropic glutamate receptor structure and pharmacology. *Psychopharmacology* **2005**, *179*, 4-29.
- Kim, J.H., Austin, J.D., Tanabe, L., Creekmore, E., and Vezina, P. Activation of group II mGlu receptors blocks the enhanced drug taking induced by previous exposure to amphetamine. *Eur. J. Neurosci.* **2005**, *21*, 295-300.
- Kingston, A.E., O'Neill, M.J., Lam, A., Bales, K.R., Monn, J.A., and Schoepp, D.D. Neuroprotection by metabotropic glutamate receptor glutamate receptor agonists: LY354740, LY379268 and LY389795. *Eur. J. Pharmacol.* **1999**, *377*, 155-165.
- Kitayama, S., Shimada, S., Xu, H., Markham, L., Donovan, D.M., and Uhl, G.R. Dopamine transporter site-directed mutations differentially alter substrate transport and cocaine binding. *Proc. Nat. Acad. Sc.* **1992**, *89*, 7782-7785.
- Kiyonaka, S., Kato, K., Nishida, M., Mio, K., Numaga, T., Sawaguchi, Y., Yoshida, T., Wakamori, M., Mori, E., Numata, T., Ishii, M., Takemoto, H., Ojida, A., Watanabe, K., Uemura, A., Kurose, H., Morii, T., Kobayashi, T., Sato, Y., Sato, C., Hamachi, I., and Mori, Y. Selective and direct inhibition of TRPC3 channels underlies biological activities of a pyrazole compound. *Proc. Natl. Acad. Sci. U.S.A.* **2009**, *106*, 5400-5405.

- Klein, D.F., and Rowland, L.P. Current psychotherapeutic drugs, Brunner/Mazel, New York, **2013**.
- Klein, S.I., Czekaj, M., Gardner, C.J., Guertin, K.R., Cheney, D.L., Spada, A.P., Bolton, S.A., Brown, K., Colussi, D., Heran, C.L., Morgan, S.R., Leadley, R.J., Dunwiddie, C.T., Perrone, M. H., and Chu, V. Identification and initial structure-activity relationships of a novel class of nonpeptide inhibitors of blood coagulation factor Xa. *J. Med. Chem.* **1998**, *41*, 437-450.
- Kline, R.H., Jr., Eshleman, A.J., Eldefrawi, M.E., and Wright, J. Synthesis of substituted 3-carbamoylecgonine methyl ester analogs: Irreversible and photoaffinity ligands for the cocaine receptor/dopamine transporter. *J. Med. Chem.* **1994**, *37*, 2249-2252.
- Kobeissy, F., Mouhieddine, T.H., Nokkari, A., Itani, M., Mouhieddine, M., Zhang, Z., Zhu, R., Gold, M.S., Wang, K.K., and Mechref, Y. Recent updates on drug abuse analyzed by neuroproteomics studies: Cocaine, methamphetamine and MDMA. *Translational Proteomics* **2014**, DOI: 10.1016/j.trprot.2014.04.001.
- Koldsoe, H., Christiansen, A.B., Sinning, S., and Schioett, B. Comparative modeling of the human monoamine transporters: Similarities in substrate binding. *ACS Chem. Neurosci.* **2013**, *4*, 295-309.
- Kolkhof, P., Bruens, A., Thede, K., Schlemmer, K.H., Hillisch, A., Lang, D., Gerisch, M., Goeller, A., Grosser, R., Schmeck, C., Woltering, E., Prien, O., Paulsen, H., and Kern, A. Preparation of 7-sulfonylmethylindoles as mineralocorticoid receptor inhibitors. PCT Int. Appl. WO 2009004305, **2009**.
- Koob, G.F. and Volkow, N.D. Neurocircuitry of addiction. *Neuropsychopharmacology* **2010**, *35*, 217-238.

- Kopajtic, T.A., Liu, Y., Surratt, C.K., Donovan, D.M., Newman, A.H., and Katz, J.L. Dopamine transporter-dependent and -independent striatal binding of the benztropine analog JHW 007, a cocaine antagonist with low abuse liability. *J. Pharmacol. Exp. Ther.* **2010**, *335*, 703-714.
- Krasnokutskaya, E.A., Semenischeva, N.I., Filimonov, V.D., and Knochel, P. A new, one-step, effective protocol for the iodination of aromatic and heterocyclic compounds *via* aprotic diazotization of amines. *Synthesis* **2007**, 81-84.
- Krishnamurthy, H. and Gouaux, E. X-ray structures of LeuT in substrate-free outward-open and apo inward-open states. *Nature* **2012**, *481*, 469-474.
- Kufahl, P.R., Watterson, L.R., Nemirovsky, N.E., Hood, L.E., Villa, A., Halstengard, C., Zautra, N., and Foster Olive, M. Attenuation of methamphetamine seeking by the mGluR2/3 agonist LY379268 in rats with histories of restricted and escalated self-administration. *Neuropharmacology* **2013**, *66*, 290-301.
- Kuhar, M., Ritz, M., and Boja, J. The dopamine hypothesis of the reinforcing properties of cocaine. *Trends in Neurosciences* **1991**, *14*, 299-302.
- Kuhar, M.J. and Pilotte, N.S. Neurochemical changes in cocaine withdrawal. *Trends Pharmacol. Sci.* **1996**, *17*, 260-264.
- Kunishima, N., Shimada, Y., Tsuji, Y., Sato, T., Yamamoto, M., Kumasaka, T., Nakanishi, S., Jingami, H., and Morikawa, K. Structural basis of glutamate recognition by a dimeric metabotropic glutamate receptor. *Nature* **2000**, *407*, 971-977.
- Kym, P.R., Carlson, K.E., and Katzenellenbogen, J.A. Progestin 16α,17α-dioxolane ketals as molecular probes for the progesterone receptor: synthesis, binding affinity, and photochemical evaluation. *J. Med. Chem.* **1993**, *36*, 1111-1119.

- Laib, A.K., Brunen, S., Pfeifer, P., Vincent, P., and Hiemke, C. Serum concentrations of hydroxybupropion for dose optimization of depressed patients treated with bupropion. *Ther. Drug. Monit.* **2014**, *36*, 473-479.
- Laizure, S.C., and DeVane, C.L. Stability of bupropion and its major metabolites in human plasma. *Ther. Drug Monit.* **1985**, *7*, 447-450.
- Laizure, S.C., DeVane, C.L., Stewart, J.T., Dommisse, C.S., and Lai, A.A. Pharmacokinetics of bupropion and its major basic metabolites in normal subjects after a single dose. *Clin. Pharmacol. Ther.* **1985**, *38*, 586-589.
- Lancelot, J.C., Robba, M., Bonnet, J.J., Vaugeois, J.M. and Costentin, J. Synthesis and preliminary study of the activity of thiophene analogues of pyrovalerone on the neuronal uptake of the monoamines. *Eur. J. Med. Chem.* **1992**, *27*, 297-300.
- Langmead, C.J., and Christopoulos, A. Functional and structural perspectives on allosteric modulation of GPCRs. *Curr Opin Cell Biol* **2014**, *27*, 94-101.
- Lapinsky, D.J. Tandem photoaffinity labeling-bioorthogonal conjugation in medicinal chemistry. *Bioorg. Med. Chem.* **2012**, *20*, 6237-6247.
- Lapinsky, D.J., Aggarwal, S., Huang, Y., Surratt, C.K., Lever, J.R., Foster, J.D., and Vaughan, R.A. A novel photoaffinity ligand for the dopamine transporter based on pyrovalerone. *Bioorg. Med. Chem.* **2009**, *17*, 3770-3774.
- Lapinsky, D.J., Aggarwal, S., Nolan, T.L., Surratt, C.K., Lever, J.R., Acharya, R., Vaughan, R.A., Pandhare, A., and Blanton, M.P. (+/-)-2-(*N*-tert-Butylamino)-3'-[($^{125}$)I]-iodo-4'-azidopropiophenone: A dopamine transporter and nicotinic acetylcholine receptor photoaffinity ligand based on bupropion (Wellbutrin, Zyban). *Bioorg. Med. Chem. Lett.* **2012**, *22*, 523-526.

- Lapinsky, D.J., Velagaleti, R., Yarravarapu, N., Liu, Y., Huang, Y., Surratt, C.K., Lever, J.R., Foster, J.D., Acharya, R., Vaughan, R.A., and Deutsch, H.M. Azido-iodo-N-benzyl derivatives of threo-methylphenidate (Ritalin, Concerta): Rational design, synthesis, pharmacological evaluation, and dopamine transporter photoaffinity labeling. *Bioorg. Med. Chem.* **2011**, *19*, 504-512.
- Lapinsky, D.J., Yarravarapu, N., Nolan, T.L., Surratt, C.K., Lever, J.R., Tomlinson, M., Vaughan, R.A., and Deutsch, H.M. Evolution of a compact photoprobe for the dopamine transporter based on (+/-)-threo-methylphenidate. *ACS Med. Chem. Lett.* **2012**, *3*, 378-382.
- Law, R.J. and Lightstone, F.C. Modeling neuronal nicotinic and GABA receptors: important interface salt-links and protein dynamics. *Biophyical Journal* **2009**, *97*, 1586-1594.
- Le Moal, M. and Koob, G.F. Drug addiction: Pathways to the disease and pathophysiological perspectives. *Eur. Neuropsychopharmacol* **2007**, *17*, 377-393.
- Leach, A.R., Gillet, V.J., Lewis, R.A., and Taylor, R. Three-dimensional pharmacophore methods in drug discovery. *J. Med. Chem.* **2010**, *53*, 539-558.
- Letchworth, S.R., Nader, M.A., Smith, H.R., Friedman, D.P., and Porrino, L.J. Progression of changes in dopamine transporter binding site density as a result of cocaine self-administration in rhesus monkeys. *J. Neuroscience* **2001**, *21*, 2799-2807.
- Lever, J.R., Zou, M.F., Parnas, M.L., Duval, R.A., Wirtz, S.E., Justice, J.B., Vaughan, R.A., and Newman, A.H. Radioiodinated azide and isothiocyanate derivatives of cocaine for irreversible labeling of dopamine transporters: Synthesis and covalent binding studies. *Bioconjugate Chem.* **2005**, *16*, 644-649.

- Lewis, J.A., Lebois, E.P., and Lindsley, C.W. Allosteric modulation of kinases and GPCRs: Design principles and structural diversity. *Curr. Opin. Chem. Biol.* **2008**, *12*, 269-280.
- Lin, S.Y., Hojjat, M., and Strekowski, L. A facile synthesis of 4-(trialkylmethyl)anilines by the reaction of 4-(trifluoromethyl)aniline with Grignard reagents. *Syn. Commun.* **1997**, *27*, 1975-1980.
- Liu, X., Wang, Z., Cheng, X., and Li, C. Silver-catalyzed decarboxylative alkynylation of aliphatic carboxylic acids in aqueous solution. *J. Am. Chem. Soc.* **2012**, *134*, 14330-14333.
- Loland, C.J. The use of LeuT as a model in elucidating binding sites for substrates and inhibitors in neurotransmitter transporters. *Biochim. Biophys. Acta* **2014**, DOI: 10.1016/j.bbagen.2014.04.011.
- Loland, C.J., Desai, R.I., Zou, M.F., Cao, J., Grundt, P., Gerstbrein, K., Sitte, H.H., Newman, A.H., Katz, J.L., and Gether, U. Relationship between conformational changes in the dopamine transporter and cocaine-like subjective effects of uptake inhibitors. *Mol. Pharmacol.* **2008**, *73*, 813-823.
- Loland, C.J., Norregaard, L., Litman, T., and Gether, U. Generation of an activating $Zn^{2+}$ switch in the dopamine transporter: Mutation of an intracellular tyrosine constitutively alters the conformational equilibrium of the transport cycle. *Proc. Natl. Acad. Sci. USA* **2002**, *99*, 1683-1688.
- Liu, Y., Paige, M., Olson, T.T., Al-Muhtasib, N., Xie, T., Hou, S., White, M.P., Cordova, A., Guo, J.L., Kellar, K.J., Xiao, Y., and Brown, M.L. Synthesis and pharmacological characterization of neuronal nicotinic acetylcholine receptor ligands derived from Sazetidine-A. *Bioorg. Med. Chem. Lett.* **2014**, *24*, 2954-2956.

- Lu, L.Y., Xue, Y.Q., Steketee, J.D., Rebec, G.V., and Sun, W.L. Regulation of cocaine-induced reinstatement by group II metabotropic glutamate receptors in the ventral tegmental area. *Psychopharmacology* **2012**, *220*, 75-85.
- Lukac, I., Kosa, C., and Weiss, R.G. Photo-crosslinking of polyethylene by mono- and diacetophenone derivatives and their precursors. *Photochem. Photobiol. Sci.* **2009**, *8*, 1389-1400.
- Lukas, R.J., Changeux, J.P., Le Novere, N., Albuquerque, E.X., Balfour, D.J., Berg, D.K., Bertrand, D., Chiappinelli, V.A., Clarke, P.B., Collins, A.C., Dani, J.A., Grady, S.R., Kellar, K.J., Lindstrom, J.M., Marks, M.J., Quik, M., Taylor, P.W., and Wonnacott, S. International union of pharmacology. XX. Current status of the nomenclature for nicotinic acetylcholine receptors and their subunits. *Pharmacol. Rev.* **1999**, *51*, 397-401.
- Lukas, R.J., Muresan, A.Z., Damaj, M.I., Blough, B.E., Huang, X., Navarro, H.A., Mascarella, S.W., Eaton, J.B., Marxer-Miller, S.K., and Carroll, F.I. Synthesis and characterization of *in vitro* and *in vivo* profiles of hydroxybupropion analogs: Aids to smoking cessation. *J. Med. Chem.* **2010**, *53*, 4731-4748.
- Lundstrom, L., Bissantz, C., Beck, J., Wettstein, J.G., Woltering, T.J., Wichmann, J., and Gatti, S. Structural determinants of allosteric antagonism at metabotropic glutamate receptor 2: mechanistic studies with new potent negative allosteric modulators. *British Journal of Pharmacology* **2011**, *164*, 521-537.
- Madras, B.K., Spealman, R.D., Fahey, M.A., Neumeyer, J.L., Saha, J.K., and Milius, R.A. Cocaine receptors labeled by [$^3$H]2β-carbomethoxy-3β-(4-fluorophenyl)tropane. *Mol. Pharmacol.* **1989**, *36*, 518-524.

- Mahale, R.D., Chaskar, S.P., Patil, K.E., Maikap, G.C., and Gurjar, M.K. Corey–Itsuno reduction of ketones: A development of safe and inexpensive process for synthesis of some API intermediates. *Org. Proc. Res. Dev.* **2012**, *16*, 710-713.
- Mahasenan, K.V., Pavlovicz, R.E., Henderson, B.J., Gonzalez-Cestari, T.F., Yi, B., McKay, D.B., and Li, C. Dicovery of novel α4β2 neuronal nicotinic receptor modulators through structure-based virtual screening. *ACS Med. Chem. Lett.* **2011**, *2*, 855-860.
- Malherbe, P., Knoflach, F., Broger, C., Ohresser, S., Kratzeisen, C., Adam, G., Stadler, H., Kemp, J.A., and Mutel, V. Identification of essential residues involved in the glutamate binding pocket of the group II metabotropic glutamate receptor. *Mol. Pharmacol.* **2001**, *60*, 944-954.
- Malherbe, P., Kratochwil, N., Knoflach, F., Zenner, M.T., Kew, J.N., Kratzeisen, C., Maerki, H.P., Adam, G., and Mutel, V. Mutational analysis and molecular modeling of the allosteric binding site of a novel, selective, noncompetitive antagonist of the metabotropic glutamate 1 receptor. *J. Biol. Chem.* **2003**, *278*, 8340-8347.
- Malherbe, P., Kratochwil, N., Zenner, M.T., Piussi, J., Diener, C., Kratzeisen, C., Fischer, C., and Porter, R.H. Mutational analysis and molecular modeling of the binding pocket of the metabotropic glutamate 5 receptor negative modulator 2-methyl-6-(phenylethynyl)-pyridine. *Mol. Pharmacol.* **2003**, *64*, 823-832.
- Manepalli, S., Surratt, C.K., Madura, J.D., and Nolan, T.L. Monoamine transporter structure, function, dynamics, and drug discovery: a computational perspective. *The AAPS J.* **2012**, *14*, 820-831.

- Marinetti, L.J. and Antonides, H.M. Analysis of synthetic cathinones commonly found in bath salts in human performance and postmortem toxicology: Method development, drug distribution and interpretation of results. *J. Anal. Toxicol.* **2013**, *37*, 135-146.
- Marotta, C.B., Rreza, I., Lester, H.A., and Dougherty, D.A. Selective ligand behaviors provide new insights into agonist activation of nicotinic acetylcholine receptors. *ACS Chemical Biology* **2014**, *9*, 1153-1159.
- Martin, M., Chen, B.T., Hopf, F.W., Bowers, M.S., and Bonci, A. Cocaine self-administration selectively abolishes LTD in the core of the nucleus accumbens. *Nat. Neurosci.* **2006**, *9*, 868-869.
- Marusich, J.A., Antonazzo, K.R., Wiley, J.L., Blough, B.E., Partilla, J.S., and Baumann, M.H. Pharmacology of novel synthetic stimulants structurally related to the "bath salts" constituent 3,4-methylenedioxypyrovalerone (MDPV). *Neuropharmacology* **2014**, DOI: 10.1016/j.neuropharm.2014.02.016
- Mash, D.C. Dopamine transporter disease states and pathology. From *Dopamine Transporters* **2008**, 29-46. Edited by Trudell, M.L. and Izenwasser, S.
- Mehta, N.B. Intermediates for biologically active ketones. Patent Canada CA977778 A, **1975**.
- Meltzer, P.C., Butler, D., Deschamps, J.R., and Madras, B.K. 1-(4-methylphenyl)-2-pyrrolidin-1-yl-pentan-1-one (pyrovalerone) analogs: A promising class of monoamine uptake inhibitors. *J. Med. Chem.* **2006**, *49*, 1420-1432.
- Meyer, M.R., Du, P., Schuster, F., and Maurer, H.H. Studies on the metabolism of the alpha-pyrrolidinophenone designer drug methylenedioxy-pyrovalerone (MDPV) in rat and

human urine and human liver microsomes using GC-MS and LC-high-resolution ms and its detectability in urine by GC-MS. *J. Mass. Spectrom.* **2010**, *45*, 1426-1442.

- Miller, L.W. and Cornish, V.W. Selective chemical labeling of proteins in living cells. *Current Opinion in Chemical Biology* **2005**, *9*, 56-61.
- Misra, M., Shi, Q., Ye, X., Gruszecka-Kowalik, E., Bu, W., Liu, Z., Schweri, M.M., Deutsch, H.M., and Venanzi, C.A. Quantitative structure-activity relationship studies of threo-methylphenidate analogs. *Bioorg. Med. Chem.* **2010**, *18*, 7221-7238.
- Miyazawa, A., Fujiyoshi, Y., and Unwin, N. Structure and gating mechanism of the acetylcholine receptor pore. *Nature* **2003**, *423*, 949-955.
- Mohr, G.J. Tailoring the sensitivity and spectral properties of a chromoreactand for the detection of amines and alcohols. *Anal. Chim. Acta* **2004**, *508*, 233-237.
- Monn, J.A., Valli, M.J., Massey, S.M., Hansen, M.M., Kress, T.J., Wepsiec, J.P., Harkness, A.R., Grutsch, J.L., Jr., Wright, R.A., Johnson, B.G., Andis, S.L., Kingston, A., Tomlinson, R., Lewis, R., Griffey, K.R., Tizzano, J.P., and Schoepp, D.D. Synthesis, pharmacological characterization, and molecular modeling of heterobicyclic amino acids related to (+)-2-aminobicyclo[3.1.0] hexane-2,6-dicarboxylic acid (LY354740): Identification of two new potent, selective, and systemically active agonists for group ii metabotropic glutamate receptors. *J. Med. Chem.* **1999**, *42*, 1027-1040.
- Monn, J.A., Valli, M.J., Massey, S.M., Wright, R.A., Salhoff, C.R., Johnson, B.G., Howe, T., Alt, C.A., Rhodes, G.A., Robey, R.L., Griffey, K.R., Tizzano, J.P., Kallman, M.J., Helton, D.R., and Schoepp, D.D. Design, synthesis, and pharmacological characterization of (+)-2-aminobicyclo[3.1.0]hexane-2,6-dicarboxylic acid (LY354740): A potent,

selective, and orally active group 2 metabotropic glutamate receptor agonist possessing anticonvulsant and anxiolytic properties. *J. Med. Chem.* **1997**, *40*, 528-537.

- Monod, J., Wyman, J., and Changeux, J.P. On the nature of allosteric transitions: A plausible model. *J. Mol. Biol.* **1965**, *12*, 88-118.
- Morishima, Y., Miyakawa, T., Furuyashiki, T., Tanaka, Y., Mizuma, H., and Nakanishi, S. Enhanced cocaine responsiveness and impaired motor coordination in metabotropic glutamate receptor subtype 2 knockout mice. *Proc. Natl. Acad. Sci. USA* **2005**, *102*, 4170-4175.
- Morris, J.L., Reddington, S.C., Murphy, D.M., Jones, D.D., Platts, J.A., and Tippman, E.M. Aryl azide photochemistry in defined protein environments. *Org. Lett.* **2013**, *15*, 728-731.
- Moussawi, K. and Kalivas, P.W. Group II metabotropic glutamate receptors (mGlu2/3) in drug addiction. *Eur. J. Pharmacol.* **2010**, *639*, 115-122.
- Moussawi, K., Pacchioni, A., Moran, M., Olive, M.F., Gass, J.T., Lavin, A., and Kalivas, P.W. N-acetylcysteine reverses cocaine-induced metaplasticity. *Nat. Neurosci.* **2009**, *12*, 182-189.
- Murthy, V., Martin, T.J., Kim, S., Davies, H.M., and Childers, S.R. *In vivo* characterization of a novel phenylisothiocyanate tropane analog at monoamine transporters in rat brain. *J. Pharmacol. Exp. Ther.* **2008**, *326*, 587-595.
- Musso, D.L. and Mehta, N.B. Separations of threo-erythro aminoalcohols by preparative HPLC. *J. Liq. Chromatogr.* **1981**, *4*, 1417-1434.

- Musso, D.L., Mehta, N.B., and Soroko, F.E. Synthesis and evaluation of the anticonvulsant activity of a series of 2-amino-1-phenyl-1-propanols derived from the metabolites of the antidepressant bupropion. *Bioorg. Med. Chem. Lett.* **1997**, *7*, 1-6.
- Musso, D.L., Mehta, N.B., Soroko, F.E., Ferris, R.M., Hollingsworth, E.B., and Kenney, B.T. Synthesis and evaluation of the antidepressant activity of the enantiomers of bupropion. *Chirality* **1993**, *5*, 495-500.
- Muto, T., Tsuchiya, D., Morikawa, K., and Jingami, H. Expression, purification, crystallization and preliminary x-ray analysis of the ligand-binding domain of metabotropic glutamate receptor 7. *Acta Cryst.* **2007**, *63*, 627-630.
- Neelarapu, R., Holzle, D.L., Velaparthi, S., Bai, H., Brunsteiner, M., Blond, S.Y., and Petukhov, P.A. Design, synthesis, docking, and biological evaluation of novel diazide-containing isoxazole- and pyrazole-based histone deacetylase probes. *J. Med. Chem.* **2011**, *54*, 4350-4364.
- Nestler, E.J. Is there a common molecular pathway for addiction? *Nat. Neurosci.* **2005**, *8*, 1445-1449.
- Neugebauer, V., Zinebi, F., Russell, R., Gallagher, J.P., and Shinnick-Gallagher, P. Cocaine and kindling alter the sensitivity of group II and III metabotropic glutamate receptors in the central amygdala. *J. Neurophysiol.* **2000**, *84*, 759-770.
- Newman, A.H., Allen, A.C., Izenwasser, S., and Katz, J.L. Novel 3. Alpha.-(diphenylmethoxy) tropane analogs: Potent dopamine uptake inhibitors without cocaine-like behavioral profiles. *J. Med. Chem.* **1994**, *37*, 2258-2261.
- Newman, A.H., Cha, J.H., Cao, J., Kopajtic, T., Katz, J.L., Parnas, M.L., Vaughan, R., and Lever, J.R. Design and synthesis of a novel photoaffinity ligand for the dopamine and

serotonin transporters based on 2β-carbomethoxy-3β-biphenyltropane. *J. Med. Chem.* **2006**, *49*, 6621-6625.

- Newton, T.F., Roache, J.D., De La Garza, R., Fong, T., Wallace, C.L., Li, S.-H., Elkashef, A., Chiang, N., and Kahn, R. Bupropion reduces methamphetamine-induced subjective effects and cue-induced craving. *Neuropsychopharmacology* **2006**, *31*, 1537-1544.
- Nicholls, A., McGaughey, R.P., Sheridan, R.P., Good, A.C., Warren, G. Mathieu, Muchmore, S.W., Brown, S.P., Grant, J.A., Haigh, J.A., Nevins, N., Jain, A.N., and Kelley, B. Molecular shape and medicinal chemistry: A perspective. *J. Med. Chem.* **2010**, *53*, 3862-3886.
- Nickell, J.R., Siripurapu, K.B., Vartak, A., Crooks, P.A., and Dwoskin, L.P. The vesicular monoamine transporter-2: An important pharmacological target for the discovery of novel therapeutics to treat methamphetamine abuse. *Adv. Pharmacol.* **2014**, *69*, 71-106.
- Nirthanan, S., Garcia, G., Chiara, D.C., Husain, S.S., and Cohen, J.B. Identification of binding sites in the nicotinic acetylcholine receptor for TDBzl-etomidate, a photoreactive positive allosteric effector. *J. Biol. Chem.* **2008**, *283*, 22051-22062.
- Niswender, C.M., and Conn, P.J. Metabotropic glutamate receptors: physiology, pharmacology, and disease. *Annu. Rev. Pharmacol. Toxicol.* **2010**, *50*, 295-322.
- Nolan, T.L., Lapinsky, D.J., Talbot, J.N., Indarte, M., Liu, Y., Manepalli, S., Geffert, L., Maos, M.E., Taylor, P.N., Madura, J.D., and Surratt, C.K. Identification of a novel selective serotonin reuptake inhibitor by coupling monoamine transporter-based virtual screening and rational molecular hybridization. *ACS Chem. Neurosci.* **2011**, *2*, 544-552.
- Nyola, A., Karpowich, N.K., Zhen, J., Marden, J., Reith, M.E., and Wang, D.N. Substrate and drug binding sites in LeuT. *Curr. Opin. Struct. Biol.* **2010**, *20*, 415-422.

- Ogawa, H., Tamada, S., Fujioka, T., Teramoto, S., Kondo, K., Yamashita, S., Yabuuchi, Y., Tominaga, M., and Nakagawa, K. Studies on positive inotropic agents. V.: Synthesis of 1-heteroaroylpiperazine derivatives. *Chem. Pharm. Bull.* **1988**, *36*, 2253-2258.
- Onishi, Y., Nishimoto, Y., Yasuda, M., and Baba, A. $InCl_3/Me_3SiBr$-catalyzed direct coupling between silyl ethers and enol acetates. *Org. Lett.* **2011**, *13*, 2762-2765.
- Ortuno, J.-C., Cordi, A., Lacoste, J.-M., Fejes, I., Burbridge, M., Hickman, J., and Pierre, A. Preparation of new dihydroindolone derivatives, particularly 3-[(1H-pyrrol-2-yl)methylene]-5-(heterocyclylalkyl)-1,3-dihydro-2H-indol-2-ones, as inhibitors of cancer cell migration and pharmacetical compositions containing them, **2011**.
- Pandhare, A., Hamouda, A.K., Staggs, B., Aggarwal, S., Duddempudi, P.K., Lever, J.R., Lapinsky, D.J., Jansen, M., Cohen, J.B., and Blanton, M.P. Bupropion binds to two sites in the torpedo nicotinic acetylcholine receptor transmembrane domain: A photoaffinity labeling study with the bupropion analogue [$^{125}$I]-SADU-3-72. *Biochemistry* **2012**, *51*, 2425-2435.
- Parekh, J.M., Sutariya, D.K., Vaghela, R.N., Sanyal, M., Yadav, M., and Shrivastav, P.S. Sensitive, selective and rapid determination of bupropion and its major active metabolite, hydroxybupropion, in human plasma by LC-MS/MS: Application to a bioequivalence study in healthy Indian subjects. *Biomed. Chromatogr.* **2012**, *26*, 314-326.
- Parikh, N., Nonnemacher, M.R., Pirrone, V., Block, T., Mehta, A., and Wigdahl, B. Substance abuse, HIV-1, and hepatitis. *Curr. HIV Res.* **2012**, *10*, 557-571.
- Park, J.Y., Kim, S.W., Lee, J.-K., Im, W.B., Jin, B.K., and Yoon, S.H. Simplified heterocyclic analogues of fluoxetine inhibit inducible nitric oxide production in lipopolysaccharide-induced BV2 cells. *Biol. Pharm. Bull.* **2011**, *34*, 538-544.

- Parnas, M.L., Gaffaney, J.D., Zou, M.F., Lever, J.R., Newman, A.H., and Vaughan, R.A. Labeling of dopamine transporter transmembrane domain 1 with the tropane ligand *n*-[4-(4-azido-3-[$^{125}$I]iodophenyl)butyl]-2β-carbomethoxy-3β-(4-chlorophenyl)tropane implicates proximity of cocaine and substrate active sites. *Mol. Pharmacol.* **2008**, *73*, 1141-1150.
- Partilla, J.S., Dempsey, A.G., Nagpal, A.S., Blough, B.E., Baumann, M.H., and Rothman, R.B. Interaction of amphetamines and related compounds at the vesicular monoamine transporter. *J. Pharmacol. Exp.l Ther.* **2006**, *319*, 237-246.
- Pavlovicz, R.E., Henderson, B.J., Bonnell, A.B., Boyd, R.T., McKay, D.B., and Li, C. Identification of a negative allosteric site on human α4β2 and α3β4 neuronal acetylcholine receptors. *Plos One* **2011**, *6*, e24949.
- Penmatsa, A. and Gouaux, E. How LeuT shapes our understanding of the mechanisms of sodium-coupled neurotransmitter transporters. *J. Physiol.* **2014**, *592*, 863-869.
- Perrine, D.M., Ross, J.T., Nervi, S.J., and Zimmerman, R.H. A short, one-pot synthesis of Bupropion (Zyban, Wellbutrin). *J. Chem. Educ.* **2000**, *77*, 1479-1483.
- Peters, J., and Kalivas, P.W. The group II metabotropic glutamate receptor agonist, LY379268, inhibits both cocaine- and food-seeking behavior in rats. *Psychopharmacology* **2006**, *186*, 143-149.
- Pieffet, G. and Petukhov, P.A. Parameterization of aromatic azido groups: application as photoaffinity probes in molecular dynamics studies. *J. Mol. Model.* **2009**, *15*, 1291-1297.
- Pierce, R.C. and Kumaresan, V. The mesolimbic dopamine system: The final common pathway for the reinforcing effect of drugs of abuse? *Neurosci. Biobehav. Rev.* **2006**, *30*, 215-238.

- Pifl, C., Drobny, H., Reither, H., Hornykiewicz, O., and Singer, E.A. Mechanism of the dopamine-releasing actions of amphetamine and cocaine: Plasmalemmal dopamine transporter versus vesicular monoamine transporter. *Mol. Pharmacol.* **1995**, *47*, 368-373.
- Pin, J.P., and Duvoisin, R. The metabotropic glutamate receptors: Structure and functions. *Neuropharmacology* **1995**, *34*, 1-26.
- Pin, J.P., Galvez, T., and Prezeau, L. Evolution, structure, and activation mechanism of family 3/C G-protein-coupled receptors. *Pharmacol. Ther.* **2003**, *98*, 325-354.
- Pinkerton, A.B., Cube, R.V., Hutchinson, J.H., James, J.K., Gardner, M.F., Rowe, B.A., Schaffhauser, H., Rodriguez, D.E., Campbell, U.C., Daggett, L.P., and Vernier, J.M. Allosteric potentiators of the metabotropic glutamate receptor 2 (mGlu2). Part 3: Identification and biological activity of indanone containing mglu2 receptor potentiators. *Bioorg. Med. Chem. Lett.* **2005**, *15*, 1565-1571.
- Pinkerton, A.B., Vernier, J.M., Cube, R.V., Hutchinson, J.H., Bonnefous, C., and Kamenecka, T. Preparation of indanone potentiators of metabotropic glutamate receptors for use against neurological and psychiatric disorders. PCT Int. Appl. WO 2006015158 A1, **2006**.
- Poe, R., Schnapp, K., Young, M.J.T., Grayzar, J., and Platz, M.S. Chemistry and kinetics of singlet pentafluorophenylnitrene. *J. Am. Chem. Soc.* **1992**, *114*, 5054-5067.
- Pokhodylo, N.T., and Matiychuk, V.S. Synthesis of new 1,2,3-triazolo[1,5-α]quinazolinones. *J. Hetero. Chem.* **2010**, *47*, 415-420.
- Poling, J., Oliveto, A., Petry, N., Sofuoglu, M., Gonsai, K., Gonzalez, G., Martell, B., and Kosten, T.R. Six-month trial of bupropion with contingency management for cocaine

dependence in a methadone-maintained population. *Arch. Gen. Psychiatry* **2006**, *63*, 219-228.

- Pomierny-Chamioło, L., Rup, K., Pomierny, B., Niedzielska, E., Kalivas, P.W., and Filip, M. Metabotropic glutamatergic receptors and their ligands in drug addiction. *Pharmacol. Ther.* **2014**, *142*, 281-305.
- Pramod, A.B., Foster, J., Carvelli, L., and Henry, L.K. SLC6 transporters: Structure, function, regulation, disease association and therapeutics. *Mol. Aspects. Med.* **2013**, *34*, 197-219.
- Pubill, D., Garcia-Rates, S., Camarasa, J., and Escubedo, E. Neuronal nicotinic receptors as new targets for amphetamine-induced oxidative damage and neurotoxicity. *Pharmaceuticals* **2011**, *4*, 822-847.
- Pudlo, M., Csányi, D., Moreau, F., Hajós, G., Riedl, Z., and Sapi, J. First Suzuki–Miyaura type cross-coupling of *ortho*-azidobromobenzene with arylboronic acids and its application to the synthesis of fused aromatic indole-heterocycles. *Tetrahedron* **2007**, *63*, 10320-10329.
- Quick, M., Winther, A.M., Shi, L., Nissen, P., Weinstein, H., and Javitch, J.A. Binding of an octylglucoside detergent molecule in the second substrate (S2) site of LeuT establishes an inhibitor-bound conformation. *Proc. Natl. Acad. Sci. U S A* **2009**, *106*, 5563-5568.
- Quick, M., Shi, L., Zehnpfennig, B., Weinstein, H., and Javitch, J.A. Experimental conditions can obscure the second high-affinity site in LeuT. *Nat. Struct. Mol. Biol.* **2012**, *19*, 207-211.

- Radchenko, E.V., Karlov, D.S., Palyulin, V.A., and Zefirov, N.S. Molecular modeling of the transmembrane domain of mGluR2 metabotropic glutamate receptor and the binding site of its positive allosteric modulators. *Biochem. Biophys.* **2014**, *454*, 13-16.
- Rahman, S. Nicotinic receptors as therapeutic targets for drug addicitve disorders. *CNS Neurol. Disord. Drug Targets* **2013**, *12*, 633-640.
- Rahman, S. and Prendergast, M.A. Cholinergic recptor system as a target for treating alcohol abuse and dependence. *Recent Patents on CNS Drug Discovery* **2012**, *7*, 145-150.
- Rasmussen, K., Hsu, M.A., and Vandergriff, J. The selective mGlu2/3 receptor antagonist LY341495 exacerbates behavioral signs of morphine withdrawal and morphine-withdrawal-induced activation of locus coeruleus neurons. *Neuropharmacology* **2004**, *46*, 620-628.
- Reddy, Y.T., Reddy, P.N., Reddy, M.N., Rajitha, B., and Crooks, P.A. Convenient and scalable process for the preparation of bupropion hydrochloride *via* efficient bromination of *m*-chloropropiophenone with N-bromosuccinimide. *Synth. Commun.* **2010**, *40*, 1566-1573.
- Reichel, C.M., Murray, J.E., Grant, K.M., and Bevins, R.A. Bupropion attenuates methamphetamine self-administration in adult male rats. *Drug Alcohol Depend.* **2009**, *100*, 54-62.
- Reid, L.W., Elifson, K.W., and Sterk, C.E. Ecstasy and gateway drugs: Initiating the use of ecstasy and other drugs. *Ann. Epidemiol.* **2007**, *17*, 74-80.
- Reid, M.S., Mickalian, J.D., Delucchi, K.L., and Berger, S.P. A nicotine antagonist, mecamylamine, reduces cue-induced cocaine craving in cocaine-dependent subjects. *Neuropsychopharmacology* **1999**, *20*, 297-307.

- Reith, M.E., Berfield, J.L., Wang, L.C., Ferrer, J.V., and Javitch, J.A. The uptake inhibitors cocaine and benztropine differentially alter the conformation of the human dopamine transporter. *J. Biol. Chem.* **2001**, *276*, 29012-29018.
- Robinette, D., Neamati, N., Tomer, K.B., and Borchers, C.H. Photoaffinity labeling combined with mass spectrometric approaches as a tool for structural proteomics. *Expert Rev. Proteomics* **2006**, *3*, 399-408.
- Rocheville, M., and Garland, S.L. An industrial perspective on positive allosteric modulation as a means to discover safe and selective drugs. *Drug Discov. Today: Technol.* **2010**, *7*, E87-E94.
- Rodrigues, J.P. and Bonvin, A.M. Integrative computational modeling of protein interactions. *FEBS J.* **2014**, *281*, 1988-2003.
- Rorick-Kehn, L.M., Johnson, B.G., Burkey, J.L., Wright, R.A., Calligaro, D.O., Marek, G.J., Nisenbaum, E.S., Catlow, J.T., Kingston, A.E., Giera, D.D., Herin, M.F., Monn, J.A., McKinzie, D.L., and Schoepp, D.D. Pharmacological and pharmacokinetic properties of a structurally novel, potent, and selective metabotropic glutamate 2/3 receptor agonist: *in vitro* characterization of agonist (-)-(1R,4S,5S,6S)-4-amino-2-sulfonylbicyclo[3.1.0]-hexane-4,6-dicarboxylic acid (LY404039). *J. Pharmacol. Exp. Ther.* **2007**, *321*, 308-317.
- Rorick-Kehn, L.M., Johnson, B.G., Knitowski, K.M., Salhoff, C.R., Witkin, J.M., Perry, K.W., Griffey, K.I., Tizzano, J.P., Monn, J.A., McKinzie, D.L., and Schoepp, D.D. *In vivo* pharmacological characterization of the structurally novel, potent, selective mGlu2/3 receptor agonist LY404039 in animal models of psychiatric disorders. *Psychopharmacology* **2007**, *193*, 121-136.

- Rose, J.E., Behm, F.M., Westman, E.C., Levin, E.D., Stein, R.M., and Ripka, G.V. Mecamylamine combined with nicotine skin patch facilitates smoking cessation beyond nicotine patch treatment alone. *Clin. Pharmacol. Ther.* **1994**, *56*, 86-99.
- Rosenbaum, D.M., Rasmussen, S.G., and Kobilka, B.K. The structure and function of G-protein-coupled receptors. *Nature* **2009**, *459*, 356-363.
- Rostovtsev, V.V., Green, L.G., Fokin, V.V., and Sharpless, K.B. A stepwise Huisgen cycloaddition process: copper(I)-catalyzed regioselective "ligation" of azides and terminal alkynes. *Angew. Chem. Int. Ed. Engl.* **2002**, *41*, 2596-2599.
- Rothman, R.B., Baumann, M.H., Prisinzano, T.E., and Newman, A.H. Dopamine transport inhibitors based on GBR12909 and benztropine as potential medications to treat cocaine addiction. *Biochem. Pharmacol.* **2008**, *75*, 2-16.
- Rothman, R.B., Mele, A., Reid, A.A., Akunne, H., Greig, N., Thurkauf, A., Rice, K.C., and Pert, A. Tight binding dopamine reuptake inhibitors as cocaine antagonists. A strategy for drug development. *FEBS Lett* **1989**, *257*, 341-344.
- Rowe, B.A., Schaffhauser, H., Morales, S., Lubbers, L.S., Bonnefous, C., Kamenecka, T.M., McQuiston, J., and Daggett, L.P. Transposition of three amino acids transforms the human metabotropic glutamate receptor (mGluR)-3-positive allosteric modulation site to mGluR2, and additional characterization of the mGluR2-positive allosteric modulation site. *J. Pharmacol. Exp. Ther* **2008**, *326*, 240-251.
- Rucktooa, P., Haseler, C.A., van Elk, R., Smit, A.B., Gallagher, T., and Sixma, T.K. Structural characterization of binding mode of smoking cessation drugs to nicotinic acetylcholine receptors through study of ligand complexes with acetylcholine-binding protein. *J. Bio. Chem.* **2012**, *287*, 23283-23293.

- Rucktooa, P., Smit, A.B., and Sixma, T.K. Insight in nachr subtype selectivity from AChBP crystal structures. *Biochem. Pharmacol.* **2009**, *78*, 777-787.
- Rueping, M., and Hubener, L. Enantioselective synthesis of quinolizidines and indolizidines *via* a catalytic asymmetric hydrogenation cascade. *Synlett* **2011**, 1243-1246.
- Runyon, S.P. and Carroll, F.I. Dopamine transporter ligands: Recent developments and therapeutic potential. *Curr. Top. Med. Chem.* **2006**, *6*, 1825-1843.
- Saario, S.M., McKinney, M.K., Speers, A.E., Wang, C., and Cravatt, B.F. Clickable, photoreactive inhibitors to probe the active site microenvironment of fatty acid amide hydrolase. *Chem. Sci.* **2012**, *3*, 77-83.
- Sadaghiani, A.M., Verhelst, S.H.L, and Bogyo, M. Tagging and detecting strategies for activity-based proteomics. *Current Opinion in Chemical Biology* **2007**, *11*, 20-28.
- Saladino, A.C., Xu, Y., and Tang, P. Homology modeling and molecular dynamics simulations of transmembrane domain structure of human neuronal nicotinic acetylcholine receptor. *Biophysical Journal* **2005**, *88*, 1009-1017.
- Sallee, F.R., Fogel, E.L., Schwartz, E., Choi, S.M., Curran, D.P., and Niznik, H.B. Photoaffinity labeling of the mammalian dopamine transporter. *FEBS Lett.* **1989**, *256*, 219-224.
- Sanghvi, M., Hamouda, A.K., Jozwiak, K., Blanton, M.P., Trudell, J.R., and Arias, H.R. Identifying the binding site(s) for antidepressants on the Torpedo nicotinic acetylcholine receptor: [$^3$H]2-azidoimipramine photolabeling and molecular dynamics studies. *Biochemica et Biophysica Acta, Biomembranes* **2008**, *1778*, 2690-2699.

- Sasse, J., Pilhatsch, M., Weikert, B., and Bauer, M. The noradrenergic and dopaminergic antidepressant bupropion. Mechanism of action and clinical profile. *Arzeimitteltherapie* **2008**, *26*, 285-289.
- Sato, T., Shimada, Y., Nagasawa, N., Nakanishi, S., and Jingami, H. Amino acid mutagenesis of the ligand binding site and the dimer interface of the metabotropic glutamate receptor 1. Identification of crucial residues for setting the activated state. *J. Biol. Chem.* **2003**, *278*, 4314-4321.
- Saxon, E. and Bertozzi, C.R. Cell surface engineering by a modified Staudinger reaction. *Science* **2000**, *287*, 2007-2010.
- Schaffhauser, H., Rowe, B.A., Morales, S., Chavez-Noriega, L.E., Yin, R., Jachec, C., Rao, S.P., Bain, G., Pinkerton, A.B., Vernier, J.M., Bristow, L.J., Varney, M.A., and Daggett, L.P. Pharmacological characterization and identification of amino acids involved in the positive modulation of metabotropic glutamate receptor subtype 2. *Mol. Pharmacol.* **2003**, *64*, 798-810.
- Schep, L.J., Slaughter, R.J., and Beasley, D.M. The clinical toxicology of metamfetamine. *Clin. Toxicol.* **2010**, *48*, 675-694.
- Schmidt, H.D., and Pierce, R.C. Cocaine-induced neuroadaptations in glutamate transmission: Potential therapeutic targets for craving and addiction. *Ann. N. Y. Acad. Sci.* **2010**, *1187*, 35-75.
- Schmitt, K.C. and Reith, M.E. Regulation of the dopamine transporter: aspects relevant to psychostimulant drugs of abuse. *Ann. N.Y Acad. Sci.* **2010**, *1187*, 316-340.

- Schmitt, K.C., Rothman, R.B., and Reith, M.E. Nonclassical pharmacology of the dopamine transporter: Atypical inhibitors, allosteric modulators, and partial substrates. *J. Pharmacol. Exp. Ther.* **2013**, *346*, 2-10.
- Schmitt, K.C., Zhen, J., Kharkar, P., Mishra, M., Chen, N., Dutta, A.K., and Reith, M.E. Interaction of cocaine-, benztropine-, and GBR12909-like compounds with wild-type and mutant human dopamine transporters: Molecular features that differentially determine antagonist-binding properties. *J. Neurochem.* **2008**, *107*, 928-940.
- Schnapp, K.A., Poe, R., Leyva, E., Soundararajan, N., and Platz, M.S. Exploratory photochemistry of fluorinated aryl azides. Implications for the design of photoaffinity labeling reagents. *Bioconjugate Chem.* **1993**, *4*, 172-177.
- Schoepp, D.D., Jane, D.E., and Monn, J.A. Pharmacological agents acting at subtypes of metabotropic glutamate receptors. *Neuropharmacology* **1999**, *38*, 1431-1476.
- Schrock, A.K. and Schuster, G.B. Photochemistry of phenyl azide: chemical properties of the transient intermediates. *J. Am. Chem. Soc.* **1984**, *106*, 5228-5234.
- Seddik, A., Holy, M., Weissensteiner, R., Zdrazil, B., Sitte, H.H., and Ecker, G.F. Probing the selectivity of monoamine transporter substrates by means of molecular modeling. *Molecular Informatics* **2013**, *32*, 409-413.
- Severinsen, K., Koldsoe, H., Thorup, K.A.V., Schjoeth-Eskesen, C., Moeller, P.T., Wiborg, O., Jensen, H.H., Sinning, S., and Schioett, B. Binding of mazindol and analogs to the human serotonin and dopamine transporters. *Mol. Pharmacol.* **2014**, *85*, 208-217.
- Shi, L., Quick, M., Zhao, Y., Weinstein, H., and Javitch, J.A. The mechanism of a neurotransmitter:sodium symporter--inward release of $Na^+$ and substrate is triggered by substrate in a second binding site. *Mol. Cell.* **2008**, *30*, 667-677.

- Shiffman, S., Johnston, J.A., Khayrallah, M., Elash, C.A., Gwaltney, C.J., Paty, J.A., Gnys, M., Evoniuk, G., and DeVeaugh-Geiss, J. The effect of bupropion on nicotine craving and withdrawal. *Psychopharmacology* **2000**, *148*, 33-40.
- Shortle, D., DiMaio, D., and Nathans, D. Directed mutagenesis. *Annual Review of Genetics* **1981**, *15*, 265-294.
- Sidique, S., Dhanya, R.P., Sheffler, D.J., Nickols, H.H., Yang, L., Dahl, R., Mangravita-Novo, A., Smith, L.H., D'Souza, M.S., Semenova, S., Conn, P.J., Markou, A., and Cosford, N.D.P. Orally active metabotropic glutamate subtype 2 receptor positive allosteric modulators: structure–activity relationships and assessment in a rat model of nicotine dependence. *J. Med. Chem.* **2012**, *55*, 9434-9445.
- Simmler, L.D., Buser, T.A., Donzelli, M., Schramm, Y., Dieu, L.H., Huwyler, J., Chaboz, S., Hoener, M.C., and Liechti, M.E. Pharmacological characterization of designer cathinones in vitro. *Br. J. Pharmacol.* **2013**, *168*, 458-470.
- Simmler, L.D., Rickli, A., Hoener, M.C., and Liechti, M.E. Monoamine transporter and receptor interaction profiles of a new series of designer cathinones. *Neuropharmacology* **2013**, *79*, 152-160.
- Simmons, S.J., and Gould, T.J. Involvement of neuronal beta subunit-containing nicotinic acetylcholine receptors in nicotine reward and withdrawal: Implications for pharmacotherapies. *J. Clin. Pharm. Ther.* **2014**.
- Singh, A., Thornton, E.R., and Westheimer, F.H. The photolysis of diazoacetylchymotrypsin. *J. Biol. Chem.* **1962**, *237*, 3006-3008.
- Singh, S.K., Yamashita, A., and Gouaux, E. Antidepressant binding site in a bacterial homologue of neurotransmitter transporters. *Nature* **2007**, *448*, 952-956.

- Singh, S.K., Piscitelli, C.L., Yamashita, A., and Gouaux, E. A competitive inhibitor traps LeuT in an open-to-out conformation. *Science* **2008**, *322*, 1655-1661.
- Sitte, H.H., Huck, S., Reither, H., Boehm, S., Singer, E.A., and Pifl, C. Carrier-mediated release, transport rates, and charge transfer induced by amphetamine, tyramine, and dopamine in mammalian cells transfected with the human dopamine transporter. *J. Neurochem.* **1998**, *71*, 1289-1297.
- Sletten, E.M. and Bertozzi, C.R. Bioorthogonal chemistry: fishing for selectivity in a sea of functionality. *Angew. Chem. Int. Ed. Engl.* **2009**, *48*, 6974-6998.
- Sliwoski, G., Kothiwale, S., Meiler, J., and Lowe, E.W. Computational methods in drug discovery. *Pharmacol. Rev.* **2013**, *66*, 334-395.
- Smith, N.J., Bennett, K.A., and Milligan, G. When simple agonism is not enough: Emerging modalities of GPCR ligands. *Mol. Cell. Endocrinol.* **2011**, *331*, 241-247.
- Sonders, M.S., Zhu, S.J., Zahniser, N.R., Kavanaugh, M.P., and Amara, S.G. Multiple ionic conductances of the human dopamine transporter: the actions of dopamine and psychostimulants. *J. Neurosci.* **1997**, *17*, 960-974.
- Speers, A.E., Adam, G.C., and Cravatt, B.F. Activity-based protein profiling in vivo using a copper(I)-catalyzed azide-alkyne [3+2] cycloaddition. *J. Am. Chem. Soc.* **2003**, *125*, 4686-4687.
- Srivastava, S., Hamouda, A.K., Pandhare, A., Duddempudi, P.K., Sanghvi, M., Cohen, J.B., and Blanton, M.P. [$^3$H]-Epibatidine photolabels non-equivalent amino acids in the agonist binding site of Torpedo and $\alpha4\beta2$ nicotinic acetylcholine receptors. *J. Biol. Chem.* **2009**, *284*, 24939-24947.

- Stahl, S.M., Pradko, J.F., Haight, B.R., Modell, J.G., Rockett, C.B., and Learned-Coughlin, S. A review of the neuropharmacology of bupropion, a dual norepinephrine and dopamine reuptake inhibitor. *Prim. Care Companion. J. Clin. Psychiatry* **2004**, *6*, 159.
- Stockner, T., Montgomery, T.R., Kudlacek, O., Weissensteiner, R., Ecker, G.F., Freissmuth, M., and Sitte, H.H. Mutational analysis of the high-affinity zinc binding site validates a refined human dopamine transporter homology model. *PLoS Comput. Biol.* **2013**, *9*, e1002909.
- Sulzer, D., Chen, T., Lau, Y., Kristensen, H., Rayport, S., and Ewing, A. Amphetamine redistributes dopamine from synaptic vesicles to the cytosol and promotes reverse transport. *J. Neurosci.* **1995**, *15*, 4102-4108.
- Sulzer, D., Sonders, M.S., Poulsen, N.W., and Galli, A. Mechanisms of neurotransmitter release by amphetamines: a review. *Prog. Neurobiol.* **2005**, *75*, 406-433.
- Sumranjit, J. and Chung, S.J. Recent advances in target characterization and identification by photoaffinity probes. *Molecules* **2013**, *18*, 10425-10451.
- Tantama, M., Lin, W.C., and Licht, S. An activity-based protein profiling probe for the nicotinic acetylcholine receptor. *J. Am. Chem. Soc.* **2008**, *130*, 15766-15767.
- Tella, S.R., Ladenheim, B., Andrews, A.M., Goldberg, S.R., and Cadet, J.L. Differential reinforcing effects of cocaine and GBR-12909: Biochemical evidence for divergent neuroadaptive changes in the mesolimbic dopaminergic system. *J. Neurosci.* **1996**, *16*, 7416-7427.
- Tomohiro, T., Morimoto, S., and Hatanaka, Y. Efficient capture, release, and detection of target protein by scissile photoaffinity biotinylation. *Photomedicine and Photobiology* **2012**, *34*, 15-16.

- Tong, E.K., Carmody, T.P., and Simon, J.A. Bupropion for smoking cessation: A review. *Compr. Ther.* **2006**, *32*, 26-33.
- Torres, G.E., Gainetdinov, R.R., and Caron, M.G. Plasma membrane monoamine transporters: Structure, regulation and function. *Nature Rev. Neurosci.* **2003**, *4*, 13-25.
- Trabanco, A.A. and Cid, J.M. mGluR2 postitive allosteric modulators (PAMs): a patent review (2009-present). *Expert Opin. Ther. Patents* **2013**, *23*, 629-647.
- Trabanco, A.A., Cid, J.M., Lavreysen, H., Macdonald, G.J., and Tresadern, G. Progress in the developement of positive allosteric modulators of the metabotropic glutamate receptor 2. *Curr. Med. Chem.* **2011**, *18*, 47-68.
- Tritsch, N.X. and Sabatini, B.L. Dopaminergic modulation of synaptic transmission in cortex and striatum. *Neuron* **2012**, *76*, 33-50.
- Tsuchiya, D., Kunishima, N., Kamiya, N., Jingami, H., and Morikawa, K. Structural views of the ligand-binding cores of a metabotropic glutamate receptor complexed with an antagonist and both glutamate and $Gd^{3+}$. *Proc. Natl. Acad. Sci. U S A* **2002**, *99*, 2660-2665.
- Uhl, G.R. and Lin, Z. The top 20 dopamine transporter mutants: Structure-function relationships and cocaine actions. *Eur. J. Pharmacol.* **2003**, *479*, 71-82.
- Ukairo, O.T., Bondi, C.D., Newman, A.H., Kulkarni, S.S., Kozikowski, A.P., Pan, S., and Surratt, C.K. Recognition of benztropine by the dopamine transporter (DAT) differs from that of the classical dopamine uptake inhibitors cocaine, methylphenidate, and mazindol as a function of a DAT transmembrane 1 aspartic acid residue. *J. Pharmacol. Exp. Ther.* **2005**, *314*, 575-583.

- Unwin, N. Refined structure of the nicotinic acetylcholine receptor at 4Å resolution. *J. Mol. Biol.* **2005**, *346*, 967-989.
- Unwin, N., and Fujiyoshi, Y. Gating movement of acetylcholine receptor caught by plunge-freezing. *J. Mol. Biol.* **2012**, *422*, 617-634.
- Uys, J.D., and Reissner, K.J. Glutamatergic neuroplasticity in cocaine addiction. *Prog. Mol. Biol. Transl. Sci.* **2011**, *98*, 367-400.
- Vaidya, A.S., Karumudi, B., Mendonca, E., Madriaga, A., Abdelkarim, H., van Breemen, R.B., and Petukhov, P.A. Design, synthesis, modeling, biological evaluation and photoaffinity labeling studies of novel series of photoreactive benzamide probes for histone deacetylase 2. *Bioorg. Med. Chem. Lett.* **2012**, *22*, 5025-5030.
- Van de Bittner, G.C., Bertozzi, C.R., and Chang, C.J. Strategy for dual-analyte luciferin imaging: *In vivo* bioluminescence detection of hydrogen peroxide and caspase activity in a murine model of acute inflammation. *J. Am. Chem. Soc.* **2013**, *135*, 1783-1795.
- van Scherpenzeel, M., Moret, E.E., Ballell, L., Liskamp, R.M., Nilsson, U.J., Leffler, H., and Pieters, R.J. Synthesis and evaluation of new thiodigalactoside-based chemical probes to label Galectin-3. *ChemBioChem* **2009**, *10*, 1724-1733.
- van Scherpenzeel, M., van den Berg, R.J., Donker-Koopman, W.E., Liskamp, R.M., Aerts, J.M., Overkleeft, H.S., and Pieters, R.J. Nanomolar affinity, iminosugar-based chemical probes for specific labeling of lysosomal glucocerebrosidase. *Bioorg. Med. Chem.* **2010**, *18*, 267-273.
- Vandergriff, J., and Rasmussen, K. The selective mGlu2/3 receptor agonist LY354740 attenuates morphine-withdrawal-induced activation of locus coeruleus neurons and behavioral signs of morphine withdrawal. *Neuropharmacology* **1999**, *38*, 217-222.

- Vaughan, R.A. Cocaine and GBR photoaffinity labels as probes of dopamine transporter structure. *Methods Enzymol.* **1998**, *296*, 219-230.
- Vaughan, R.A. and Foster, J.D. Mechanisms of dopamine transporter regulation in normal and disease states. *Trends in Pharmacological Sciences* **2013**, *34*, 489-496.
- Vaughan, R.A. and Kuhar, M.J. Dopamine transporter ligand binding domains. Structural and functional properties revealed by limited proteolysis. *J. Biol. Chem.* **1996**, *271*, 21672-21680.
- Vaughan, R.A., Agoston, G.E., Lever, J.R., and Newman, A.H. Differential binding of tropane-based photoaffinity ligands on the dopamine transporter. *J. Neurosci.* **1999**, *19*, 630-636.
- Vaughan, R.A., Gaffaney, J.D., Lever, J.R., Reith, M.E.A., and Dutta, A.K. Dual incorporation of photoaffinity ligands on dopamine transporters implicates proximity of labeled domains. *Mol. Pharmacol.* **2001**, *59*, 1157-1164.
- Vaughan, R.A., Parnas, M.L., Gaffaney, J.D., Lowe, M.J., Wirtz, S., Pham, A., Reed, B., Dutta, S.M., Murray, K.K., and Justice, J.B. Affinity labeling the dopamine transporter ligand binding site. *J. Neurosci. Methods* **2005**, *143*, 33-40.
- Vaughan, R.A., Sakrikar, D.S., Parnas, M.L., Adkins, S., Foster, J.D., Duval, R.A., Lever, J.R., Kulkarni, S.S., and Hauck-Newman, A. Localization of cocaine analog [$^{125}$I]RTI 82 irreversible binding to transmembrane domain 6 of the dopamine transporter. *J. Biol. Chem.* **2007**, *282*, 8915-8925.
- Vervacke, J.S., Funk, A.L., Wang, Y., Strom, M., Hrycyna, C.A., and Distefano, M.D. Diazirine-containing photoactivatable isoprenoid: synthesis and application in studies with isoprenylcysteine carboxyl methyltransferase. *J. Org. Chem.* **2014**, *79*, 1971-1978.

- Vodovozova, E.L. Photoaffinity labeling and its application in structural biology. *Biochemistry (Moscow)* **2007**, *72*, 1-20.
- Volz, T.J., and Schenk, J.O. A comprehensive atlas of the topography of functional groups of the dopamine transporter. *Synapse* **2005**, *58*, 72-94.
- Watterson, L.R., Kufahl, P.R., Nemirovsky, N.E., Sewalia, K., Grabenauer, M., Thomas, B.F., Marusich, J.A., Wegner, S., and Olive, M.F. Potent rewarding and reinforcing effects of the synthetic cathinone 3,4-methylenedioxypyrovalerone (MDPV). *Addict. Biol.* **2014**, *19*, 165-174.
- Wee, S., Carroll, F.I., and Woolverton, W.L. A reduced rate of in vivo dopamine transporter binding is associated with lower relative reinforcing efficacy of stimulants. *Neuropsychopharmacology* **2006**, *31*, 351-362.
- West, R., Baker, C.L., Cappelleri, J.C., and Bushmakin, A.G. Effect of varenicline and bupropion SR on craving, nicotine withdrawal symptoms, and rewarding effects of smoking during a quit attempt. *Psychopharmacology* **2008**, *197*, 371-377.
- Woltersdorf, O.W., deSolms, S.J., Schultz, E.M., and Cragoe, E.J. (Acylaryloxy)acetic acid diuretics. 1. (2-Alkyl- and 2,2-dialkyl-1-oxo-5-indanyloxy)acetic acids. *J. Med. Chem.* **1977**, *20*, 1400-1408.
- Wood, M.R., Hopkins, C.R., Brogan, J.T., Conn, P.J., and Lindsley, C.W. "Molecular switches" on mGluR allosteric ligands that modulate modes of pharmacology. *Biochemistry* **2011**, *50*, 2403-2410.
- Woolverton, W.L. and Johnson, K.M. Neurobiology of cocaine abuse. *Trends Pharmacol. Sci.* **1992**, *13*, 193-200.

- Woolverton, W.L., Rowlett, J.K., Wilcox, K.M., Paul, I.A., Kline, R.H., Newman, A.H., and Katz, J.L. 3'-and 4'-chloro-substituted analogs of benztropine: Intravenous self-administration and in vitro radioligand binding studies in rhesus monkeys. *Psychopharmacology* **2000**, *147*, 426-435.
- Wright, R.A., Arnold, M.B., Wheeler, W.J., Ornstein, P.L., and Schoepp, D.D. [$^3$H]LY341495 binding to group II metabotropic glutamate receptors in rat brain. *J. Pharmacol. Exp. Ther.* **2001**, *298*, 453-460.
- Wu, H., Wang, C., Gregory, K.J., Han, G.W., Cho, H.P., Xia, Y., Niswender, C.M., Katritch, V., Meiler, J., and Cherezov, V. Structure of a class C GPCR metabotropic glutamate receptor 1 bound to an allosteric modulator. *Science* **2014**, *344*, 58-64.
- Wu, X. and Gu, H.H. Cocaine affinity decreased by mutations of aromatic residue phenylalanine 105 in the transmembrane domain 2 of dopamine transporter. *Mol. Pharmacol.* **2003**, *63*, 653-658.
- Xie, X., and Steketee, J.D. Effects of repeated exposure to cocaine on group II metabotropic glutamate receptor function in the rat medial prefrontal cortex: Behavioral and neurochemical studies. *Psychopharmacology* **2009**, *203*, 501-510.
- Xie, X., and Steketee, J.D. Repeated exposure to cocaine alters the modulation of mesocorticolimbic glutamate transmission by medial prefrontal cortex group II metabotropic glutamate receptors. *J. Neurochem.* **2008**, *107*, 186-196.
- Yamashita, A., Singh, S.K., Kawate, T., Jin, Y., and Gouaux, E. Crystal structure of a bacterial homologue of $Na^+/Cl^-$-dependent neurotransmitter transporters. *Nature* **2005**, *437*, 215-223.

- Yeniceli, D., Sener, E., Korkmaz, O.T., Dogrukol-Ak, D., and Tuncel, N. A simple and sensitive LC-ESI-MS (ion trap) method for the determination of bupropion and its major metabolite, hydroxybupropion in rat plasma and brain microdialysates. *Talanta* **2011**, *84*, 19-26.
- Zawilska, J.B. and Wojcieszak, J. Designer cathinones - an emerging class of novel recreational drugs. *Forensic Sci. Int.* **2013**, *231*, 42-53.
- Zhang, N., Tomizawa, M., and Casida, J.E. 5-Azidoepibatidine: an exceptionally potent photoaffinity ligand for neuronal $\alpha4\beta2$ and $\alpha7$ nicotinic acetylcholine receptors. *Bioorg. Med. Chem. Lett.* **2003**, *13*, 525-527.
- Zhao, C. and Noskov, S.Y. The role of local hydration and hydrogen-bonding dynamics in ion and solute release from ion-coupled secondary transporters. *Biochemistry* **2011**, *50*, 1848-1856.
- Zhao, Y., Dayas, C.V., Aujla, H., Baptista, M.A., Martin-Fardon, R., and Weiss, F. Activation of group II metabotropic glutamate receptors attenuates both stress and cue-induced ethanol-seeking and modulates c-FOS expression in the hippocampus and amygdala. *J. Neurosci.* **2006**, *26*, 9967-9974.
- Zhao, Y., Terry, D., Shi, L., Weinstein, H., Blanchard, S.C., and Javitch, J.A. Single-molecule dynamics of gating in a neurotransmitter transporter homologue. *Nature* **2010**, *465*, 188-193.
- Zhao, Y., Terry, D.S., Shi, L., Quick, M., Weinstein, H., Blanchard, S.C., and Javitch, J.A. Substrate-modulated gating dynamics in a $Na^+$-coupled neurotransmitter transporter homologue. *Nature* **2011**, *474*, 109-113.

- Zhou, Z., Zhen, J., Karpowich, N.K., Goetz, R.M., Law, C.J., Reith, M.E., and Wang, D.N. LeuT-desipramine structure reveals how antidepressants block neurotransmitter reuptake. *Science* **2007**, *317*, 1390-1393.
- Zhou, Z., Zhen, J., Karpowich, N.K., Law, C.J., Reith, M.E., and Wang, D.N. Antidepressant specificity of serotonin transporter suggested by three LeuT-SSRI structures. *Nat. Struct. Mol. Biol.* **2009**, *16*, 652-657.
- Zhu, A.Z., Cox, L.S., Nollen, N., Faseru, B., Okuyemi, K.S., Ahluwalia, J.S., Benowitz, N.L., and Tyndale, R.F. CYP2B6 and bupropion's smoking-cessation pharmacology: the role of hydroxybupropion. *Clin. Pharmacol. Ther.* **2012**, *92*, 771-777.
- Zhu, J. and Reith, M.E. Role of the dopamine transporter in the action of psychostimulants, nicotine, and other drugs of abuse. *CNS Neurol. Disord. Drug Targets* **2008**, *7*, 393-409.
- Zimmerman, J.L. Cocaine intoxication. *Crit. Care Clin.* **2012**, *28*, 517-526.
- Zou, M.F., Kopajtic, T., Katz, J.L., Wirtz, S., Justice, J.B., and Newman, A.H. Novel tropane-based irreversible ligands for the dopamine transporter. *J. Med. Chem.* **2001**, *44*, 4453-4461.
- Zou, M., Kopajtic, T., Katz, J.L., and Newman, A.H. Structure-activity relationship comparison of (*S*)-2β-substituted 3α-(bis[4-fluorophenyl]methoxy)tropanes and (*R*)-2β-substituted 3β-(3,4-dichlorophenyl)tropanes at the dopamine transporter. *J. Med. Chem.* **2003**, *46*, 2908-2916.

## APPENDIX

### A.1. Radiosynthesis, Pharmacological Evaluation, and Photoaffinity Labeling Experiments of Racemic 4-Azido-3-Iodo-Pyrovalerone ((±)-[$^{125}$I]-4.16) for DAT Structure-Function Studies

With the novel pyrovalerone derivatives aniline (±)-**5.6**, 4-amino-3-iodo (±)-**5.7** and 4-azido-3-iodo (±)-**4.16** in hand (see Section 5.1), ligand affinities ($K_i$ values) were determined for inhibition of [$^3$H]-WIN-35,428 (**1.15**) binding and [$^3$H]-dopamine uptake inhibition in hDAT expressed in N2A neuroblastoma cells by Dr. Christopher Surratt's group (Duquesne University). Although the DAT affinity of target photoprobe (±)-**4.16** (hDAT $K_i$ = 78 ± 18 nM) was 10-folds less than pyrovalerone (±)-**1.19** (hDAT $K_i$ = 8 ± 2 nM) (Table A.1), it was still in an acceptable pharmacological range of pyrovalerone, which justified its further development into a potential DAT photoaffinity probe.

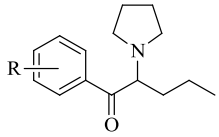


| Compound No. | Aromatic substituent (R) | [$^3$H]-WIN binding inhibition $K_i$ (nM) | [$^3$H]-DA reuptake inhibition $IC_{50}$ (nM) |
|---|---|---|---|
| **(±)-4.16** | 4-$N_3$-3-I | 78 ± 18 | 264 ± 78 |
| **(±)-5.6** | 4-$NH_2$ | 5 ± 1 | 7 ± 2 |
| **(±)-5.7** | 4-$NH_2$-3-I | 28 ± 8 | 175 ± 59 |

Each $K_i$ and $IC_{50}$ value represents data from at least three independent experiments with each data point on the curve performed in duplicate.

**Table A.1.** Inhibition of [$^3$H]-WIN 35,428 binding and [$^3$H]-dopamine reuptake of pyrovalerone-based compounds at hDAT N2A neuroblastoma cells (Lapinsky *et al.*, 2009).

Given that wash-resistant binding experiments on non-radioactive azido-containing compounds frequently give false positives in the assessment of covalent attachment (Agoston *et al.*, 1997), a radio-iodinated [$^{125}$I] version of **(±)-4.16** was pursued to determine if photoactivation could produce covalent ligation to the hDAT protein. In this regard, **(±)-[$^{125}$I]-**

**4.16** was synthesized by Dr John Lever (University of Missouri-Columbia) *via* electrophilic radioiodination of aniline **(±)-4.16** with [$^{125}$I]-NaI (1.67 mCi) under no-carrier-added conditions using Chloramine-T (*N*-chloro-4-toluenesulfonamide trihydrate) as an oxidant, followed by diazotization and subsequent treatment with $NaN_3$ (Scheme A.1). Reversed-phase HPLC purification provided the final photoprobe **(±)-[$^{125}$I]-4.16** in 20% isolated yield with high purity (>99%) and high specific activity (1946 mCi/lmol).

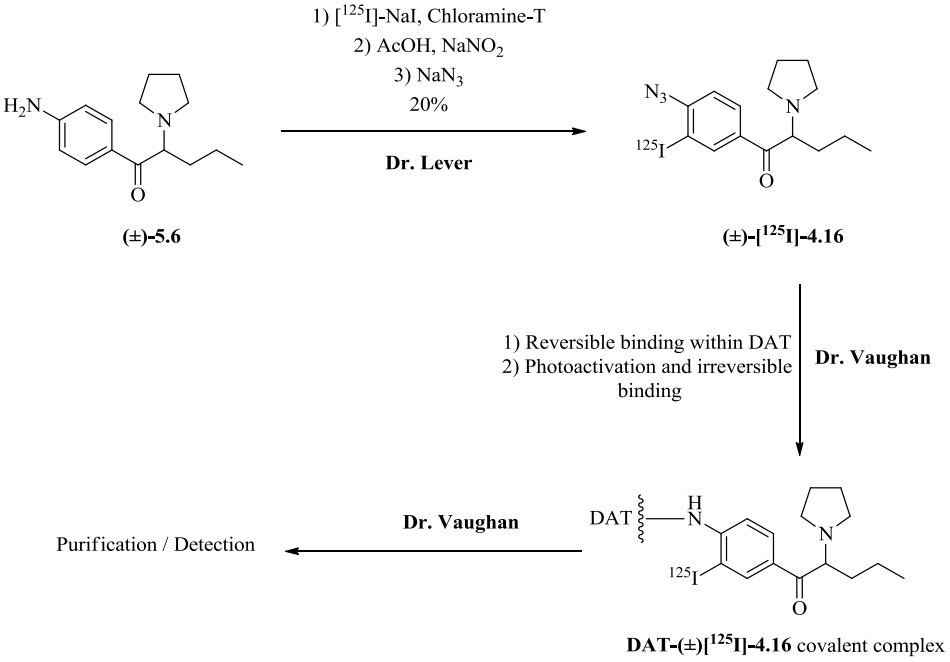


**Scheme A.1.** Radioiodination and DAT covalent ligation of pyrovalerone-based photoprobe **(±)-[$^{125}$I]-4.16** (Lapinsky *et al*., 2009).

With radioactive photoprobe **(±)-[$^{125}$I]-4.16** in hand, Dr Roxanne A. Vaughan's group (University of North Dakota) conducted preliminary photoaffinity labeling experiments with the DAT. In particular, LLC-PK$_1$ cells expressing rat DAT and HEK 293 cells expressing 6Xhis-human DAT were incubated with **(±)-[$^{125}$I]-4.16** in the absence or presence of 100 μM cocaine. Cells were then irradiated with 254 nm UV light for 45 seconds to photoactivate the azido group and allow irreversible binding of the probe to DAT. Next, the cells were solubilized and then

sequentially subjected to immunoprecipitation, SDS-PAGE and autoradiography. The isolated ~80 kDa labeled proteins clearly demonstrated the photoincorporation of **(±)-[$^{125}$I]-4.16** into DAT that was blocked by cocaine (see Figure A.1). This demonstrated that **(±)-[$^{125}$I]-4.16** specifically labeled DAT as opposed to a nonspecific cell binding site.

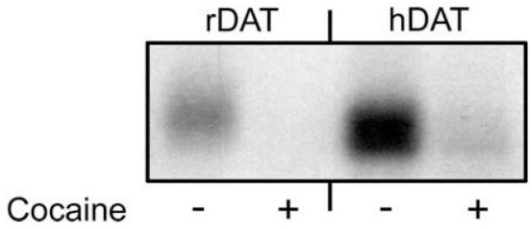


**Figure A.1.** Photoaffinity labeling of rat and human DAT with **(±)-[$^{125}$I]-4.16** performed by the Vaughan group. Cells expressing rDAT or 6X-his-hDAT were photoaffinity labeled with **(±)-[$^{125}$I]-4.16** in the absence or presence of 100 μM (-)-cocaine. Cells were solubilized and DATs were immunoprecipitated with DAT antibody 16 (rDAT) or anti-his antibody (hDAT) followed by SDS–PAGE and autoradiography (Lapinsky *et al*., 2009. Reprinted with permission from *Bioorg. Med. Chem.* **2009**, *17*, 3770-3774. Copyright 2009, Elsevier)

In conclusion, **(±)-[$^{125}$I]-4.16** represents the first successful example of a non-tropane DAT photoaffinity ligand based on pyrovalerone **(±)-4.16** with the photoaffinity labeling group directly on the inhibitor pharmacophore, thus representing an important contribution to the arsenal of chemical probes useful for characterizing DAT function and 3-D structure. This work has been published in Lapinsky *et al.*, 2009.

## A.2. Radiosynthesis, Pharmacological Evaluation and Photoaffinity Labeling Experiments of Racemic 4-Azido-3-Iodo-Bupropion ((±)-[$^{125}$I]-4.20) for DAT and nAChR Structure-Function Studies

With bupropion probe **(±)-4.20** in hand, preliminary DAT ligand affinity was determined by Dr. Surratt's group *via* inhibition of [$^{3}$H]-WIN-35,428 binding to hDAT in N2A neuroblastoma cells (Lapinsky *et al*., 2012). Given the DAT affinity of bupropion-based photoprobe **(±)-4.20** (hDAT $K_i$ = 3071 ± 497 nM) was seven-fold lower than bupropion **(±)-1.20**

(hDAT $K_i$ = 441 ± 174 nM), but still bioactive within the range of bupropion, this justified further photoaffinity labeling experimentation. Synthesized aniline **(±)-5.31** (see Section 5.2.1) was utilized by Dr. John Lever to prepare a radioactive version of probe **(±)-4.20** (Scheme A.2) for photoaffinity labeling studies within hDAT and selected nAChRs using methodology previously described (Section A.1, Scheme A.1). Briefly, aniline **(±)-5.31** was subjected to electrophilic radioiodination with [$^{125}$I]-NaI (1.67 mCi) under no-carrier-added conditions using Chloramine-T (*N*-chloro-4-toluenesulfonamide trihydrate) as oxidant, followed by diazotization and subsequent treatment with $NaN_3$ (Scheme A.2). Final reversed-phase HPLC isolation provided **(±)-[$^{125}$I]-4.20** in 65% yield with high purity (> 99%) and high specific activity (2057 mCi/lmol). The radioligand also exhibited a chromatographic profile identical to that of its non-radioactive version.

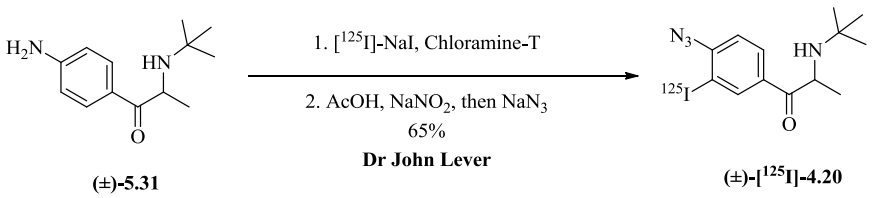


**Scheme A.2.** Synthesis of radio-iodinated photoprobe **(±)-[$^{125}$I]-4.20** by Dr. John Lever (Lapinsky *et al.*, 2012)

To determine if the DAT underwent irreversible labeling with **(±)-[$^{125}$I]-4.20**, Dr Roxanne Vaughan's group used LLCPK1 cells expressing 6Xhis-hDAT for photoaffinity labeling with **(±)-[$^{125}$I]-4.20** in the absence or presence of 10 μM or 100 μM (±)-bupropion or (-)-cocaine (Figure A.2). Labeled cells were then detergent-solubilized and the lysates were immunoprecipitated and analyzed by SDS–PAGE/autoradiography. Labeled proteins of ~80 kDa were obtained from LLCPK1 hDAT cells (Figure A.2), thus demonstrating incorporation of **(±)-[$^{125}$I]-4.20** into the DAT. Incorporation of the ligand was blocked by 40–70% by either (±)-

bupropion or (-)-cocaine in a dose-dependent manner, demonstrating the appropriate pharmacological specificity of **(±)-[$^{125}$I]-4.20** attachment to the DAT (Figure A.2).

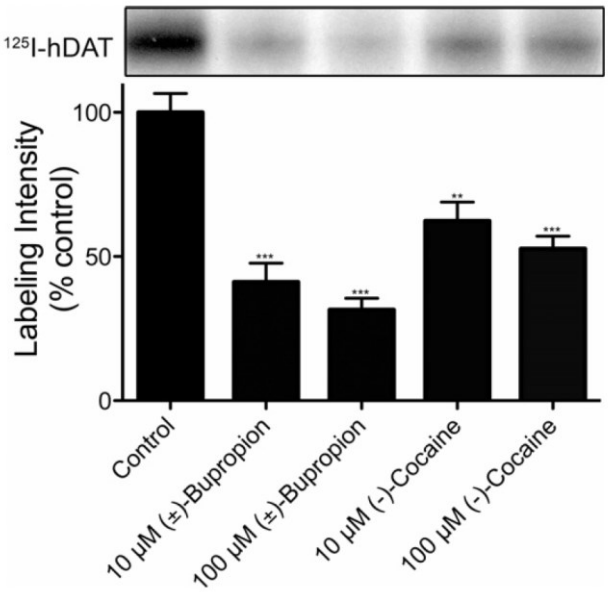


**Figure A.2.** Photoaffinity labeling of hDAT with **(±)-[$^{125}$I]-4.20** performed by the Vaughan group. LLCPK1 cells expressing 6Xhis-hDAT were photoaffinity labeled with 10 nM (±)-[$^{125}$I]-**4.20** in the absence or presence of 10 or 100 μM (±)-bupropion or (-)-cocaine. Cells were solubilized and DATs were immunoprecipitated followed by analysis by SDS–PAGE and autoradiography. The relevant portion of a representative autoradiograph is pictured followed by a histogram that quantitates relative band intensities (means ± SE of three independent experiments; ***P < 0.0001 versus control; **P < 0.001 versus control). (Lapinsky *et al*., 2012. Reprinted with permission from *Bioorg. Med. Chem. Lett.* **2012**, *22*, 523-526. Copyright 2012, Elsevier)

Similarly, nAChR pharmacology and photoaffinity labeling experiments were also performed with photoprobe **(±)-[$^{125}$I]-4.20** (Figure A.3). In this regard, Dr. Hugo Arias's group at California Northstate University demonstrated that BP inhibited **(±)-[$^{125}$I]-4.20** binding to human α4β2 nAChRs expressed in HEK cells with an $IC_{50}$ value of 8.3 μM (Arias *et al*., 2012), a value consistent with those previously reported (Arias, 2010). In addition, binding affinity of **(±)-4.20** in *Torpedo* nAChRs was studied in different conformational states in radioligand binding assays. In this regard, *Torpedo* nAChR-rich membranes were incubated with 15 nM [$^3$H]-TCP in the presence of 1 μM α-bungarotoxin (α-BTx) (resting/α-BTx-bound state) or of 1 mM CCh (desensitized/CCh-bound state) with increasing concentrations of **(±)-4.20** or BP.

Probe **(±)-4.20** demonstrated 100% inhibition of the specific binding of [$^3$H]-TCP in a concentration-dependent fashion in either the desensitized or resting state, as was observed for BP (Figure A.3).

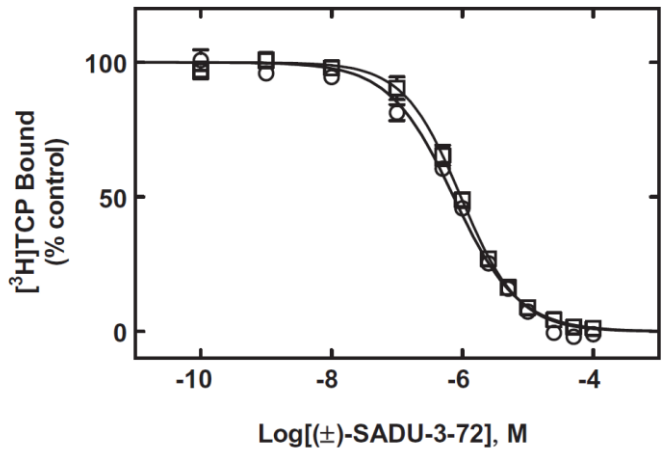


**Figure A.3.** (±)-SADU-3-72-induced inhibition of [$^3$H]-TCP binding to *Torpedo* AChRs in different conformational states performed by the Arias group (Arias *et al.* 2012). *Torpedo* AChR native membranes (0.3 μM) were equilibrated (2 h) with 15 nM [$^3$H]-TCP, in the presence of 1 μM α-BTx (○) (resting/α-BTx-bound state) or 1 mM CCh (□) (desensitized/CCh-bound state), and increasing concentrations of (±)-SADU-3-72. (Arias *et al*., 2012. Reprinted with permission from *Neurochem. Int.* **2012**, *61*, 1433-1441. Copyright 2012, Elsevier)

Furthermore, Dr. Michael Blanton's group at Texas Tech University Health Sciences Center performed photoaffinity labeling studies wherein affinity-purified and lipid-reincorporated (DOPC/DOPA/CH-3:1:1) human α4β2 neuronal nAChRs (~ 45 μg) were photolabeled with 78 nM **(±)-[$^{125}$I]-4.20** at 365 nm UV light in the absence or presence of 160 μM (±)-bupropion. The photolabeled polypeptides were then gel-fractionated, visualized by Coomassie Blue staining, and processed for autoradiography (Figure A.4). Significant reduction in **(±)-[$^{125}$I]-4.20** labeling in the presence of an excess of (±)-bupropion was observed, which proved that **(±)-[$^{125}$I]-4.20** specifically photoincorporated into neuronal α4β2 nAChRs (Figure A.4).

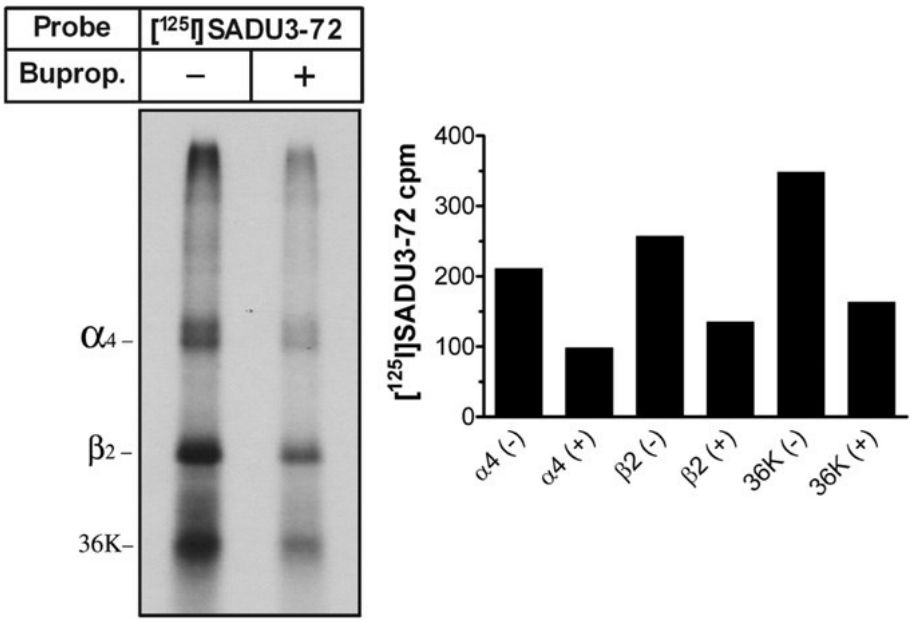


**Figure A.4.** Photoincorporation of **(±)-[$^{125}$I]-4.20** ((±)-[$^{125}$I]-SADU-3-72) into human α4β2 neuronal nAChR performed by Dr. Michael Blanton's group. UV irradiation at 365 nM proceeded for 10 min. Left panel, autoradiograph of an 8% SDS–polyacrylamide gel (1-week exposure) showing (±)-[$^{125}$I]-**4.20** photoincorporation into the α4 and β2 subunits, and into a ~36 kDa proteolytic fragment of the β2 subunit, in the absence (-) or presence (+) of 160 μM (±)-bupropion. Right panel, (±)-[$^{125}$I]-**4.20** photoincorporation of each band was quantified by gamma counting where inclusion (+) of (±)-bupropion (160 μM) inhibited labeling of each band by ~50%. ). (Lapinsky *et al*., 2012. Reprinted with permission from *Bioorg. Med. Chem. Lett.* **2012**, *22*, 523-526. Copyright 2012, Elsevier)

With the successful outcome of **(±)-[$^{125}$I]-4.20** in a macrolevel photoaffinity labeling experiment, Dr. Blanton's group performed the microlevel analysis of photoincorporation of **(±)-[$^{125}$I]-4.20** within the T*orpedo* nAChR. The photoincorporation of **(±)-[$^{125}$I]-4.20** was characterized in the resting and desensitized states of *Torpedo* nAChR. Briefly, *Torpedo* nAChR-rich membranes were photolabeled with 1.5 nM **(±)-[$^{125}$I]-4.20** in the presence of 5μM α-bungarotoxin (α-BgTx; nAChR competitive antagonist that stabilizes the resting state) or 400 μM carbamylcholine (Carb; nAChR agonist that stabilizes the desensitized state), followed by the separation of nAChR subunits *via* SDS-PAGE with autoradiograph monitoring. SDS-PAGE autoradiograph showed photoincorporation into each nAChR subunit which was inhibited by tetracaine (a resting state selective channel blocker) in nAChR resting state (+α-BgTx). In the

nAChR desensitized state (+Carb), photolabeling in nAChR subunits was reduced as compared to resting state, except in the α subunit. In the nAChR desensitized state, TCP inhibited **(±)-[$^{125}$I]-4.20** photolabeling in the γ- and δ-subunits by ~35%, while photolabeling in the α-subunit was increased by ~15%, and β-subunit labeling was unchanged (see Figure A.5). In addition, bupropion also inhibited the extent of **(±)-[$^{125}$I]-4.20** photolabeling with high affinity in the desensitized state and with lower affinity in the resting state.

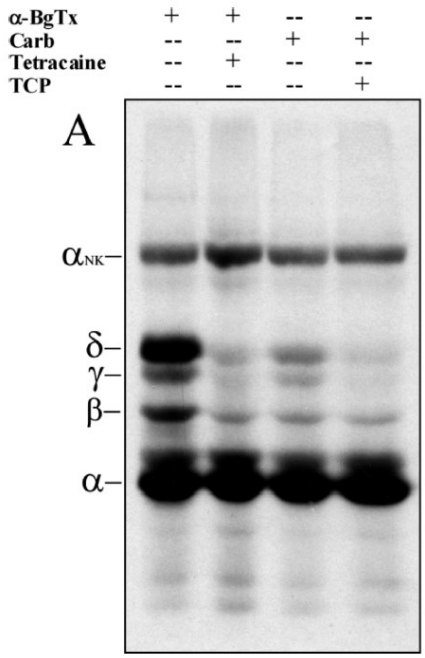


**Figure A.5.** Photoincorporation of [$^{125}$I]-SADU-3-72 (**(±)-[$^{125}$I]-4.20**) into the *Torpedo* nAChR in the absence and the presence of Carb performed by Dr Blanton's group. An autoradiograph (12−24 h exposure with intensifying screen) of an 8% SDS-PAGE gel containing native *Torpedo* nAChR-rich membranes photolabeled with [$^{125}$I]-SADU-3-72 in the absence (−) and/or the presence (+) of the agonist Carbamylcholine (Carb), the competitive antagonist α-bungarotoxin (αBgTx), the resting state-selective channel blocker tetracaine, or the desensitized state-selective channel blocker thienycyclohexylpiperidine (TCP). The migration of individual nAChR subunits and the alpha subunit of Na/K ATPase (αNK) is also indicated as a control. (Pandhare *et al.*, 2012, Reprinted with permission from *Biochemistry* **2012**, *51*, 2425-2435. Copyright 2012 ACS Publications).

To determine the exact location of **(±)-[$^{125}$I]-4.20** labeling, the labeled subunit fragments were isolated from the SDS-PAGE electrophoresis gel with limited digestion by *S. aureus* V8 protease. The isolated subunit fragments were further treated with trypsin for 5 days at room temperature. The digested material was then resolved *via* Tricine SDS-PAGE gel

electrophoresis and the radiolabeled fragments were then purified by reversed-phase HPLC. Furthermore, the amino acid sequence analysis of *Torpedo* nAChR subunit fragments was performed *via* Edman degradation. These experiments identified two distinct **(±)-[$^{125}$I]-4.20**/bupropion binding sites in the *Torpedo* nAChR (Figure A.6). The results showed that one site is at the middle of the *Torpedo* nAChR ion channel (M2-9) where **(±)-4.20**/bupropion binds with micromolar affinity in the resting and desensitized states to δLeu265 and βLeu257 located at position M2-9 (represented in red color in Figure A.6, B), and is likely to contribute to their functional inhibition of the *Torpedo* nAChR. The second site of **(±)-[$^{125}$I]-4.20** /bupropion binding resides within a desensitized state pocket in the proximity of αTyr213 in αM1 (represented in blue color, Figure A.6, B) (Pandhare *et al.*, 2012).

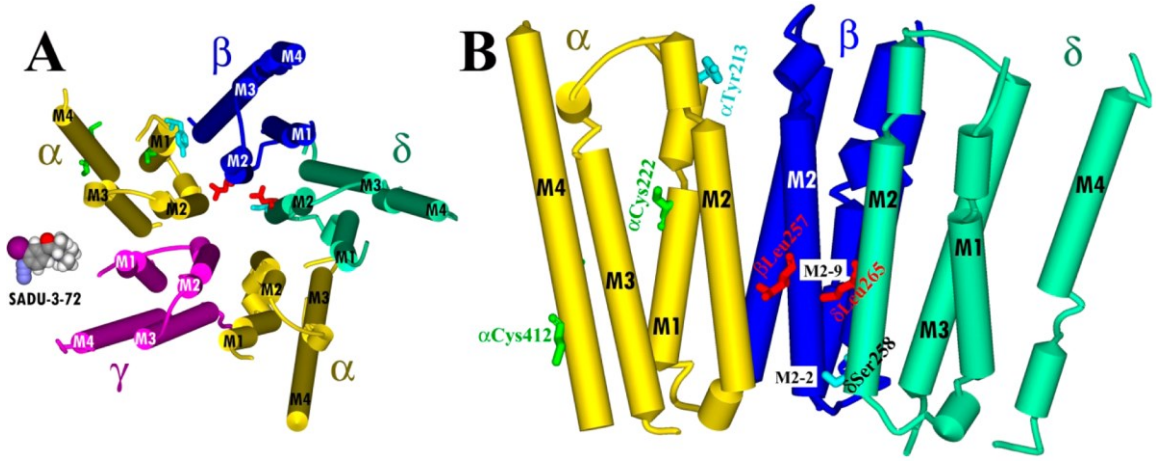


**Figure A.6.** Molecular model of binding sites of [$^{125}$I]-SADU-3-72 (**(±)-[$^{125}$I]-4.20**) labeling in the *Torpedo* nAChR structure (PDB # 2BG9) (A) looking down the channel from the base of the extracellular domain and (B) looking parallel to the membrane with 2 subunits removed for clarity, rotated 90° from (A). Subunits are color-coded: α, yellow; β, blue; and δ, green. Residues photolabeled by [$^{125}$I]-SADU-3-72 are included in stick format, color-coded by domain and conformation: ion channel, resting state (red); ion channel, desensitized state (cyan); lipid−protein interface (green). (Pandhare *et al.*, 2012, Reprinted with permission from *Biochemistry* **2012**, *51*, 2425-2435. Copyright 2012 ACS Publications)

In summary, analog **(±)-[$^{125}$I]-4.20** represents the first successful example of a DAT and nAChR photoaffinity ligand based on the bupropion scaffold, thus representing an important contribution to the growing arsenal of probes useful for characterizing the function and 3D

structure of the DAT and nAChRs as therapeutically significant proteins. The research work related to the synthesis, pharmacological evaluation, and photoaffinity labeling results of probe **(±)-[$^{125}$I]-4.20** within DAT and nAChRs have been successfully published in Arias *et al.*, 2012, Lapinsky *et al.*, 2012 and Pandhare *et al.*, 2012.

## A.3. Radiosynthesis, Pharmacological Evaluation, and Photoaffinity Labeling Experiments of Iodo-Isostere of Racemic Bupropion ((±)-[$^{125}$I]-4.21)

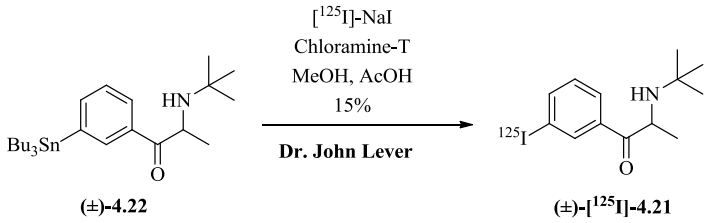


**(±)-4.22** **(±)-[$^{125}$I]-4.21**

**Scheme A.3.** Radiosynthesis of radioiodinated photoprobe **(±)-[$^{125}$I]-4.21** performed by Dr. John Lever

The synthesis of a radioiodinated ($^{125}$I) version of **(±)-[$^{125}$I]-4.21** was pursued to test whether the iodo isostere of bupropion could function as a natural acetophenone-based photoprobe. In this regard, precursor **(±)-4.22** (synthesized in Section 5.2.2) was converted to radioactive iodine derivative **(±)-[$^{125}$I]-4.21** by Dr. John Lever at the University of Missouri-Columbia. As shown in Scheme A.3, Dr. Lever treated stannyl derivative **(±)-4.22** with [$^{125}$I]-NaI (1.53 mCi) in the presence of Chloramine-T, followed by reversed-phase HPLC isolation to provide **(±)-[$^{125}$I]-4.21** in 15% yield in high radioactive purity (98%). Furthermore, this radioligand exhibited a chromatographic profile identical to that of non-radioactive **(±)-4.21**. To test if **(±)-[$^{125}$I]-4.21** was capable of undergoing UV-induced photoactivation and crosslinking, Dr Michael Blanton (Texas Tech University Health Sciences Center) performed photoaffinity labeling experiments within *Torpedo* nAChRs. However, probe **(±)-[$^{125}$I]-4.21** was found not to contribute significantly to the photoaffinity labeling as the level of photoincorporation within

*Torpedo* nAChR was ~1% with respect to the photolabeling intensity displayed by [$^{125}$I]-SADU-3-72 (**(±)-[$^{125}$I]-4.20**). This suggested that the aryl azide in **(±)-[$^{125}$I]-4.20** was the functional group responsible for covalent attachment of this probe to the *Torpedo* nAChR, not the acetophenone moiety

## A.4. Preliminary Pharmacological Characterization of a BINA-Based Clickable Photoprobe ((±)-4.25) for mGlu2 Structure-Function Studies

Given the need for structural characterization of allosteric binding sites within mGlu2, clickable photoprobe **(±)-4.25** was designed (in Section 4.8.1) and synthesized (in Section 5.3.2) for structure-function studies of binding sites of positive allosteric modulators within mGlu2. Dr. Karen Gregory (Monash University, Australia) performed pharmacological evaluation of **(±)-4.25** in HEK-293 cells expressing mGlu2. Briefly, the cells were exposed to varying concentrations of **(±)-4.25** under a fixed glutamate concentration, and resulting intracellular $Ca^{2+}$ mobilization was measured with FlexStation in 96-well plates using a $Ca^{2+}$-sensitive fluorescent dye, Fluo-4. The results showed that functional potency of **(±)-4.25** ($pEC_{50}$ = 6.0, $E_{max}$ = 117 %) was comparable to the parent compound **(±)-1.74** ($pEC_{50}$ = 6.0, $E_{max}$ = 135%) and the lead compound BINA **(±)-1.71** ($pEC_{50}$ = 5.2, $E_{max}$ = 114%). This justified its further progression towards photoaffinity labeling studies.

As of the writing of this dissertation, photoprobe **(±)-4.25** is currently being evaluated in mGlu2 tandem photoaffinity labeling-bioorthogonal conjugation experiments in Dr. Karen Gregory's laboratory at Monash University as shown in Scheme A.4.

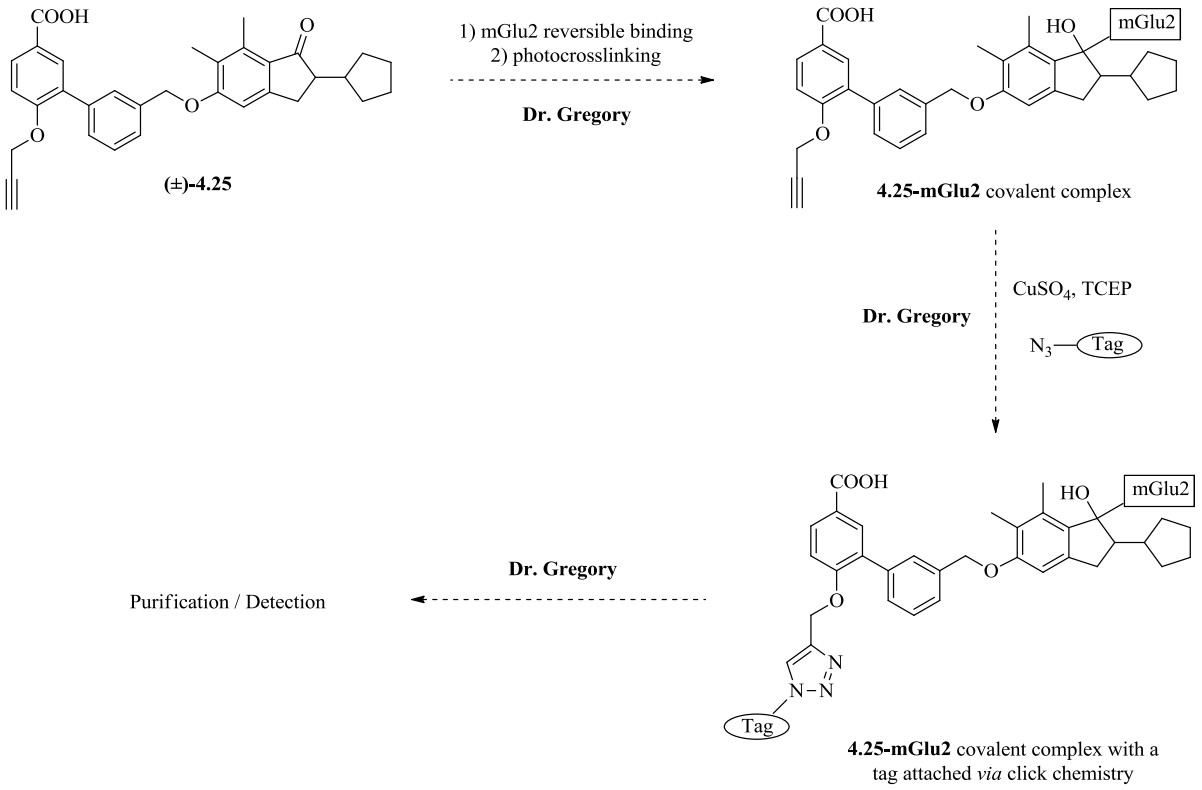


**Scheme A.4.** Proposed schematic representation of mGlu2 tandem photoaffinity labeling-bioorthogonal conjugation experiment of clickable BINA-based mGlu2 PAM photoprobe **(±)-4.25**

In this regard, the mGlu2 transfected cells will be incubated with **(±)-4.25** to enable reversible binding within an mGlu2 allosteric site, and then will be subsequently irradiated with UV light to enable photocrosslinking of the probe within the mGlu2 allosteric site. The resulting **4.25**-mGlu2 covalent complex will then be "clicked" with an azide containing tag (e.g., a fluorescent dye or biotin) to allow further purification and detection of labeled proteins for characterization of mGlu2 3-D structure and function.